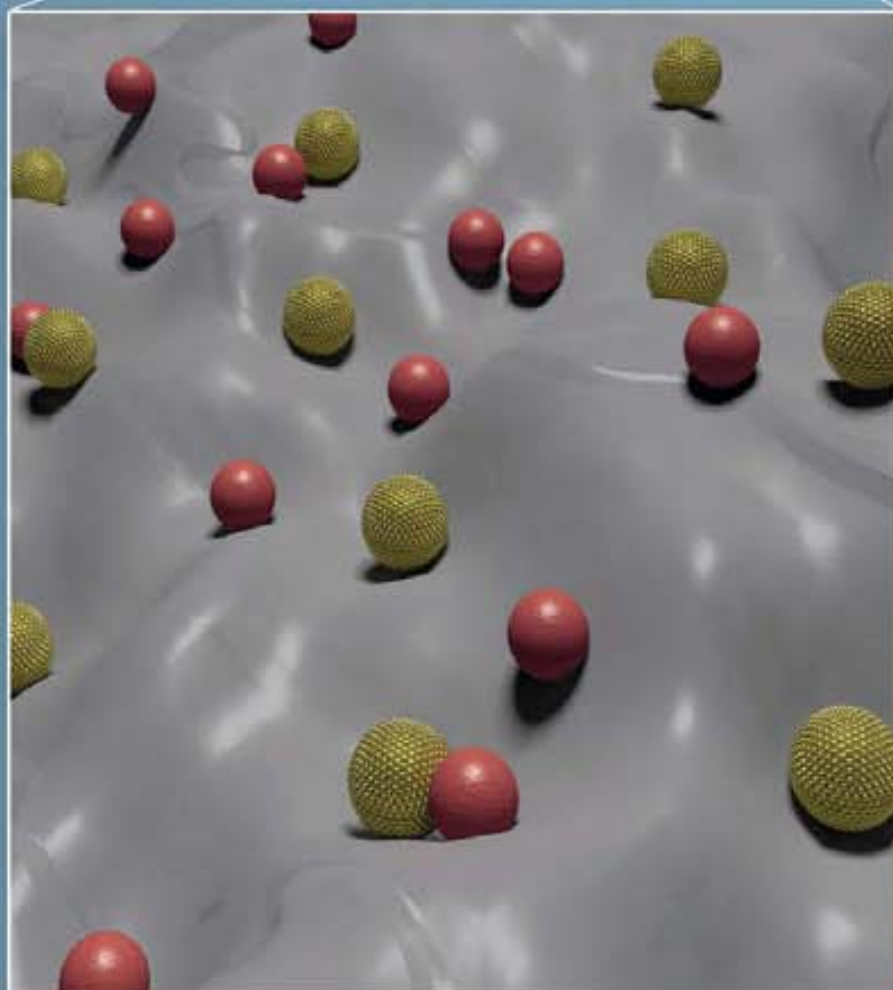


# Plastic and paper platforms for nanoparticle based immunosensors

## PhD Thesis

PhD in Biotechnology, Department of genetic and microbiology,  
Faculty of Biosciences, Autonomous University of Barcelona.

Catalan Institute of Nanoscience and Nanotechnology



Presented by:  
**Claudio Parolo**

Directors  
**Prof. Arben Merkoçi**  
**Dr. Alfredo de la Escosura Muñiz**



Tutor:  
**Prof. Antoni Villaverde Corrales**



**Bellaterra (Barcelona), 2013**



# **Plastic and paper platforms for nanoparticle based immunosensors**

**Claudio Parolo**

PhD Thesis

PhD in Biotechnology – Department of genetic and microbiology

Faculty of Biosciences – Autonomous University of Barcelona

Directors

**Prof. Arben Merkoçi and Dr. Alfredo de la Escosura Muñiz**

Catalan Institute of Nanoscience and Nanotechnology

Tutor

**Prof. Antoni Villaverde Corrales**

**2013**



Memòria presentada per aspirar al Grau de Doctor per Claudio Parolo

Claudio Parolo

Vist i plau

Prof. Dr. Arben Merkoçi Hyka

Investigador ICREA

Nanobioelectronics & Biosensors Group

Institut Català de Nanociència i Nanotecnologia (ICN2)

Dr. Alfredo de la Escosura Muñiz

Nanobioelectronics & Biosensors Group

Institut Català de Nanociència i Nanotecnologia (ICN2)

Bellaterra, 19 de Juny de 2013



**Acknowledgment for the economic and logistic support:**





## Index

<b>Preface</b> .....	I
<b>Optical Abstracts</b> .....	III
<b>Thesis Overview</b> .....	V
<b>Chapter 1 – Introduction</b> .....	1
1.1 – General introduction .....	3
1.2 – Antibodies: structure and modifications with nanoparticles .....	4
1.3 – Electrical detection .....	6
1.3.1 - Direct electrical detections .....	6
1.3.2 - Indirect electrical detections .....	7
1.3.3 - Quartz crystal microbalances and microcantilevers .....	9
1.3.4 - NPs as modifiers of electrotransducing surfaces .....	10
1.4 – Paper-based Biosensors .....	11
1.4.1 - Different types of paper-based biosensors .....	11
1.4.2 - Different types of detection .....	12
1.4.3 - What nanotechnology can bring .....	13
1.4.4 - Protein detection .....	14
1.5 – Conclusions .....	16
1.6 – Bibliography .....	17
 <b>Chapter 2 – Objectives</b> .....	 23
 <b>Chapter 3 – Electrochemical immunosensors based on gold nanoparticles</b> .....	 27
3.1 – Introduction .....	29
3.1.1 - Why AuNPs as electrochemical labels.....	29
3.1.2 - Fabrication of Screen Printed Carbon Electrodes .....	29
3.1.3 - Magnetosandwich immunoassay strategy .....	30
3.2 – Effect of the AuNP size on the direct electrochemical detection .....	30
3.2.1 - Direct electrochemical detection of gold nanoparticles .....	31

3.2.2 - Size-effect on the voltammetric response for the same number of gold nanoparticles .....	33
3.2.3 - Size-effect on the voltammetric response for the same concentration of total gold .....	35
3.2.4 - Application in a magnetoimmunoassay .....	37
3.3 – Oriented functionalization for more efficient AuNP labels .....	39
3.3.1 - Conjugates characterization .....	40
3.3.2 - Effective labels for signal amplification in a magneto-sandwich immunoassay .....	42
3.4 – Conclusions .....	44
3.5 – Bibliography .....	46

## **Chapter 4 – Lateral Flow Immunoassay based on gold nanoparticles .....**

4.1 – Introduction .....	51
4.2 - First amplification strategy: simple changes in the geometry of LFIA	52
4.2.1 - Assay procedure .....	52
4.2.2 - Mathematical simulations.....	54
4.2.3 - Effect of the architecture of the sample pad .....	55
4.2.4 - Effect of different architectures for both sample and conjugation pad .....	57
4.3 - Second amplification strategy: use of AuNPs as carriers of enzymes.	59
4.3.1 - AuNP/antibody conjugates characterization .....	61
4.3.2 - Evaluation of the LFIA performance using AuNPs as both direct labels and carriers of enzymatic labels.....	61
4.4 - Conclusions.....	64
4.5 - Bibliography.....	64

## **Chapter 5 – Paper-based electrodes for nanoparticles detection .....**

5.1 - Introduction .....	69
5.2 - Characterization of paper-based SPCEs .....	70
5.3 - Electrochemical detection of NPs using paper-based SPCEs .....	74

5.4 - Conclusions and perspectives.....	76
5.5 - Bibliography.....	77

<b>Chapter 6</b> – General conclusions and future perspective .....	81
6.1 - General conclusions.....	83
6.2 - Future Perspectives .....	84
6.3 - Bibliography.....	84

**Annex A** – Electrochemical DNA Sensors based on Nanoparticles

**Annex B** – Antibody-oriented functionalization of gold nanoparticle labels for very sensitive electrochemical biosensing

**Annex C** – Compendium of Publications

**Acknowledgments/Agraïments/Agradecimientos/Ringraziamenti**



## Preface

The present PhD thesis has been carried out mainly in the Nanobioelectronics and Biosensors Group of the Catalan Institute of Nanoscience and Nanotechnology (ICN2). According to the decision of the PhD Commission of the Autonomous University of Barcelona, this PhD thesis is presented as a compendium of publications.

All the publications and manuscripts are listed below following their appearance in the thesis:

- 1) De la Escosura-Muñiz, A.; Parolo, C.; Merkoçi, A. Immunosensing using nanoparticles. *Materials Today*, Oxford (UK) 2010, 13, 24–34.
- 2) Parolo, C.; Merkoçi, A. Paper-based nanobiosensors for diagnostics. *Chemical Society Reviews*, London (UK) 2013, 42, 450–457.
- 3) De la Escosura-Muñiz, A.; Parolo, C.; Maran, F.; Merkoçi, A. Size-dependent direct electrochemical detection of gold nanoparticles: application in magnetoimmunoassays. *Nanoscale*, London (UK) 2011, 3, 3350–3356.
- 4) Parolo, C.; Medina-Sánchez, M.; De la Escosura-Muñiz, A.; Merkoçi, A. Simple paper architecture modifications lead to enhanced sensitivity in nanoparticle based lateral flow immunoassays. *Lab on a chip*, London (UK) 2013, 13, 386–90.
- 5) Parolo, C.; De la Escosura-Muñiz, A.; Merkoçi, A. Enhanced lateral flow immunoassay using gold nanoparticles loaded with enzymes. *Biosensors and Bioelectronics*, Amsterdam (NHL) 2012, 40, 412–416.
- 6) Parolo, C.; Medina-Sánchez, M.; Montón, H.; De la Escosura-Muñiz, A.; Merkoçi, A. Paper-based electrodes for nanoparticles detection. *Particle & Particle System Characterization*, Weinheim (DE) 2013, DOI: 10.1002/ppsc.201200124.



## Thesis Overview

This PhD thesis describes two different platforms for the detection of proteins. One platform is based on the use of screen printed carbon electrodes (SPCEs) for the electrochemical detection of magnetosandwich immunoassays, with gold nanoparticles (AuNPs) used as electrochemical label. The second one consists in a lateral flow immunoassay (LFIA), where AuNPs are used both as optical labels and carriers of enzymes. All the presented biosensors were developed using as model protein the Human Immunoglobulin G.

The first two manuscripts, used in this work as introduction (**Chapter 1**), are two reviews that clarify the importance of the developed technologies in the field of biosensors. In detail, the first review, titled “*Immunosensing using nanoparticles*” (Materials Today, 2010, 13, 24–34), besides giving a general knowledge on what an antibody is and how it is connected to a nanoparticle, shows all the techniques in which the nanoparticles have an active role in the detection of proteins, ranging from colorimetric to electrochemical detections. The second review, “*Paper-based nanobiosensors for diagnostics*” (Chemical Society Reviews, 2013, 42, 450–457), focuses more on the use of nanoparticles in paper-based sensor. It wants to point out the huge possibilities, in the development of new biosensors, existing by combining a very low cost and disposable material, such as paper, with the unique properties of nanoparticles.

In **Chapter 2** the objectives of the thesis are explained.

The third chapter (**Chapter 3**) presents two manuscripts related with the use of AuNPs, as electrochemical labels in immunosensors: “*Size-dependent direct electrochemical detection of gold nanoparticles: application in magnetoimmunoassays*” (Nanoscale, 2011, 3, 3350–3356) and “*Antibody-oriented functionalization of gold nanoparticle labels for very sensitive electrochemical biosensing*” (Submitted to Anal. Chem. 2013). The first paper shows how the size of the AuNPs affects their electrochemical detection. In particular, we found that for the direct detection of AuNPs in a SPCE the Brownian motions influence negatively the AuNPs with a diameter smaller than 20 nm. This phenomenon was theoretically and experimentally explained developing a magnetosandwich immunoassay. The second manuscript, presents a new oriented functionalization of AuNPs with antibodies. This technique consists in taking advantage of oriented ionic interactions that happen when negatively charged AuNPs

are in solution with positively charged antibodies. The ionic interaction is further changed for a covalent bond. The new labels were used in a magnetosandwich immunoassay and compared with AuNPs randomly modified with the same antibody. The results clearly show a better limit of detection using the oriented functionalized AuNPs, which were finally used for the detection of HlgG in real human serum.

**Chapter 4** is based on two publications related to AuNP-based LFIA. The first one, “*Simple paper architecture modifications lead to enhanced sensitivity in nanoparticle based lateral flow immunoassays*” (Lab on a chip, 2013, 13, 386–90), describes how simple changes in the geometry of a LFIA, as increasing the size of the different pads, can produce better performances, resulting in an improved sensitivity of about one order of magnitude. The experimental part is also supported by computer simulations, which shows the different flow speeds for the different geometries proposed. The second article, “*Enhanced lateral flow immunoassay using gold nanoparticles loaded with enzymes*” (Biosensors and Bioelectronics, 2012, 40, 412–416), presents a way to obtain two different ranges of detection in a LFIA using the AuNPs both as optical label and carrier of enzymes. In fact, in this work the AuNPs were modified with an antibody already modified with HRP. In this way the obtained signal can be read just by considering the red color produced by the plasmon of AuNP or can be enhanced applying the HRP-substrate directly onto the detection line of the LFIA.

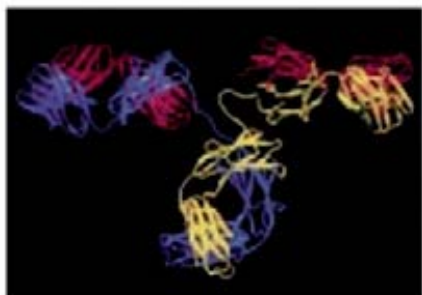
In **Chapter 5** the manuscript “*Paper-based electrodes for nanoparticles detection*” (Particle & Particle System Characterization, 2013, DOI: 10.1002/ppsc.201200124) wants to be the conjunction of the electrochemical and paper-based sensors, since it describes the production, characterization and application of paper-based SPCEs for the detection of nanoparticles. Furthermore, its performances were compared with those of a polyester SPCE showing that the porous structure of paper increases the sensitivity in the detection of both AuNPs and CdSe@ZnS QDs.

Finally, in **Chapter 6** the general conclusions and the future perspectives are discussed.

In addition, **Annex A** reports a book chapter which presents the different electrochemical techniques used in the DNA detection that involves nanoparticles. The **Annex B** includes the manuscript submitted to Anal Chem. and discussed in Chapter 3. The **Annex C** lists all the publications (including the relative supporting information) used in this thesis.

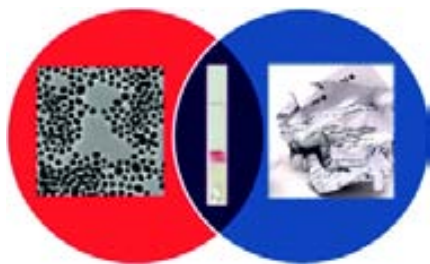
## Optical Abstracts:

### 1) De la Escosura-Muñiz, A.; Parolo, C.; Merkoçi, A. Immunosensing using nanoparticles. *Materials Today, Oxford (UK)* 2010, 13, 24–34.



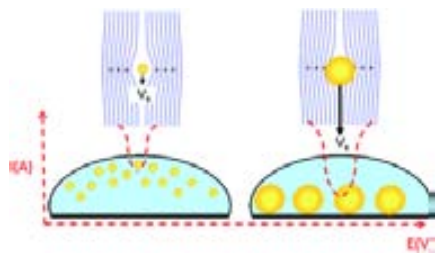
In this review, it is shown how immunosensing technology is taking advantage of the latest developments in material science and in particular from the nanomaterial field. Because of their unprecedented optical tenability, as well as electrical and electrochemical qualities, we are seeing significant developments in the design of novel immunoassays. Various conventional optical and electrical platforms, which will be used for future applications in several fields, are being discussed. Properties of nanoparticles, such as light absorption and dispersion, are bringing interesting immunosensing alternatives. Nanoparticles are improving the sensitivity of existing immunoassays based on Surface Plasmon Resonance, Quartz Crystal Microbalance, Fluorescence spectroscopy etc. Electrochemical techniques are also taking advantage of electrical properties of nanoparticles. Redox behaviors of metal based nanoparticles, surface impedance and conductance changes, when nanoparticles are used as labeling tags or modifiers of transducer surfaces, are also improving the technology. In most of the reported examples, biosensing systems based on nanoparticles are being offered as excellent screening and superior alternatives to existing conventional strategies/assays, with interest in clinical analysis, food quality, safety and security.

### 2) Parolo, C.; Merkoçi, A. Paper-based nanobiosensors for diagnostics. *Chemical Society Reviews, London (UK)* 2013, 42, 450–457.



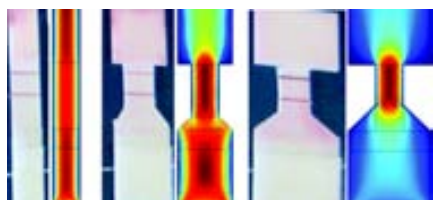
In this review, we discuss how nanomaterials can be integrated in diagnostic paper-based biosensors for the detection of proteins, nucleic acids and cells. In particular, first the different types and properties of paper-based nanobiosensors and nanomaterials are briefly explained. Then, several examples of their application in diagnostics of several biomarkers are reported. Finally, our opinions regarding future trends in this field are discussed.

**3) De la Escosura-Muñiz, A.; Parolo, C.; Maran, F.; Mekoçi, A. Size-dependent direct electrochemical detection of gold nanoparticles: application in magnetimmunoassays. *Nanoscale, London (UK)* 2011, 3, 3350–3356.**



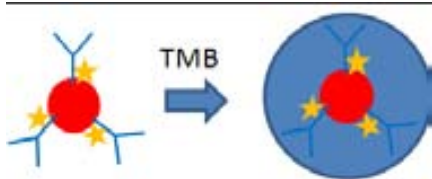
The effect of the AuNPs size, ranging from 5 nm to 80 nm, on the electrochemical response of screen-printed carbon electrodes (SPCEs) used as electrochemical transducers is investigated for the first time. A simple hydrodynamic modeling and calculation at the nanoscale level is applied so as to find the effect of the size of AuNP upon the electrochemical response. The results show that the best electrochemical response for AuNP suspension for the same concentration of total gold is obtained for the 20 nm sized nanoparticles. It is concluded that the Brownian motions avoid a better response for smaller AuNPs that should in fact be related with the best electrochemical signal due to their higher surface area. Finally, the size effect is studied for AuNPs acting as electroactive labels in an immunosensor that employs magnetic beads as platforms of the bioreactions. The best response for the 5 nm AuNPs in this case is due to the fact that in the immunosensing conditions the Brownian motions are minimized because the AuNPs contact with the electrotransducer surface is induced by the immunoreaction and the fast magnetic collection of the nanoparticles used as antibody labels upon application of a magnetic field.

**4) Parolo, C.; Medina-Sánchez, M.; De la Escosura-Muñiz, A.; Mekoçi, A. Simple paper architecture modifications lead to enhanced sensitivity in nanoparticle based lateral flow immunoassays. *Lab on a chip, London (UK)* 2013, 13, 386–90.**



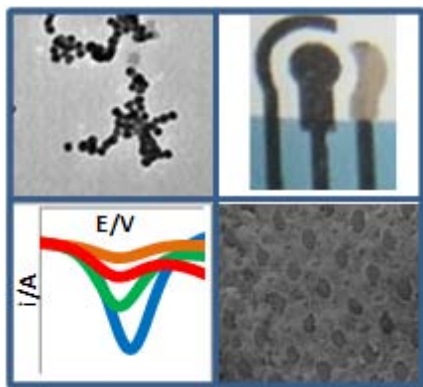
Lateral flow immunoassays (LFIA) are ideal biosensors to detect proteins, but their lack of sensitivity hinders their extensive use. We report a strategy that yields up to an 8-fold improvement in the sensitivity of a gold nanoparticles-based LFIA by changing the sizes of the pads. Theoretical flow simulations of the developed LFIA architectures are in accordance with the experimental results.

5) Parolo, C.; De la Escosura-Muñiz, A.; Merkoçi, A. Enhanced lateral flow immunoassay using gold nanoparticles loaded with enzymes. *Biosensors and Bioelectronics, Amsterdam (NHL)* 2012, 40, 412–416.



The use of gold nanoparticles (AuNPs) as labeling carriers in combination with the enzymatic activity of the Horseradish Peroxidase (HRP) in order to achieve an improved optical lateral flow immunoassay (LFIA) performance is here represented. Briefly in a LFIA with an immunosandwich format AuNPs are functionalized with a detection antibody already modified with HRP, obtaining an “enhanced” label. Two different detection strategies have been tested: the first one produced just by the red color of the AuNPs and the second one obtained using a substrate for the HRP (3 different substrates are evaluated), which produces a red color that enhances the intensity of the previous red color of the unmodified AuNPs. In such very simple way it is gained sensitivity (up to 1 order of magnitude) without losing the simplicity of the LFIA format, opening the way to other LFIA applications including the on-demand tuning of the performance according the analytical scenario

6) Parolo, C.; Medina-sánchez, M.; Montón, H.; Escosura-muñiz, A. De; Merkoçi, A. Paper-based electrodes for nanoparticles detection. *Particle & Particle System Characterization, Weinheim (DE)* 2013. DOI: 10.1002/ppsc.201200124



In this manuscript, the fabrication, characterization and applications of paper-based screen printed carbon electrodes (SPCE) are discussed. In particular, microscopy technique images of the working electrode surfaces show a reproducible 3-D pattern that enhances the performances of the device comparing with those of a polyester-based SPCE. Gold nanoparticles and CdSe@ZnS quantum dots are detected using different electrochemical techniques.

# Chapter 1

## Introduction

This introductory chapter wants to give the reader the basis to understand the importance of immunosensing, as well as why nanoparticles are so extensively used in biosensing. Particular focus is given to the electrochemical detection techniques and paper-based sensors, which use nanoparticles as electrochemical or optical labels. For this and for the next chapters, the contents are extracted from the related publications.

### Related Publications

- 
- 1) DelaEscosura-Muñiz, A.; Párola, C.; Merkoçi, A. Immunosensing using nanoparticles. *Materials Today*, 2010, 13, 24–34.
  - 2) Párola, C.; Merkoçi, A. Paper-based nanobiosensors for diagnostics. *Chemical Society Reviews*, 2013, 42, 450–457.
-



### 1.1 General introduction

In the last years the development of new biosensors has increased significantly, especially in diagnostics, since it has been shown that an early diagnosis can change dramatically the development of a disease.<sup>1</sup> In particular, in the third world the availability of biosensors for the most common diseases could save many lives.<sup>2</sup> Unfortunately, the cost of biosensors and the lack of equipped centres and trained people are probably the hardest obstacles to the diffusion of adequate biosensors in these regions.<sup>3,4</sup> The World Health Organization defined that diagnostics for developing countries should be defined as ASSURED: affordable, sensitive, specific, user-friendly, rapid and robust, equipment free and deliverable to end-users.<sup>5</sup>

On the other hand, recent developments in nanotechnology are significantly impacting different industries ranging from electronics to biomedical engineering by producing a new group of nanomaterials such as nanoparticles (NPs), including quantum dots (QDs), with unique semiconducting and light-emitting properties between other characteristics. Nanomaterials are defined as having a size regime of less than 100 nanometers and, more specifically, QDs range from 2-10 nanometers. From the material point of view, NPs are so small that they exhibit characteristics that are often not observed in the bulk materials. For example, gold nanoparticles (AuNPs) have unique properties such as a strong absorption in the UV-Vis up to the NIR region. QDs have unique properties because, at this size, they behave differently to their bulk equivalents and exhibit unprecedented tunability, enabling completely new applications in science and technology. This has required the continuous search for novel synthesis routes of NPs fabricated from different materials such as Au, Pt, Fe, Co, CdS, Pd, Cu etc.

Although nanotechnology contains high level of integrated technologies and knowledge, it is also bringing simple sensing and biosensing concepts and technologies that are making possible the development of even more easy-to-use and efficient biosensors for several areas such as clinical analysis,<sup>6,7</sup> environmental monitoring<sup>8</sup> as well as safety and security between others.

In this optic, paper-based nanobiosensors are the excellent example of ASSURED devices developed as the result of the synergy between nanotechnology and biosensing technology.

## 1.2 Antibodies: structure and modifications with nanoparticles

The structure of IgG, the most used antibody in immunosensing assays, has been determined by X-ray crystallography (Fig. 1.1A, upper part) which shows a Y-shape form consisting of three equal-sized portions, loosely connected by a flexible tether.<sup>9</sup> The antibodies are constituted by two heavy and two light polypeptide chains that are linked between them as shown in Fig. 1.1A (lower part). The C regions of the heavy chains determine the isotype of the antibody whereas the variable regions of one heavy and one light chain constitute an antigen binding site (ABS). The digestion of antibody with pepsin (Fig. 1.1B upper part) and papain (Figure 1.1B lower part) proteases produces several smaller fragments that may be used instead of the original antibody for immunosensing applications.

Immunoassays are based on the interaction between the antibody and the antigen, in particular between the ABS and the epitope. In fact this interaction gives high specificity and sensitivity to the immunoassay. In order to functionalize the Ig, the connection of labels through three main groups:  $-NH_2$ ,  $-COOH$  and  $-SH$  have been performed. Fig. 1.1C (upper part) shows two examples of conjugation of mono-sulfo-NHS-AuNPs with an antibody through the amino group. A conjugation of monomaleimido AuNPs (Fig. 1.1C, lower part) with an antibody, through the  $-SH$  group, is also shown. The use of the thiol group for the functionalization is a good way to control the direction of the bond between the label and the antibody, and prevent the involvement of the ABS. Fig. 1.1D is an example of conjugation through the carboxyl group reported by Ahirwal et al.<sup>10</sup> They connected the carboxi-term of the antibody with a AuNP by glutathione used as a spacer. The C-term region is a good point to attach the label, since it is far from the ABS and should allow the molecule interaction with the antigen. The AuNP modification with protein can even be observed by TEM (Fig. 1.1E).<sup>11</sup>

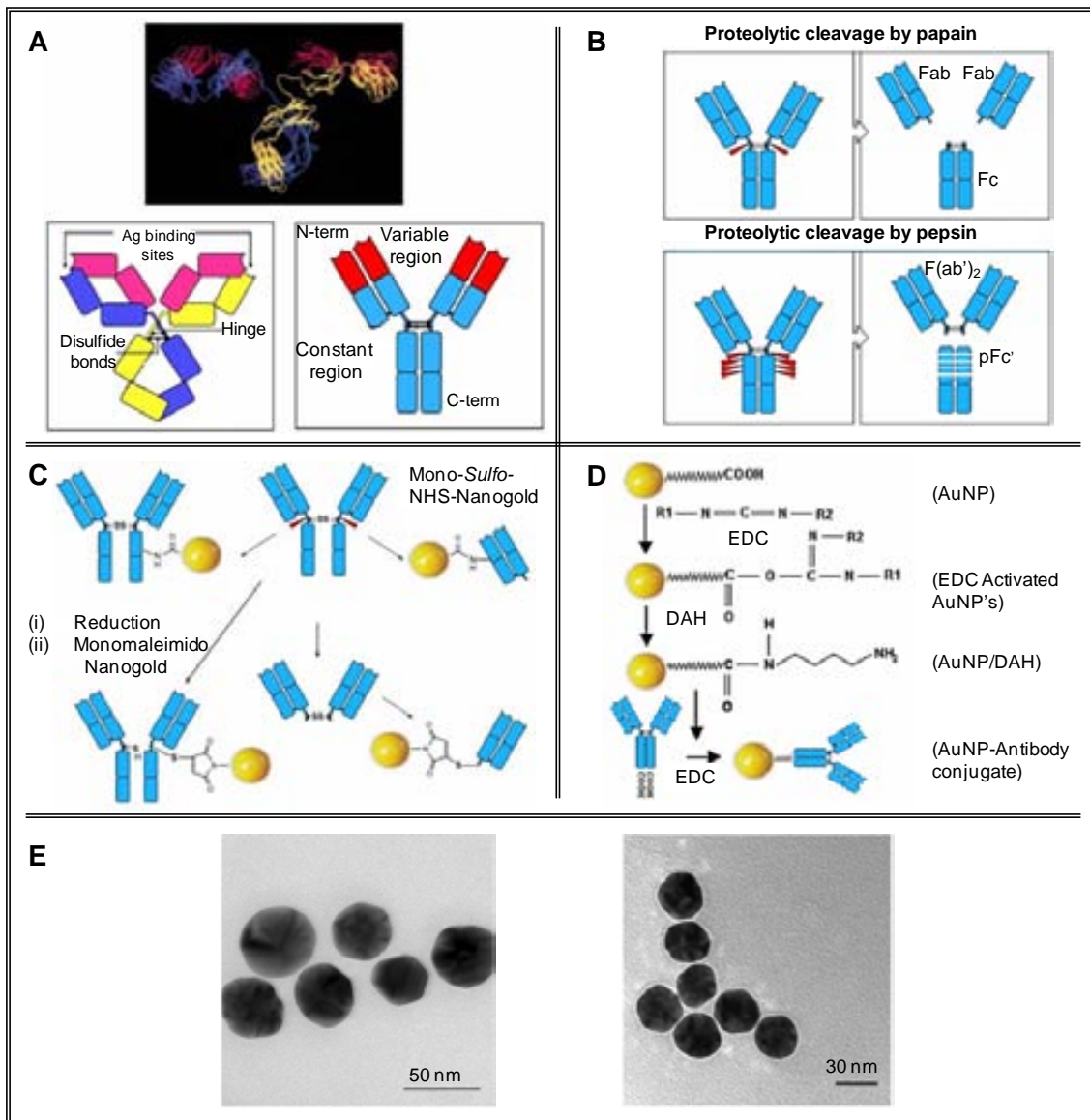


**Fig. 1.1** (A) X-ray crystallographic structure of an IgG antibody (upper part); A schematic representation of IgG and a simplified scheme of the antibody's structure (lower part). (B) The papain (upper part) and the pepsin (lower part) cleavages. (C), Functionalization of a whole IgG or a Fab by a Mono-Sulfo-NHS-AuNP via free amino groups (upper part); monomaleimido AuNP binds the S atom after the reduction of the disulfide bond starting from the whole IgG (lower part, left) or from F(ab')<sub>2</sub>. (D) A n a c t i v a t e d by E D C A u N P c o a t e d w i t h g l u t a t h i o n e, a s s p a c e r a r m, r e a c t s w i t h a n I g G, a l s o a c t i v a t e d b y E D C. (E) TEM images of AuNPs (left part) and AuNPs conjugated with IgG (right part). Image shows a thin white layer, called "halo" effect, surrounding the surface of the AuNPs indicating coating with protein. Adapted with permission from <http://www.nanoprob.es.com> and ref 9, 10, 11.

### 1.3 Electrical detection

The excellent electroactivity of i.e. AuNPs and heavy metal based QDs (i.e. CdS, ZnS, PbS QDs) allows the use of both electrical or electrochemical techniques for their detection, reaching low limits of detection (LOD) and consequently low concentrations of proteins to be detected.<sup>12</sup> NPs can be directly detected due to their own red-ox properties (i.e. of the gold or heavy metals atoms constituents) or indirectly due to their electrocatalytic properties toward other species (i.e. silver reduction etc.).

#### 1.3.1 Direct electrical detection

Several NPs present excellent electroactivity, making possible their direct electrical detection, being not necessary any preliminary dissolution step to liberate the metal ions in solution. This direct electrical detection of NPs comprises solid state analysis, where the metals forming the NPs are electrically detected. However, this type of detection needs direct contact between the electrode surface and the metal and excludes from detection a large portion of non-touching particles. This phenomenon could result in a loss of sensitivity, in comparison with techniques exploiting the total NP dissolution where all metal ions are detected. However, more rapid responses with acceptable LODs and moreover with a shorter analysis time and a more compact / integrated immunosensing assays are achieved with this direct detection.

The first work describing direct electrochemical detection of NPs was reported by Costa-Garcia et al.<sup>13</sup> After that, our group and others have made important contributions to direct electrochemical characterization or detection of metal and semiconductor NPs, reporting some works regarding the voltammetric analysis of AuNPs and CdS QDs. In the case of the AuNPs,<sup>14</sup> the procedure consists in the absorption of AuNPs onto the electrode, followed by their electrochemical oxidation in a hydrochloric medium. The resulting tetrachloroaurate ions generated near the electrode surface are detected by differential pulse voltammetry. For CdS QDs,<sup>15,16</sup> the procedure is quite similar, but in this case the Cd (II) ions contained as defects in the CdS QDs crystalline structure are electrochemically reduced to Cd (0) and then immediately electro-oxidized to Cd (II), registering the oxidation peak. Based on these fundamentals, solid-state detection of AuNPs<sup>17</sup> (Fig. 1.2A) and CdS QDs<sup>18</sup> have been applied in immunoassays for the detection of human IgG and carcinoembryonic antigen respectively at pM levels.

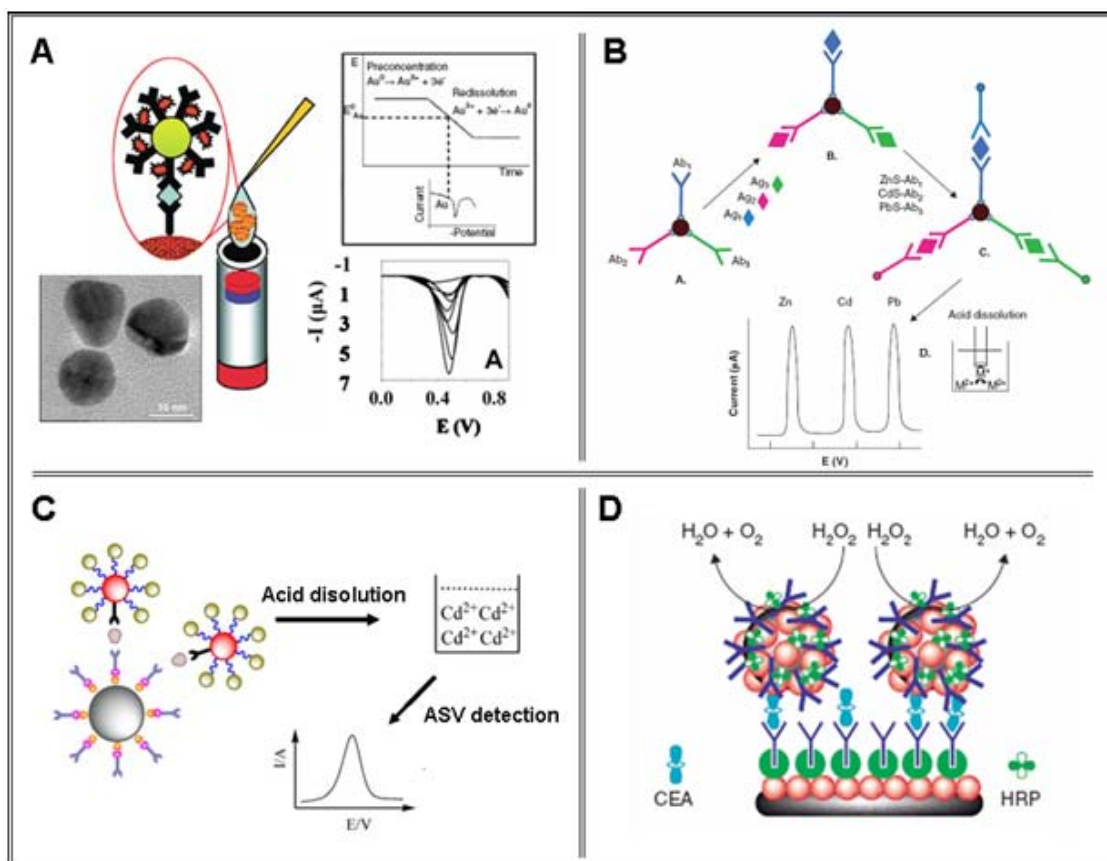


**Fig. 1.2** Electrical detection of NPs. (A) Direct electrical detection of AuNPs tags without acidic dissolving, based on a pre-oxidation and later reduction of Au(III) ions generated. (B) Electrochemical detection of NPs. The electrochemical stripping detection of different QDs labels after their acidic dissolution, allows the multiple detection of multiple proteins. (C) NPs as carriers of other NPs. AuNPs can be used as carriers of a high number of CdS QDs, giving rise to an amplified signal in the further stripping detection after acidic dissolution. (D) NPs as carriers of enzymes. AuNPs can also be used as carriers of a high number of HRP enzymes, exerting an amplification effect in the electrochemical enzymatic signal. Adapted with permission from ref 17, 23, 24, 25.

### 1.3.2 Indirect electrical detections

The most reported way to electrochemically detect NPs involved in bioassays consists in their preliminary oxidative dissolution in acidic mediums, followed by the detection of the metal ions by a sensitive powerful electroanalytical technique such as anodic stripping voltammetry. Very low LODs, in the order of pM, are achieved due to the release of a large number of metal ions from each NP and its effective “built-in” preconcentration step ensured by electrochemical stripping analysis. Dequaire et al.<sup>19</sup> pioneered the application of this NP detection method for the quantification of IgG as model analyte at pg/mL levels. From that to now, AuNPs as well as other NPs, such as CdS@ZnS QDs,<sup>20,21</sup> CdSe@ZnS QDs<sup>22</sup> have been used for the sensitive detection

(always in the pM level) of proteins as prostate specific antigen or interleukin 1- $\alpha$  respectively. Furthermore, one of the most important advantages that offers the use of QDs as electroactive labels is their ability to perform multidetection by using QDs made of different inorganic crystals, with different electrochemical responses. This electrochemical coding technology has been approached by Liu et al.<sup>23</sup> for the simultaneous measurements of proteins ( $\beta_2$ -microglobulin, IgG, bovine serum albumin, and C-reactive protein) using as tracers ZnS, CdS, PbS and CuS QDs. (Fig. 1.2B).

It must also be mentioned that the high surface coupled with the easy bioconjugation, make NPs excellent carriers of other electroactive labels in immunoassays.. The loading of NPs with other NPs (i.e. AuNPs loaded by CdS QDs)<sup>24</sup> (Fig. 1.2C) and with enzymes (i.e. AuNPs loaded by HRP<sup>25</sup> and SiNPs loaded by HRP<sup>26</sup> or AP<sup>27</sup>) (Fig. 1.2D) so as to obtain labels with an enhanced signal have been reported as interesting alternative for electrochemical immunosensing systems.

Another alternative to detect NPs used as labels in protein detection assays consists in using their catalytic properties toward reactions of other species. The well-known catalytic properties of the AuNPs on the silver chemical reduction have been extensively approached in the last years. Recently, our group has developed a very sensitive methodology based on the selective electroreduction of silver ions on the surface of AuNPs in magnetosandwich assays, achieving LODs of human IgG in the fM level,<sup>28</sup> and has also exploited the catalytic properties of AuNPs on the hydrogen ions electroreduction in an acidic medium for the antigen-antibody interaction monitoring, applied for cancer cells detection<sup>29</sup> (Fig. 1.3).

Silver nanoparticles (AgNPs) also exhibit catalytic activity on the chemical reduction of silver ions added as 'substrate'. After that, the silver can be i.e. dissolved in an acidic medium and measured by anodic stripping voltammetry. This property has been exploited in sandwich immunoassays, for the sensitive detection of human IgG<sup>30</sup> at pM level.

Finally, in addition to the catalytic activity on metal ions reduction the catalysis of other electrochemical reactions is also reported. For example, the catalytic activity of PtNPs on the reduction of H<sub>2</sub>O<sub>2</sub> to H<sub>2</sub>O<sup>31</sup>, and of the core-shell Au@Pd NPs on the O<sub>2</sub> reduction to H<sub>2</sub>O<sup>32</sup> have been exploited by Polsky et al. for the detection of thrombin (nM levels) and cytokine TNF- $\alpha$  (fM levels) respectively.

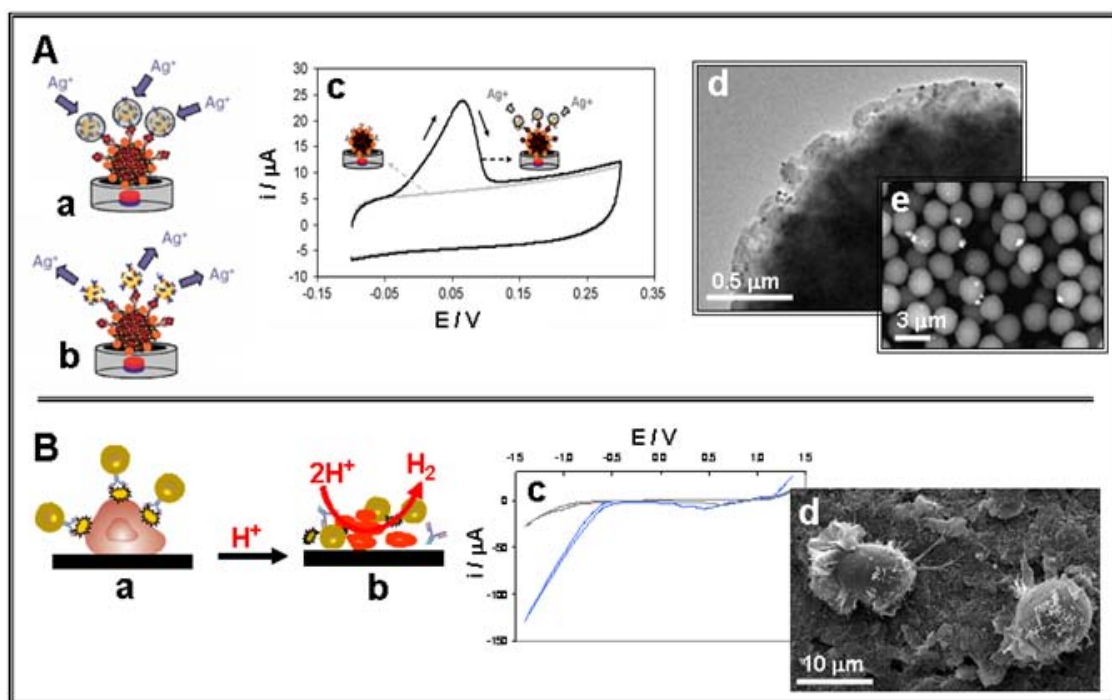


**Fig. 1.3** Electrocatalytic detection of AuNPs. (A) Detection based on the catalytic properties of AuNPs on the silver electroreduction in a magnetosandwich immunoassay (a); the further silver reoxidation (b) gives rise to a peak current that can be related with the protein concentration (c); the AuNPs (small black points) can be observed by TEM analysis around the magnetic beads used as immobilization platforms (big black sphere) (d); the silver crystals formed after the silver electrodeposition (white points) can be observed by SEM analysis around the magnetic beads (e). (B) Detection of cells (a) based on the catalytic properties of AuNPs on the hydrogen evolution in an acidic medium (b); the presence of AuNPs gives rise to a shift in the reduction potential of the hydrogen ions to hydrogen (lower voltammetric curve) (c); the cells on the electrotransducer surface can be observed by SEM (d). Adapted with permission from ref 28, 29.

### 1.3.3 Electromechanical detection: quartz crystal microbalances and microcantilevers

Microcantilevers and quartz crystal microbalances have emerged in the last years as versatile biosensors demonstrating the prominent performances such as high sensitivity and label free detection.<sup>33–35</sup> In the case of the quartz crystal microbalance, the bioreaction generates a change in the mass, reordering the charges in the surface of the piezoelectric material and giving rise to a change in the resonant frequency of the microbalance. The use of NP labels in sandwich assays can increase both the surface stress and the mass of the immunocomplex, allowing the increasing of the sensitivity of these electromechanical assays.

This is the case of the work reported by Lee et al.<sup>36</sup> for the detection of prostate specific antigen at pg/mL levels using SiNPs as labels in a dynamic mode

microcantilever based biosensor. In a similar way, quartz crystal microbalance biosensors have been developed using AuNPs, as amplification agents for the detection of human IgG and aflatoxin B1<sup>37</sup> at clinical relevant levels.

#### *1.3.4 NPs as modifiers of electrotransducing surfaces*

The presence of NPs on the electrotransducer surface promotes the electron transfer, improving the electrochemical response coming from potentiometric and conductimetric responses. Furthermore, some NPs provide congenial microenvironment similar to that of red-ox proteins in a native system for retaining their bioactivity giving the protein molecules more freedom in orientation and avoiding their denaturation. The introduction of NPs into the transducing platform is commonly achieved by their adsorption onto conventional electrode surfaces in various forms including that of a composite.

PtNPs directly electrogenerated,<sup>38</sup> AuNPs adsorbed,<sup>39</sup> AuNPs integrated in composites,<sup>40,41</sup> or AuNPs immobilised on the electrotransducer surface through electrostatic forces on cationic polymeric layers<sup>42</sup> are representative examples of these nanostructured surfaces built for the detection of proteins such as human IgG,  $\alpha$ -fetoprotein, prostate specific antigen and hepatitis B surface antigen at clinical relevant levels.

Furthermore, in addition to the final conductometric, potentiometric and voltammetric detections it must be remarkable the use of nanostructured surfaces containing AuNPs,<sup>43,44</sup> ZrO<sub>2</sub> NPs<sup>45</sup> and CoFe<sub>2</sub>O<sub>4</sub>@SiO<sub>2</sub> NPs<sup>46</sup> for improving the performance of quartz crystal microbalance based immunosensors.

## 1.4 Paper-based Biosensors

Paper-based biosensors can be one of the answers to this demand. In fact they are affordable, paper is inexpensive and abundant; sensitive and specific, they can be based on immunoreactions or nucleic acid hybridizations; user-friendly, the pregnancy test is one of the most used point-of-care (PoC) biosensors; rapid and robust, within few minutes or less the response is developed; equipment free, they are mainly read by the naked eye, or, if a quantitative detection is required, the equipments are small and cheap; and finally deliverable to end-users, they are quite stable to a wide range of temperature and time.<sup>47</sup> Furthermore they can be developed using inkjet<sup>48</sup>, wax printing<sup>49</sup> or screen printing<sup>50</sup> technology making them amenable to in-situ fabrication<sup>51</sup> with interest to be delivered or even produced in areas with limited resources..

The first paper-based sensor can be considered the invention of paper chromatography by Martin and Synge, who were awarded with the Nobel Prize in chemistry in 1952. Another milestone in the field was the commercialization of the pregnancy test, which can be considered one of the most used PoC biosensors and one of the first lateral flow assays (LFAs).<sup>6</sup> After the pregnancy test, other diagnostic PoC paper-based devices for diabetes and for the detection of biomarkers of pathogens and infectious diseases appeared in the market.<sup>52</sup> More recently the development in this field has been extended toward the microfluidic paper analytical devices ( $\mu$ PADs).<sup>53</sup>

### 1.4.1 Different types of paper-based biosensors

The paper-based biosensor can be divided into three main categories: the dipstick assays, the LFAs and the  $\mu$ PADs (Table 1.1).

The dipstick assays are the simplest ones, since they are based on the blotting of the sample onto a paper pre-stored with reagents; the best known example is the pH strip. Their main disadvantage is the impossibility to design more sophisticated assays, which for diagnostic purposes are often necessary.

The LFAs have all the reagents pre-stored in the strip, as the dipstick, but they integrate also the flow of the sample. The flow gives a very important advantage to the sample: it passes through the different zones of the strip, which have different reagents for different functions. In this way many different assay designs like sandwich and competitive formats or multi-detection can be used. In particular a LFA is generally made of 4 different parts: the sample pad, the conjugation pad, the detection pad and the absorbent pad. The sample pad, made of cellulose, filters the sample from impurities

and stores the dried assay buffer, which assures the optimal conditions for the analyte during all the flux.

The conjugation pad, made of glass fibers, is used as dry-reagents storage for the labels. In this pad the binding reaction between the labels and the analyte starts. In the detection pad, made of nitrocellulose, the capture reagents are fixed and the signal is developed. Finally, cellulose filters are used as absorbent pad. The function of the absorbent pad is to wick the fluid through the membrane, in this way the amount of sample can be increased resulting in an increased sensitivity. The main drawbacks of the LFAs are the difficulty in obtaining multiplex and quantitative analysis.<sup>54</sup>

These drawbacks can be overcome using the  $\mu$ PADs. The  $\mu$ PADs are devices which integrate the paper advantages with those of microfluidics. In fact they are very cheap and do not need any pump or external source of energy to make the liquid flow through the channel, but at the same time they require a very low amount of sample and can be used for multiplexed and quantitative analysis.<sup>55</sup> They are made creating hydrophilic channels in the hydrophobic paper. Many techniques such as photolithography, polydimethylsiloxane (PDMS) plotting, inkjet etching, plasma etching, cutting, and wax printing have been used to produce  $\mu$ PADs.<sup>56</sup>

#### *1.4.2 Different types of detection.*

The three different types of paper-based platforms exemplify differences in the type of detection. In fact the dip stick assays tend to an easy optical detection, which is done by the naked eye, like pH strips, in the most cases. Regarding the LFAs, optical detection is the most frequent and is based on the use of strip readers when quantitative results are required<sup>57</sup>, although integration of electrochemical detection within the LFA is also reported<sup>58</sup>. Finally the  $\mu$ PADs, besides being simple and using optical detection, can employ more sophisticated devices and techniques, like microplate readers<sup>59</sup>, chemiluminescence<sup>60,61</sup>, electrochemistry<sup>62</sup>, transmission of light through paper<sup>4</sup>, or piezoresistive MEMS sensors<sup>63</sup>. All these techniques would be useless in third world countries due to the price of the devices and the lack of trained people. To solve this problem Martinez *et al.* integrate the use of a normal digital camera. The camera can digitalize the optical signal of the paper-based sensor and send it to trained personnel, who can send back a quantitative response.<sup>64</sup>

Type of paper-based biosensor	Possible detection methods	Advantages	Disadvantages
<b>Dipstick</b>	<ul style="list-style-type: none"> <li>Optical</li> </ul>	<ul style="list-style-type: none"> <li>Easy design</li> <li>Fast optimization</li> </ul>	<ul style="list-style-type: none"> <li>Just one step</li> <li>Only optical detection</li> <li>Mostly no quantification</li> </ul>
<b>LFA</b>	<ul style="list-style-type: none"> <li>Optical</li> <li>Electrochemical</li> </ul>	<ul style="list-style-type: none"> <li>Versatile</li> <li>Flow</li> <li>Electrochemical detection</li> <li>Possible quantification</li> </ul>	<ul style="list-style-type: none"> <li>Long optimization times</li> <li>Long fabrication</li> <li>Sample volume (around 100 <math>\mu\text{L}</math>)</li> </ul>
<b><math>\mu\text{PAD}</math></b>	<ul style="list-style-type: none"> <li>Optical</li> <li>Electrochemical</li> <li>Chemiluminescence</li> <li>MEMS</li> </ul>	<ul style="list-style-type: none"> <li>Versatile</li> <li>Flow</li> <li>Different detection methods</li> <li>Quantification</li> <li>Small sample volume (less than 10 <math>\mu\text{L}</math>)</li> <li>Massive production</li> </ul>	<ul style="list-style-type: none"> <li>Long optimization times</li> </ul>

**Table 1.1:** Detection methods, advantages and disadvantages of the different paper-based biosensor

#### 1.4.3 What nanotechnology can bring.

In this context nanotechnology can improve the quality of the paper-based devices with the unique properties of the nanomaterials.<sup>65</sup> In the paper biosensors the nanomaterials are mainly used as labels or carriers<sup>66</sup> (Fig. 1.4A), but other special functions such as photocatalytic, antibacterial, anti-counterfeiting, Surface Enhanced Raman Scattering (SERS) and Surface Plasmon Resonance (SPR) on the paper have also been reported.<sup>67</sup> The most used nanomaterial in paper-based devices are gold nanoparticles (AuNPs).<sup>68</sup> AuNPs have many properties, which make them excellent labels: easy functionalization, easy manipulation, biocompatibility, a strong red color, a characteristic surface Plasmon resonance and electrochemical activity that can be used in optical<sup>69</sup> (Fig. 1.4B) or electrical detection of antibodies, nucleic acids and even cancer cells. The AuNPs are not the only NPs used in paper-based devices. Magnetic nanoparticles<sup>70</sup>, quantum dots (QDs)<sup>71</sup>, liposomes<sup>72</sup>, carbon nanoparticles<sup>73,74</sup> and ceria

nanoparticles<sup>75</sup> have also been reported.

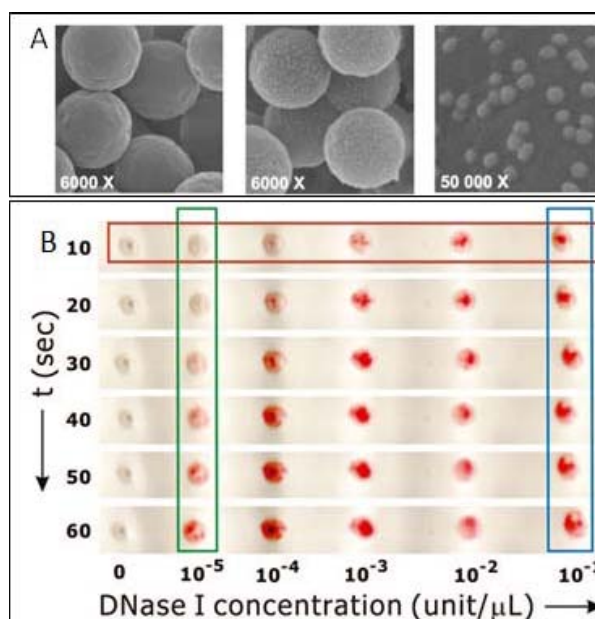


**Fig. 1.4** Nanomaterials in paper biosensors. A) From the left to the right: Scanning electron microscopy (SEM) images of the microspheres deposited on the diagnostic membrane alone, with nanoparticles, and with nanoparticles at a larger magnification. B) DNase I-sensing assays on hydrophobic paper as functions of assay time and DNase I concentration. More red color is observed when more target analyte is added (red box) or longer assay time was utilized (green box). Note that the color intensity eventually reaches a plateau. For example, when a target analyte at a high concentration (10<sup>-1</sup> unit/μL) was applied (blue box), a maximum signal was reached very quickly (~10-20 s), after which no further color change was observed. Adapted with permission from ref 66, 69.

#### 1.4.4 Protein detection

The development of sensitive, easy-to-use and cheap biosensors for the detection of proteins is of tremendous interest for diagnostics applications. In fact many diseases can be related to the higher/lower presence of a protein or to its different isoforms.<sup>76</sup> Many paper-based sensors have been developed using different strategies. Here we try to summarize the different techniques and NPs that can be used.

The main format used in paper nanobiosensors to detect proteins is the sandwich assay, based on a pair of antibodies (immunosandwich formation) as reported below. Li *et al.* detected nitrated ceruloplasmin, a significant biomarker for cardiovascular disease, lung cancer, and stress response to smoking, using a sandwich assay LFA based on the measurement of the QD fluorescence using a portable device (Fig. 1.5A). The authors reached a limit of detection (LoD) of 8 ng/mL in spiked human plasma sample.<sup>77</sup> Other works enhanced the sensitivity of the sandwich format. One was

proposed by Parolo *et al.* using the AuNPs both as labels reaching a LoD of 6 ng/mL of HIgG and as carriers of HRP, achieving a LoD of 200 pg/mL.<sup>78</sup> A different mechanism of enhancement was proposed by Choi *et al.* Combining two different size AuNPs in the same sandwich to detect the Troponin I with a LoD of 10 pg/mL (Fig. 1.5B) in serum samples of patients with myocardial infarction.<sup>79</sup> The sandwich format also has been used by Lin *et al.* to develop an electrochemical LFA reaching a LoD of 20 pg/mL of prostate specific antigen in human serum. In this case the authors used core-shell CdSe-ZnS nanoparticles as labels.<sup>21</sup>

The following two works are based also in sandwich format but instead of using antibodies, the authors used aptamers or DNA sequences. Xu *et al.* detected thrombin in human plasma, achieving a LoD of 2.5 nM, using a LFA based on the use of aptamers combined with AuNPs. They demonstrated that aptamers are equivalent or superior to antibodies in terms of specificity and sensitivity for thrombin detection, respectively (Fig. 1.5C).<sup>80</sup> Fang *et al.* developed a LFA for the rapid detection of the DNA-binding protein c-jun. They used the sandwich format using AuNPs functionalized with a DNA probe specific for the c-jun and a capture antibody specific for the same protein in the test line. The biosensor was tested with crude HeLa cells lysate and it visually detected c-jun activity in 100g of protein lysate.<sup>81</sup>

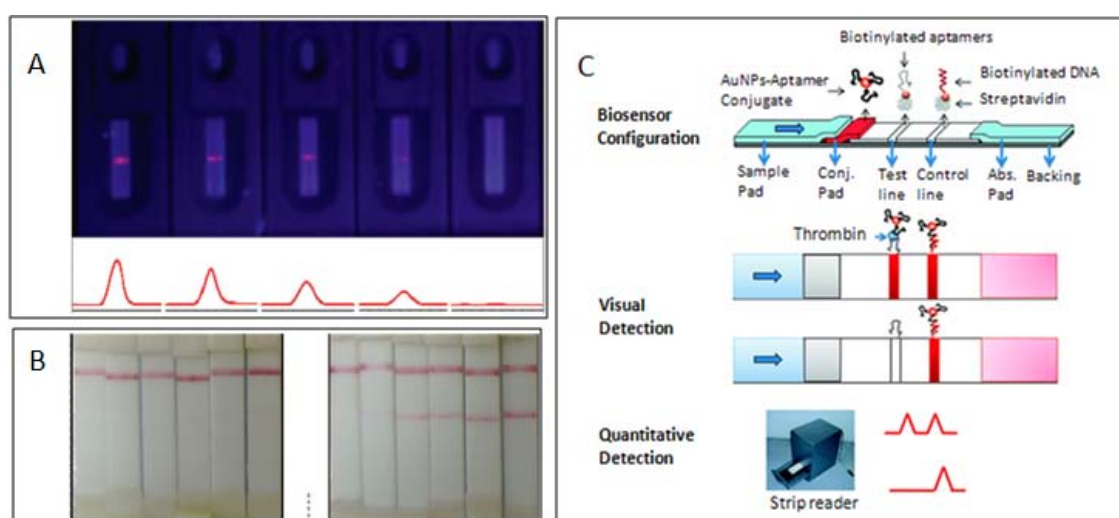


**Fig. 1.5** Paper-based biosensor for protein detection. A) Fluorescence imaging of QD-based LF for (from the left to the right) 10 g/mL, 1  $\mu$ g/mL, 100 ng/mL, 10 ng/mL nitrated ceruloplasmin and 10  $\mu$ g/mL ceruloplasmin without nitration. The bottom curves are the corresponding readout using a strip reader. B) Detection of troponin I with varying concentrations by the conventional LFA (left) and the dual AuNP conjugate-based LFA (right). C) Schematic illustration of the configuration and measurement principle of the aptamer-based strip biosensor. Adapted with permission from ref 77, 79, 81.

Some very interesting works about the detection of proteins in paper-based biosensors, based on enzymatic reactions have been published; in a near future such devices will probably integrate NPs in order to enhance their performances. Martinez *et al.* were the first in creating a  $\mu$ PAD for the detection of protein. They could detect the total amount of protein in a urine sample, as low as  $0.38 \mu\text{M}$ , integrating the tetrabromophenol blue in a  $\mu$ PAD.<sup>53</sup> Particularly interesting is the work of Cheng *et al.*, who developed a paper-based ELISA (P-ELISA). They obtained a 96 well paper device which can be read with a normal spectrophotometer to perform the classical ELISA test. P-ELISA showed to be faster and cheaper than a conventional ELISA and with similar level of sensitivity and specificity. In particular the authors obtained a limit of detection of 54 fmol/zone, which is approximately ten times lower than that obtained by ELISA experiments in 96-well plates for the same antigen/antibody pair<sup>82</sup>. The paper-based ELISA format was recently used by Wang *et al.* to perform a multi detection of tumoral markers. In their work the authors introduced, beside the chemiluminescence detection, the modification with chitosan of the surface to enhance the efficiency of immobilization of the antibodies. They reached to detect with a linear range: 0.1 - 35.0 ng/mL for  $\alpha$ -fetoprotein, 0.5 - 80.0 U/mL for cancer antigen 125 and 0.1 - 70.0 ng/mL for carcinoembryonic antigen.<sup>60</sup>

### 1.5 Conclusions

This chapter gives a brief overview of a rapidly increasing research field such as immunosensing using NPs. The research and applications in this field are located at the crossroads of materials research, nanosciences, and molecular biotechnology. Since the NPs and biomolecules, such as antibodies, typically meet at the same nanometer length scale, this interdisciplinary approach will contribute to the establishment of a novel field, descriptively termed immunosensing nanotechnology or nanoimmunosensing.

The future development of immunosensing technology will keep profiting from the rapid current advances in materials science in general and particularly that of nanomaterials science that will bring novel NPs with improved physical and chemical properties. In addition, the current proteome research will also be beneficial for this field, since it provides data that allow producing of even more suitable bioreceptors, such as antibodies, which are crucial for such a technology. This might open the door to more effective nanoimmunosensors with interest for biomedical applications.

In addition to long term perspectives, today's NPs based immunosensing systems are showing to offer new and versatile protein detection alternatives. In most of the reported applications NPs are offered as immunoassays labels achieving higher sensitivities and multiplexing analysis. They are also used as modifiers of the electrochemical or optical transducing platforms.

On the other hand, the paper-based nanobiosensors are showing to be excellent tools for diagnostics. In particular their nature makes them available for PoC applications since they are portable and easy to be used. Furthermore the fast response is essential in many situations such as illness diagnostics which later require a fast treatment. The integration of small strip reader or electrochemical sensor in a paper-based device improves the quantification of the analytes, reaching higher sensitivity and lower detection limits. Paper-based diagnostics are suitable for large scale production, since they can be fabricated using even already existing or similar office machines making them a very cheap and efficient technology. Finally the integration of nanomaterials within these devices is expected to bring advances to their stability/robustness, shelf lifetime and bringing novel detection opportunities including multidetection capability beside other improvements of their analytical performance.

## 1.6 Bibliography

- (1) Ali, M. M.; Aguirre, S. D.; Xu, Y.; Filipe, C. D. M.; Pelton, R.; Li, Y. *Chemical communications (Cambridge, England)* **2009**, 6640–2.
- (2) Mabey, D.; Peeling, R. W.; Ustianowski, A.; Perkins, M. D. *Nature reviews. Microbiology* **2004**, 2, 231–40.
- (3) Yager, P.; Edwards, T.; Fu, E.; Helton, K.; Nelson, K.; Tam, M. R.; Weigl, B. H. *Nature* **2006**, 442, 412–8.
- (4) Ellerbee, A. K.; Phillips, S. T.; Siegel, A. C.; Mirica, K. a; Martinez, A. W.; Striehl, P.; Jain, N.; Prentiss, M.; Whitesides, G. M. *Analytical chemistry* **2009**, 81, 8447–52.
- (5) Peeling, R. W.; Holmes, K. K.; Mabey, D.; Ronald, a *Sexually transmitted infections* **2006**, 82 Suppl 5, v1–6.
- (6) Agasti, S. S.; Rana, S.; Park, M.-H.; Kim, C. K.; You, C.-C.; Rotello, V. M. *Advanced drug delivery reviews* **2010**, 62, 316–28.

- (7) Durner, J. *Angewandte Chemie (International ed. in English)* **2010**, 49, 1026–51.
- (8) Palchetti, I.; Mascini, M. *The Analyst* **2008**, 133, 846–54.
- (9) Janeway, C.; Travers, P.; Walport, M.; Shlomchik, M. *Immunobiology: The Immune System in Health and Disease*; Taylor & Francis Group, Ed.; 6th editio.; New york, 2005.
- (10) Ahirwal, G. K.; Mitra, C. K. *Biosensors & bioelectronics* **2010**, 25, 2016–20.
- (11) Thobhani, S.; Attree, S.; Boyd, R.; Kumarswami, N.; Noble, J.; Szymanski, M.; Porter, R. a *Journal of immunological methods* **2010**, 356, 60–9.
- (12) De la Escosura-Muñiz, A.; Ambrosi, A.; Merkoçi, A. *TrAC Trends in Analytical Chemistry* **2008**, 27, 568–584.
- (13) Garcfa, M. B. G.; Garcfa, A. C. **1995**, 38, 389–395.
- (14) Pumera, M.; Aldavert, M.; Mills, C.; Merkoçi, A.; Alegret, S. *Electrochimica Acta* **2005**, 50, 3702–3707.
- (15) Merkoçi, A.; Marín, S.; Castañeda, M. T.; Pumera, M.; Ros, J.; Alegret, S. *Nanotechnology* **2006**, 17, 2553–9.
- (16) Merkoçi, A.; Marcolino-Junior, L. H.; Marín, S.; Fatibello-Filho, O.; Alegret, S. *Nanotechnology* **2007**, 18, 035502.
- (17) Ambrosi, A.; Castañeda, M. T.; Killard, A. J.; Smyth, M. R.; Alegret, S.; Merkoçi, A. *Analytical chemistry* **2007**, 79, 5232–40.
- (18) Ho, J. A.; Lin, Y.-C.; Wang, L.-S.; Hwang, K.-C.; Chou, P.-T. *Analytical chemistry* **2009**, 81, 1340–6.
- (19) Dequaire, M.; Degrand, C.; Limoges, B. *Analytical chemistry* **2000**, 72, 5521–8.
- (20) Liu, G.; Lin, Y.; Wang, J.; Wu, H.; Wai, C. M.; Lin, Y. *Analytical chemistry* **2007**, 79, 7644–7653.
- (21) Lin, Y.-Y.; Wang, J.; Liu, G.; Wu, H.; Wai, C. M.; Lin, Y. *Biosensors & bioelectronics* **2008**, 23, 1659–65.
- (22) Wu, H.; Liu, G.; Wang, J.; Lin, Y. *Electrochemistry Communications* **2007**, 9, 1573–1577.
- (23) Liu, G.; Wang, J.; Kim, J.; Jan, M. R.; Collins, G. E. *Analytical chemistry* **2004**, 76, 7126–30.

- (24) Ding, C.; Zhang, Q.; Zhang, S. *Biosensors & bioelectronics* **2009**, *24*, 2434–40.
- (25) Tang, D.; Yuan, R.; Chai, Y. *Analytical chemistry* **2008**, *80*, 1582–8.
- (26) Wu, Y.; Chen, C.; Liu, S. *Analytical chemistry* **2009**, *81*, 1600–7.
- (27) Qu, B.; Chu, X.; Shen, G.; Yu, R. *Talanta* **2008**, *76*, 785–90.
- (28) De la Escosura-Muñiz, A.; Maltez-da Costa, M.; Merkoçi, A. *Biosensors & bioelectronics* **2009**, *24*, 2475–82.
- (29) De la Escosura-Muñiz, A.; Sánchez-Espinel, C.; Díaz-Freitas, B.; González-Fernández, A.; Maltez-da Costa, M.; Merkoçi, A. *Analytical chemistry* **2009**, *81*, 10268–74.
- (30) Chen, Z.-P.; Peng, Z.-F.; Luo, Y.; Qu, B.; Jiang, J.-H.; Zhang, X.-B.; Shen, G.-L.; Yu, R.-Q. *Biosensors & bioelectronics* **2007**, *23*, 485–91.
- (31) Polsky, R.; Gill, R.; Kaganovsky, L.; Willner, I. *Analytical chemistry* **2006**, *78*, 2268–71.
- (32) Polsky, R.; Harper, J. C.; Wheeler, D. R.; Dirk, S. M.; Rawlings, J. a; Brozik, S. M. *Chemical communications (Cambridge, England)* **2007**, *1*, 2741–3.
- (33) Fritz, J. *The Analyst* **2008**, *133*, 855–63.
- (34) Wu, G.; Datar, R. H.; Hansen, K. M.; Thundat, T.; Cote, R. J.; Majumdar, a *Nature biotechnology* **2001**, *19*, 856–60.
- (35) Milburn, C.; Zhou, J.; Bravo, O.; Kumar, C.; Soboyejo, W. O. *Journal of Biomedical Nanotechnology* **2005**, *1*, 30–38.
- (36) Lee, S.-M.; Hwang, K. S.; Yoon, H.-J.; Yoon, D. S.; Kim, S. K.; Lee, Y.-S.; Kim, T. S. *Lab on a chip* **2009**, *9*, 2683–90.
- (37) Jin, X.; Jin, X.; Chen, L.; Jiang, J.; Shen, G.; Yu, R. *Biosensors & bioelectronics* **2009**, *24*, 2580–5.
- (38) Huang, Y.; Wen, Q.; Jiang, J.-H.; Shen, G.-L.; Yu, R.-Q. *Biosensors & bioelectronics* **2008**, *24*, 600–5.
- (39) Ding, C.; Zhao, F.; Ren, R.; Lin, J.-M. *Talanta* **2009**, *78*, 1148–54.
- (40) Liu, Y. *Thin Solid Films* **2008**, *516*, 1803–1808.
- (41) Tang, D.; Yuan, R.; Chai, Y.; Zhong, X.; Liu, Y.; Dai, J. *Clinical biochemistry* **2006**, *39*, 309–14.

- (42) Proteins, B.; Gold, U.; Mani, V.; Chikkaveeraiah, B. V.; Patel, V.; Gutkind, K. J. S.; Rusling, J. F. **2009**, 3, 585–594.
- (43) Ding, Y.; Liu, J.; Wang, H.; Shen, G.; Yu, R. *Biomaterials* **2007**, 28, 2147–54.
- (44) Zhang, Q.; Huang, Y.; Zhao, R.; Liu, G.; Chen, Y. *Journal of colloid and interface science* **2008**, 319, 94–9.
- (45) Wang, H.; Wang, J.; Choi, D.; Tang, Z.; Wu, H.; Lin, Y. *Biosensors & bioelectronics* **2009**, 24, 2377–83.
- (46) Tang, D.; Yuan, R.; Chai, Y.; An, H. *Advanced Functional Materials* **2007**, 17, 976–982.
- (47) Zhao, W.; Van der Berg, A. *Lab on a chip* **2008**, 8, 1988–91.
- (48) Su, S.; Ali, M. M.; Filipe, C. D. M.; Li, Y.; Pelton, R. *Biomacromolecules* **2008**, 9, 935–41.
- (49) Carrilho, E.; Martinez, A. W.; Whitesides, G. M. *Analytical chemistry* **2009**, 81, 7091–5.
- (50) Savolainen, A.; Zhang, Y.; Rochefort, D.; Holopainen, U.; Erho, T.; Virtanen, J.; Smolander, M. *Biomacromolecules* **2011**, 12, 2008–15.
- (51) Martinez, A. W.; Phillips, S. T.; Whitesides, G. M.; Carrilho, E. *Analytical chemistry* **2010**, 82, 3–10.
- (52) Leuvering, J. H.; Thal, P. J.; Van der Waart, M.; Schuurs, A. H. *Journal of immunoassay* **1980**, 1, 77–91.
- (53) Martinez, A. W.; Phillips, S. T.; Butte, M. J.; Whitesides, G. M. *Angewandte Chemie (International ed. in English)* **2007**, 46, 1318–20.
- (54) Posthuma-Trumpie, G. a; Korf, J.; Van Amerongen, A. *Analytical and bioanalytical chemistry* **2009**, 393, 569–82.
- (55) Rezk, A. R.; Qi, A.; Friend, J. R.; Li, W. H.; Yeo, L. Y. *Lab on a Chip* **2012**, 12, 773–779.
- (56) Wijitar Dungchai, O. C. and C. S. H. *Analyst* **2011**, 136, 77–82.
- (57) Dudek, M. M.; Kent, N. J.; Gu, P.; Fan, Z. H.; Killard, A. J. *The Analyst* **2011**, 136, 1816–25.
- (58) Carvalhal, R. F.; Kfour, M. S.; Piazzetta, M. H. D. O.; Gobbi, A. L.; Kubota, L. T. *Analytical chemistry* **2010**, 82, 1162–5.

- (59) Carrilho, E.; Phillips, S. T.; Vella, S. J.; Martinez, A. W.; Whitesides, G. M. *Analytical chemistry* **2009**, *81*, 5990–8.
- (60) Wang, S.; Ge, L.; Song, X.; Yu, J.; Ge, S.; Huang, J.; Zeng, F. *Biosensors & bioelectronics* **2012**, *31*, 212–8.
- (61) Shi, C.-G.; Shan, X.; Pan, Z.-Q.; Xu, J.-J.; Lu, C.; Bao, N.; Gu, H.-Y. *Analytical chemistry* **2012**, *84*, 3033–8.
- (62) Nie, Z.; Nijhuis, C. a; Gong, J.; Chen, X.; Kumachev, A.; Martinez, A. W.; Narovlyansky, M.; Whitesides, G. M. *Lab on a chip* **2010**, *10*, 477–83.
- (63) Liu, X.; Mwangi, M.; Li, X.; O'Brien, M.; Whitesides, G. M. *Lab on a chip* **2011**, *11*, 2189–96.
- (64) Martinez, A. W.; Phillips, S. T.; Carrilho, E.; Thomas, S. W.; Sindi, H.; Whitesides, G. M. *Analytical chemistry* **2008**, *80*, 3699–707.
- (65) Song, S.; Qin, Y.; He, Y.; Huang, Q.; Fan, C.; Chen, H.-Y. *Chemical Society reviews* **2010**, *39*, 4234–43.
- (66) Elenis, D. S.; Ioannou, P. C.; Christopoulos, T. K. *Nanotechnology* **2011**, *22*, 155501.
- (67) Ngo, Y. H.; Li, D.; Simon, G. P.; Garnier, G. *Advances in colloid and interface science* **2011**, *163*, 23–38.
- (68) Lou, S.; Ye, J.-Y.; Li, K.-Q.; Wu, A. *The Analyst* **2011**, *137*, 1174–1181.
- (69) Zhao, W.; Ali, M. M.; Aguirre, S. D.; Brook, M. A.; Li, Y. *Analytical chemistry* **2008**, *80*, 8431–8437.
- (70) Puertas, S.; Moros, M.; Fernández-Pacheco, R.; Ibarra, M. R.; Grazú, V.; De la Fuente, J. M. *Journal of Physics D: Applied Physics* **2010**, *43*, 474012.
- (71) Zhu, X.; Chen, L.; Shen, P.; Jia, J.; Zhang, D.; Yang, L. *Journal of agricultural and food chemistry* **2011**, *59*, 2184–9.
- (72) Shukla, S.; Leem, H.; Kim, M. *Analytical and bioanalytical chemistry* **2011**, *401*, 2581–90.
- (73) Blažková, M.; Javůrková, B.; Fukal, L.; Rauch, P. *Biosensors & bioelectronics* **2011**, *26*, 2828–34.
- (74) Kalogianni, D. P.; Boutsika, L. M.; Kouremenou, P. G.; Christopoulos, T. K.; Ioannou, P. C. *Analytical and bioanalytical chemistry* **2011**, *400*, 1145–52.
- (75) Ornatska, M.; Sharpe, E.; Andreescu, D.; Andreescu, S. *Analytical chemistry* **2011**, *83*, 4273–80.

- (76) Mohammed, M.-I.; Desmulliez, M. P. Y. *Lab on a chip* **2011**, *11*, 569–95.
- (77) Li, Z.; Wang, Y.; Wang, J.; Tang, Z.; Pounds, J. G.; Lin, Y. *Analytical chemistry* **2010**, *82*, 7008–14.
- (78) Parolo, C.; De la Escosura-Muñiz, A.; Merkoçi, A. *Biosensors and Bioelectronics* **2012**, *40*, 412–416.
- (79) Choi, D. H.; Lee, S. K.; Oh, Y. K.; Bae, B. W.; Lee, S. D.; Kim, S.; Shin, Y.-B.; Kim, M.-G. *Biosensors & bioelectronics* **2010**, *25*, 1999–2002.
- (80) Xu, H.; Mao, X.; Zeng, Q.; Wang, S.; Kawde, A.-N.; Liu, G. *Analytical chemistry* **2009**, *81*, 669–75.
- (81) Fang, Z.; Ge, C.; Zhang, W.; Lie, P.; Zeng, L. *Biosensors & bioelectronics* **2011**, *27*, 192–6.
- (82) Cheng, C.-M.; Martinez, A. W.; Gong, J.; Mace, C. R.; Phillips, S. T.; Carrilho, E.; Mirica, K. a; Whitesides, G. M. *Angewandte Chemie (International ed. in English)* **2010**, *49*, 4771–4.

## **Chapter 2**

### **Objectives**

In this Chapter the objectives of this thesis are presented.



The general objective of this PhD thesis is the development of point-of-care, cheap and easy-to-use immunosensors based on the use of nanoparticles for diagnostic application. The development of such immunosensors is of great interest, especially for third world countries, where the lack of resources makes the diagnostic not available for all the population. On the other hand, they would be extensively used also in developed countries for diagnostic in ambulatories or even at home.

More in detail the objectives of this thesis can be summarized as following:

- The optimization of the use of gold nanoparticles (AuNPs) as labels in electrochemical and optical biosensors;
- The development of a new functionalization technique to obtain new antibody-oriented AuNP conjugates, which give better sensing performances;
- The improvement of the sensitivity of lateral flow immunoassays (LFIA) by simply modifying the geometry of the device;
- The development of a double label based on AuNPs and Horseradish Peroxidase (HRP) to have a better limit of detection and a modulation of the signal obtained in LFIA;
- The development of paper-based screen printed carbon electrodes (SPCEs) to be used as platform for the detection of nanoparticles.



## Chapter 3

### Electrochemical immunosensors based on gold nanoparticles

This chapter summarizes the achievements obtained for the electrochemical detection of proteins in magnetosandwich immunoassays. It can be divided in three main parts, The first part is a general introduction, where it is explained i) why we use AuNPs as labels and the principles of the two electrochemical techniques used, ii) how to fabricate SPCE and iii) the principle of magnetosandwich immunoassays. The second part summarizes and discusses the results obtained in the study of the effect of AuNP size on their direct electrochemical detection. Finally, in the third part the study of a novel strategy for the oriented functionalization of AuNPs is also summarized and discussed (the complete manuscript can be found in Annex B). Both studies are finally applied for the detection of proteins in magnetosandwich immunoassays.

#### Related Publications

---

3) De la Escosura-Muñiz, A.; Parolo, C.; Maran, F.; Mekoçi, A. Size-dependent direct electrochemical detection of gold nanoparticles: application in magnetoimmunoassays. *Nanoscale*, 2011, 3, 3350–3356.

---



### 3.1 Introduction

#### 3.1.1 *Why AuNPs as electrochemical labels*

Gold nanoparticles (AuNPs) stand out from the variety of other nanoparticles and quantum dots because of their easy preparation and modification, their biocompatibility<sup>1</sup> and unique electronic, optical, and catalytic properties.<sup>2–5</sup> In particular, AuNPs applications are extensively investigated and tested in immunocytochemistry and cell biology.<sup>6</sup> AuNPs have also been used in a variety of analytical,<sup>7,8</sup> and sensing applications, including DNA,<sup>9,10</sup> and immuno-sensing.<sup>11</sup> Although the majority of existing sensing systems rely on the optical properties of AuNPs, we are currently observing a noticeable growth of AuNP-based immuno<sup>12</sup> and DNA electrochemical assay.<sup>13,14</sup> The vast majority of these electrochemical approaches is based on chemical dissolution of AuNPs in toxic solutions (i.e. HBr/Br<sub>2</sub>) followed by accumulation and stripping analysis of the resulting Au (III) solution. These solutions are highly toxic and therefore alternative approaches based on direct electrochemical detection of AuNPs to replace the chemical oxidation agent are sought. We<sup>15–17</sup> and others<sup>18,19</sup> developed two electrochemical methods to detect AuNPs: one direct and one indirect.

The direct detection method consists of three steps: first the adsorption of the AuNPs on the surface of the electrotransducer, then the electrooxidation of the AuNPs to Au (III), and finally the reverse electroreduction to Au (0). This last step generates a well defined cathodic peak, which constitutes the analytical signal.

In the indirect method, the AuNPs catalyze the hydrogen formation in acidic solution (1M HCl). This reaction produced a current, measured by chronoamperometry (holding the working electrode at a potential of +1.35 V for 1 min followed by a negative potential of -1.00 V for 100 s), which current intensity is directly related to the amount of AuNPs.<sup>20</sup>

#### 3.1.2 *Fabrication of Screen Printed Carbon Electrodes*

The full size of the SPCE was 29 mm x 6.7 mm, and the working-electrode diameter was 3 mm. The fabrication of the SPCEs was carried out in three steps. First, a graphite layer was printed onto the polyester sheet, using the screen-printing machine with the stencil (where it is the electron pattern). After curing for 15 minutes at 95°C, an Ag/AgCl layer was printed and cured for 15 minutes at 95°C. Finally, the insulating ink was printed and cured at 95°C for 20 minutes.

### 3.1.3 Magnetosandwich immunoassay strategy

Magnetosandwich immunoassay presents several advantages in terms of sensitivity and selectivity, due to the pre-concentration of the analyte, the separation from the matrix of the sample and the immobilization/collection on the transducer surface, achieved using a magnetic field.

Briefly, it consists in the immobilization of biotin-modified anti-human IgG antibodies onto the surface of streptavidin-coated magnetic beads followed by the human IgG capturing from the sample. Finally the sandwich is completed through the immunoreaction with anti-human IgG-AuNP.

In order to perform the electrochemical detection, a drop of 25  $\mu$ L of the magnetoimmuno complex is deposited onto SPCE and the complex is accumulated onto the working electrode surface by a magnet in order to be detected.

### 3.2 Effect of the AuNP size on the direct electrochemical detection

The direct electrochemical detection of AuNPs was previously optimized for 20-nm AuNPs on carbon paste and graphite-epoxy electrodes, but the effect of the AuNPs size on the electrochemical signal and the use of other kinds of electrotransducers, such as screen-printed electrodes, has not yet been studied and possibly exploited in biosensors. The size-dependence of the optical properties of AuNPs has been extensively studied, but this effect on the electrochemical properties has not yet been clarified.

Here, we report the size-dependent direct electrochemical detection of AuNPs (5, 20 and 80 nm in diameter, Fig. 3.1A) using screen-printed carbon electrodes (SPCEs) as electrochemical transducers.

A key step of our procedure for the direct electrochemical detection of AuNPs consists in an efficient adsorption of AuNPs onto the surface of the electrotransducer, which will allow their further oxidation and then reduction of the ensuing oxidized gold species. The efficient adsorption of 20-nm AuNPs onto the surface of the SPCEs, according to the experimental procedure detailed in experimental section, seems to be evidenced in the SEM images shown in Fig. 3.1B, where in spite of the rugosity of the carbon surface it seems that the AuNPs are adsorbed and spread onto the carbon surface without agglomerates formation; this is important for allowing a reproducible electrochemical detection in the further steps.

Our group previously reported results about the direct electrochemical detection of AuNPs on graphite-epoxy composite electrodes.<sup>15–17</sup> We are now reporting data concerning further important issues. One aspect we addressed was to study the electrochemical features of this AuNP-based approach by using SPCEs, which provide an advantageous platform in terms of miniaturization, low volume of samples, single use possibilities, and convenient mass-production related technology. In addition to the use of a novel transducing surface, main objective of this work was to study the effect of the AuNP size on the electrochemical signal. In particular, we anticipated that this issue would have had important effects on both the sensitivity and the reproducibility of the affinity bioassays (i.e. DNA sensors or immunosensor) requiring the use of labels.

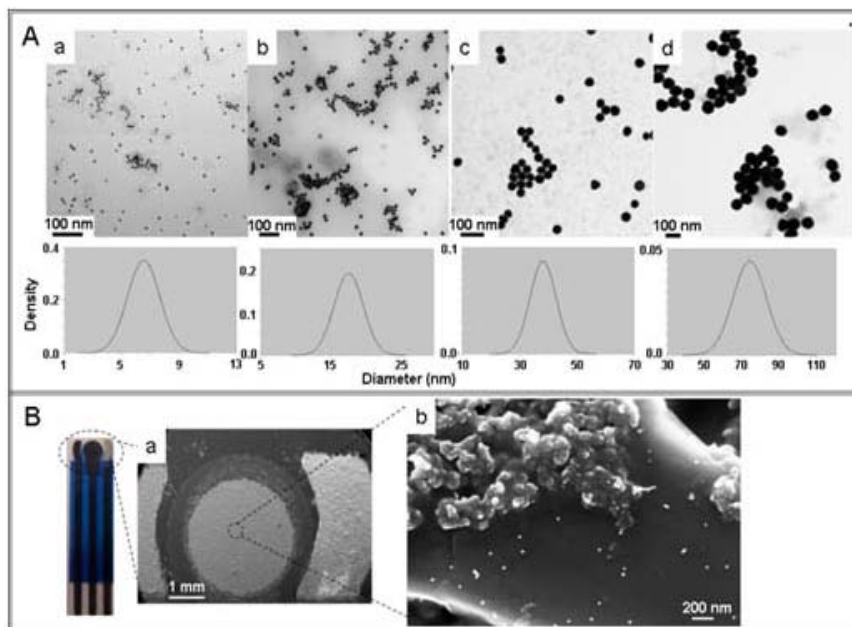


**Fig. 3.1**(A) TEM images obtained for 5-nm (a), 20-nm (b), 40-nm (c) and 80-nm (d) AuNPs solutions and the corresponding sizes distribution. (B) SEM images of the SPCE electrotransducer (a) and the 20-nm AuNPs deposited on the carbon working area from a solution of  $1 \times 10^{10}$  AuNPs mL<sup>-1</sup>, following the experimental procedure detailed in experimental section at 100.000 X amplifications (b).

### 3.2.1 Direct electrochemical detection of gold nanoparticles

Fig. 3.2A shows cartoons of the detection steps pertaining to AuNPs with three different sizes (small, medium, large); AuNP suspensions consist of the same number of AuNPs. After the AuNPs are deposited onto the SPE surface from the appropriate suspension (step 1), their partial electrochemical oxidation (step 2), generating a high surface concentration of Au(III) ions by the electrotransducer, occurs. Anodic stripping of the adsorbed AuNPs is then followed by a potential scan to reductive potentials (step

3): the peak current for reduction of Au(III) ions to Au(0) is related to the original surface concentration of the AuNPs.

For the same number of AuNPs, AuNPs of different sizes were also expected to provoke different behaviors in terms of reduction peak potentials for Au(0) deposition. The value of the peak current was expected to be higher for larger AuNPs (for the same number of AuNPs) due to their higher surface area generating a higher surface concentration of released gold ions during the oxidation step. As depicted in the cartoon of step 3, deposition of gold occurs onto smaller, residual AuNPs, as during the stripping step AuNPs are partially oxidized (being their size slightly reduced). Due to an ‘incomplete stripping’<sup>21</sup>, the remaining AuNPs, of different area, act as an array of nanoelectrodes that catalyze the further electrodeposition, that consequently should occur at different potentials in comparison to the bare carbon electrode.

On the other hand, it is conceivable that if one starts from the same total gold ion concentration (see Fig. 3.2B), smaller AuNPs would result in the detection of larger peak currents, as small NPs are present in a larger number, provide a higher quantity of surface atoms (the ratio between the surface and the core gold atoms increases as the NP is made smaller), and increase the area of contacting surface between them and the electrotransducing surface. Furthermore, the reduction potential of the gold ions should be shifted to less negative potentials, due to a better array-like effect for smaller compared to larger sizes NPs.

To verify our expectations, we carried out experiments focusing on two sets of conditions for the AuNP suspensions. In the first set we used AuNP suspensions with varying core sizes but with the same number of AuNPs. In the second set we kept the total amount of gold constant: because of the different core sizes, this procedure resulted in AuNP suspensions containing a different number of AuNPs.

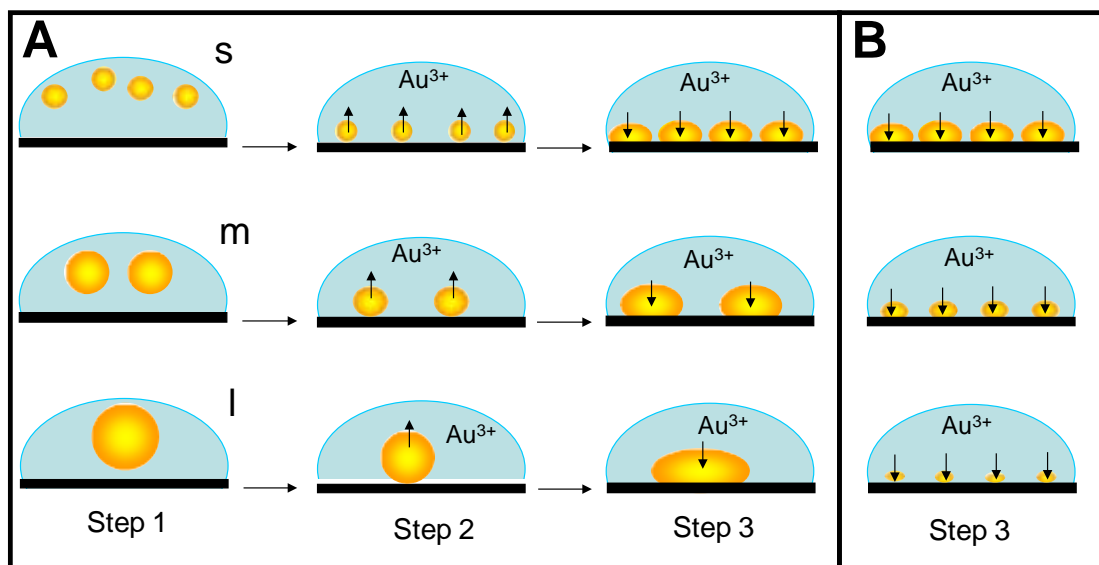
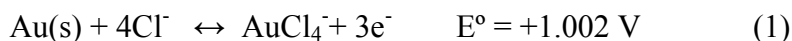


**Fig. 3.2(A).** Schematic, not in scale, of the three steps used for introduction and detection of small (s), medium (m) and large (l) size AuNP suspension of the same number of AuNPs using a SPCE. Step 1 corresponds to AuNP deposition onto SPE surface. Step 2 corresponds to gold ion release/oxidation upon the application of a +1.25 V potential during 120s. Step 3 corresponds to gold ion deposition/reduction onto the SPE by scanning from +1.25 V to 0.0 V. (B). Schematic of the third step if the total gold concentration is the same.

### 3.2.2 Size-effect on the voltammetric response for the same number of gold nanoparticles

As a first step, the effect of the AuNPs size on the electrochemical signal for the same concentration of AuNPs, previously determined by UV-Vis spectrophotometry, was evaluated. As it is detailed in experimental section, an oxidation potential of +1.25 V was applied to the adsorbed AuNPs in order to release the Au (III) ions (step 2, Fig. 3.2A). In the case of gold, the standard state in the pure crystalline bulk metal, and the generation of Au (III) ions from the AuNPs in a hydrochlorhydric medium is given by<sup>22</sup>:



For convenience, the shape of AuNPs is taken as that of a perfect sphere and, accordingly, the volumes of single 5-, 20- and 80-nm-diameter particles are calculated to be  $5.23 \times 10^{-19}$ ,  $2.09 \times 10^{-18}$  and  $8.36 \times 10^{-18} \text{ cm}^3$ , respectively. By taking the density of the AuNP to be that of bulk gold ( $\rho$ ),  $19.3 \text{ g cm}^{-3}$  the atomic mass ( $M$ ) to be  $196.967 \text{ g mol}^{-1}$ , and Avogadro's number ( $N_A$ ) to be  $6.022 \times 10^{23}$ , the approximate numbers of atoms per particle ( $N$ ) are 3859, 246960 and 15806976, respectively, according with the

following equation<sup>23,24</sup>:

$$N = \frac{\rho D^3 N_A}{6M} \quad (2)$$

where  $D$  is the diameter of the NP.

These values are much greater than the more than 100 atoms needed to start producing “bulk character”<sup>25,26</sup> and, as such, to have the same standard potential,  $E^\circ$ , of gold, as this value is quoted for all species in their standard states. The range of particle sizes considered in this work, in a similar mode as for Compton’s silver nanoparticles<sup>27</sup> is narrow, and therefore, it is assumed that the value of this standard potential is the same for the different-sized AuNPs studied. It means that the potential of +1.25 V applied is oxidative enough to oxidize the surface of the AuNPs and to generate Au (III) ions.

After the oxidation step, we applied a negative-going differential pulse voltammetry (DPV) scan to the SPCE and obtained voltammograms such as those shown in figure 3A. The results show that gold ion reduction onto larger AuNPs occurs at less negative potentials (~60 mV shift) than observed for smaller size particles, due to an increased nanoarray like effect (Fig. 3. 2A, step 3). Regarding the peak current, directly related to the quantity of gold ions and indirectly to the AuNP quantity, Fig. 3.3A shows that the maximum analytical signals, obtained by following the experimental procedure described in experimental section, were obtained for the largest NP employed, i.e., the 80-nm AuNPs. The same behavior was observed for different AuNP concentrations, as shown in the plots of Fig. 3.3B. As for the peak potential, the increase of the DPV peaks as the AuNP size also increases are in agreement with the expected behavior, because for the same number of NPs the number of released gold ions (and, consequently, of those available for the following reduction step) can be related with the number of surface atoms in the AuNPs, which in turn is related to the size of the AuNPs (Fig. 3.2A, step 2).

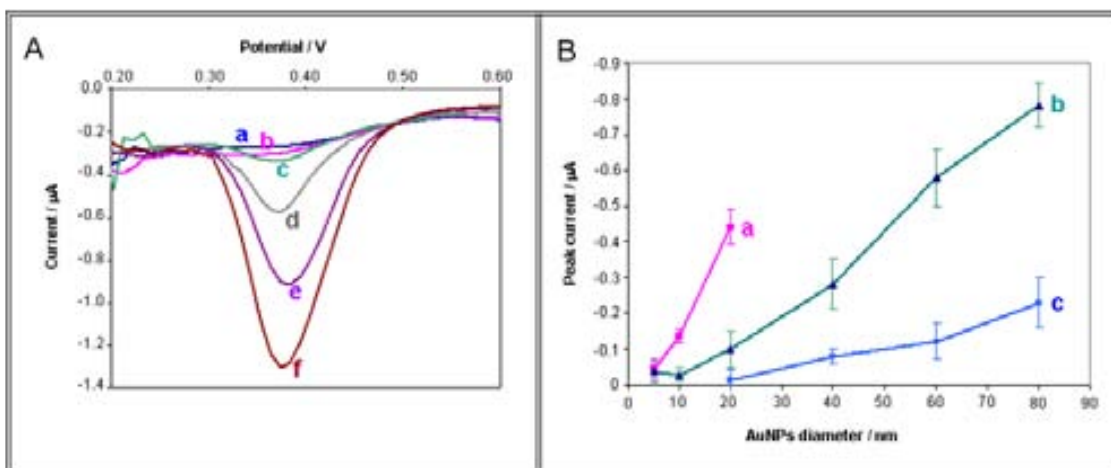


**Fig. 3.3**(A) Differential pulse voltammograms obtained for AuNPs of different diameters in solutions containing  $1 \times 10^{10}$  AuNPs  $\text{mL}^{-1}$ . (a) 5 nm, (b) 10 nm, (c) 20 nm, (d) 40 nm, (e) 60 nm, (f) 80 nm. Step potential: 10mV, modulation amplitude: 50mV, scan rate  $33.5 \text{ mV s}^{-1}$  (non-stirred solution). (B) AuNPs size dependence on the analytical signal for different AuNPs concentrations: (a)  $1 \times 10^{11}$ , (b)  $1 \times 10^{10}$ , (c)  $1 \times 10^9$  AuNPs  $\text{mL}^{-1}$ .

### 3.2.3 Size-effect on the voltammetric response for the same concentration of total gold

The effect of the AuNPs size onto the electrochemical response for the same concentration of total gold, previously determined by inductively-coupled plasma mass spectrometry (ICP-MS), was also studied. We expected (Fig. 3.2B) that for the same quantity of total gold, smaller AuNPs would have yielded a higher electrochemical signal, as for smaller AuNPs a higher surface area, implying a higher number of surface atoms, is in contact with the working electrode surface. Consequently, a higher number of Au (III) ions would be released from the bulk metal due to the electrochemical oxidation step, giving rise to a higher voltammetric peak recorded during the ions reduction step. The DPVs obtained for different AuNPs at a total gold concentration of 200  $\mu\text{M}$  are shown in Fig. 3.4A. The predicted behavior is indeed observed in the range 20-80 nm (c,d,e voltammograms). In these experiments, a positive shift of the reduction potential ( $\sim 30 \text{ mV}$ ) was observed for the smaller AuNPs. This can be attributed again to array effect of the remaining AuNPs and its promoting role on the reduction of Au(III) ions to Au(0). As also predicted, the peak current is smaller for larger AuNPs. However, for AuNPs in the range from 5 to 20 nm (voltammograms a, b, and c: voltammogram c, corresponding to the 20 nm AuNP, is included for comparison purposes) we found the opposite effects in terms of both reduction potential and peak current intensity. The shift of the reduction potential ( $\sim 80 \text{ mV}$ ) is even more pronounced. This general trend was

consistently observed for different total gold concentrations tested, as shown in the plots of figure 3.4B.

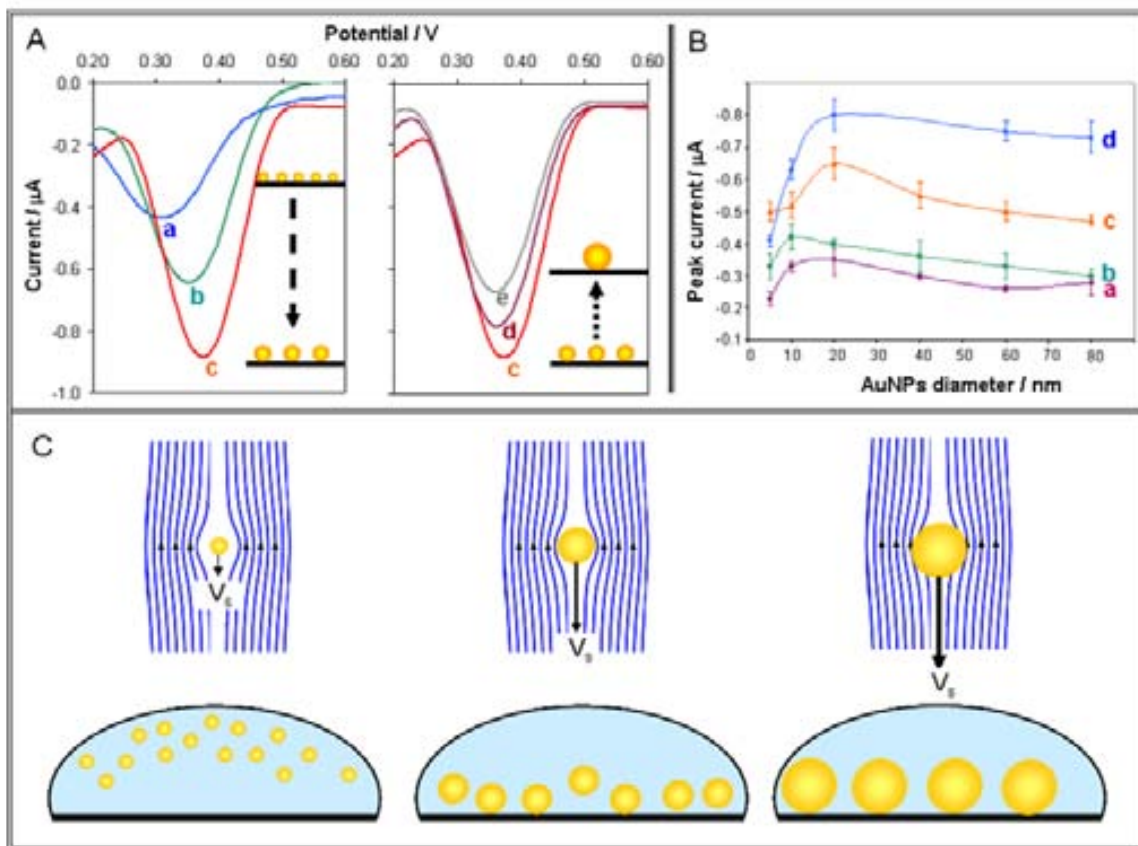


**Fig. 3.4** (A) Differential pulse voltammograms obtained for AuNPs of different sizes – (a) 5 nm, (b) 10 nm, (c) 20 nm, (d) 60 nm, (e) 80 nm - containing a concentration of total gold of 200  $\mu\text{M}$ . DPV parameters as in figure 3A. (B) AuNPs size dependence on the analytical signal for different total gold concentrations: (a) 10  $\mu\text{M}$ , (b) 20  $\mu\text{M}$ , (c) 50  $\mu\text{M}$ , (d) 200  $\mu\text{M}$ . (C) Scheme of the process occurring on the electrode surface for the different AuNPs sizes.  $V_s$  stands for “settling velocity” as detailed in experimental section.

An explanation to these contradictory results may be related to the Brownian effects<sup>28</sup> governing the motion of these smaller particles. Any minute particle suspended in a liquid (or gas) moves chaotically under the action of collisions with surrounding molecules. The frictional force -also called drag force- exerted on spherical objects with very small Reynolds numbers (e.g., AuNPs) in a continuous viscous fluid can be calculated by the Stokes Law: if the particles are falling in a viscous fluid by their own weight due to gravity, then a terminal velocity, also known as the settling velocity, is reached when this frictional force combined with the buoyant force exactly balance the gravitational force. From equations derived from this law, the settling velocity of the AuNPs of different sizes from the suspension to the electrode surface and the necessary

falling time to the electrode surface from an arbitrary distance can be estimated. These approximated calculations are detailed in the *supplementary information* of the manuscript, showing that for the 5-nm AuNPs, the expected time of AuNPs deposition of those situated at a distance of, say, 50 nm (an arbitrary distance chosen as long enough to put in evidence the different behaviors between the smaller and the larger AuNPs in relatively short, i.e. 2 minutes, adsorption time) over the electrotransducer surface would be 32 minutes. This means that, after drop casting the AuNPs suspension onto the electrode surface, a deposition time of 2 minutes (used in the detection procedure) is not long enough to guarantee quantitative adsorption of AuNPs smaller than 20 nm onto the electrode surface. If part (or even most) of the AuNPs are still not adsorbed onto the electrotransducer surface, the electrochemical signal coming from the AuNPs will dramatically decrease. On the other hand, the AuNPs of 20-80 nm situated at the same 50 nm distance from the electrode surface will be totally adsorbed within the 2 minutes deposition time. A cartoon of the process hypothesized to occur on the electrode surface is shown in Fig. 3.4C.

Overall, the results obtained under the same experimental protocol indicate that, for the same quantity of total gold, efficiency is optimized with the 20-nm AuNPs. In other words, for the same quantity of gold the best way to exploit the electrochemical properties of AuNPs is to use the 20-nm sized ones. Smaller AuNPs suffer the problem of the longer times required to be adsorbed onto the electrode surface due to Brownian effects.

#### 3.2.4 Application in a magnetoimmunoassay

We also studied the effect of the AuNPs size on the electrochemical signal when the NPs are used as labels in an immunoassay system based on the use of magnetic particles (MB) as immobilization platform. Under these conditions, we expected that the Brownian effects would have been minimized because independently of their size all AuNPs would be attracted onto the electrotransducer surface upon application of the magnetic field.

To study the effect of size, AuNPs of different sizes were conjugated with antibodies and used as labels in a magnetosandwich immunoassay that we previously optimized for 20-nm AuNPs<sup>15,29</sup>, using magnetic beads (MB) as platforms of the immunoreactions. Fig. 3.5A shows the electrochemical signals obtained for the same total concentration of gold with different AuNPs sizes (5, 20, and 80 nm) used as labels

in the described magnetoimmunoassay. The DPV peak-current values show that a higher peak current was obtained for the 5-nm AuNPs. In addition, the peak potential was found to shift to less negative potentials as the AuNP size decreased. These results confirm that the Brownian effects are not relevant when the AuNPs are attached to the MBs through the immunoreaction (as schematized in Fig. 3.5B) being these attracted afterward by a magnet placed under the working electrode surface. Therefore, under magnetosandwich conditions, the higher surface area of the smaller AuNPs gives rise to the best electrochemical response.

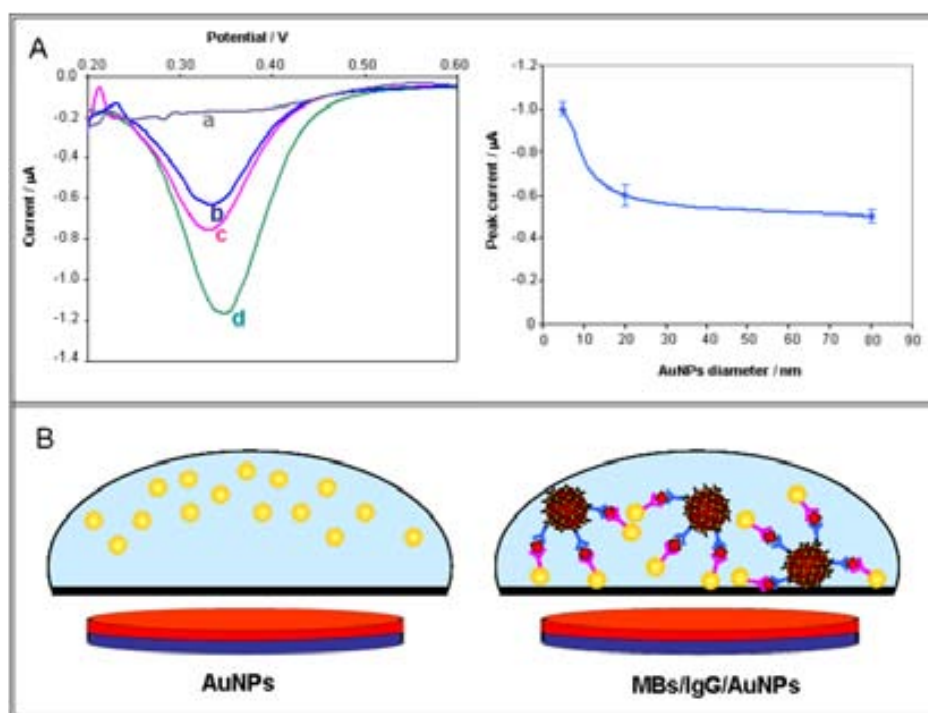


**Fig. 3.5**(A) (Left) Differential pulse voltammograms obtained for magnetosandwich immunoassays performed using AuNPs labels of different sizes: (b) 80 nm, (c) 20 nm and (d) 5 nm. (a) Curve corresponds to a blank immunoassay carried out with goat IgG instead of human IgG and AuNPs labels of 5 nm. (Right) Corresponding AuNPs labels size dependence on the analytical signals obtained for the magnetosandwich immunoassay using as electrochemical labels AuNPs of different sizes prepared from solutions of 84  $\mu\text{M}$  of total gold as detailed in experimental section. Experimental procedure also detailed in experimental section. DPV parameters as in figure 3A. (B) Scheme of the process on the electrode surface – where a magnet has been placed under the working electrode area- for only AuNPs (left) and for the AuNPs attached to magnetic beads through the immunoassay (right).

### 3.3 Oriented functionalization for more efficient AuNP labels

The special intrinsic properties of AuNPs are not enough to make them great labels in bioassays.<sup>30</sup> In fact, the specificity of an affinity biosensor (immunosensors or DNA biosensor) is achieved by the biomolecules that are attached to the label that should recognize the analyte. Considering immunosensors case, a label-antibody conjugate that maintains the antigen binding sites available to capture the antigen is of extremely importance to obtain good performances from the devices.<sup>12</sup>

In this section, we show how a proper antibody orientation affects the limit of detection (LoD) of an AuNP-label based immunosensor. In order to obtain a controlled functionalization, which leaves accessible the antigen binding sites, a two steps coupling reaction has been adapted.<sup>31,32</sup> This methodology couples an oriented ionic attraction with a strong covalent bond formation using carbodiimide chemistry.<sup>33</sup> The technique is based on the high concentration of positive charges in the major plane of an antibody, when the pH of the solution is lower than its isoelectric point (Fig. 3.6A). In such condition the  $\text{NH}_2$ -groups of Lys residues are protonated generating  $\text{NH}_3^+$ . In this way, if the antibodies are in solution with negatively charged AuNPs, the probability of interaction between the surface of AuNPs and the major plane of the antibody are maximized. This controlled approximation allows the antigen binding sites to be available for the capture of the antigen. In order to charge negatively the AuNP surface and to allow the formation of the covalent bond, the NPs were covered with a carboxylated poly(ethylene glycol)(PEG). In fact, using the carbodiimide chemistry, a stable intermediate, an amine reactive sulfur ester, is formed onto the AuNP surface. This group is negatively charged and catalyzes the formation of the peptide bond between the carboxylic groups of the PEG and the amino-groups of the Lys-residues (Fig. 3.6B).

In order to prove the better performances of this new label compared with those of a random functionalized AuNP (Fig. 3.6C), we used two different antibodies: an  $\alpha\text{HRP}$  and an  $\alpha\text{HIgG}$ . The first was used just as optical tool to verify that for a saturating amount of antigen the new label could bind more HRP molecules, whereas the second was tested in an electrochemical magnetosandwich immunoassay. Finally, after providing the evidences that our new label works better than the other, we used it in the analysis of a real human serum.

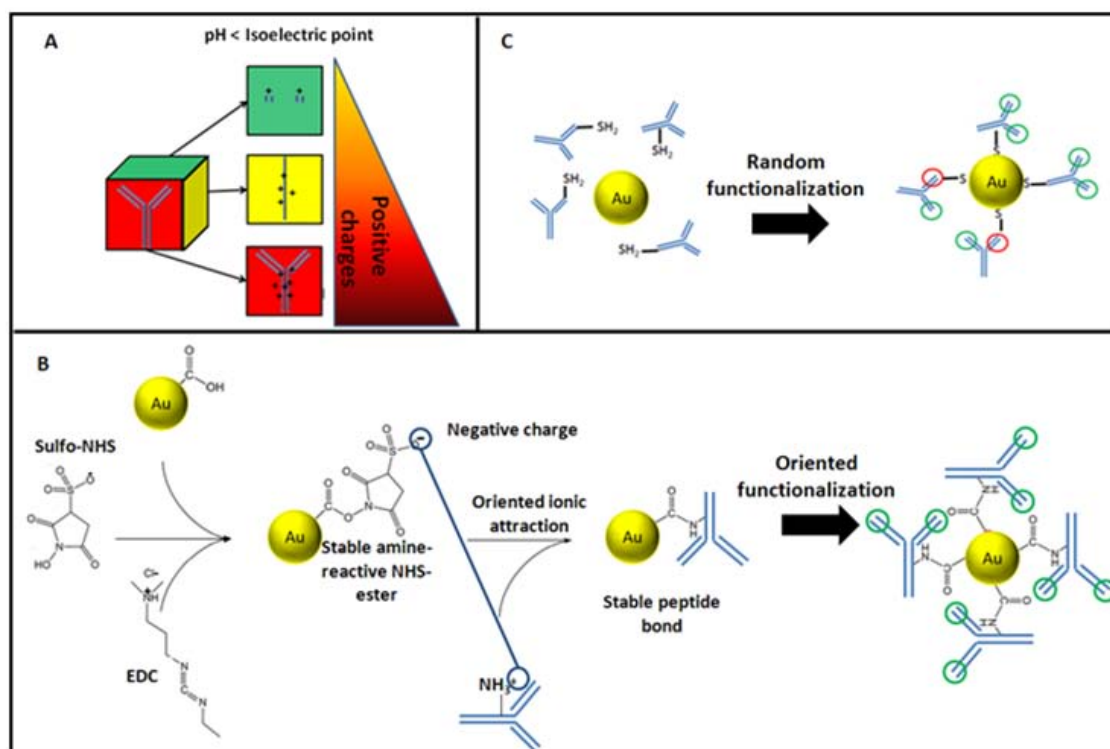


**Fig. 3.6** (A) Density of the positive charges on the antibody structure for pH lower than the isoelectric point of the antibody. The major plane (corresponding to the red square at the bottom) has the highest density. (B) Scheme of the oriented functionalization proposed based on the oriented ionic attraction and the formation of the peptide bond. (C) Scheme of the random adsorption of antibody onto the surface of AuNPs. NOTE: the schemes are not in scale.

### 3.3.1 Conjugates characterization

First the TEM of AuNPs was performed to verify the good homogeneity of the AuNPs (Fig. 3.7A)

The measurements of the isoelectric points of  $\alpha$ HRP and  $\alpha$ HIgG produced several bands; this was due to the fact that we were using antiserums and so other serum proteins were present in the solution (Fig. 3.7B). However, comparing the two different gels, we can estimate that the isoelectric points of both antibodies are around 7, since the most intense bands, corresponding to the  $\alpha$ HRP and  $\alpha$ HIgG can be found at pH 7. From this result, the MES buffer at pH 5 was chosen to carry out all the oriented functionalization.

The evidence that, working at pH 5, there was ionic attraction between negatively charged AuNPs and antibodies was given by the Bradford assay measurements. The experiment was carried out without the activation of the COOH-groups with the EDC-chemistry; in this way, the formation of the peptide bond between the COOH-group of

the PEG and the  $\text{NH}_2$ -group of the antibody was not catalyzed, and so we assumed that the interaction between NPs and antibodies was due mainly to ionic interactions. We found that in the supernatant of the first sample the concentration of antibodies, which were not ionically adsorbed onto the AuNP, was  $13.87 \pm 5.52 \mu\text{g/mL}$ ; whereas in the second supernatant the concentration of the antibodies, which were ionically adsorbed onto the AuNP and then released by the carbonate buffer pH8, was  $12.74 \pm 2.21 \mu\text{g/mL}$ . The sum of the values is  $\sim 26 \mu\text{g/mL}$ , which was the concentration of antibody that we used for the incubation with the AuNPs. In addition, the concentration of the ionically adsorbed antibody is close to those of the GAT ( $15 \mu\text{g/mL}$ ), indicating that the entire surface of the AuNPs was fully covered with antibodies.

The next step was to prove that the conjugation was covalent. For this reason, the new labels were incubated in carbonate buffer pH 8, since it could desorb all the ionically adsorbed antibodies (as shown by the previous Bradford results), but not those that are covalently attached. In this case, the supernatants were analyzed by SDS-PAGE. The results showed that all the antibodies of the new label were covalently attached to the surface of the AuNPs, since no bands can be seen in the raw of the gel corresponding to this sample. On the other hand, the previous supernatants, which were obtained without the activation of the  $\text{COOH}$ -groups, revealed the two typical bands of the antibodies, corresponding to the light and heavy chains (Fig. 3.7C).

These two controls confirmed the ionic adsorption and the peptide bond formation.

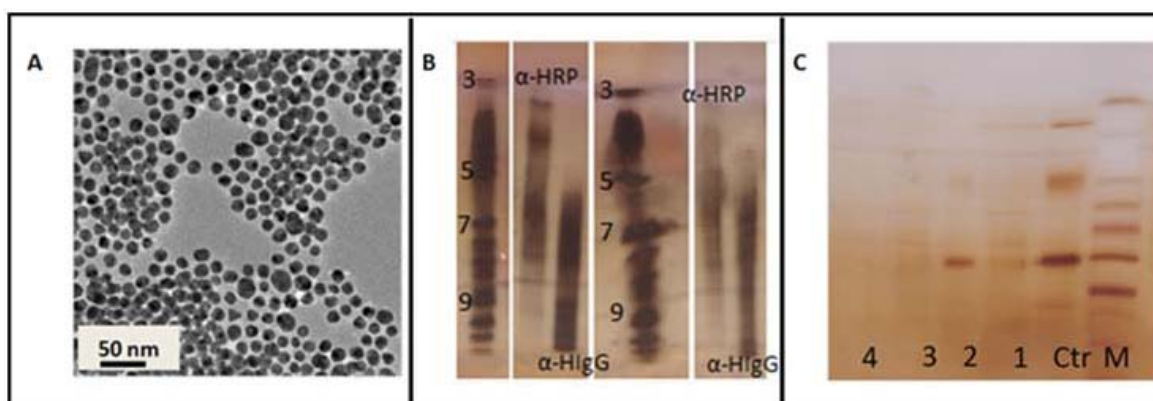


**Fig.3.7** (A) Transmission Electron Microscopy image of the synthesized AuNPs. (B) Isoelectric point measurement; both  $\alpha$ HRP and  $\alpha$ HIgG antibodies have an isoelectric point of 7. (C) SDS gel of supernatants after conjugates centrifugation, from the right to the left: M) marker, Ctr)  $\alpha$ HRP, 1) Ionic absorption without EDC, 2) Ionic desorption without EDC in Carbonate buffer pH 8, 3) Conjugates  $\alpha$ HRP/AuNP, 4) Conjugates  $\alpha$ HRP/AuNPs in Carbonate buffer pH 8.

The advantage of using the  $\alpha$ HRP antibody was that the antigen, the horseradish peroxidase, is an enzyme that can catalyze a reaction that generates color in the presence of the proper substrate (Fig. 3.8A). This is a powerful tool to check how much antigen the antibodies have captured. In fact, it is possible to link the kinetic of the enzyme reaction with the amount of enzyme present in solution. This experiment gives qualitative information about the orientation of the antibodies onto the AuNP surface, since the amount of captured antigen is strictly related to the orientation of the antigen binding sites. The experiment was carried out using a saturated concentration of HRP with the aim to see which label could capture more antigens, considering the same amount of antibodies and AuNPs. The results (Fig. 3.8B) showed that the oriented functionalization allowed the recognition of an amount of HRP molecules of around 5 times more than the random technique.

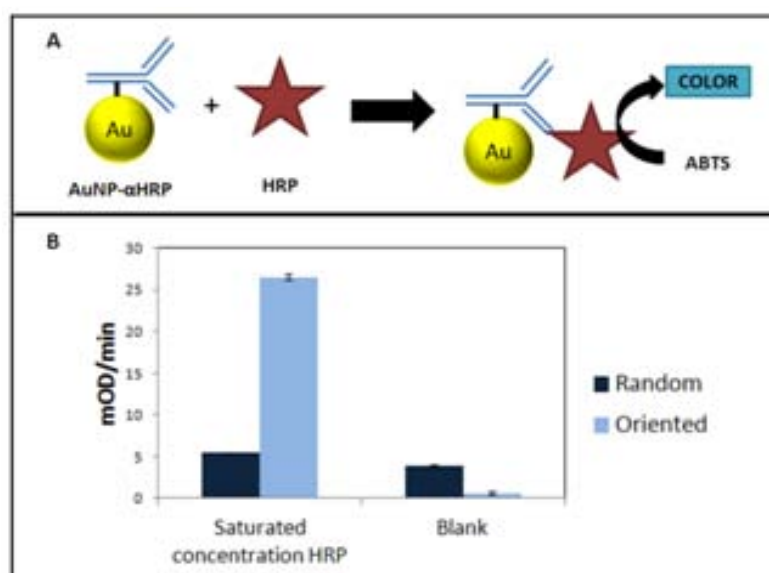


**Fig. 3.8** (A) Scheme of the optical method used to qualitatively evaluate the orientation of the  $\alpha$ HRP antibody onto the AuNP surface. (B) Comparison of the results obtained using the random and oriented conjugation for a blank sample (without HRP) and for a saturated concentration of HRP.

### 3.3.2 Effective labels for signal amplification in a magneto-sandwich immunoassay

The efficiency of both oriented and random conjugated AuNP labels were also compared in a magnetosandwich immunoassay for the electrochemical detection of HIgG in PBS buffer. The detection method is based on the AuNP ability of catalyzing the formation of hydrogen gas from hydrogen ions; this reaction generates a current that can be chronoamperometrically measured (Fig. 3.9A). In this way, it is possible to

correlate the current intensity recorded at a fixed time (180 seconds) with the concentration of AuNPs in solution and so to the concentration of the antigen captured by the magnetosandwich. The obtained results are plotted in the Fig. 3.9B. A logarithmic relationship (correlation coefficient of 0.999 in both cases) between the HIgG concentration and the current intensity is found in the range of 0.5 to 500 ng/ml and of 5 to 500 ng/ml for the oriented and random label respectively. The reproducibility of the method shows a relative standard deviation (RSD) of 7% for the oriented label and 5% for the random one ([HIgG]: 5 ng/mL;  $n = 6$ ). The estimated limit of detection (LoD), calculated as the concentration of HIgG corresponding to three times the standard deviation of the estimate, was 0.19 and 1.9 ng/mL respectively using the oriented label and the random. This means that using the oriented label was possible to improve the LoD of almost one order of magnitude. This reflects the fact that there are more antigen binding sites available in the new label and so the probability of a recognition event between antibody and antigen is higher than using the random label.

Once proved that the new label could achieve the detection of less amount of analyte, we applied it for the detection of HIgG in a human serum to prove that it could be used also for real samples. Standard additions method was used to estimate the concentration of the sample minimizing the matrix effects. A linear relationship between the standard addition of HIgG and the voltammetric peak current is found in the range 10–70 ng/mL, with a correlation coefficient of 0.998, adjusted to the following equation: peak current ( $\mu\text{A}$ ) =  $-0.1958 [\text{added HIgG (ng/mL)}] + 1.7359$ . (Fig. 3.9C). The estimated concentration of HIgG in serum was  $8.86 \pm 0.4 \text{ mg/mL}$  (Standard addition: 0 ng/mL;  $n = 3$ ). This value is within the expected range of IgG in serum, between 6 and 11 mg/mL.<sup>34,35</sup>

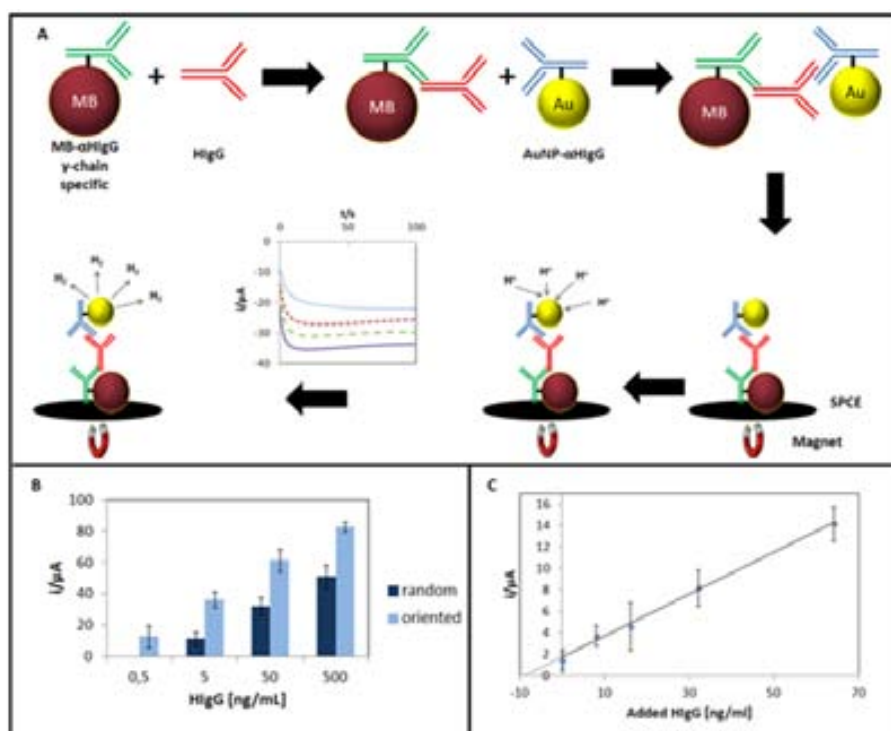


**Fig. 3.9** A) Scheme of the magnetosandwich immunoassay used to detect HgG. In the inset a representative chronoamperometric results obtained using the new label (from up to down): .... 0, ---- 8, - - - 32, \_\_\_\_ 64 ng/ml of HgG. (B) Results obtained subtracting the blank in HCl 1M for random and oriented  $\alpha$ HgG/AuNP labels. (C) Correlation curve obtained with the method of the standard additions of HgG in human serum.

### 3.4 Conclusions

The electrochemical properties of AuNPs suspensions are strongly depended on the size and the hydrodynamic properties of the solvent. By considering only the NPs' size and for a fixed quantity of gold, smaller size NPs generate higher DPV signals. On the other hand, owing to the solvent effect and while working at a constant electrochemical measuring time, larger NPs generate higher signals. Our analysis points to Brownian effects as the main factor governing the efficiency of smaller size NPs. Conversely, while working in a bioassay system such as magnetoimmunoassay employing magnetic particles, the mentioned effect is suppressed due to the fact that the NPs labels are attracted to the electrotransducer surface upon application of a magnetic field as witnessed by the increase of the DPV signal for the smallest NPs.

However, we consider that the Brownian effect should be carefully considered according to the experimental conditions. For example, in an integrated biosensing system where the antibodies (or DNA capture probes) are directly immobilized onto the transducing surface the approaching of NPs upon the recognition event would highly

depend on the size. This consideration should be crucial for microfluidics based biosensing systems (i.e. lab-on-a-chip) designs employing NPs based labelling technology. The design of optical based biosystems also might take advantages of such an approximation that would enlarge the importance of such a phenomenon.

These results are considered to provide an important piece of information to obtain a better understanding of the properties of AuNPs and, more generally, for the optimization of AuNPs-based electrochemical bioassays relevant not only to proteins but also to DNA and cells sensing.

On the other hand, a new electrochemical label based on the oriented functionalization of AuNPs with Abs has been developed. It took advantage of non-specific oriented ionic interaction between the negatively charged AuNP surface and the positively charged major plane of Abs, when they are in a solution with pH lower than their isoelectric point. In a second step, the formation of a covalent bond between the carboxylic groups of the AuNPs covered with PEG and the amino group of the Lys of the Ab was catalyzed using the EDC chemistry. The bond formation is forced to happen via the major plane of the Ab, since it is the part in contact with the AuNP surface. The method has been tested with two different Abs, anti-HRP and anti-HIgG showing its big range of applicability.

Furthermore, the conjugates obtained with this oriented method were compared as optical and electrochemical labels, with those obtained with a random method based on the formation of bonds between the thiol group of the antibodies and the Au atoms of the AuNP surface. In the direct optical detection of HRP the oriented conjugates obtained an improving of the signal of 5 times the one obtained with the random conjugates. In the electrochemical detection of HIgG in PBS, based on the formation of a magneto-sandwich immunoassay the improvement was of one order of magnitude.

Finally, after proving their applicability as labels in biosensors, the oriented conjugates were used to detect HIgG in real human serum. The value obtained of 8.86 mg/ml was in accordance with bibliography values.

We expect that this oriented antibody immobilization approach, developed for AuNP, the most used AuNP in biosensing technology, will have a great impact in several other electrochemical biosensing applications with interest not only for proteins but also for cells (ex. cancer cells reported earlier<sup>36,37</sup>) or even plasmonic based detection of biomarkers.<sup>38</sup>

### 3.5 Bibliography

- (1) Daniel, M.-C.; Astruc, D. *Chemical reviews* **2004**, 104, 293–346.
- (2) Wang, J.; Liu, G.; Polsky, R.; Merkok, A. **2002**, 4, 722–726.
- (3) Liu, G.; Wu, H.; Wang, J.; Lin, Y. *Small (Weinheim an der Bergstrasse, Germany)* **2006**, 2, 1139–43.
- (4) Jha, N.; Ramaprabhu, S. *Nanoscale* **2010**, 2, 806–10.
- (5) Seydack, M. *Biosensors & bioelectronics* **2005**, 20, 2454–69.
- (6) Aslan, K. **2002**, 6059–6065.
- (7) Faulk, W. P.; Taylor, G. M. *Immunochemistry* **1971**, 8, 1081–1083.
- (8) Pumera, M.; Wang, J.; Grushka, E.; Polsky, R. *Analytical chemistry* **2001**, 73, 5625–8.
- (9) Alivisatos, A. P.; Johnsson, K. P.; Peng, X.; Wislon, T. E.; Loweth, C. J.; Bruchez, M. P.; Schultz, P. G. *Nature* **1996**, 382, 609–611.
- (10) Demers, L. M.; Mirkin, C. a; Mucic, R. C.; Reynolds, R. a; Letsinger, R. L.; Elghanian, R.; Viswanadham, G. *Analytical chemistry* **2000**, 72, 5535–41.
- (11) Hayat, M. A. *Colloidal Gold, Principles, Methods and Applications*; Press, A., Ed.; New York, 1989.
- (12) De la Escosura-Muñiz, A.; Parolo, C.; Merkoçi, A. *Materials Today* **2010**, 13, 24–34.
- (13) Katz, E.; Willner, I.; Wang, J. *Electroanalysis* **2004**, 16, 19–44.
- (14) Wang, J. *Analytica Chimica Acta* **2003**, 500, 247–257.
- (15) Ambrosi, A.; Castañeda, M. T.; Killard, A. J.; Smyth, M. R.; Alegret, S.; Merkoçi, A. *Analytical chemistry* **2007**, 79, 5232–40.
- (16) Pumera, M.; Aldavert, M.; Mills, C.; Merkoçi, A.; Alegret, S. *Electrochimica Acta* **2005**, 50, 3702–3707.
- (17) Pumera, M.; Castañeda, M. T.; Pividori, M. I.; Eritja, R.; Merkoçi, A.; Alegret, S. *Langmuir: the ACS journal of surfaces and colloids* **2005**, 21, 9625–9.
- (18) De la Escosura-Muñiz, A.; Ambrosi, A.; Merkoçi, A. *TrAC Trends in Analytical Chemistry* **2008**, 27, 568–584.
- (19) Merkoçi, A. *The FEBS journal* **2007**, 274, 310–6.
- (20) Maltez-da Costa, M.; De la Escosura-Muñiz, A.; Merkoçi, A. *Electrochemistry Communications* **2010**, 12, 1501–1504.

- (21) Hyde, M. E.; Banks, C. E.; Compton, R. G. *Electroanalysis* **2004**, *16*, 345–354.
- (22) Lingane, J. L. *J. Electroanal. Chem.* **1962**, *4*, 332–342.
- (23) Liu, X.; Atwater, M.; Wang, J.; Huo, Q. *Colloids Surf. B* **2007**, *58*, 3–7.
- (24) Terrill, R. H.; Postlethwaite, T. A.; Chen, C. H.; Poon, C. D.; Terzis, A.; Chen, A.; Hutchison, J. E.; Clark, M. R.; Wignal, G. *J. Am. Chem. Soc.* **1995**, *117*, 12537–12548.
- (25) Sardar, R.; Funston, A. M.; Mulvaney, P.; Murray, R. W. *Langmuir* **2009**, *25*, 13840–13851.
- (26) Murray, R. W. *Chem. Rev.* **2008**, *108*, 2688–2720.
- (27) Ward-Jones, S. E.; Campbell, F. W.; Baron, R.; Xiao, L.; Compton, R. G. *J. Phys. Chem. C* **2008**, *112*, 17820–17827.
- (28) Brown, R. *Philos. Mag.* **1828**, *4*, 161–173.
- (29) De la Escosura-Muñiz, A.; Maltez-da Costa, M.; Merkoçi, A. *Biosensors & bioelectronics* **2009**, *24*, 2475–82.
- (30) Mout, R.; Moyano, D. F.; Rana, S.; Rotello, V. M. *Chemical Society reviews* **2012**, *41*, 2539–44.
- (31) Puertas, S.; Batalla, P.; Moros, M.; Polo, E.; Del Pino, P.; Guisan, J. M.; Grazú, V.; De la Fuente, J. M. *ACS nano* **2011**, *5*, 4521–8.
- (32) Puertas, S.; Moros, M.; Fernández-Pacheco, R.; Ibarra, M. R.; Grazú, V.; De la Fuente, J. M. *Journal of Physics D: Applied Physics* **2010**, *43*, 474012.
- (33) Sanz, V.; Conde, J.; Hernández, Y.; Baptista, P. V.; Ibarra, M. R.; Fuente, J. M. *Journal of Nanoparticle Research* **2012**, *14*, 917.
- (34) Stiehm, E. R.; Fudenberg, H. H. *Pediatrics* **1966**, *37*, 715.
- (35) Gonzalez-Quintela, a; Alende, R.; Gude, F.; Campos, J.; Rey, J.; Meijide, L. M.; Fernandez-Merino, C.; Vidal, C. *Clinical and experimental immunology* **2008**, *151*, 42–50.
- (36) Maltez-da Costa, M.; De la Escosura-Muñiz, A.; Nogués, C.; Barrios, L.; Ibáñez, E.; Merkoçi, A. *Nano letters* **2012**, *12*, 4164–71.
- (37) Maltez-da Costa, M.; De la Escosura-Muñiz, A.; Nogués, C.; Barrios, L.; Ibáñez, E.; Merkoçi, A. *Small* **2012**, *8*, 3605–12.
- (38) De la Rica, R.; Stevens, M. M. *Nature Nanotechnology* **2012**, *7*, 821–824.



## Chapter 4

### Lateral Flow Immunoassay based on gold nanoparticles

In this chapter, it is first presented how to perform a lateral flow immunoassay (LFIA) and its function principles. Then two different strategies for the improvement of the LFIA performance are presented. In the first one, the effect of the geometry of the strips is studied while in the second one AuNPs are used not only as direct optical labels but also as carriers of enzymes so as to amplify the signal.

#### Related Publications

---

4) Parolo, C.; Medina-Sánchez, M.; Dela Escosura-Muñiz, A.; Merkoçi, A. Simple paper architecture modifications lead to enhanced sensitivity in nanoparticle based lateral flow immunoassays. *Lab on a chip*, London (UK) Octubre 2013, 13, 386–90.

5) Parolo, C.; Dela Escosura-Muñiz, A.; Merkoçi, A. Enhanced lateral flow immunoassay using gold nanoparticles loaded with enzymes. *Biosensors and Bioelectronics*, Amsterdam (NHL) Junio 2012, 40, 412–416.

---



#### 4.1 –Introduction

As already explained in Chapter 2, the sensitive detection of proteins is of tremendous interest in everyday diagnostic, since many of them are biomarkers of diseases.<sup>1</sup> An early detection of such biomarkers could allow starting a treatment in an early stage of disease, making possible to save many lives. This is particularly important in third world countries, where advanced and expensive technologies are precluded to the foremost of people.<sup>2,3</sup> The same situation can be found in extreme regions or battlefields, where the conditions do not allow the use of complicated devices and trained personnel cannot be present. For these reasons, it is of extremely importance the development of biosensors, which fulfill the requirements of an ASSURED biosensor<sup>4</sup>: affordable, sensitive, specific, user-friendly, rapid and robust, equipment free and deliverable to end-users.

Lateral flow immunoassays (LFIA) can be considered as biosensors which fit the definition of ASSURED technology. Since the first pregnancy test, sold in the mid-1970s, the LFIAs have gained much more importance in the field of biosensing.<sup>5</sup> However, some limitations have avoided their extensive diffusion to other fields, where quantitative analyses together with a better sensitivity are required. In order to answer these demands, we present two easy modifications of the LFIA.

Before entering in the details of the proposed solutions, a description of how a LFIA is fabricated is given. In particular a LFA is generally made of 4 different parts: the sample pad, the conjugation pad, the detection pad and the absorbent pad. The sample pad, made of cellulose, filters the sample from impurities and stores the dried assay buffer, which assures the optimal conditions for the analyte during all the flux.

Regarding the experimental preparation: the sample pad was pre-treated by dipping it into 10 mM PBS buffer pH 7.4, containing 5% BSA and 0.05% Tween20 and then dried for 30 min at 60° C. The conjugation pad was dipped into the AuNPs solution and then dried for 1 hour under vacuum. The control and the detection lines were obtained dispensing respectively the antibody  $\alpha$ HIgG whole molecule and the  $\alpha$ GIgG onto the detection pad. The antibody solutions at 1 mg/mL in 10 mM phosphate buffer pH 7.4 were dispensed with a rate of 1  $\mu$  L/cm using the IsoFlow reagent dispensing system. The pad was then dried at 37° C for 30 min. After that, the different pads were laminated on the backing card in the following order: first the detection pad, then the absorbent pad at the end of the backing card and overlapping the detection pad, after

that the conjugation pad overlapping the detection pad and finally the sample pad on the beginning of the backing card and overlapping the conjugation pad (see Fig. 4.1A). All the overlaps were around 1 mm.

The assay followed an immunosandwich format: the  $\alpha$ HIgG ( $\gamma$ -chain specific) antibodies, attached to the AuNPs, recognized the  $\gamma$ -chain of the HIgG of the sample. The conjugates AuNPs-  $\alpha$ HIgG ( $\gamma$ -chain specific)-HIgG are further stopped at the detection line by the  $\alpha$ HIgG (whole molecule) antibodies fixed at the detection line. Stronger is the red color of the AuNPs at the detection line and higher is the concentration of the analyte (HIgG) present in the sample (Fig. 4.1B). Furthermore the  $\alpha$ GIgG of the control line recognized the  $\alpha$ HIgG ( $\gamma$ -chain specific) of the complexes which are not stopped at the detection line, confirming that the assay worked properly.

## **4.2 First amplification strategy: simple changes in the geometry of LFIA**

In this section, we show theoretically and experimentally how simple changes in the architecture of an AuNPs based LFIA, such as the width of the sample and conjugation pads, can be transduced to an increased sensitivity and improved detection limit of this analytical device.

Two different set-ups were used: changing just the sample pad size and changing both the sample and the conjugation pad sizes. In both cases the surface area studied was 1X, 2X and 3X the original one.

### *4.2.1 Assay procedure*

For the 1X, 2X and 3X strip sizes, the assays were performed pipetting at the bottom of the sample pad 200, 400 and 600  $\mu$ L of the HIgG solution respectively. A blank and three different concentrations of HIgG were studied: 6, 60 and 600 ng/mL in 10 mM PBS pH 7.4. The assay took around 10 min to develop the color of the lines and 10 min for the washing step, performed pipetting the same amount of buffer. The strip was finally cut with a uniform wide of 8 mm in order to be read by the strip reader.

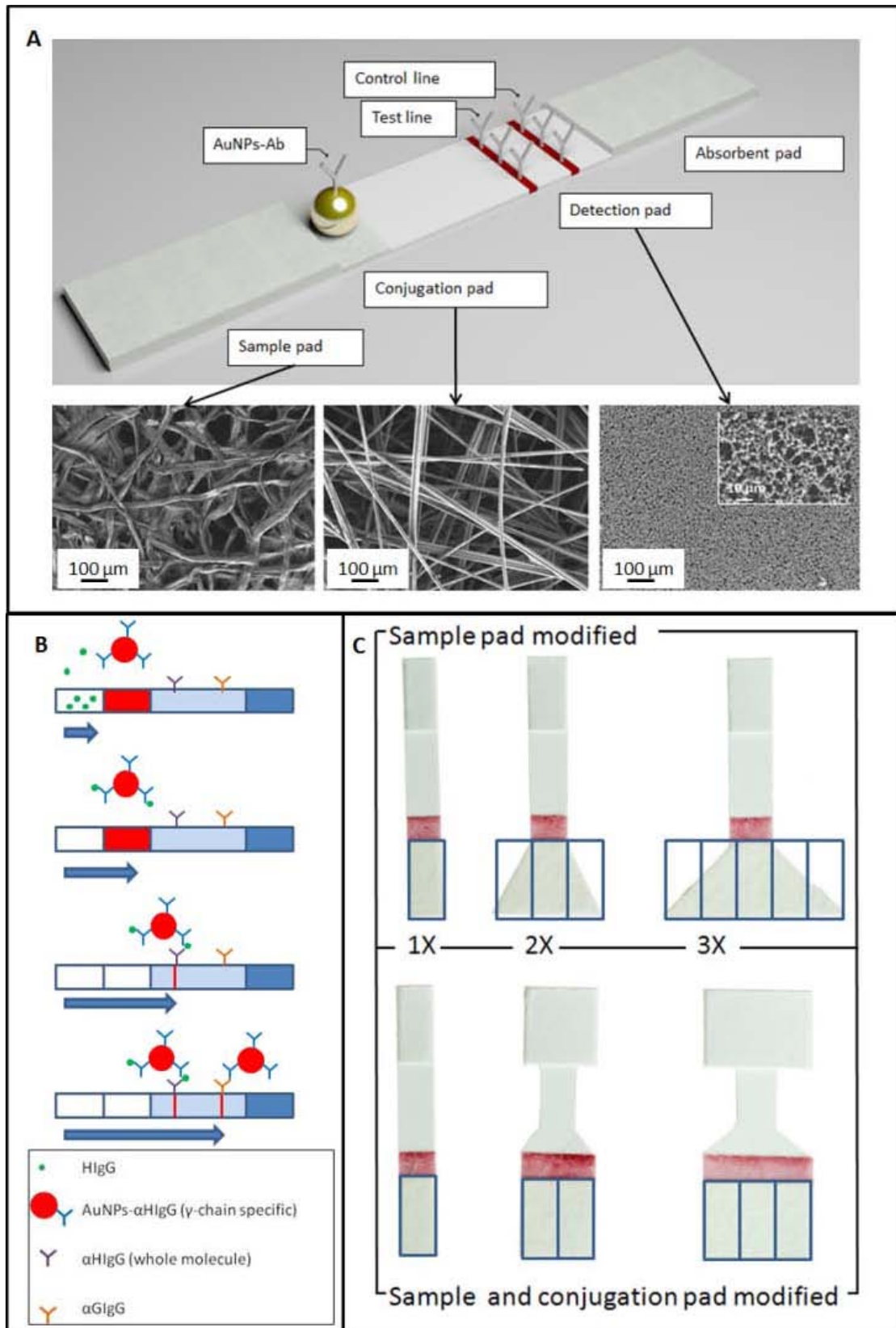


**Fig. 4.1**(A) Scheme, not in scale, of a LFIA strip based on a sandwich format (up) and SEM images of the different pads (down). (B) Scheme of the formation of the immunocomplex during the flow. (C) Different sets up of the LFIA: with only the sample pad 1X, 2X and 3X (up) and with both the conjugation and sample pads 1X, 2X and 3X (down).

#### 4.2.2 Mathematical simulations

The flow in the strip membranes is usually described by the Navier-Stokes equation (pores-free region), and using the Brinkman equations (porous region). The most common way to deal with pores-free and porous media flow in a system is to couple Darcy's law, which does not account for viscous effects, with the Navier-Stokes equations. However, depending on the pore size distribution of the porous media and the fluid's properties, it is not always appropriate to neglect viscous effects. The Brinkman equations account for momentum transport through viscous effects and through pressure gradients in porous media, and can be considered an extension of Darcy's Law, which is a derived constitutive equation that describes the flow of a fluid through a porous medium (see equation 1)<sup>6</sup>:

$$Q = \frac{kA}{\mu} \left( \frac{dP}{dL} \right) \quad (1)$$

where  $Q$  is the flow rate (in units of volume for time unit),  $k$  is the relative permeability (typically in millidarcies),  $A$  is the cross sectional area (in square meters),  $\mu$  is the viscosity of the fluid (in centipoises),  $L$  the length of the porous media (in meters) and  $dP/dL$  is the pressure change per unit length. The constants for the different pads were calculated empirically measuring the volume of water absorbed by each pad. In this way it was possible to estimate the porosity and the permeability of the different pads (see supplementary information of the manuscript).

The initial conditions defined for the simulation were: porosity and permeability of the membranes (empirically calculated, as detailed at the supplementary information of the manuscript) and viscosity and density of the fluid (water). On the other hand, for the boundary conditions the initial velocity was calculated from the volume of the liquid introduced in the membrane (200, 400, and 600  $\mu\text{L}$  for the 1X, 2X and 3X strip respectively), the cross area and the time necessary to absorb the respective volume. So for 1X, 2X and 3X strip the velocity was  $1.47 \times 10^{-3} \text{ m/s}$ ,  $2.94 \times 10^{-3} \text{ m/s}$  and  $4.41 \times 10^{-3} \text{ m/s}$  respectively.

#### 4.2.3 *Effect of the architecture of the sample pad*

A scheme of the LFIA performed for the detection of H IgG as model analyte is shown in Fig. 4.1B. It was first evaluated how the changes in only the sample pad size could affect the sensitivity of the LFIA. The sample pads were designed to have a trapezoid shape to facilitate the flow. In order to obtain the sample pad area 2 and 3 times bigger, the smaller base of the trapezoid, the one in contact with the conjugation pad, was fixed at 8 mm wide, whereas the bigger base was increased respectively to 24 mm and 40 mm, as detailed in Fig. 4.1C. The strip reader gives as output % values corresponding to the intensity of the lines: weaker is the intensity of the line and higher is the % value. The blank of each strip was subtracted to the results obtained to compensate possible non-specific interactions.

In Fig. 4.2A it is possible to see how the strips look like after an assay with 60 ng/mL of H IgG. There are not clear differences in the sensitivity for the different geometries used. In fact as schematized in Fig. 4.2B there are two opposite effects that influenced the assay: the amount of analyte and the speed of the flow. Using bigger sample pads it is possible to use more volume of the sample, and consequently more analyte is available, but this induces an increment in the speed of the flow, which reduces the time that the AuNPs labels have to bind the analyte. The flow is also faster in the detection pad, decreasing the time to recognize the immunocomplexes formed by the antibodies of the test and control lines. As represented by the arrows in the Fig. 4.2, in the 1X format the AuNP speed is low giving enough time to have a good recognition of the analyte, but the analyte amount is not high. The 2X format has a flow speed higher than the 1X but still not enough fast to compromise the interaction between the antibodies and the analyte; furthermore the amount of analyte is bigger, increasing the possibility of recognition by the AuNPs. Finally, in the 3X format the speed is very fast giving not enough time to the AuNP complexes to interact with the antigen, consequently decreasing the limit of detection of the assay even if the amount of analyte is bigger.

These phenomena were also evaluated by mathematical simulations (see Fig. 4.2C). For each design, the flow speed was calculated at the level of the conjugation pad and the test line. For 1X geometry the speeds resulted to be respectively  $2.1 \times 10^{-3}$  and  $1.95 \times 10^{-3}$  m/s, whereas for the 2X they were  $8 \times 10^{-3}$  and  $7.2 \times 10^{-3}$  m/s and finally  $18 \times 10^{-3}$  and  $16 \times 10^{-3}$  m/s for the 3X.

The graph in Fig. 4.2D shows the results obtained with the strip reader. They are in accordance with the theoretical calculations. In fact, there is not any clear positive effect

in the LFIA sensitivity changing only the sample pad size. For the strips with the sample pad 2 times bigger it is possible to observe a slight increased sensitivity of the assay, probably due to the higher volume of sample, which implies a higher amount of analyte. However, the results obtained using the strips with the sample pad 3 times bigger show that the sensitivity of the assay is lower than the one obtained with the sample pad of the original size. This can be explained considering that in the 3X configuration the flow has a speed of approximately one order of magnitude higher than the 1X. Furthermore the AuNPs are re-suspended by a fixed amount of liquid and they are dragged by it. This means that just the analyte present in such volume of liquid can be recognized by the AuNP labels, making not useful using an excess of volume.

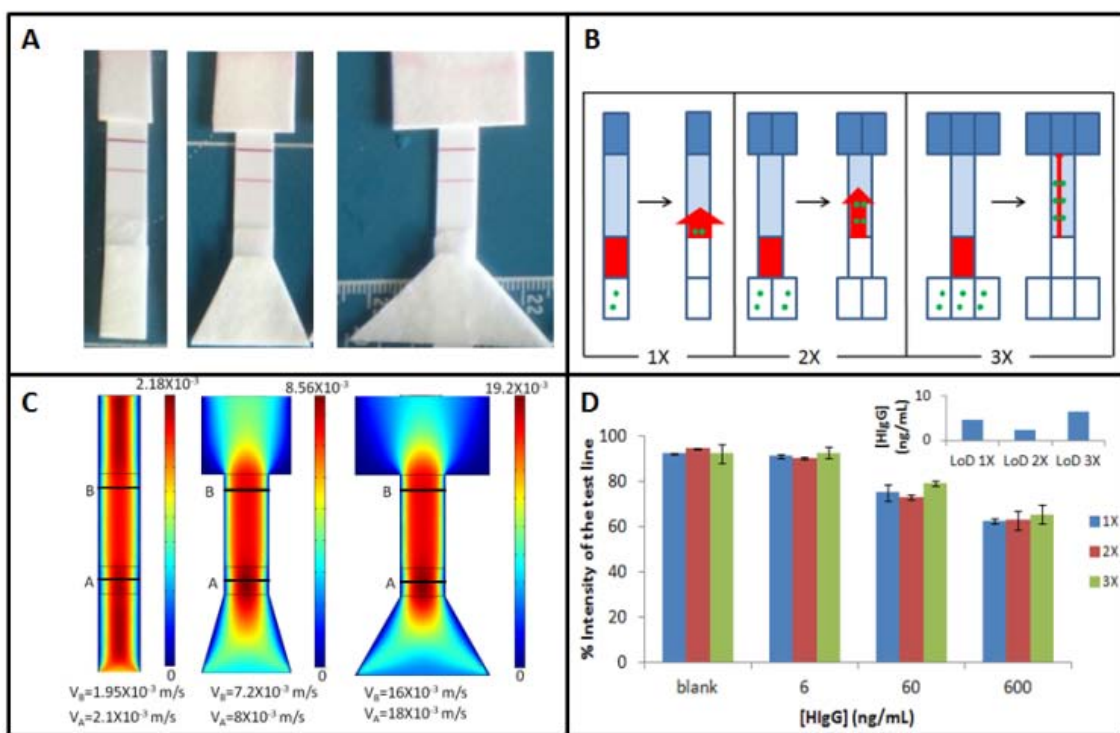


**Fig. 4.2** (A) Photos of LFIA with different sample pad architectures for 60 ng/mL HIgG. (B) Scheme of the two opposite effects: the amount of analyte vs the speed of the flow for the LFIA using a bigger sample pad. The red arrows represent the speed of the AuNPs in the flow and the green point stated for the analyte. (C) Results of the flow speed simulations for sample pads with different sizes. (D) Effect of the sample pad relative size on the quantitative measurement for different HIgG concentrations and the corresponding LODs obtained (inset).

#### 4.2.4 Effect of different architectures for both sample and conjugation pad.

In the second study, both the conjugation and the sample pads were changed. Here, the shapes of the sample and conjugation pads remain rectangular, so they are simply made 2 and 3 times bigger (Fig. 4.1C). In Fig. 4.3A it is possible to observe how the strips look like after an assay for 60 ng/mL of HIgG. It is evident an increase in the intensity of the band increasing the sizes of sample and conjugation pads. In fact, as schematized in Fig. 4.3B, using these configurations the flow speed in the conjugation pads should not change significantly, giving enough time to the AuNPs labels to recognize the analyte. In addition, using a bigger volume there were more analyte molecules to be detected and at the same time, since also the conjugation pad is bigger, more AuNPs to be used as labels. This brought out the formation of a higher number of immuno-complexes. Just when the flow passed to the detection pad, there was an increment in the flow speed, but this phenomenon was compensated by the bigger number of labels, which recognized the analyte. The theory was confirmed by the mathematical simulations (Fig. 4.3C): for the conjugation pad the speed values were of the same order:  $2.1 \times 10^{-3}$ ,  $4.4 \times 10^{-3}$  and  $4.4 \times 10^{-3}$  m/s for 1X, 2X and 3X respectively. However for the detection pad a high increase in the value is obtained when increasing the size, being  $1.95 \times 10^{-3}$ ,  $7.8 \times 10^{-3}$  and  $17.8 \times 10^{-3}$  m/s respectively. The results obtained with the strip reader (Fig. 4.3D) confirmed all the previous data, showing limits of detection for the strips 1X, 2X and 3X to be respectively: 5.89, 1.83 and 0.7 ng/mL. This means that increasing 3 times the width of the conjugation and sample pads it is possible to obtain an 8-fold improvement in the limit of quantification.

These results could be further improved by increasing the difference between the width of the detection pad and those of the conjugation and sample pads. This can be achieved making wider the conjugation and sample pad and/or making smaller the detection pad. However, some drawbacks are previewed: with bigger conjugation and sample pads, more volume of the sample as well as more amount of label is required. On the other hand, smaller detection pads would not be compatible with the strip reader. Another point to be considered is the shape of the strips: longer strips would allow a softer pre-concentration, which would probably produce more reproducible results. This can also be achieved placing the detection line closer to the end of the detection pad.

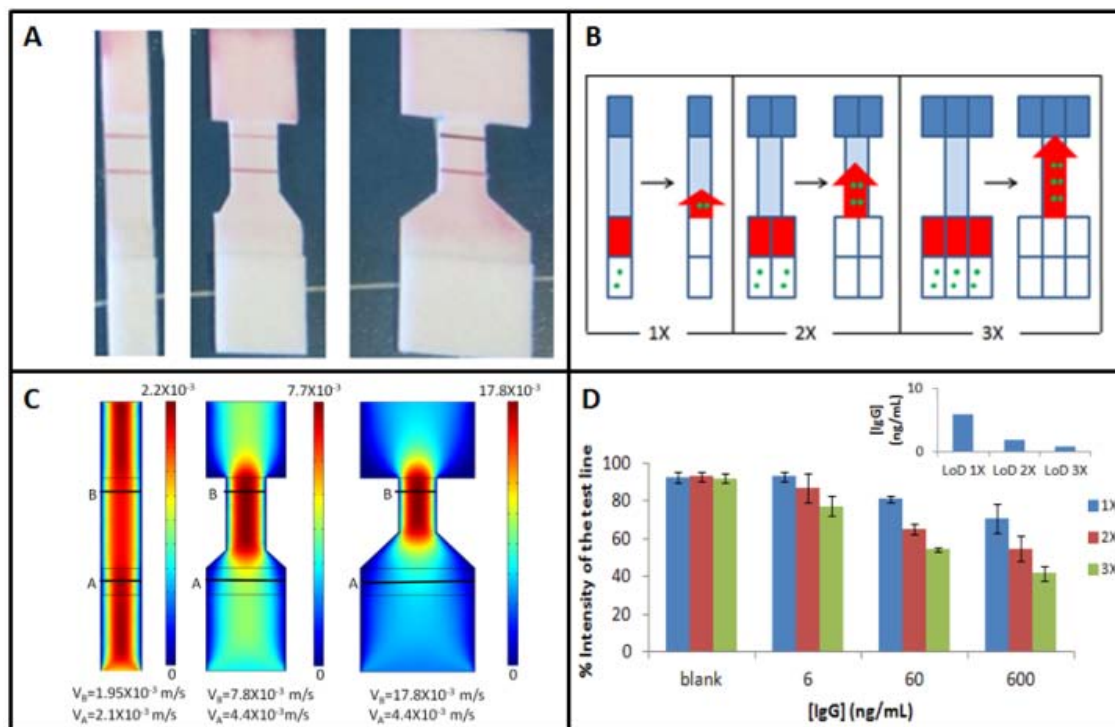


**Fig. 4.3**(A) Photos of LFIA with different sample and conjugation pads architectures for 60 ng/mL HIgG. (B) Scheme of the two opposite effects: the amount of analyte vs the speed of the flow for the LFIAs using bigger sample and conjugation pads. The red arrows represent the speed of the AuNPs in the flow and the green point stated for the analyte. (C) Results of the flow speed simulations for sample and conjugation pads with different sizes. (D) Effect of the sample and conjugation pads relative sizes on the quantitative measurement for different HIgG concentrations and the corresponding LODs obtained (inset).

### 4.3 Second amplification strategy: use of AuNPs as carriers of enzymes

In this section we use the AuNPs as carriers of a high number of enzymes so as to increase their availability to catalyze the detection reaction (Fig. 4.4A). This approach was already performed in different biosensors like ELISA <sup>7</sup> and lateral flow for nucleic acid <sup>8,9</sup>.

AuNPs produce red bands at the detection and control lines of the LFIA when acting as direct labels; but if they are coupled with an antibody modified with HRP they can also act as carriers. 3',5',5' -Tetramethylbenzidine (TMB); 3-Amino-9-ethylcarbazole (AEC); 3,3' -Diaminobenzidine tetrahydrochloride (DAB) with Metal Enhancer as substrates of the HRP are evaluated since they produce insoluble chromogens which cannot be moved by the flow, concentrating the color at the lines (Fig. 4.4 B). The developed LFIAs offer two different detection alternatives: one produced just by the red color of the AuNPs and one more sensitive produced by the substrate of the HRP achieving an 'on-demand' tuning of the biosensing performance. Its application for protein detection, after related optimizations, could open the way to several uses with interest in diagnostics, safety and security between other fields.

The assay procedure consisted in first dispensing of 200  $\mu$ l of sample solution onto the sample pad and waiting during 15 minutes until the flow is stopped. Then 200  $\mu$ l PBS were dispensed in order to wash away the excess of AuNPs/antibody. The strips were read with the strip reader to obtain the calibration curve corresponding to the AuNPs used as 'direct' labels. After the first reading step, the LFIA strips were dipped for 5 min into the different HRP substrates and washed with MQ water to stop the reaction and prevent a saturation of the signals. The strips were finally read again with the reader.

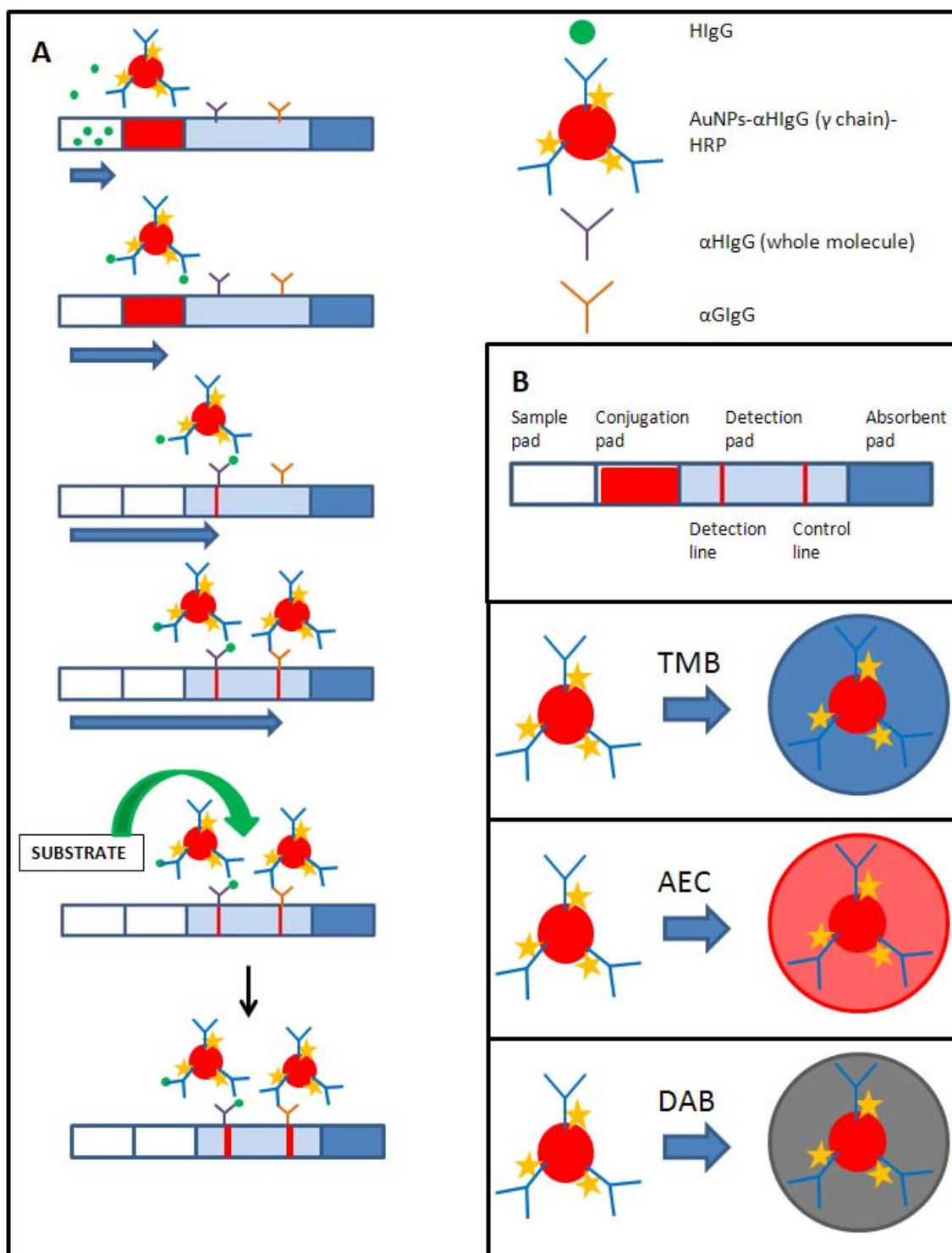


**Fig. 4.4** (A) Scheme of the LFIA for the detection of HlgG. (B) Detail of the different parts of a LFIA strip and cartoons representing the AuNP modified with the antibody anti-human IgG  $\gamma$  chain specific HRP modified, and the different colors expected for the different substrates

#### 4.3.1 AuNP/antibody conjugates characterization

The AuNPs were characterized by UV-vis and TEM to define their sizes (Fig. 4.5A-B). The detection lines obtained for different concentrations of HIgG were visualized also by scanning electron microscopy (SEM). In the Fig. 4.5C it is possible to see the AuNPs (the white spots) in the test line of a LFIA after detecting 500 ng/mL of HIgG, whereas Fig. 4.5D shows another zone of the detection pad without AuNPs.

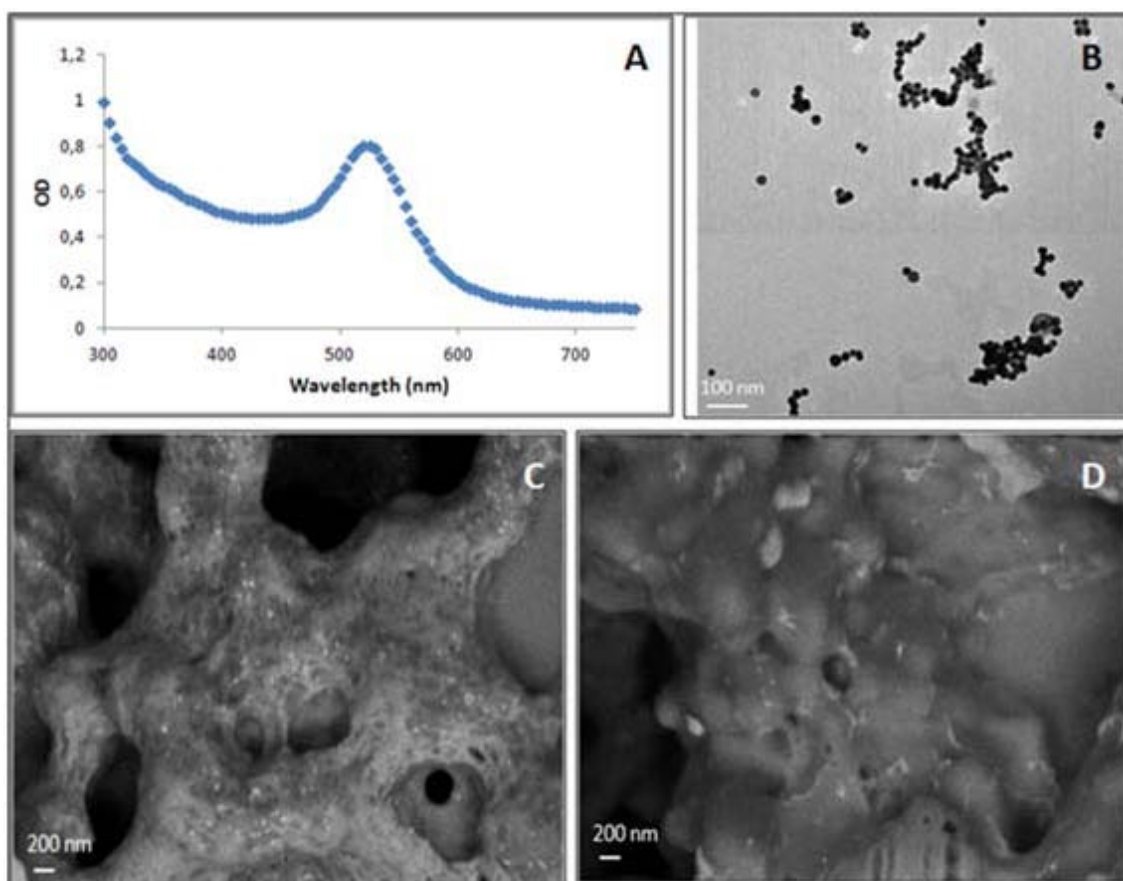


**Fig. 4.5** (A) UV-Vis spectra of AuNPs. (B) TEM image of AuNPs. (C) SEM image of the test line of the LFIA detecting 500 ng/mL HIgG; the white spots represent the AuNPs. (D) SEM image of the detection pad without AuNPs.

#### 4.3.2 Evaluation of the LFIA performance using AuNPs as both direct labels and carriers of enzymatic labels

The prepared LFIA strips gave rise to two different signals. The first one consists in the red color of the AuNPs, whereas the second one corresponds to the color of the chromogen produced by the enzymatic activity of the HRP. The red color of the AuNPs enables to detect up to around 50 ng/mL of HIgG with naked eyes. The strip reader gives as output a % value corresponding to the intensity of the lines: stronger the color,

lower is the % value (Fig. 4.6). A linear relationship between this value and the logarithm of the HIgG concentration was found (see Supplementary Material of the manuscript). The limit of detection using the reader was calculated (also for all the formats described below) as the concentration of HIgG corresponding to three times the standard deviation of the estimate, giving a value of 2 ng/mL of HIgG. Although the obtained sensitivity can be considered adequate for some applications, it is not enough for others, which required lower detection limits. For this reason the TMB, AEC and DAB with metal enhancer were tested as HRP substrates in the developed LFIA.

The first HRP substrate tested was the TMB. As stated in the *experimental section* the TMB used in these experiments produced an insoluble blue-violet chromogen, which is deposited at the level of the control and test lines (as shown in Fig. 4.6); in this way the color is not dispersed along the strip. After stopping the HRP activity the strips were read with the strip reader. The results obtained are shown in the graph of Fig. 4.6, where the improvement in the sensitivity seems to be clear. By using non-modified AuNPs as labels it was difficult to distinguish between a blank and 5 ng/mL of HIgG with the naked eye; on the other hand using the TMB the difference between the blank and the samples is evident, even at 5 ng/mL. The limit of detection obtained using the reader was of 200 pg/mL.

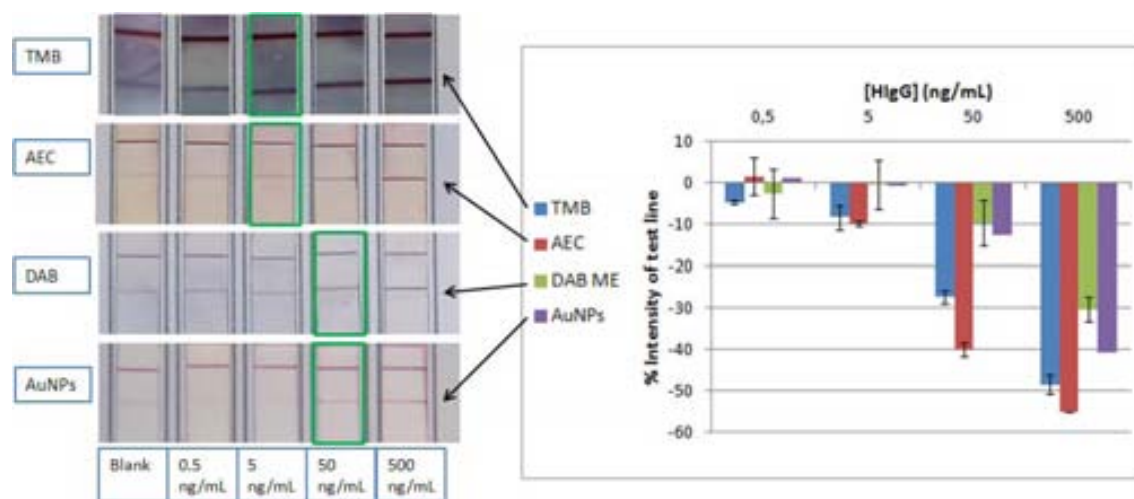


**Fig. 4.6** (Left) Photos of the LFIA strips for different concentrations of HIgG and the different substrates. The limits of detection obtained for the naked eyes are highlighted. (Right) Graph of the results obtained with the strip reader. Experimental conditions as explained in the text.

The second substrate used was the AEC, which produces an insoluble red chromogen. This substrate was already used by Liu's group in a LF for the detection of

nucleic acids<sup>89</sup>. As in the case of TMB substrate also the AEC enables increasing the sensitivity of the assay, allowing detecting up to 5 ng/mL with the naked eye as shown in Fig. 4.6. The limit of detection using the strip reader was in this case 0.31 ng/mL.

Finally the DAB with metal enhancer was tested. This HRP-substrate developed a grey/black insoluble compound. Surprisingly, it did not produce any appreciable increment in the sensitivity of the LFIA, being the minimum concentration detected with the naked eye of around 50 ng/mL, as also shown in Fig. 4.6. The limit of detection using the reader (1.6 ng/mL) was only a little bit lower than the one obtained for the unmodified AuNPs (2 ng/mL, as explained before).

It is also noticed a higher colored background in the case of the enzymatic reactions, probably due to a not completely washing of the strips.

The reproducibility of responses ( $n = 3$ ) for a 50 ng/mL HIgG concentration was also studied, and relative standard deviations (RSD) of 1.3% for AuNPs, 5.6% for TMB, 1.5% for AEC and 16% for DAB were obtained.

The obtained results show that the use of the enzymatic reactions catalyzed by the HRP loaded on AuNPs using TMB and AEC as substrates of the enzyme allows an enhancing of the sensitivity of the LFIA of around one order of magnitude compared to the results obtained just from the direct measurement of the AuNPs as non modified optical labels. In particular the TMB was the substrate which gave the best limit of quantification compared with the others (Fig. 4.6). TMB is also cheaper compared with DAB. Furthermore it has an important advantage compared to the other substrates studied in this work: it is ready to use. In fact both AEC and DAB need to be prepared freshly, using deionized water and mixing of at least two reagents. These characteristics make these two substrates not so suitable for LFIA applications, since they are more time consuming and could increase the possibility of human errors leading to an increase of the irreproducibility of the results. It has also to be noted that the AEC produces a red chromogen which color can be added to the red color of the AuNPs and the background resulted less intense than the one of the TMB.

#### 4.4 Conclusions

We have demonstrated that very simple changes of the LFIA architecture, like increasing the size of both the conjugation and the sample pads, can improve its performance in terms of sensitivity of the assay. Flow speed simulations also corroborate the experimental achievements and can represent useful tools in designing novel lateral flow architectures. The proposed designs can be easily applied in any type of LF strips without changing their fabrication method; moreover it is simple and cheap, fostering its use for point-of-care applications, even at the doctor's office or in undeveloped countries.

On the other hand, a LFIA strip was obtained using AuNPs loaded with HRP enzymatic labels. The use of such a label allows increasing an order of magnitude the limit of quantification in a LFIA for the detection of Human IgG used as model protein. The strips prepared gave two different detection ranges: one less sensitive considering just the red color of the AuNPs and one more sensitive considering the color produced by the HRP substrates. Three different HRP substrates were tested and the TMB was resulted the most suitable for LFIA applications compared with AEC and DAB with metal enhancer. This result could open the way to the use of LFIA in more diagnostics applications, especially in an ambulatory/laboratory context, due to the lower limit of quantification obtained. Furthermore, the use of various substrates offers the possibility to the 'on-demand' tuning of the sensitivity of the device adapting it to the analytical scenario.

#### 4.5 Bibliography

- (1) Mabey, D.; Peeling, R. W.; Ustianowski, A.; Perkins, M. D. *Nature reviews. Microbiology* **2004**, 2, 231–40.
- (2) Yager, P.; Edwards, T.; Fu, E.; Helton, K.; Nelson, K.; Tam, M. R.; Weigl, B. H. *Nature* **2006**, 442, 412–8.
- (3) Ellerbee, A. K.; Phillips, S. T.; Siegel, A. C.; Mirica, K. a; Martinez, A. W.; Striehl, P.; Jain, N.; Prentiss, M.; Whitesides, G. M. *Analytical chemistry* **2009**, 81, 8447–52.
- (4) Peeling, R. W.; Holmes, K. K.; Mabey, D.; Ronald, a *Sexually transmitted infections* **2006**, 82 Suppl 5, v1–6.
- (5) Posthuma-Trumpie, G. a; Korf, J.; Van Amerongen, A. *Analytical and bioanalytical chemistry* **2009**, 393, 569–82.

- (6) Chen, S.; Doolen, G. D. *Annu. Rev. Fluid Mech.* **1998**, *30*, 329–64.
- (7) Ambrosi, A.; Airò, F.; Merkoçi, A. *Analytical chemistry* **2010**, *82*, 1151–6.
- (8) He, Y.; Zhang, S.; Zhang, X.; Baloda, M.; Gurung, A. S.; Xu, H.; Zhang, X.; Liu, G. *Biosensors & bioelectronics* **2011**, *26*, 2018–24.
- (9) Mao, X.; Ma, Y.; Zhang, A.; Zhang, L.; Zeng, L.; Liu, G. *Analytical chemistry* **2009**, *81*, 1660–8.



## Chapter 5

### Paper-based electrodes for nanoparticles detection

In this chapter it is firstly explained why it is important the integration of an electrode in a paper-based device. Then, the characterization of paper-based screen-printed carbon electrodes (SPCEs) is discussed. Finally, the results obtained in the electrochemical detection of AuNPs and CdSe@ZnS QDs using paper-based devices are compared with those of polyester SPCEs.

#### Related Publications

---

6) Parolo, C.; Medina-Sánchez, M.; Montón, H.; De la Escosura-Muñiz, A.; Merkoçi, A. Paper-based electrodes for nanoparticles detection. *Particle & Particle System Characterization*, accepted manuscript, 2013, DOI: 10.1002/ppsc.201200124

---



## 5.1 Introduction

Generally, the success of a sensor depends not only on the efficient recognition of the analyte, but it is also affected by the detection method and the platform used.<sup>1</sup> In this context, the development of sensitive, robust and cheap electrodes is essential for the progress of electrochemical based (bio)sensors. Many different kinds of electrodes, used as sensing platform, are reported: glassy carbon electrodes, gold electrodes, microelectrodes, screen printed carbon electrodes (SPCEs), etc.<sup>2</sup> In our opinion, the integration of SPCEs in a point of care platform, such as lateral flow sensor, is easier, and the resulting device easy to be used.<sup>3-5</sup> In addition, due to their small sizes, low cost, fast and versatile fabrication, using screen printing technology, the resulting device is cheaper in comparison to other types of electrodes, such as those based on sputtering or other micro and nanofabrication technologies. SPCEs are usually printed on polymeric materials, like polyester, due to overall the mechanical properties of this platform, beside their low cost. These materials have two main drawbacks: they are not safely disposable and the sample to be analyzed needs pre-treatments (i.e. incubations, washings, labeling etc.) outside the electrode. These problems can be overcome by the use of paper as platform for the production of SPCEs, instead of plastic materials.<sup>6-8</sup> In fact, paper electrodes can be safely disposed by burning them. Their inherent microfluidic capability combined with an easy insertion of sample pretreatment pads including electrochemical detectors makes these devices the best candidate in terms of full integration of all the steps required for the detection of a sample.<sup>9,10</sup>

Paper-based nanobiosensors are showing to be the best sensing platforms for point of care applications.<sup>11</sup> They combine the advantages of the paper with those of nanomaterials, in general and especially of nanoparticles. The paper-based nanobiosensors, developed so far, are based mainly on optical detection of gold nanoparticles (AuNPs) plasmon signal.<sup>12</sup> Although such detection technologies are successfully applied for DNA,<sup>13</sup> proteins<sup>14</sup> or cells,<sup>15</sup> there is still a big demand to improve the sensitivity and decrease the detection limits. Given the simplicity and robustness of electrochemical detection, its integration with lateral flow seems to be the best choice. The efforts to achieve such integration are usually limited to a simple mechanical approximation of electrochemical detector with lateral flow paper platform. In fact, it is possible to develop paper-based sensors (like lateral flow assays, microfluidic paper-based devices, etc.), where the paper SPCEs can be easily integrated

and the entire device can be easily burned after use.<sup>16</sup> Furthermore, the sensitivity of such electrodes is generally expected to be higher than the others, because the surfactants of the inks can be absorbed by the paper, making the conductive material more exposed. In addition, they have a bigger electroactive surface available, since the matrix of the paper has a porous 3D structure.<sup>17</sup> To clarify such phenomena, characterizations of paper SPCEs and polyester SPCEs by scanning electron microscopy (SEM), confocal laser scanning microscopy (CLSM), and the studies of their hydrophobicity and porosity are firstly discussed. Then, the results obtained using paper SPCEs are compared with those obtained with polyester SPCEs for the detection of AuNPs and CdSe@ZnS quantum dots (QDs) with different electrochemical techniques. These very sensitive paper SPCEs are reproduced by combining screen printing, wax printing and plasma cleaner.

## 5.2 Characterization of paper-based SPCEs

First, we characterized the surface of the electrodes by SEM. Fig. 5.1A-B shows the images of the paper and polyester platforms before printing any ink. A higher porosity of the paper can be clearly observed. In Fig. 5.1C-D, it is possible to see the carbon based working electrodes (WE) of polyester SPCE and paper SPCE respectively. In the paper SPCE, it is observed that in addition to the higher porosity of the substrate, the carbon ink is also printed in a microporous like pattern of a round 185  $\mu\text{m}$ , which apparently increases the roughness of the WE and, in addition, may allow free space for an easy penetration of the sample. Such structures, in addition to the porous nature of the paper, make the WE having an enhanced electroactive surface easily accessible by the analyte. These ink-printed structures are observed only after printing (they are not present in Fig. 5.1B) and are due to the nitrocellulose properties. We suggest that during the screen-printing process, when the ink is squeezed out of the mesh, the surfactants are quickly absorbed by the paper, making the carbon material accumulated into certain areas ordered according to the micropore distribution in the used mask. Such ordered carbon areas cannot be observed when the same ink is printed onto polyester, due to the fact that the ink once is getting out from the mesh, keeps containing the same amount of solvent and consequently the same fluidity, causing an almost uniform coverage with carbon. As expected, the printed WE on the polyester surface (SPCE) is very flat compared with the one of paper SPCE. This difference in the WE structure is probably

one of the most important factors in the better electrochemical behavior of paper SPCEs compared with the polyester ones, as will be shown below. In the case of the silver layers, no observable differences are noticed between polyester and paper, as shown in Fig. 5.1E-F, due to the different behavior (more fluidity) in comparison to the carbon ink.

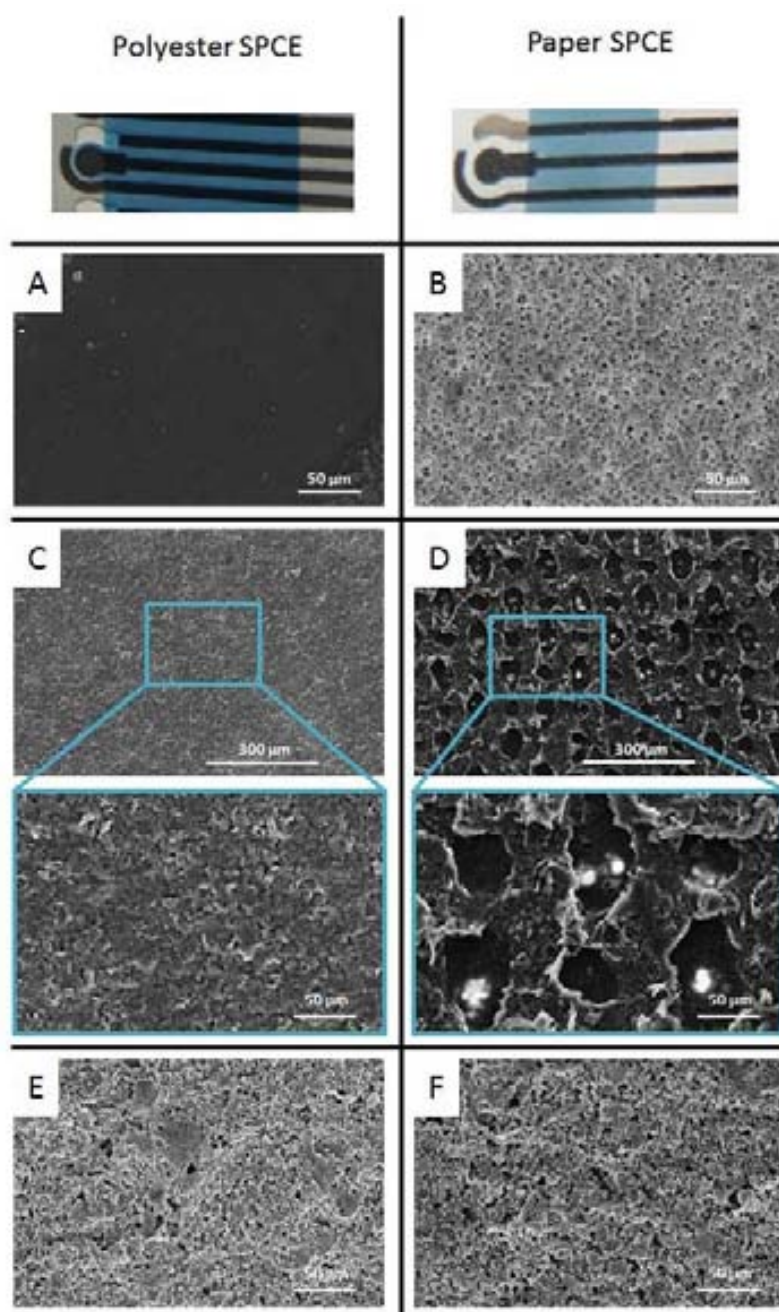


**Fig. 5.1** Pictures of both polyester and paper-based SPCEs and Scanning Electron Microscopy characterizations of: Polyester sheet (A.); Nitrocellulose membrane (paper) (B); Carbon ink printed on polyester (C) and in paper (D) at two different magnifications; Silver ink printed in polyester (E) and in paper (F).

CLSM was used to confirm such observations by scanning the depth of the electrode along the z-axis using the reflection mode and z-stacks (Fig. 5.2A-B). The periodic pattern in the WE of the paper SPCE and the much more homogenous surface of the WE in polyester are evidenced in the plan view. Moreover, in order to see in depth the X and Y profiles of the WEs, a cross section of the z-stack was performed (the dashed cross represents the exact site where the virtual cuts are performed). It is possible to see the periodic changes in the surface both in the X and Y profiles of the paper SPCE, while in the polyester one no remarkable changes of the surface can be observed.

The study of the hydrophilicity, of both carbon printed surfaces, was also performed after plasma exposition. This plasma treatment is applied in order to introduce hydroxyl groups. The presence of such groups increases the hydrophilicity of the surface, causing a better and faster entrance of the sample into the porous surface of the WE, and increasing the contact area between the WE and the analyte. The increment in the wettability was confirmed by contact angle studies, as shown in Fig. 5.2C-D. As expected, the untreated polyester is more hydrophobic than the untreated paper, as shown by the resulting contact angles of  $80 \pm 0.5^\circ$  and  $22 \pm 0.5^\circ$  respectively. The contact angle of the polyester decreased to  $40 \pm 0.5^\circ$  after the plasma treatment (1 min of exposure). The value of the paper could not be measured, because the liquid was immediately absorbed. The obtained results indicate that the plasma treatment is effective in making the paper SPCE more hydrophilic, enabling its application in water medium sensing.

The improved characteristics of the paper SPCEs were evaluated for the electrochemical detection of gold nanoparticles (AuNPs) and CdSe@ZnS quantum dots (QDs), which are of great interest for further applications in bioassays, where these NPs will be used as electroactive labels. To obtain a better sensing performance, all the electrochemical measurements were performed using the electrodes treated with plasma. The detailed experimental conditions for the detection of each NPs are detailed at the supporting information of the manuscript.

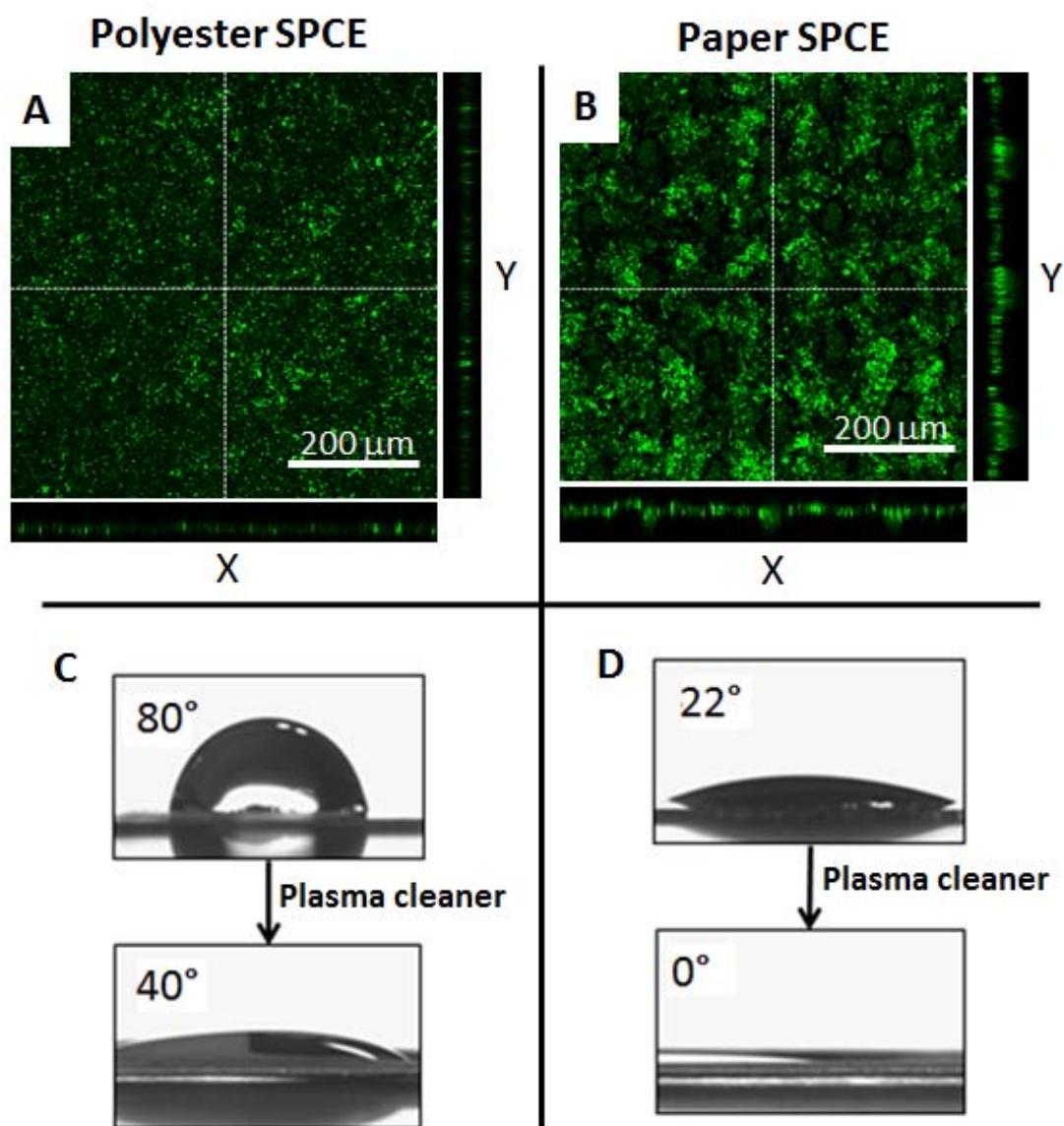


**Fig. 5.2** CLSM and hydrophilicity characterizations of the carbon WE printed in polyester (left column) and in paper (right column). CLSM plan views and cross-section of the z-stack (A,B); Contact angle study (C,D) before (up) and after (down) plasma treatment.

### 5.3 Electrochemical detection of NPs using paper-based SPCEs

In the case of the AuNPs, two different methods, previously optimized on polyester SPCEs for the detection of these NP labels in immunoassays, were tested with the two kinds of electrodes. Firstly, suspensions of 20 nm AuNPs (Fig. 5.3A) of different concentrations were voltammetrically detected following a previously optimized method<sup>18</sup>. It consists in the electrochemical oxidation of the Au(0) to  $\text{AuCl}_4^-$ , followed by the differential pulse voltammetric (DPV) reduction back to Au(0) (Fig. 5.3B), which generates a peak of current directly related with the quantity of AuNPs. The results obtained, shown in Fig. 5.3C, demonstrate that also with paper SPCEs was possible to directly detect AuNPs, obtaining sensitivity and reproducibility values of the same order of magnitude of polyester SPCEs, noticing even a slightly better sensitivity in the case of the paper. In particular, the limits of detection for paper SPCEs and polyester SPCEs were respectively 15 pM and 25 pM of AuNPs.

The second method tested was based on the hydrogen evolution reaction (HER) catalyzed by AuNPs and was followed chronoamperometrically. The value of the current registered at a 100s is related with the quantity of AuNPs. This method leads to an efficient indirect detection of AuNPs by measuring the current produced during  $\text{H}_2$  formation catalyzed by AuNPs (Fig. 5.3D). This AuNP quantification technique is known to be more sensitive than the direct voltammetric detection and has been used in many biosensors ranging from protein<sup>19</sup> to cancer cell<sup>20,21</sup> detections. The results show a clear increment in the signal using paper SPCEs. The limits of detection obtained were respectively 3 pM and 24 pM for paper SPCEs and polyester SPCEs. The bigger improvement obtained using paper instead of polyester, respect the direct detection of gold, can be related to the 3D structure of the WE, which allows an easier flow of protons toward the electrode area, pushing forward the  $\text{H}_2$  evolution (hydrogen gas also escape faster through the generated micropores) reaction. This makes the paper SPCE an excellent platform to perform the whole catalytic cycles, with interest for an efficient AuNP quantification.

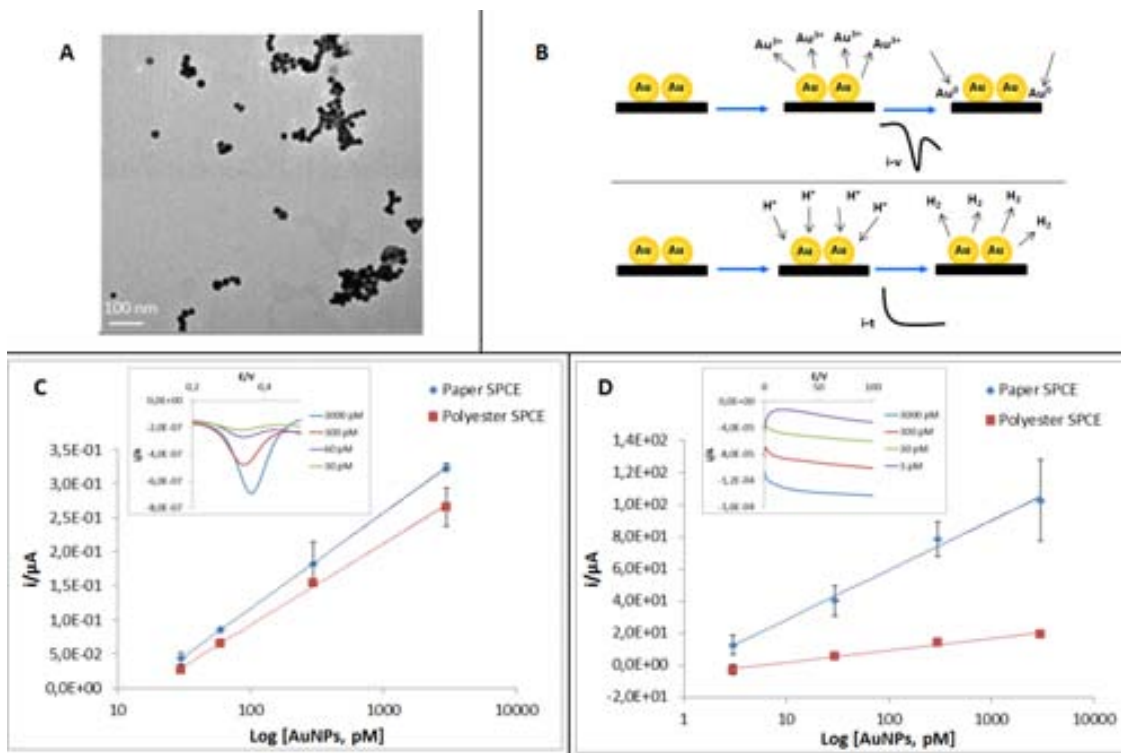


**Fig. 5.3** A) TEM images of AuNPs. B) Electrochemical principles for the detection of AuNPs: Direct voltammetric detection (top) and catalytic detection of AuNPs through the HER - Hydrogen Evolution Reaction (bottom). C) Calibration curves of direct voltammetric detection of AuNPs, obtained measuring the peak values; in the inset representative signals obtained with paper SPCE at different concentration of AuNPs. D) Calibration curves of catalytic detection of AuNPs obtained considering the current values at 100 sec; in the inset representative signals obtained with paper SPCE at different concentration of AuNPs are shown.

Finally, the last application of paper SPCEs was the direct voltammetric detection of CdSe@ZnS QDs (Fig. 5.4A) in PBS buffer, without the need of a previous acidic dissolution of the NPs. This methodology has also been previously reported for QD detection on polyester SPCEs<sup>22</sup>. It consists in the electrochemical reduction of the Zn(II), contained in the NP, to Zn(0) followed to a square wave voltammetric (SWV) oxidation back of the Zn(0) to Zn(II), which generates a peak of currents at -0.9V which is related with the quantity of these NPs (Fig. 5.4B). The results showed a very good trend, reaching a limit of detection of 11 nM of QDs in a PBS solution (Fig. 5.4C) using paper SPCEs. In this experiment the data obtained with polyester SPCE are not shown, because such electrodes could not detect even the highest concentration of QDs evaluated.

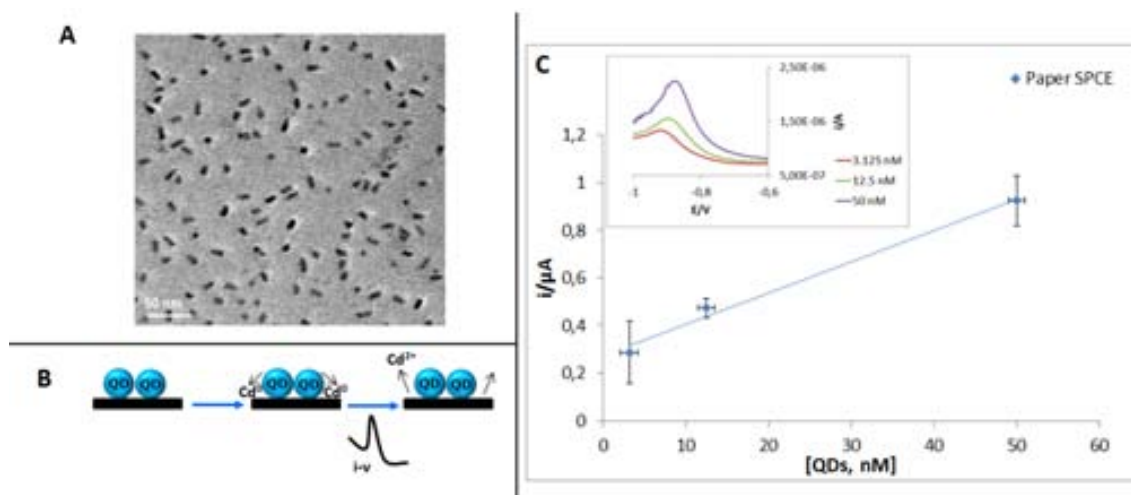


**Fig. 5.4** A) TEM images of CdSe@ZnS QDs. B) Electrochemical principle for the direct voltammetric detection of QDs. C) Calibration curve of direct voltammetric detection of QDs; in the inset representative signals obtained with paper SPCE at different concentration of QDs are shown. (The response of polyester SPCE were not representative)

#### 5.4 Conclusions and perspectives

In conclusion, we have developed very sensitive paper SPCEs by combining screen printing, wax printing and plasma cleaner. This complete integrated paper-based SPCE shows a better response in comparison to state of the art screen-printed platforms, such as polyester. We have also clarified such better response, due to the 3D structure of the electrode and the formation of microporous structures, which allowed a higher surface interaction between the nanoparticles and the WE. Furthermore, the use of plasma exposition makes the surface more hydrophilic. The detections of AuNPs and CdSe@ZnS QDs demonstrate that paper SPCEs can be used with a wide range of electrochemical techniques. Finally, the better electrochemical responses, compared with those obtained with polyester SPCE, make evident that the paper SPCE can be integrated in many biosensing platforms for several applications, where nanoparticles are used as labels either for DNA, protein or even cells detection. In addition, fast and sensitive detection of electroactive nanoparticles with interest for environmental control can be done.

The developed paper-based sensor may improve, in a significant mode, the lateral flow based devices, and opens the way to new real world applications of electrochemical sensing technology, which is still lacking from the separation between sample introduction, pretreatment and incubations (immunoreactions, DNA reactions) with detection. Having the electrochemical detector well integrated within paper

microfluidics will further strengthen the efficiency of the resulting biosensing technologies. We envisage that, given the easy deposition of electrodes onto paper, combined with the flexibility and variability of paper platforms and wax printing, paper-based electrodes and sensors will be strong devices, with interest, not only in (bio)sensing, but also energy related applications<sup>23–25</sup>, where efficient ‘green solutions’ are always welcome.

## 5.5 Bibliography

- (1) De la Escosura-Muñiz, A.; Parolo, C.; Merkoçi, A. *Materials Today* **2010**, *13*, 24–34.
- (2) Kimmel, D. W.; LeBlanc, G.; Meschievitz, M. E.; Cliffl, D. E. *Analytical chemistry* **2012**, *84*, 685–707.
- (3) Ge, L.; Yan, J.; Song, X.; Yan, M.; Ge, S.; Yu, J. *Biomaterials* **2012**, *33*, 1024–31.
- (4) Wang, P.; Ge, L.; Yan, M.; Song, X.; Ge, S.; Yu, J. *Biosensors & bioelectronics* **2012**, *32*, 238–43.
- (5) Nie, Z.; Nijhuis, C. a; Gong, J.; Chen, X.; Kumachev, A.; Martinez, A. W.; Narovlyansky, M.; Whitesides, G. M. *Lab on a chip* **2010**, *10*, 477–83.
- (6) Dungchai, W.; Chailapakul, O.; Henry, C. S. *Analytical chemistry* **2009**, *81*, 5821–6.
- (7) Carvalhal, R. F.; Kfour, M. S.; Piazzetta, M. H. D. O.; Gobbi, A. L.; Kubota, L. T. *Analytical chemistry* **2010**, *82*, 1162–5.
- (8) Zang, D.; Ge, L.; Yan, M.; Song, X.; Yu, J. *Chemical communications (Cambridge, England)* **2012**, *48*, 4683–5.
- (9) Ge, S.; Ge, L.; Yan, M.; Song, X.; Yu, J.; Huang, J. *Chemical communications (Cambridge, England)* **2012**, *48*, 9397–9.

- (10) Liu, X.; Mwangi, M.; Li, X.; O'Brien, M.; Whitesides, G. M. *Lab on a chip* **2011**, *11*, 2189–96.
- (11) Parolo, C.; Merkoçi, A. *Chemical Society Reviews* **2013**, *42*, 450–457.
- (12) Saha, K.; Agasti, S. S.; Kim, C.; Li, X.; Rotello, V. M. *Chemical reviews* **2012**, *112*, 2739–79.
- (13) Lie, P.; Liu, J.; Fang, Z.; Dun, B.; Zeng, L. *Chemical communications (Cambridge, England)* **2012**, *48*, 236–8.
- (14) Parolo, C.; De la Escosura-Muñiz, A.; Merkoçi, A. *Biosensors and Bioelectronics* **2012**, *40*, 412–416.
- (15) Li, C.-Z.; Vandenberg, K.; Prabhulkar, S.; Zhu, X.; Schneper, L.; Methee, K.; Rosser, C. J.; Almeida, E. *Biosensors & bioelectronics* **2011**, *26*, 4342–4348.
- (16) Nie, Z.; Deiss, F.; Liu, X.; Akbulut, O.; Whitesides, G. M. *Lab on a chip* **2010**, *10*, 3163–9.
- (17) Zang, D.; Ge, L.; Yan, M.; Song, X.; Yu, J. *Chemical communications (Cambridge, England)* **2012**, 4683–4685.
- (18) De la Escosura-Muñiz, A.; Parolo, C.; Maran, F.; Mekoçi, A. *Nanoscale* **2011**, *3*, 3350–3356.
- (19) M. Maltez-da Costa, A. de la Escosura-Muñiz, A. Merkoçi, ^  
*Electrochemistry Communications* **2010**, *12*, 1501–1504.
- (20) Maltez-da Costa, M.; De la Escosura-Muñiz, A.; Nogués, C.; Barrios, L.; Ibáñez, E.; Merkoçi, A. *Nano letters* **2012**, *12*, 4164–71.
- (21) Maltez-da Costa, M.; De la Escosura-Muñiz, A.; Nogués, C.; Barrios, L.; Ibáñez, E.; Merkoçi, A. *Small (Weinheim an der Bergstrasse, Germany)* **2012**, *1*–8.

- (22) Medina-Sánchez, M.; Miserere, S.; Marín, S.; Aragay, G.; Merkoçi, A. *Lab on a chip* **2012**, *12*, 2000–5.
- (23) Thom, N. K.; Yeung, K.; Pillion, M. B.; Phillips, S. T. *Lab on a chip* **2012**, *12*, 1768–70.
- (24) Yuan, L.; Xiao, X.; Ding, T.; Zhong, J.; Zhang, X.; Shen, Y.; Hu, B.; Huang, Y.; Zhou, J.; Wang, Z. L. *Angewandte Chemie (International ed. in English)* **2012**, 4934–4938.
- (25) Ge, L.; Wang, P.; Ge, S.; Li, N.; Yu, J.; Yan, M.; Huang, J. *Analytical chemistry* **2013**.



## **Chapter 6**

### **General conclusions and future perspectives**

Since the specific conclusions are already written at the end of each chapter, in this paragraph just the general conclusions of the whole thesis are reported. Furthermore, some future perspectives are considered.



## 6.1 General conclusions

Two different types of platforms with interest for immuno-sensing applications have been developed. The first one is based on the use of polyester screen printed carbon electrodes (SPCE) for the detection of a magneto-sandwich immunoconjugate, which uses AuNPs as electrochemical labels. Two different electrochemical methods have been used for the detection of AuNPs: a direct and an indirect method, obtaining with both of them very good analytical performances allowing for future applications as point of care and cost / efficient devices.

The other type of immunosensor used is a lateral flow immune analysis (LFIA). Innovative architecture (platform shapes) and detection (enhancement of label signal) related modifications that have enhanced the sensitivity of the developed LFIA without losing its simplicity have been achieved. The discovered strategies clearly avoid the sensitivity drawback of current nanoparticle based LFIA technology extending the range of its applicability in many applications where achieving lower detection limits and higher sensitivity is crucial.

Finally, an attempt to integrate the two platforms, SPCE with paper, fabricating a paper-based SPCE is also demonstrated. This new device showed to have better performance than polyester SPCE for the detection of nanoparticles. We believe this is due to its porous structure which enhances the electroactive surface of the electrode.

The novel devices designed and fabricated during this thesis have shown to be:

- *easy-to-use*: few (just one for the LFIA) and overall only easy to be performed operations are required by the final user,
- *point-of-care*: all the devices and related signal readers can be small or easy to be miniaturized which make them suitable for in-field / POC applications,
- *sensitive*: the limit of detections of the developed devices for proteins used as proof of concept analytes are in the order of ng/ml or pg/ml, which are enough for the most applications in diagnostics,
- *fast*: the LFIA takes as much as 15 minutes to develop the signal, whereas the magneto-sandwich immuno-complex electrochemical detection required less than 2 hours to complete all the protocol, which make the developed assays competitive to conventional techniques (i.e. ELISA).

-

## 6.2 Future perspectives

The applicability of the reported technologies is undoubted, especially considering the LFIA devices. Nevertheless, to compete in the market is necessary to offer something different from the existing devices. In this scenario, the Chapter 5 of this thesis is the first step to combine the advantages of the electrochemical detections presented with those of the paper-based devices. In fact, the development of an electrochemical LFIA would integrate in one device the simplicity and qualitative detection of the paper-strips with the quantification capability and sensitivity of the electrochemical detection.

Furthermore, it can be expected that in the near future to improve the applicability of point-of-care biosensors an important alternative to bring these devices to end users should be the possibility to communicate the results to specialized personnel. In this way some works related to paper-based diagnostic technology and communication system have been already reported, especially by Martinez *et al.*<sup>1,2</sup> The authors used a normal phone camera to send the result of the assay to a laboratory where a specialized person can analyze it and send back to the biosensor user the response of the test (Fig. 6.1). This technology will tremendously enhance the healthcare in extreme places like the developing world and battle fields, but also it will be probably the starting point for a real home-diagnostic.

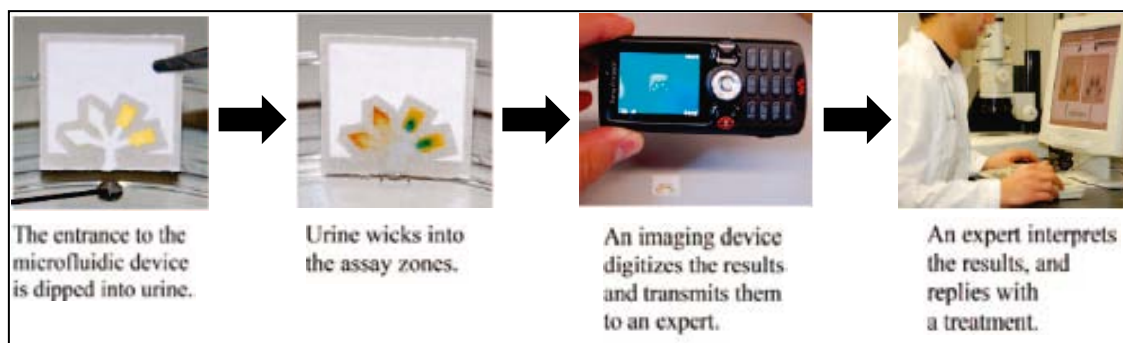


**Fig.6.1** General strategy for performing inexpensive bioassays in remote locations and for exchanging the results of the tests with offsite technicians. Adapted with permission from ref 1, 2.

## 6.3 Bibliography

- (1) Martinez, A. W.; Phillips, S. T.; Carrilho, E.; Thomas, S. W.; Sindi, H.; Whitesides, G. M. *Analytical chemistry* **2008**, 80, 3699–707.
- (2) Martinez, A. W.; Phillips, S. T.; Whitesides, G. M.; Carrilho, E. *Analytical chemistry* **2010**, 82, 3–10.

## **Annex A**

### **Electrochemical DNA Sensors based on Nanoparticles**

#### **Related Publications**

---

8) Parolo, C.; De la Escosura-Muñiz, A.; Merkoçi, A. Electrochemical DNA Sensors based on Nanoparticles. Book Chapter. Manuscript 2013

---



## **Electrochemical DNA Sensors based on Nanoparticles**

*Claudio Parolo, Alfredo de la Escosura-Muñiz, Arben Merkoçi*

*Nanobioelectronics & Biosensors Group, Institut Català de Nanotecnologia, CIN2 (ICN-CSIC), Campus UAB, Bellaterra, Barcelona, 08193, Spain*

*ICREA, Institució Catalana de Recerca i Estudis Avançats, Barcelona, 08010, Spain*

*arben.merkoci@icn.cat*

### **7.1 Introduction**

The identification/quantification of specific DNA sequences is of crucial importance for many fields. For example, the detection of DNA mutations is already correlated to specific diseases. The most frequent of these mutations are single nucleotide polymorphisms (SNPs), the change of just one base in a DNA sequence which can provoke serious damages to the organisms. Furthermore specific DNA sequences can be indicators of pathogens which can be related to food and water contamination. Finally forensic applications need to be as fast and specific as possible to correlate DNA sequences with person's identification. In this optic the development of sensitive, specific, easy to use, fast and cheap DNA biosensors is of extremely importance.<sup>1,2</sup>

In most cases, the DNA analysis using nanomaterials (NMs) based biosensors consists in the detection of the DNA sequence of interest using single-stranded DNA (ssDNA) as bioreceptor and final optical or electrochemical transducing, while using NMs in any of the sensing technology steps. The specificity of the device depends on the hybridization between two ssDNA molecules (see more details on the main DNA biosensor components at section 7.2.4). Given the relatively complicated technology or the employment of harmful reagents from other DNA sensor technologies, the electrochemical based devices seem to take advantages of the inherent properties of the electrochemical techniques. Electrochemical sensors have many advantages: they have a very fast response and are cheap, sensitive, specific and can be easily miniaturized. All these characteristics make them the perfect technology to study DNA with interest in different fields of research and diagnostics.<sup>3–10</sup>

Nanomaterials (NMs) with their unique electrical and optical properties thanks to their nanometer size scale are showing to be important building blocks in the design and fabrication of novel or improved biosensors. Between various NMs, nanoparticles (NPs)

are extensively used in biosensors, since they can act as labels, label carriers and modifiers of transducers.<sup>11–13</sup>

The purpose of this chapter is to show the latest trends in the use of NPs in the development of electrochemical DNA sensors.

## **7.2 General aspects of DNA and nanoparticles**

### **7.2.1 DNA structure**

DNA is a linear polymer, whose each monomer unit consists of three components: a sugar (deoxyribose), a phosphate, and a nitrogenized base (Figure 1A). The base sequence characterizes uniquely a DNA molecule. The deoxyribose molecules are linked to each other by phosphodiester bridges creating the back bone of the polymer. Specifically, the 3-hydroxyl (3-OH) group of the sugar moiety of one nucleotide is esterified to a phosphate group, which is, in turn, joined to the 5-hydroxyl group of the adjacent sugar. The bases vary from one monomer to the other. Two of the bases are derivatives of purine: adenine (A) and guanine (G), and two of pyrimidine: cytosine (C) and thymine (T). Each purine base can form hydrogen bonds just with a pyrimidine base, in particular: A binds with T and C binds with G. The two types of base pairs form different numbers of hydrogen bonds, AT forming two hydrogen bonds, and GC forming three hydrogen bonds. The connections within bases allow the formation of a helical structure consisting of two anti-parallel strands. DNA with high GC-content is more stable than DNA with low GC-content, but contrary to popular belief, this is not due to the extra hydrogen bond of a GC base-pair but rather the contribution of stacking interactions; hydrogen bonding merely provides specificity of the pairing, not stability. So all the information carried by a DNA molecule is contained in its sequence of bases. Any change in the sequence would produce a new molecule carrying new information. It is both the percentage of GC base pairs and the overall length of a DNA double helix that determine the strength of the association between the two strands of DNA. As hydrogen bonds are not covalent, they can be broken, for example by heating, and rejoined relatively easily. Strands may also be separated by adding acid or alkali to ionize the nucleotide bases and disrupt base pairing. All these properties of DNA molecule are essential for the design of a good DNA biosensor.<sup>14</sup>

### 7.2.2 DNA amplification techniques

Although the truly objective of the DNA biosensing consists in the direct detection of DNA extracted from real samples, the small quantity of the specific DNA wanted to be detected in the immense matrix of total DNA make often necessary a previous amplification.<sup>15</sup>

In this context, a revolutionary milestone in the scientific research was the development of the polymerase chain reaction (PCR), and for its invention Kary Mullis won the Nobel Prize in chemistry in the 1993.<sup>16</sup> The PCR is a technique capable of generating an incredible amount of a specific sequence DNA molecule in a short period of time. The PCR was essential to complete the sequencing of the human genome. It brought an enormous amount of data regarding DNA sequences, which are far from being completely understood. A wide knowledge of the human genome would open the way to personal medicine increasing incredibly the quality of life of the human beings.<sup>17</sup>

The PCR is based on the activity of the DNA Polymerase, an enzyme that synthesizes new strands of DNA in a 5'-3' direction from a single strand template (Figure 1B). The PCR allows having billion copies of the target DNA starting from just few molecules. Essentially two primers (oligonucleotides of 20-30 bases) flank and define the target sequence to be amplified. These primers hybridize to opposite strands of the DNA to serve as initial points for the synthesis of new DNA strand. The DNA polymerase catalyzes this synthesis. The reagents to carry out a PCR are generally: a pair of primers that hybridize with the flanking sequences of the target, all four deoxyribonucleoside triphosphates, a heat-stable DNA polymerase, the enzyme buffer and a amount of magnesium chloride. The reaction is done in a Thermalcycler, a machine which allows a rapid change in the temperature for several cycles. A general PCR cycle consists of three steps:

- Denaturation step - The solution is heating up to 94-95°C to separate the two strands of the target DNA; in fact at this temperature just the hydrogen bonds are broken whereas the bonds of the backbone stay intact.
- Hybridization step - The temperature of this step depends on the primers' features, such as length and base composition, because the aim is the specific anneal of the primers to the target sequence. One primer hybridizes to the 3' end of the target on

one strand, and the other primer hybridizes to the 3' end on the complementary target strand.

- Extension step - The solution temperature is raised up to 72°C at which the DNA Polymerase starts the amplification of the new dsDNA molecules, which are identical to the target DNA.

The detection of PCR products, called also amplicons, is generally done by gel electrophoresis, which involves the use of DNA intercalators, which are generally toxic. The main disadvantage of the PCR for DNA sensing is the need of a strictly temperature control, which involves the use of a thermalcycler. Furthermore the integration of such temperature controller in a portable device results in a very complicate process. For this reason many techniques which allow the amplification of DNA molecules at a constant temperature have been developed. Detailed information about these techniques has been extensively reported in the literature.<sup>18</sup>

### ***7.2.3 What nanoparticles can bring to DNA sensors***

NMs and especially NPs have been extensively used in various optical and electrochemical DNA sensors. NP properties such as large fraction of surface atoms, high surface energy, spatial confinement and reduced imperfections do not exist in the corresponding bulk materials<sup>19</sup> making them with interest in the design of DNA sensors. Gold nanoparticles (AuNPs) are the most used NPs in biosensing not only of nucleic acids but also of other biomolecules. AuNPs have some unique features such as: an easy synthesis, a surface plasmon resonance effect, a catalytic activity, a good biocompatibility and an easy functionalization. In particular the functionalization is essential in the development of a biosensor and in the case of AuNPs it happens generally through the Au-S bond, using biomolecules modified with a thiol group. In the case of DNA, generally a ssDNA is modified with a thiol group on its 3' or 5' end. Beside AuNPs other types of NPs are also considered in this chapter: silver NPs (AgNPs), lead sulfide NPs (PbSNPs), cadmium sulfide NPs (CdSNPs), magnetic NPs, etc. In general all the mentioned NPs act as labels or carriers of other labels while being employed in DNA detection. AuNPs, beside few other metallic NPs, are also used as modifiers of the electrotransducers in order to enhance their electroactive surface.<sup>20,21</sup>

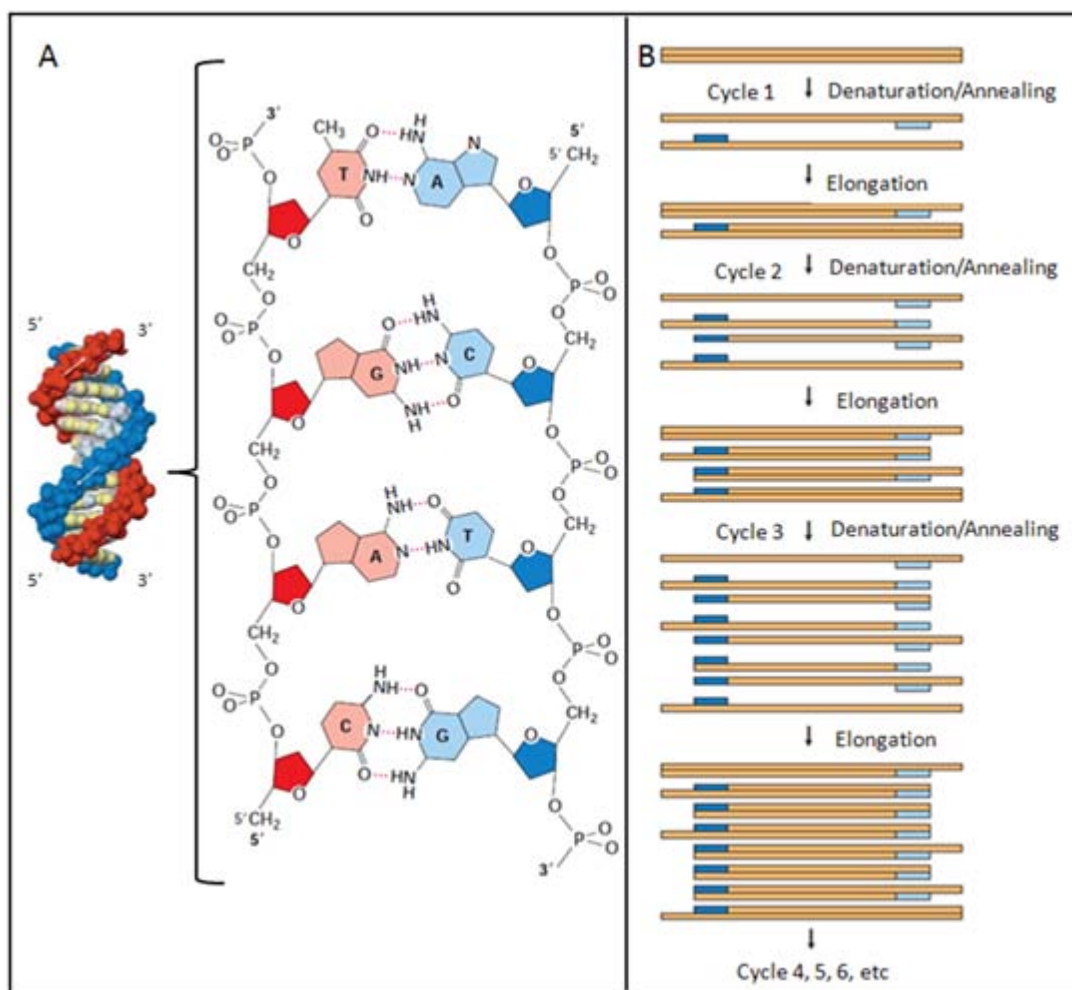


Fig.1: A) Space filling model and chemical structure of DNA double helix; B) PCR scheme. Adapted with permission from ref 22-24.

#### 7.2.4 Designs of electrochemical DNA biosensors

The first and most used DNA sensor design is based on the formation of a “sandwich” between a capture probe, the DNA target and a detection probe (Figure 2A). The three DNA molecules involved are ssDNA. The capture probe and the detection probe are complementary to the two different ends of the target molecule. The capture probe is generally attached directly to the electrode surface or to the surface of magnetic beads and its function is to recognize the target sequence. In a second step the detection probe recognizes the captured target DNA and this hybridization is followed by a second

hybridization step with the detection probe bearing an electroactive label ( i.e. AuNPs).<sup>9,22</sup>

It is also possible to design a DNA sensor starting from the dsDNA produced by PCR (Figure 2 B). In this case it is important to label the two primers with two different molecules obtaining in this way at the end of the PCR many dsDNA molecules modified at each end with a specific label. Generally one primer carries biotin, to perform in a second step the streptavidin/biotin bond, and the other primer a thiol or a protein ( i.e. digoxigenin ), to be attached to NPs directly or through an antibody ( i.e. anti-digoxigenin) attached to the NPs.<sup>23</sup>

Another way to detect DNA, in particular SNPs, is based on the use of monobases labeled with a marker (Figure 2C). In fact when a mismatch is present in a dsDNA, there is an error in the hybridization and the conformation of the dsDNA is not so closed, making the base of the mismatch available to interact with a free base. In this way using a solution of a known monobase modified with a label, such as AuNPs, it is possible to electrochemically detect if a SNP is present in the dsDNA target.<sup>24</sup>

A quite new approach consists in the use of stem loop ssDNA (Figure 2D). These molecules are a particular kind of ssDNA able to hybridize in two regions of their own sequence. This makes them obtaining a conformation where the two ends of the ssDNA are closed. If the target ssDNA is present, it hybridizes with the stem loop opening the conformation and making the two ends free.<sup>25</sup>

Finally it has to be mentioned that DNA can interact not only with other DNA molecules, but also with DNA binding proteins, peptide nucleic acid and ribonucleic acid (RNA).<sup>26</sup>

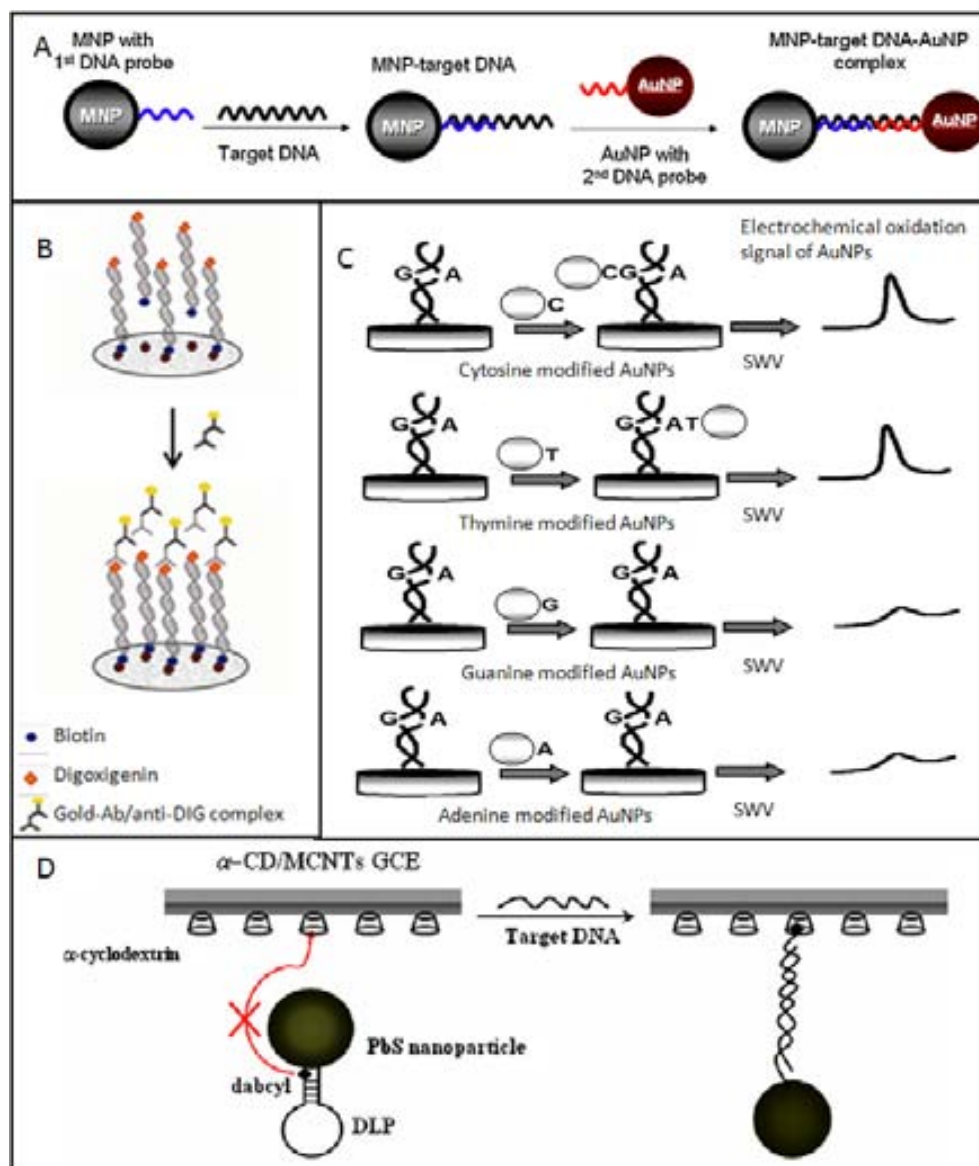


Fig. 2: Designs of electrochemical DNA biosensors. A) example of magneto-sandwich assay. B) Stem-loop based DNA sensor. C) Labeled mono-base DNA sensor scheme. D) DNA sensor based on double labeled PCR product scheme. Adapted with permission from ref. 25-28

## 7.3 Applied technologies

### 7.3.1 Gold nanoparticles based technologies

The excellent electroactivity of metallic NPs together with their easy bioconjugation, has given rise to their extensive use as labels in DNA sensors. Several electrochemical routes have been exploited for the sensitive detection of these NPs tags in bioassays.

In this section several examples of electrochemical DNA biosensors based on the use of AuNPs as labels/carriers first or as electrodes modifiers are considered.

#### 7.3.1.1 Gold nanoparticles as electroactive and catalytic labels

The excellent electroactivity of AuNPs together with their catalytic activity towards other reactions have allowed their application in various DNA sensing strategies.

For example, Yeung et al.<sup>27</sup> developed DNA biosensors integrated in a microchip for the multiplexed detection of *Escherichia coli* and *Bacillus subtilis* cells. The developed device contains a thin-film heater and temperature sensor patterned on the silicon substrate while indium tin oxide electrodes integrated inside the reaction microchamber are used as transduction element modified with DNA strands. The chip performed all the steps required: the thermal lysis of pathogens, the magnetic particle-based isolation of the target genomes, the asymmetric PCR, and the electrochemical sequence-specific detection using AuNP labels. In this case, the catalytic activity of the AuNPs on the silver reduction is approached to selectively deposit silver on their surface, followed by the electrochemical oxidative dissolution of the silver ions which is measured and related with the concentration of cells at levels of  $10^2$  cells/sample.

A similar approach based on the use of streptavidin modified AuNPs and biotinylated probes was performed by Pinijsuwan et al.<sup>28</sup> taking advantage also of the use of latex microspheres as carriers of the AuNPs labels (Figure 3A). The authors immobilized the target DNA onto a screen printed carbon electrode and then the hybridization with a complementary sequence modified with biotin was performed. Finally the AuNPs-Streptavidin loaded onto the latex microspheres were captured by the streptavidin-biotin bond. The AuNPs were detected by anodic stripping voltammetry after the NP chemical dissolution/oxidation obtaining a limit of detection of 0.5 fM.

Castañeda et al.<sup>29</sup> took advantage of the easy isolation of specific DNA sequence by magnetic particles (Figure 3B). In fact the authors used the AuNPs as labels in a magneto-sandwich assay. In details they detected two sequences: one related to BRCA1 and one to cystic fibrosis. They used magnetic microparticles modified with streptavidin, in order to easily attach the capture probe modified with biotin, to concentrate the target sequences. Then the use of a detection sequence functionalized with AuNP allowed them to detect the analyte performing in this case a direct voltammetric detection of the AuNPs without previous dissolving, by simply electrochemical oxidizing their surface. Then the detection was done measuring the electrochemical reduction of the generated Au(III) ions by differential pulse voltammetry on graphite-epoxy electrodes (modified with a magnet) reaching a limit of detection of 0.198 µg/mL.

A similar approach was performed by Torres-Chavolla et al.<sup>22</sup> They detected the *Mycobacterium tuberculosis*, combining the thermophilic helicase-dependent isothermal amplification, amine-terminated magnetic particles and dextrin coated AuNPs. In particular the authors first amplified the DNA of interest by the thermophilic helicase-dependent isothermal amplification, and then the amplicons produced were hybridized in a sandwich like assay. The AuNPs were finally detected by the same direct voltammetric approach explained above, using screen-printed carbon electrodes and obtaining a detection limit of 0.01 ng/µL of isothermally amplified target.

A different platform was used by Liao and coworkers.<sup>30</sup> The authors developed a very sensitive DNA sensor for the detection of the mutated B-RAF gene associated with papillary thyroid carcinomas based on a 96 well micro-plate streptavidin modified. The authors first attached to the wells the biotinylated capture probes; then the target sequence modified also with biotin was added and allowed to hybridize with the capture probe. Streptavidin-modified AuNPs were then added and finally dissolved in bromide, being the generated gold ions detected by square wave stripping voltammetry technique using a glassy carbon electrode. The authors obtained a limit of detection of 0.35 aM.

A DNA biosensor based on the use of stem loop instead of sandwich was proposed by Fan and collaborators (Figure 3C).<sup>31</sup> They developed a device based on a stem loop ssDNA which was modified with AuNPs on one end and with dabycil on the other end. In ssDNA conformation the two ends of the ssDNA are very close, making the dabycil impossible to interact with the cyclodextrin immobilized on glassy carbon electrodes modified with multiwalled carbon nanotubes. On the other hand in the presence of the

complementary sequence the dabcyl was free to interact with the cyclodextrin attaching the dsDNA, and consequentially the AuNPs, to the electrode. Detecting the AuNPs by the direct voltammetric approach explained before, a limit of detection of  $2.6 \times 10^{-10}$  M DNA target was reached, differentiating also single mismatches.

An example of the approaching of the catalytic properties on the reduction of chemical compounds is the work of Selvaraju et al.<sup>32</sup>, where the AuNPs were used as catalyzers of the generation of p-aminophenol starting from p-nitrophenol and NaBH<sub>4</sub> (Figure 3D). The p-aminophenol is then electrooxidized to p-quinoneimine at the electrode. The p-aminophenol redox cycling by NaBH<sub>4</sub> offers large signal amplification. The authors used a magnetosandwich format to concentrate the AuNPs onto an indium tin oxide electrode. In this way a limit of detection of 1 fM of target ssDNA was reached.

It deserves to be mentioned also the different approach reported by Kerman and coworkers.<sup>24</sup> The authors detected SNP using monobase-modified AuNPs. In fact the monobase can hybridize the dsDNA just in the presence of a SNP using the DNA polymerase. In this way it was possible not only to detect the presence of SNPs but also which bases were involved detecting in this case the oxidation signal of Au by square wave voltammetry.

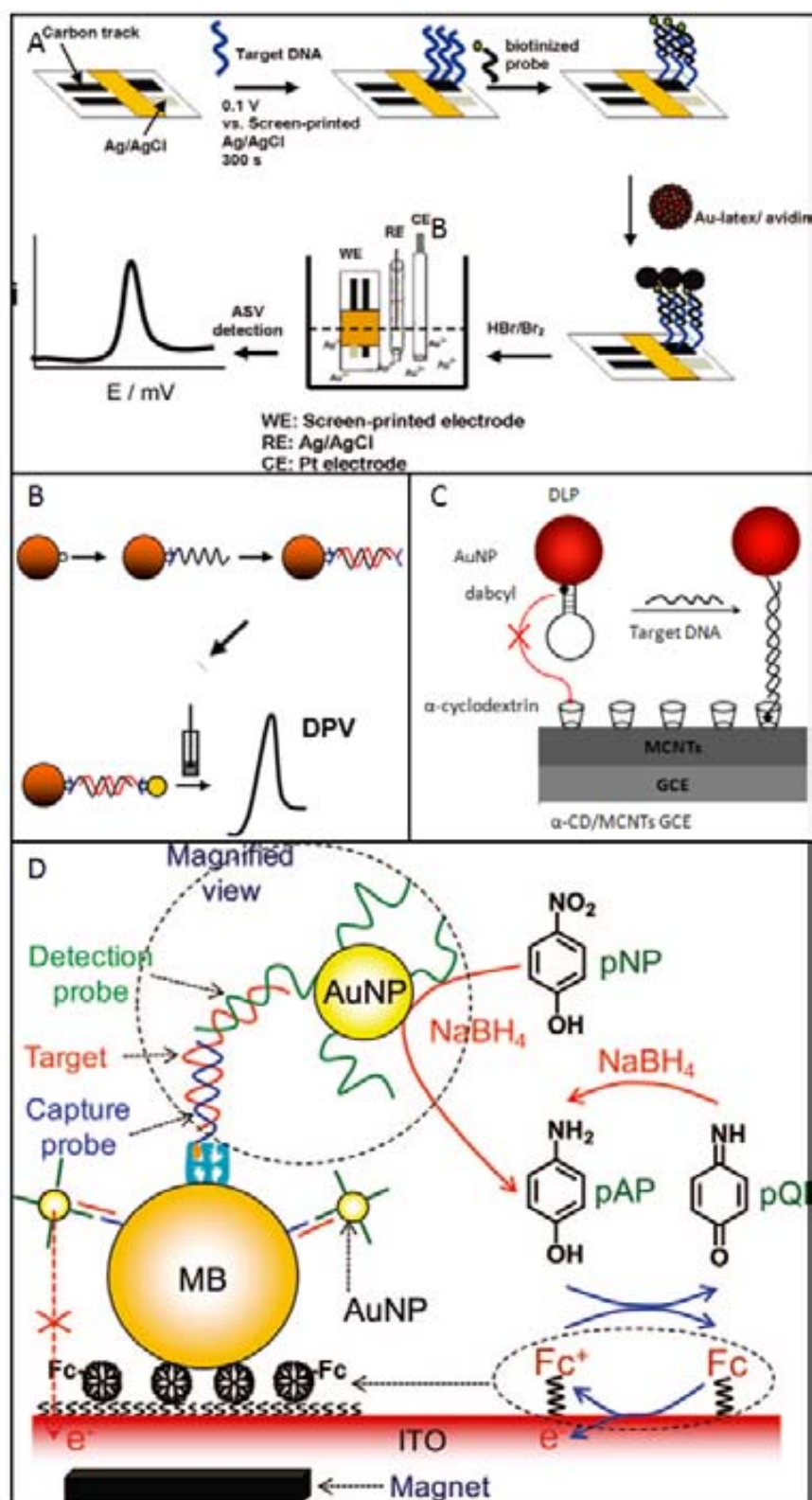


Fig. 3: AuNPs as electroactive and catalytic labels. A) Magneto sandwich assay using AuNPs. B) AuNPs used in a stem loop based DNA biosensor. C) AuNPs carried by Latex microspheres. D) AuNPs as catalyst. Adapted from [31,32,34,35]

### 7.3.1.2 Gold nanoparticles as signal amplifiers and carriers of other labels

The presence of AuNPs attached to the electrotransducer surface through the DNA hybridization reaction produces an increase in the conductivity of the surface, exerting an amplification effect in detection strategies based in both conductimetric/impedimetric measurements.

Park et al.<sup>33</sup> used the catalytic silver deposition onto AuNPs to detect DNA, taking advantage in this case of the changes in the conductivity of a microelectrode (60-nm Au on 5-nm Ti) produced by the presence of the silver catalytically deposited on the AuNPs. First they performed a classical sandwich assay with the AuNPs attached to the detection probe, and then they measured the difference in conductivity after silver deposition, which is enhanced by the presence of AuNPs. In this way a limit of detection of 500 fM was achieved.

The changes on the electron transfer resistance on the electrode surface by the presence of AuNPs without any amplification were approached by Gao et al.<sup>34</sup> for the DNA detection (Figure 4A). The authors first immobilized onto a gold electrode ssDNA, and then AuNPs were attached to the ssDNA. In this way the electron transfer resistance decreased. In the presence of the complementary sequence the AuNPs were displaced resulting in an increase of the impedance, indicating the hybridization events.

Bonanni et al.<sup>[26]</sup><sup>23</sup> took advantage of the strength of the PCR in order to amplify specifically the target sequence and, at the same time, using modified primers, obtaining a dsDNA modified with biotin in one end and with digoxin on the other end of the dsDNA. In this way they could concentrate the PCR amplicons to the streptavidin modified electrode surface. In a second step the digoxin was recognized by an antibody specific for the digoxin. Finally using a secondary antibody functionalized with AuNP the authors could increase the impedimetric response of an avidin bulk-modified graphite-epoxy biocomposite electrode from 4fM to 0,04 fmol.

A special case of the use of AuNPs as signal amplifiers was recently proposed by De la Escosura-Muñiz et al.<sup>35</sup> The authors developed an innovative DNA hybridization biosensor based on the use of nanoporous alumina filter membranes attached onto the working area of a SPCE (Figure 4B). The membrane contained nanochannels (200 nm in diameter and thickness of 60 nm) which were functionalized by a capture ssDNA probe and the presence of the complementary ssDNA target was detected through the decrease in the voltammetric signal of the  $[\text{Fe}(\text{CN})_6]^{4-/3-}$  redox system, due to both

steric and electrostatic effects. Using AuNPs labels as additional blockage agents, they detected ssDNA at levels of 42 ng/mL.

Finally, an example of the use of AuNPs as carriers of other electrochemical labels was the work of Thiruppathiraja et al.<sup>36</sup> The authors could detect the genomic DNA of *Mycobacterium* s.p. in a clinical specimen using AuNPs loaded with an alkaline phosphatase enzyme as signal amplifier. The authors first modified the indium tin oxide electrode surface with AuNPs in order to attach easily a capture probe. Then, they incubated the electrode with the sample and finally with a dual label AuNPs, which carried a DNA detection sequence and the enzyme. The alkaline phosphatase hydrolyses the para-nitrophenol phosphate and the reaction was characterized by voltammetric and impedimetric measurements. The authors studied both genomic DNA and spotted samples, reaching a detection limit of 1.25 ng/mL of genomic DNA.

AuNPs has also been used as carriers of other NPs<sup>37</sup> which are finally detected taking advantage of their electroactive properties, as it will be explained in section 7.3.2.4.

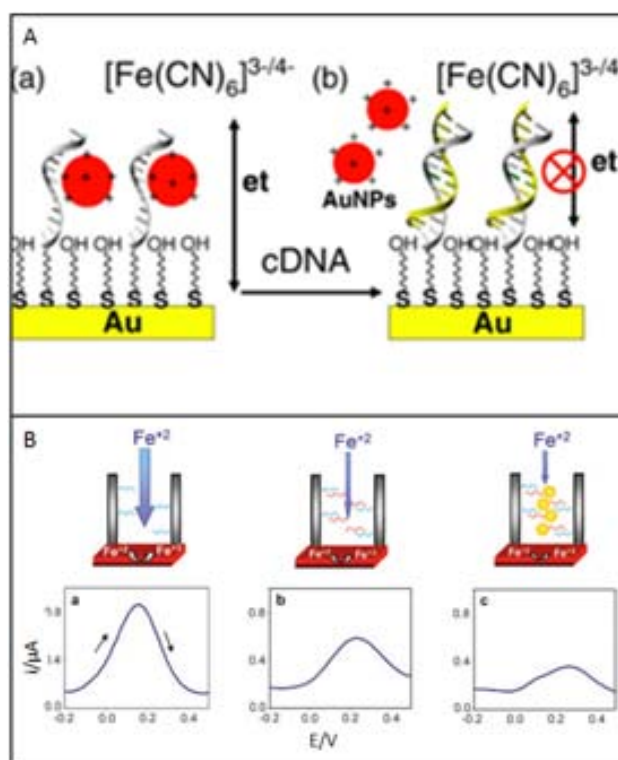


Fig. 4: AuNPs used as amplifiers. A) Displacement of AuNPs by hybridization affects electron transfer B) AuNPs as amplifiers in a nanochannels based DNA sensor. Adapted from [37,38]

### 7.3.1.3 Gold nanoparticles as modifiers of electrotransducers

Attempts to develop DNA hybridization assays using nanostructured surfaces have been reported in the last few years. The introduction of NPs into the transducing platform is generally achieved by their integration within conventional electrodes in various forms, including that of a composite.<sup>38</sup>

Li et al.<sup>39</sup> generated a mercaptophenyl film onto a glassy carbon electrode by electrografting. Then the modified electrode surface was dipped in AuNP solution for 6 hours in order to obtain AuNP modified electrode. In a second step the thiolated DNA probe was attached to the AuNPs. Finally the hybridization was detected by differential pulse voltammetry of  $\text{Co(phen)}_3^{3+}$  as the electrochemical indicator with a limit of detection of  $7.2 \times 10^{-11}$  M. In a previous work<sup>40</sup> the same authors proposed a similar approach but based on the use of mercapto-diazoaminobenzene monolayer obtaining a detection limit of  $9.10 \times 10^{-11}$  M.

Instead of using classical AuNPs, Li et al.<sup>41</sup> produced a very sensitive electrode for DNA sensing based on the formation of dendritic gold nanostructures onto a planar gold electrode applying a potential of -1.5V and a solution of 2.8mM  $\text{HAuCl}_4$  and 0.1M  $\text{H}_2\text{SO}_4$  (Figure 5A). With such electrode the authors studied the hybridization events of two DNA sequences, reaching a detection limit of 1 fM performing cyclic voltammetry and differential pulse voltammetry of methylene blue, used as electrochemical hybridization indicator.

Also Liu et al.<sup>42</sup> developed a DNA hybridization biosensor based on hollow gold nanospheres prepared using Co nanoparticles as sacrificial templates (Figure 5B). After the immobilization of the hollow gold nanospheres onto the gold electrode, the authors functionalized them with capture ssDNA to detect the hybridization events. A limit of detection of 1 pM was achieved with a range of detection between 1pM and 10 nM measuring the cyclic voltammetry and differential pulse voltammetry of  $\text{Co(phen)}_3^{3+}$ , which has high affinity for dsDNA and not for ssDNA.

A different approach was proposed by Spain et al.<sup>43</sup> They developed a DNA biosensor based on the growth of AuNPs onto Polyaniline nanofibres. The nanocomposite material produced was deposited onto a gold electrode. Then a sandwich assay, which detected a DNA sequence specific of *S. aureus*, was performed with a DNA strand

modified with horseradish peroxidase (HRP) as a detection probe. The signal measured was the reduction of a hydroquinone mediator in solution. A limit of detection of pM level was obtained, without the need of amplification. Also Hu and coworkers<sup>44</sup> used a nanocomposite material combining graphene sheets and AuNPs to obtain a DNA sensor. First they modified the graphene sheets with 3,4,9,10-perylene tetracarboxylic acid to obtain a good separation of them and increase the number of negatively-charged  $-\text{COOH}$  sites. In this way the efficiency of decoration of the graphene sheets with AuNPs was increased. The AuNPs were synthesized by reduction of  $\text{HAuCl}_4$  by amine-terminated ionic liquid ( $\text{NH}_2\text{-IL}$ ). This green synthesis produced 3 nm homogeneously dispersed  $\text{NH}_2\text{-IL}$  protected AuNPs, which, in combination with the highly negatively charged graphene sheets, allow the electrostatic interaction and adsorption of DNA without the need of its modification. Finally, impedimetric measurements allow them to detect the hybridization event, obtaining a limit of detection of  $3.4 \times 10^{-14} \text{ M}$ .

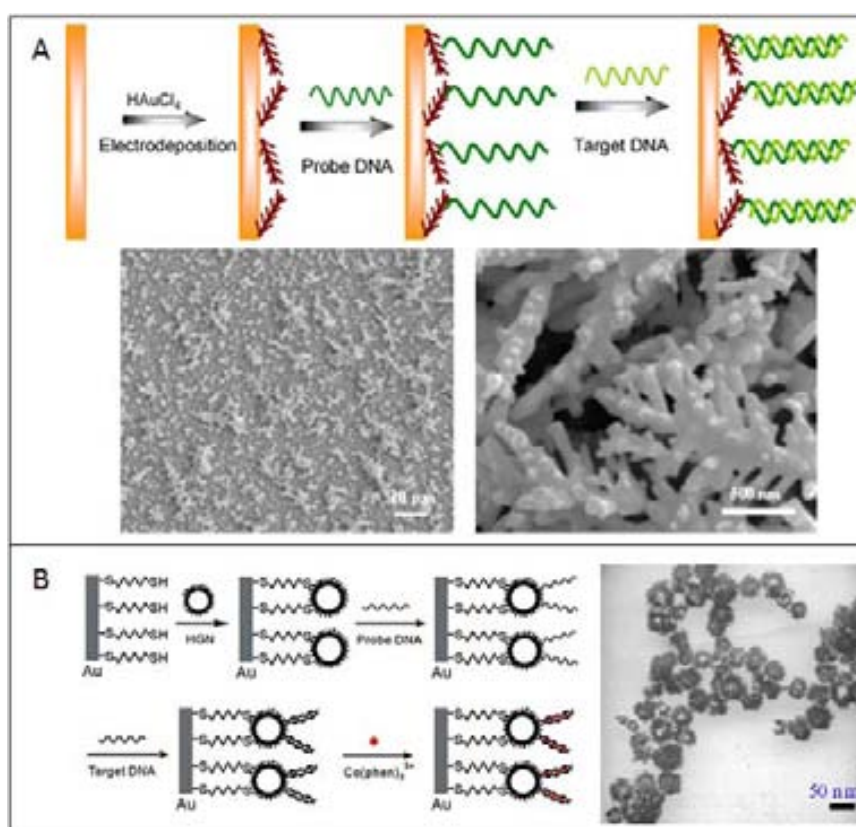


Fig 5: AuNPs used as transducer modifiers. A) Dendritic gold nanosstructure used in a planar gold electrode. B) Hollow gold nanospheres onto a gold electrode. Adapted from [44,45]

### 7.3.2 *Other nanoparticles*

#### 7.3.2.3 *Silver nanoparticles*

Silver nanoparticles (AgNPs) are other NPs with high interest in electrochemical biosensors due to their high electroactivity, although some drawbacks related to their synthesis and toxicity has minimized their extensive use. Kong et al.<sup>45</sup> took advantage of the use of AgNPs for the detection of DNA by measuring the differences in conductance in interdigitated microelectrodes. First they immobilized peptide nucleic acid in the gaps of the electrodes, and then the complementary DNA sequence hybridized with the peptide nucleic acid molecules. In the next step hematin molecules were introduced into the DNA strand via zirconium-phosphate and zirconium-carbonate chemistries. The hematin catalyzed the reduction of silver ions into AgNPs, which span the gap between electrodes. The limit of detection of 1 fM was achieved.

A different approach was proposed by Jian and coworkers.<sup>46</sup> They developed a DNA biosensor based on the aggregation of AgNPs. First they modified a gold electrode with a capture ssDNA, which recognizes the short target ssDNA. Then biotinylated AgNPs functionalized with signalling ssDNA were associated to the target strands. In a further step streptavidin was added to bind the biotin of the AgNPs. Finally solution of unlabelled biotinylated AgNPs was added inducing the aggregation of the NPs. The aggregates were detected taking advantage of impedimetric measurements, allowing a detection limit of 10 fM.

#### 7.3.2.4. *Semiconductor nanoparticles*

The use of semiconductor nanoparticles with different compositions the so-called quantum dots, has enormous potential in multidetection designs, since each of these materials can give rise to a specific electrochemical signal characteristic of the contained metal (i.e. Pb, Cd, Zn etc.). Furthermore, the conditions for the electrochemical detection are generally less aggressive (less acidic conditions, lower potentials) which can be advantageous for some biosensing designs.

Fan et al.<sup>25</sup> developed a biosensor to study the hybridization events based on the use of a double tagged stem loop: on one end with dabcyl, on the other end with PbNPs, a similar conformation as the commented in section 7.3.1.1. In the closed conformation

the dabycil cannot interact with the  $\alpha$ -cyclodextrin present on the surface of the multi walled carbon nanotube modified /glassy carbon electrode, but when the stem loop is opened with the complementary DNA sequence the dabycil interact with the  $\alpha$ -cyclodextrin making possible the PbNPs detection. In this way, it was possible obtaining a limit of detection of  $7.1 \times 10^{-10}$  M by measuring the voltammetric signal of Pb in a mercury-film electrode. The same authors proposed a similar approach based on the use of CdS-NPs.<sup>47</sup> In this work the electrode was  $\alpha$ -CD modified Poly(N-acetylaniline) glassy carbon electrode.<sup>48</sup> The stem loop probes were used also by Kjällman et al in combination with CdTe NPs to detect up to 4,7 fM DNA molecules by impedance spectroscopy in a gold electrode.

Different uses of PbNPs and CdSNPs were reported by Hu et al. and Zhu et al. In the first work [40]<sup>37</sup> the authors report a DNA hybridization biosensor based on bio barcode using PbNPs and nanoporous gold glassy carbon electrode. The device is based on the formation of a sandwich between the capture probe attached to the glassy carbon electrode and the detection probe of the label. In this case the label consists of AuNPs carrying the PbNPs and the detection sequence. The authors reached a limit of detection of  $2.6 \times 10^{-16}$  M DNA target detecting the Pb released from the NPs by anodic stripping voltammetry. In the work of Zhu et al.<sup>49</sup>, the hybridization of DNA was detected by the use of CdS nanocluster and mercury modified glassy carbon electrode. First they modified the electrode surface with pyrrole in order to attach the target DNA and then they hybridized it with CdSNPs modified DNA. They used the ASV to detect the released Cd ions and obtained a limit of detection of 0.2 pmol/L.

Dong et al., created a new label based on the functionalization of poly(styrene-co-acrylic acid) microbeads with CdTe quantum dots. The quantum dots were carried by the microbeads and functionalized with streptavidin in order to bind the biotin of a detection probe of a sandwich assay, where the capture probe was attached to a glassy carbon electrode. In this way up to 0.52 fM DNA sequence related to breast cancer was detected.<sup>50</sup> A different type of DNA hybridization biosensor was developed by Chen et al.<sup>51</sup> taking advantage of the specificity of the BfuCI nuclease for a particular 4 nucleotides long dsDNA. In detail a stem loop modified with CdSe/ZnS core shell NPs can be cleaved having the enzyme recognition sequence, making the quantum dots washed away. On the other hand if the complementary sequence was present the nuclease was not able to cut the strand (in fact it would hybridize in a different region leaving the nuclease recognition site in a ssDNA conformation). In this work two

different electrodes were used: first a gold electrode to perform all the hybridization events and then, after the dissolution of Cd into nitric acid solution, a mercury modified electrode to detect the Cd ions. In this way it was possible to achieve a detection limit of  $3.3 \times 10^{-14} \text{ M}$ .

Finally an interesting multidetection DNA hybridization biosensor design was developed by Hansen et al. The authors used three different sulfide NPs to detect electrochemically three different target sequences: CdS, ZnS and PbS (Figure 6A). Each type of NP was functionalized with a specific sequence complementary to one of the three sequence immobilized onto the electrode. Then using stripping analysis after the NPs dissolving/oxidation it was possible to detect the three different NP labels down to 100 aM.<sup>52</sup>

#### 7.3.2.3 Other nanoparticles

The advantageous properties of NPs with different compositions than the detailed in previous sections have also approached, in a minor extent, for the electrochemical detection of DNA.

A classical sandwich assay was proposed by Cai et al.<sup>53</sup> using Cu@Au alloy nanoparticles as labels. The electrochemical signal was recorded by using a glassy carbon electrode and performing the ASV of released Cu ions obtaining a detection limit of 5.0 pM.

Dong et al., developed a DNA biosensor based on the use of electrochemically reduced graphene oxide modified electrode, where they adsorbed thiolated DNA strands, which hybridize with DNA strands attached to AuNPs (Figure 6B).<sup>54</sup> In a further step the target DNA modified with biotin hybridizes with the DNA of the AuNPs. Finally carbon nanoparticles modified with streptavidin and HRP were used as labels. The limit of detection of 5 aM was reached measuring the differential pulse voltammetry signal of the HRP. The range of detection was between  $1 \times 10^{-17} \text{ M}$  and  $1 \times 10^{-13} \text{ M}$ . Another work based on the use of HRP as label was reported by Li et al.<sup>55</sup> They could detect up to 0.01 pM of DNA target or 500 cfu/ml of *E. Coli* cells, without nucleic acid amplification step, using Fe<sub>2</sub>O<sub>3</sub>@Au core/shell nanoparticles and a probe modified with HRP in a sandwich assay. The Fe<sub>2</sub>O<sub>3</sub>@Au core/shell nanoparticles have two functions: the functionalization with the capture sequence through the gold and the magnetic separation thanks to the Fe<sub>2</sub>O<sub>3</sub> paramagnetic properties. The amperometric detection of

the enzymatic reaction of reduction of 2,2'-diaminoazobenzene catalyzed by the HRP was finally detected.

Another enzyme was used by Chen et al.<sup>56</sup> The authors developed a biosensor based on a sandwich assay and the use of glucose oxidase as a label. The detection probe was modified with streptavidin to bind the avidin-labeled glucose oxidase. The capture probe was attached to the gold electrode. The signal was produced by enzyme-catalyzed deposition of cupric hexacyanoferrate (CuHCF) nanoparticles in the presence of glucose, cupric ions and ferricyanide. The limit of detection was 1 fM, obtained with differential pulse voltammetry measurements of the oxidation of the deposited NPs.

Similar to Fe<sub>2</sub>O<sub>3</sub>@Au core/shell nanoparticles, also alginic acid-coated cobalt magnetic beads used by Geng et al.<sup>57</sup> can be used both as a carrier and magnetic platforms. The beads capped with a 5-(NH<sub>2</sub>) oligonucleotide were used to detect a specific gene of E. Coli. The electrochemical detection was based on the use of daunomycin. It was observed that if the target sequence hybridizes with the target sequence the reduction peak of daunomycin decreases proportionally to the concentration of the hybridized target. With this method a limit of detection of 10 cells/mL in a real water sample, after an enrichment process, was obtained. In the work of Pal et al.<sup>58</sup> electrically active magnetic polymer (EAM) nanoparticles were also used as magnetic platforms and as labels in a sandwich type assay (Figure 6C). In particular the capture probe was modified with EAM NPs, whereas the detection probes with biotin. The complexes were washed using the magnetic properties of EAM NPs and captured to the surface of a streptavidin modified screen printed carbon electrode and the cyclic voltammetry registered reaching a detection limit of 0.01 ng/μL.

A different approach was followed by Kerman et al.<sup>59</sup> who developed a DNA biosensor based on ferrocene-conjugated chitosan nanoparticles and nuclease S1. On a gold electrode surface peptide nucleic acid sequence complementary to the target was fixed, and then the sample was added to the surface. If the hybridization was perfect the nuclease would not cut the DNA target, but if a mismatch was present the DNA target would be degraded. The ferrocene-conjugated chitosan nanoparticles were sensitive to DNA target only in the way that when it was present the label got accumulated and consequently an increase of the voltammetric signal of the ferrocene appears reaching a detection limit up to 1 fM.

Liao et al.<sup>60</sup> used liposomes to carry [Ru(NH<sub>3</sub>)<sub>6</sub>]<sup>3+</sup> as redox indicator in a DNA sensor. First they modified SPCE with AuNPs in order to attach the capture probe. Then they

incubate with the target sequence and the liposomes, functionalized with a competitive DNA sequence. The limit of detection obtained measuring the voltammetric signal of the red-ox indicator was 0.75 amol (equivalent to the amount present in 5  $\mu$ L of a 0.15 pM solution) for a DNA sequence specific of *E. Coli*.

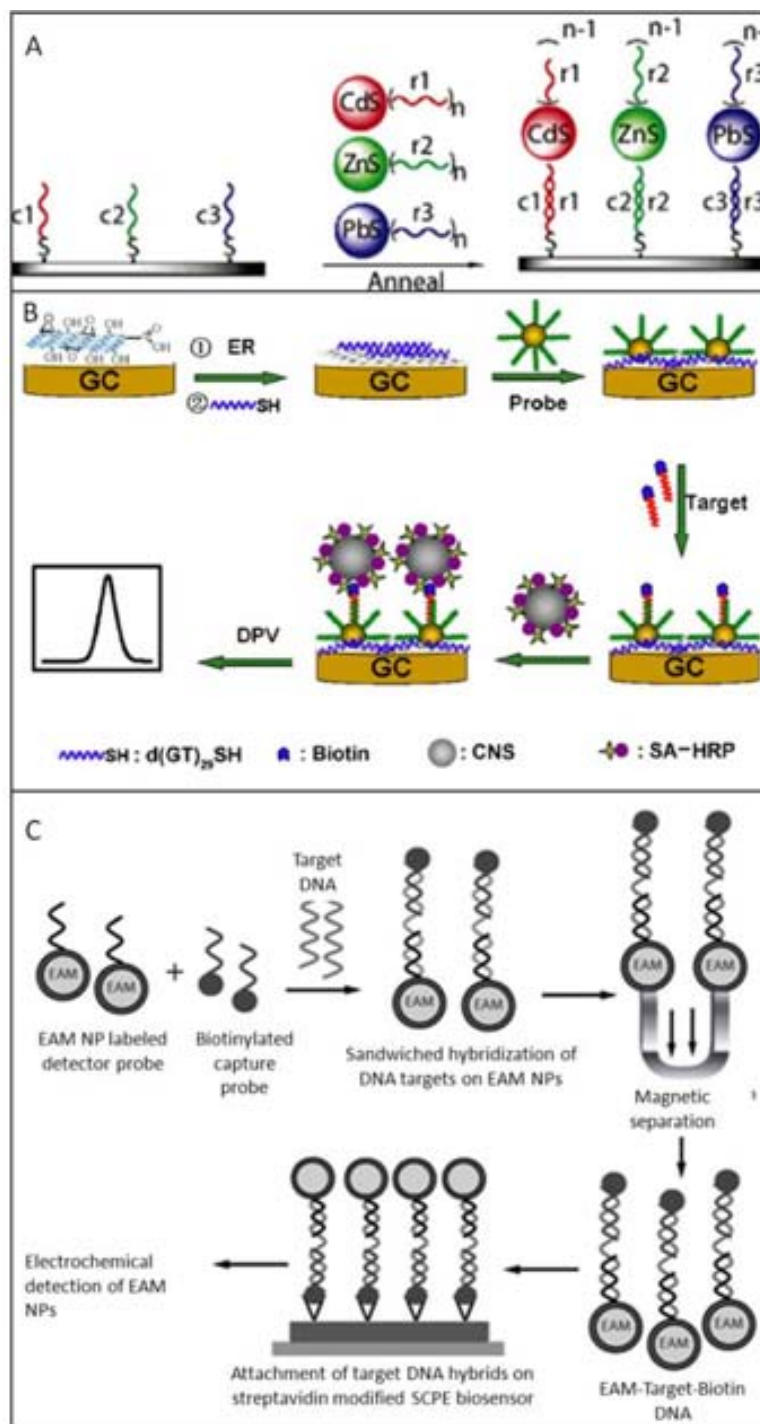


Fig.6: Other NPs. A) Sulfide based NPs for multiplex DNA detection. B) EAM NPs based DNA sensor. C) Triplex amplification based on graphene, AuNPs, Carbon NPs and HRP. Adapted with the permission from ref. 52, 54, 58 .

## 7.4 Conclusion and future perspective

Due to their sensitivity and specificity electrochemical DNA biosensors seem to be excellent devices for the detection of DNA. Furthermore electrochemical biosensors are easy to be integrated in various platforms (i.e. microfluidics) where the various assay steps can be included making them a good alternative for DNA detection in real samples. The synergy between the electrochemical detection and the use of NPs, as labels or as carriers, is giving to these devices higher sensitivities beside higher stability if compared to other technologies where enzymes or other labels are being used. Given the advances in nanotechnology in general and particularly that of NMs the cost of the NP based DNA biosensors is expected to go in line with mass production doing them ideal tools for future point of care and easy to use devices, for diagnostics, environmental and security applications.

An increase in the electrochemical DNA biosensor based on microchip devices can be noticed. Microfluidics platforms (lab on a chip or lateral flow devices) are the excellent avenues for an integrated DNA technology. These platforms are already integrating in a single device all the steps required for the detection of DNA: sample pre-treatment, amplification reaction, labeling, pre-concentration, detection. Such an integration level is expecting to better approach the DNA technology to point of care applications in many places with less resources and lack of specialized personnel to perform such analysis.

To further increase the sensitivity of DNA detection the integration of isothermal amplification techniques with electrochemical detection may expect to bring significant advantages. This integration may simplify much more the design and operation of DNA biosensors. The possibility to perform multi-detection of different DNA sequences or different SNPs in the same run (sample) can be simply reached by using various nanoparticles (with various electrochemical /catalytic properties). The parallel study of different DNA sequences with a cheap, fast and easy to use biosensor would significantly simplify the screening of mutations beside other applications.

## 7.5 References

- (1) Sassolas, A.; Leca-Bouvier, B. D.; Blum, L. J. *Chemical reviews* **2008**, *108*, 109–39.
- (2) Pérez-López, B.; Merkoçi, A. *Trends in Food Science & Technology* **2011**, 1–15.
- (3) Bonanni, a; Del Valle, M. *Analytica chimica acta* **2010**, *678*, 7–17.
- (4) Manuscript, A. *Aerospace Engineering* **2011**, *67*, 458–468.
- (5) de-los-Santos-Alvarez, P.; Lobo-Castañón, M. J.; Miranda-Ordieres, A. J.; Tuñón-Blanco, P. *Analytical and bioanalytical chemistry* **2004**, *378*, 104–18.
- (6) Erdem, A. *Talanta* **2007**, *74*, 318–25.
- (7) Hvastkovs, E. G.; Buttry, D. a *The Analyst* **2010**, *135*, 1817–29.
- (8) Tosar, J. P.; Brañas, G.; Laíz, J. *Biosensors & bioelectronics* **2010**, *26*, 1205–17.
- (9) Odenthal, K. J.; Gooding, J. J. *The Analyst* **2007**, *132*, 603–10.
- (10) Mir, M.; Homs, A.; Samitier, J. *Electrophoresis* **2009**, *30*, 3386–97.
- (11) De la Escosura-Muñiz, A.; Parolo, C.; Merkoçi, A. *Materials Today* **2010**, *13*, 24–34.
- (12) Perfézou, M.; Turner, A.; Merkoçi, A. *Chemical Society reviews* **2011**, *41*, 2606–2622.
- (13) Medina-Sánchez, M.; Miserere, S.; Merkoçi, A. *Lab on a Chip* **2012**, *12*.
- (14) Krishnan, Y.; Simmel, F. C. *Angewandte Chemie (International ed. in English)* **2011**, *50*, 3124–56.
- (15) Caliendo, A. M. *Clinical infectious diseases*: an official publication of the Infectious Diseases Society of America **2011**, *52 Suppl 4*, S326–30.
- (16) Mullis KB, F. F. *Methods Enzymol* **1987**, *155*, 335–50.
- (17) Beaudet, A. L.; Belmont, J. W. *Annual review of medicine* **2008**, *59*, 113–29.
- (18) Yang, S.; Rothman, R. E. **1830**, 337–348.
- (19) Merkoçi, A. *Biosensors & bioelectronics* **2010**, *26*, 1164–77.
- (20) Lord, H.; Kelley, S. O. *Journal of Materials Chemistry* **2009**, *19*, 3127.
- (21) Willner, I.; Willner, B. *Nano letters* **2010**, *10*, 3805–15.
- (22) Torres-Chavolla, E.; Alocilja, E. C. *Biosensors & bioelectronics* **2011**, *26*, 4614–8.

- (23) Bonanni, A.; Pividori, M. I.; Campoy, S.; Barbé, J.; Del Valle, M. *The Analyst* **2009**, *134*, 602–8.
- (24) Kerman, K.; Saito, M.; Morita, Y.; Takamura, Y.; Ozsoz, M.; Tamiya, E. *Analytical chemistry* **2004**, *76*, 1877–84.
- (25) Fan, H.; Zhao, K.; Lin, Y.; Wang, X.; Wu, B.; Li, Q.; Cheng, L. *Analytical biochemistry* **2011**, *5–9*.
- (26) Brandt, O.; Hoheisel, J. D. *Trends in biotechnology* **2004**, *22*, 617–22.
- (27) Yeung, S.-W.; Lee, T. M.-H.; Cai, H.; Hsing, I.-M. *Nucleic acids research* **2006**, *34*, e118.
- (28) Pinijsuwan, S.; Rijiravanich, P.; Somasundrum, M.; Surareungchai, W. *Analytical chemistry* **2008**, *80*, 6779–84.
- (29) Castañeda, M. T.; Merkoçi, a; Pumera, M.; Alegret, S. *Biosensors & bioelectronics* **2007**, *22*, 1961–7.
- (30) Liao, K.-T.; Cheng, J.-T.; Li, C.-L.; Liu, R.-T.; Huang, H.-J. *Biosensors & bioelectronics* **2009**, *24*, 1899–904.
- (31) Fan, H.; Xu, Y.; Chang, Z.; Xing, R.; Wang, Q.; He, P.; Fang, Y. *Biosensors & bioelectronics* **2011**, *26*, 2655–9.
- (32) Selvaraju, T.; Das, J.; Jo, K.; Kwon, K.; Huh, C.-H.; Kim, T. K.; Yang, H. *Langmuir: the ACS journal of surfaces and colloids* **2008**, *24*, 9883–8.
- (33) Park, S.-J.; Taton, T. A.; Mirkin, C. a *Science (New York, N.Y.)* **2002**, *295*, 1503–6.
- (34) Gao, Q.; Zhang, W.; Guo, Y.; Qi, H.; Zhang, C. *Electrochemistry Communications* **2011**, *13*, 335–337.
- (35) De la Escosura-Muñiz, A.; Mekoçi, A. *Chemical communications (Cambridge, England)* **2010**, *46*, 9007–9.
- (36) Thiruppathiraja, C.; Kamatchiammal, S.; Adaikkappan, P.; Santhosh, D. J.; Alagar, M. *Analytical biochemistry* **2011**, *417*, 73–9.
- (37) Hu, K.; Liu, P.; Ye, S.; Zhang, S. *Biosensors & bioelectronics* **2009**, *24*, 3113–9.
- (38) Liu, S.; Liu, J.; Wang, L.; Zhao, F. *Bioelectrochemistry (Amsterdam, Netherlands)* **2010**, *79*, 37–42.
- (39) Li, F.; Feng, Y.; Dong, P.; Yang, L.; Tang, B. *Biosensors & bioelectronics* **2011**, *26*, 1947–52.
- (40) Li, F.; Feng, Y.; Dong, P.; Tang, B. *Biosensors & bioelectronics* **2010**, *25*, 2084–8.
- (41) Li, F.; Han, X.; Liu, S. *Biosensors & bioelectronics* **2011**, *26*, 2619–25.

- (42) Liu, S.; Liu, J.; Han, X.; Cui, Y.; Wang, W. *Biosensors & bioelectronics* **2010**, *25*, 1640–5.
- (43) Spain, E.; Kojima, R.; Kaner, R. B.; Wallace, G. G.; O’Grady, J.; Lacey, K.; Barry, T.; Keyes, T. E.; Forster, R. J. *Biosensors & bioelectronics* **2011**, *26*, 2613–8.
- (44) Hu, Y.; Hua, S.; Li, F.; Jiang, Y.; Bai, X.; Li, D.; Niu, L. *Biosensors & bioelectronics* **2011**, *26*, 4355–61.
- (45) Kong, J. M.; Zhang, H.; Chen, X. T.; Balasubramanian, N.; Kwong, D. L. *Biosensors & bioelectronics* **2008**, *24*, 793–7.
- (46) Jiang, X.; Chen, K.; Han, H. *Biosensors & bioelectronics* **2011**, *28*, 464–468.
- (47) Kjällman, T. H. M.; Peng, H.; Soeller, C.; Travas-Sejdic, J. *The Analyst* **2010**, *135*, 488–94.
- (48) Fan, H.; Xing, R.; Xu, Y.; Wang, Q.; He, P.; Fang, Y. *Electrochemistry Communications* **2010**, *12*, 501–504.
- (49) Zhu, N.; Zhang, A.; He, P.; Fang, Y. *The Analyst* **2003**, *128*, 260–264.
- (50) Dong, H.; Yan, F.; Ji, H.; Wong, D. K. Y.; Ju, H. *Advanced Functional Materials* **2010**, *20*, 1173–1179.
- (51) Chen, J.; Zhang, J.; Yang, H.; Fu, F.; Chen, G. *Biosensors & bioelectronics* **2010**, *26*, 144–8.
- (52) Hansen, J. a; Mukhopadhyay, R.; Hansen, J. Ø.; Gothelf, K. V *Journal of the American Chemical Society* **2006**, *128*, 3860–1.
- (53) Cai, H.; Zhu, N.; Jiang, Y.; He, P.; Fang, Y. *Biosensors and Bioelectronics* **2003**, *18*, 1311–1319.
- (54) Dong, H.; Zhu, Z.; Ju, H.; Yan, F. *Biosensors and Bioelectronics* **2012**, *33*, 228–232.
- (55) Li, K.; Lai, Y.; Zhang, W.; Jin, L. *Talanta* **2011**, *84*, 607–13.
- (56) Chen, X.; Xie, H.; Seow, Z. Y.; Gao, Z. *Biosensors & bioelectronics* **2010**, *25*, 1420–6.
- (57) Geng, P.; Zhang, X.; Teng, Y.; Fu, Y.; Xu, L.; Xu, M.; Jin, L.; Zhang, W. *Biosensors & bioelectronics* **2011**, *26*, 3325–30.
- (58) Pal, S.; Alocilja, E. C. *Biosensors & bioelectronics* **2010**, *26*, 1624–30.
- (59) Kerman, K.; Saito, M.; Tamiya, E. *Analytical and bioanalytical chemistry* **2008**, *391*, 2759–67.
- (60) Liao, W.-C.; Ho, J.-A. A. *Analytical chemistry* **2009**, *81*, 2470–6.

## **Annex B**

Antibody-oriented functionalization of gold nanoparticle labels  
for very sensitive electrochemical biosensing



# Antibody-oriented functionalization of gold nanoparticle labels for very sensitive electrochemical biosensing

Claudio Parolo<sup>1</sup>, Alfredo de la Escosura-Muñiz<sup>1</sup>, Ester Polo<sup>2</sup>, Valeria Grazú<sup>2</sup>, Jesús M. de la Fuente<sup>2,3</sup> and Arben Merkoçi<sup>1,4\*</sup>

<sup>1</sup> ICN2 - Institut Català de Nanociència i Nanotecnologia, Campus UAB, 08193 Bellaterra (Barcelona), Spain;

<sup>2</sup> Instituto de Nanociencia de Aragón (INA), University of Zaragoza, Campus Río Ebro, Edificio I+D, Mariano Esquillor, s/n, 50018 Zaragoza, Spain

<sup>3</sup> Fundación ARAID, Zaragoza, Spain

<sup>4</sup> ICREA - Institutio Catalana de Recerca i Estudis Avançats, 08010 Barcelona, Spain

**KEYWORDS:** Gold nanoparticle labels, Antibodies, Oriented functionalization, Electrochemical biosensing, Immunosensor

---

**ABSTRACT:** We describe the development of a more efficient label for immunosensing, which is based on the oriented functionalization with antibodies of gold nanoparticles (AuNPs). The proposed method takes advantage of the high density of positive charges on the major plane of antibodies, when the pH of the solution is lower than the isoelectric point of the antibody. In this way, the interaction between the negatively charged AuNP surface and the antibodies happens via their major plane, allowing the free movement of the antigen binding sites for the maximum recognition of the analyte. The oriented ionic interaction is further fixed by the formation of a peptide bond between the amino group of the Lys residues and the carboxylic groups of the AuNP surface. The new label is characterized and its electrochemical performances are compared against a random AuNP-antibodies conjugate. The improvement in the limit of detection is of one order of magnitude. Finally, it is used for the detection of Human IgG in a real human serum.

---

## 1. Introduction

In the last two decades, many different types of nanomaterials such as gold nanoparticles (AuNPs), carbon nanotubes, quantum dots etc. have been integrated in different biosensing platforms.<sup>1,2</sup> They have been used taking advantage of their special properties that appear just at the nanometer scale. These behaviors can be used to improve already existing biosensing strategies or to develop new sensing methods. Between others, AuNPs are one of the most used nanomaterials, since they are not very toxic,<sup>3</sup> they can be easily prepared, modified and used in different sensing approaches.<sup>4,5</sup> In particular, the AuNPs can be prepared using different synthesis, which give rise to different sizes and shapes that reflect different properties, like plasmon resonance and catalytic activity, being of great relevance for their use as labels in various bioassays (including electrochemical sensing of DNA,<sup>6</sup> proteins,<sup>7</sup> cells<sup>8-10</sup> or even optical sensing<sup>11,12</sup>).<sup>13-15</sup> Anyway, these special intrinsic properties of AuNPs are not enough to make them great labels in bio-

assays.<sup>16</sup> In fact, the specificity of an affinity biosensor (immunosensors or DNA biosensor) is achieved by the biomolecules that are attached to the label that should recognize the analyte. Considering immunosensors case, a label-antibody conjugate that maintains the antigen binding sites available to capture the antigen is of extremely importance to obtain good performances from the devices.<sup>17</sup>

In this paper, we show how a proper antibody orientation affects the limit of detection (LoD) of an AuNP-label based immunosensor. In order to obtain a controlled functionalization, which leaves accessible the antigen binding sites, a two steps coupling reaction has been adapted.<sup>18,19</sup> This methodology couples an oriented ionic attraction with a strong covalent bond formation using carbodiimide chemistry.<sup>20</sup> The technique is based on the high concentration of positive charges in the major plane of an antibody, when the pH of the solution is lower than its isoelectric point (Fig. 1A). In such condition the NH<sub>2</sub>-groups of Lys residues are protonated generating

$\text{NH}_3^+$ . In this way, if the antibodies are in solution with negatively charged AuNPs, the probability of interaction between the surface of AuNPs and the major plane of the antibody is maximized. This controlled approximation allows the antigen binding sites to be available for the capture of the antigen. In order to charge negatively the AuNP surface and to allow the formation of the covalent bond, the NPs were covered with a carboxylated poly(ethylene glycol)(PEG). In fact, using the carbodiimide chemistry, a stable intermediate, an amine reactive sulfur ester, is formed onto the AuNP surface. This group is negatively charged and catalyzes the formation of the peptide bond

between the carboxylic groups of the PEG and the amino-groups of the Lys-residues (Fig. 1B).

In order to prove the better performances of this new label compared with those of a random functionalized gold nanoparticle (Fig. 1C), we used two different antibodies: an  $\alpha\text{HRP}$  and an  $\alpha\text{HIgG}$ . The first was used just as optical tool to verify that for a saturating amount of an antigen the new label could bind more HRP molecules, whereas the second was tested in an electrochemical magnetosandwich immunoassay. Finally, after providing the evidences that our new label works better than the other, we used it in the analysis of a real human serum.

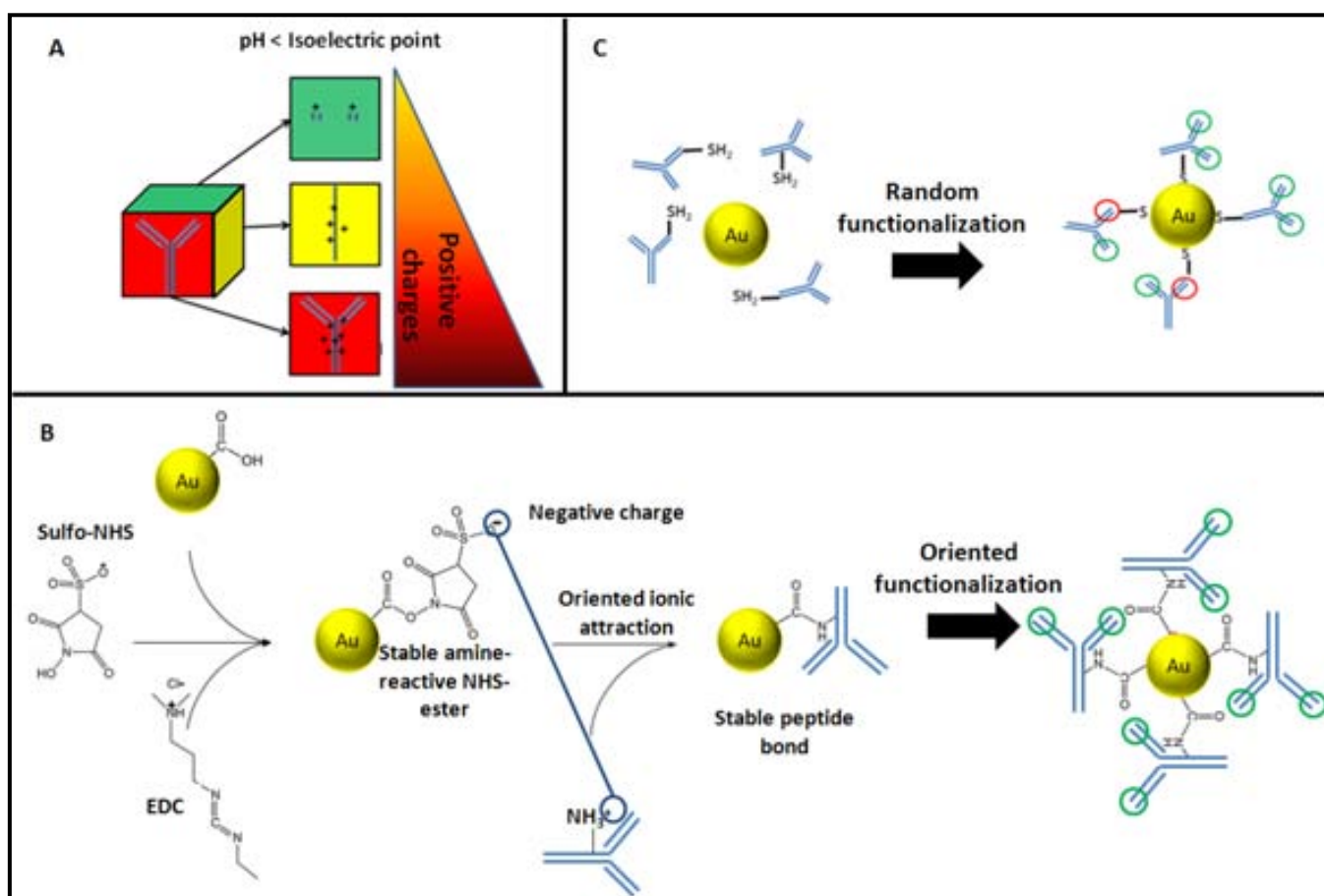


Fig.1: (A) Density of the positive charges on the antibody structure for pH lower than the isoelectric point of the antibody. The major plane (corresponding to the red square at the bottom) has the highest density. (B) Scheme of the oriented functionalization proposed based on the oriented ionic attraction and the formation of the peptide bond. (C) Scheme of the random adsorption of antibody onto the surface of AuNPs. NOTE: the schemes are not in scale.

## 2. Experimental Section

### 2.1. Chemicals and instruments

A Transmission Electron Microscope (TEM) Jeol JEM-2011 (Jeol Ltd, Japan) was used to characterize the AuNPs.

An ultrasonic bath (JP Selecta, Spain) was used to prevent agglomeration in the AuNP suspensions.

The isoelectric focusing of the Abs was carried out using the Pharmacia Phast System and PhastGel® IEF 3-9. The Bradford reagent (B6916) was purchased by Sigma Aldrich (Spain).

A thermostatic centrifugator Sigma 2-16 PK (Fisher Bioblock Scientific, France) was used to purify the conjugates of AuNPs with antibodies. Spectrophotometric measurements were performed using a Spectramax\_M2e multi-mode microplate reader (Molecular Devices Inc, UK).

A semi-automatic screen-printing machine DEK248 (DEK International, Switzerland) was used for the fabrication of the screen-printed carbon electrodes (SPCEs) (Fig S1 of S.I.). The reagents used for this process were Autostat HT5 polyester sheet (McDermid Autotype, UK), Electrodeag 423SS carbon ink, Electrodeag 6037SS silver/silver chloride ink, and Minico 7000 Blue insulating ink (Acheson Industries, The Netherlands). The detailed fabrication procedure is explained in S.I. Electrochemical measurements were performed at room temperature with an Autolab 20 (Eco-chemie, The Netherlands) connected to a PC.

Streptavidin-coated Magnetic Beads (M-280), with 2.8  $\mu\text{m}$  size, were purchased from Dynal Biotech (Invitrogen, Spain) and were used in the magnetosandwich immunoassay.

Hydrogen tetrachloroaurate (III) trihydrate ( $\text{HAuCl}_4 \cdot 3\text{H}_2\text{O}$ , 99.9%) and trisodium citrate ( $\text{Na}_3\text{C}_6\text{H}_5\text{O}_7$ ), were purchased from Sigma-Aldrich (Spain) and were used in the synthesis of AuNPs.

Bifunctional poly(ethylene glycol) SH-EG(8)-(CH<sub>2</sub>)<sub>2</sub>-COOH was purchased from Iris Biotech.

ABTS 2,2'-azino-bis (3-ethylbenzothiazoline-6-sulfonic acid) di ammonium salt, purchased from Sigma-Aldrich, was used as HRP substrate.

Human IgG whole molecule (I2511), antibody anti-human IgG whole molecule (produced in goat) (I1886), antibody anti-human IgG  $\gamma$ -chain specific biotinylated (produced in goat) (B1140), antibody  $\alpha$ HRP (produced in rabbit) (P7899), and peroxidase from horseradish Type VI, HRP (P8375) were purchased from Sigma Aldrich (Spain).

All buffer reagents and other inorganic chemicals were supplied by Sigma, Aldrich or Fluka, unless otherwise stated.

### 2.2. Gold Nanoparticle Synthesis and PEGylation

AuNPs of 14 nm were synthesized following the Turkevich<sup>21</sup> synthesis and analyzed by TEM (Fig. 2A). Briefly, first a solution of 0.508 mM  $\text{HAuCl}_4 \cdot 3\text{H}_2\text{O}$  [254  $\mu\text{M}$ ] in 49.492 mL  $\text{H}_2\text{O}$  was heated at 150°C and stirred. When the solution was boiling, 5 mL of sodium citrate [40 mM] were added rapidly. In the next 10 min of heating and stirring, the solution changed color from pale yellow to red and then was stirred for another 15 min at 25°C. The reflux was used for all the time to prevent loss of volume. The AuNPs were protected from light and stored at 4°C.

In order to use the AuNPs in the oriented functionalization, citrate prepared nanoparticles were covered with a dense layer of a bifunctional poly(ethylene glycol) SH-EG(8)-(CH<sub>2</sub>)<sub>2</sub>-COOH, with a thiol end to get covalently linked to the gold surface and a carboxylated residue to allow further functionalization using carbodiimide chemistry.<sup>20</sup> A solution of 0.5 mg/mL AuNPs, was mixed with SDS (0.025%) and PEG (0.024 mg/mL) under basic conditions for 16 h. PEGylated AuNPs were obtained after purification by centrifugation for 30 minutes at 13400 rpm.

### 2.3. Random AuNPs/antibodies conjugation

The random adsorption of antibodies onto the AuNP surface is based on the interaction between

the thiol groups of the antibodies (Cys-residues) with the gold atoms on the surface of the AuNPs (Fig 1C). First, the optimum conditions of pH and concentrations were found, performing a gold aggregation test (GAT).<sup>11</sup> The GAT consists in incubating, for 20 min at 650 rpm and 25° C in a 96 well microplate, 10 µL of antibodies at different concentrations (7.5, 10, 12.5, 15, 20 µg/mL in mQ water) with 150 µL of 3 nM AuNP solution, at pH 7, 8 and 9 (pH corrected with borate buffer 10 mM pH 9.2). After the incubation, 25 µL of NaCl 10% in mQ water were added, and the solutions were incubated for 5 min at 650 rpm and 25° C. At the end of the incubation, the absorbance spectra of the solutions were measured, from 300 to 700 nm of wavelength, in order to find the best conjugation condition, which is the pH that allows the use of the less amount of antibody to stabilize the AuNPs (the results obtained for αHRP are shown in S.I. as example).

According to the results obtained from the GAT, the conjugates were prepared incubating, at 25° C for 20 min, 1.5 mL of 3 nM AuNP solution with 100 µL of 20 µg/mL of the αHlgG at pH 9, or with 100 µL of 15 µg/mL of the αHRP at pH 7. After that, the conjugates were blocked by incubating the solution with 100 mL of 1 mg/mL BSA in mQ water, at 25° C for 20 min. Finally, a centrifugation (at 14000 X g at 4° C for 20 min) was carried out in order to purify the conjugates AuNPs/Abs and to re-suspend the pellets in mQ water.

#### 2.4. Oriented AuNPs/antibodies conjugation

The isoelectric points of the αHRP and the αHlgG antibodies were measured using the Pharmacia Phast System and PhastGel® IEF 3-9. Two different pH gradient gels were performed (one dispensing the samples at pH 3 and one at pH 7) according to Phast System Technique File No.100. 2 µL of 100 µg/mL antibodies were separated under 2000 V potential. Isoelectric focusing calibration kit for isoelectric point determination of proteins in the range of pH between 3 and 10 was used to generate standard curves from which isoelectric point of different antibodies were read. Proteins were fixed into the gels in

10% trichloroacetic acid immediately after the run and gels were silver stained according to the instructions of Pharmacia's Phast system.

All the steps of the oriented conjugation was performed in MES buffer pH 5 10 mM, unless otherwise stated. A solution of 20 µL at 10 mg/mL of EDC was mixed with 3.8 µL at 100 mg/mL of sulfo-NHS for 10 min at room temperature. Then, 23.8 µL of this solution were mixed with 0.5 mg of AuNPs covered with PEG and the total volume was raised to 500 µL with MES buffer. The solution was incubated for 30 min at 37° C at 650 rpm, to activate the carboxylic groups of the PEGylated AuNPs. After the incubation, the excess of EDC-sulfo-NHS was eliminated centrifuging the solution in Amicon Ultra 0.5 filters, with a cut off of 50K, at 14000 rpm for 5 min. The obtained conjugate solution, around 30 µL, was mixed with 10 µg of antibody in a final volume of 500 µL in MES pH 5 and incubated for 60 min at 37° C and 650 rpm. The obtained conjugates were centrifuged at 14000 rpm at 4° C for 20 min and, they were washed with 500 µL Bicarbonate buffer 10 mM pH 8 for 30 min at 37° C and 650 rpm. Finally, after the conjugates were centrifuged at 14000 rpm 4° C for 20 min, they were blocked with 2% BSA in MES 10 mM pH 6. The obtained solution was placed for 5 sec in the ultrasonic bath to separate the aggregated complexes, and then incubated for 60 min at 37° C and 650 rpm. Finally, after centrifugation, the oriented complexes AuNPs/Abs were re-suspended in mQ water.

#### 2.5. Characterization of the oriented conjugates

For the characterization we used just the αHRP antibodies.

First, we verified that, at pH lower than its isoelectric point, an antibody is attracted to the surface of a negatively charged NP. In order to achieve this goal, we used PEGylated AuNPs, which were not activated with EDC/sulfo-NHS. We incubated the AuNPs with 500 µL of 26 µg/mL antibody solution for 30 min at 37° C, and then the solution was centrifuged and the supernatant stored. Then, we used 500 µL of carbonate

buffer pH 8 to break the ionic bonds between the antibodies and the AuNPs. After a second centrifugation, all the supernatants were checked with Bradford test (experimental details in S.I.) to verify the amount of Abs that was ionically adsorbed.

Then, we wanted to prove that the formation of a covalent bond between the C OOH-groups of PEG and the NH<sub>2</sub>-groups of the antibodies was occurring. Thus, the previous procedure was repeated using also the oriented conjugates. In this case, instead of the Bradford test, we performed a SDS-PAGE (experimental details in S.I.) to check the nature of the bond.

Finally, the random and oriented conjugates, using the  $\alpha$ HRP antibody, were used to optically prove that, for a saturating concentration of antigen and almost the same concentration of antibody onto the AuNP surface, the new label allowed the capture of more antigen molecules. Briefly, 150  $\mu$ L of each conjugate were mixed with 12  $\mu$ g of HRP in sodium phosphate buffer 10 mM pH 7 and the resulting solutions were incubated at 37° C for 30 min. After centrifugation at 14000 rpm for 20 min at 4° C, the pellets were re-suspended in 1.5 mL of sodium phosphate buffer. Then in a 96 wells plate 10  $\mu$ L of each sample were mixed with 300  $\mu$ L of a solution of ABTS 1 mM + H<sub>2</sub>O<sub>2</sub> 1 mM. As soon as the ABTS solution was added the measurements of the kinetics of the reaction were started measuring every 1 min for 1 hour.

## 2.6. Magnetosandwich immunoassay and electrochemical detection of HIgG

The magnetosandwich immunoassay was performed following a method that we previously optimized.<sup>22</sup> Briefly, 120  $\mu$ g of streptavidin-coated MBs were washed twice with 120  $\mu$ L of

PBS-0.05%Tween20 and then used to immobilize 30  $\mu$ L the biotinylated  $\alpha$ HIgG  $\gamma$ -chain specific antibody (0.5  $\mu$ g/mL in PBS), incubating for 30 min at 25° C at 650 rpm. After two washing steps in PBS, the MBs were blocked with 120  $\mu$ L of BSA 5% in PBS overnight at 4° C. Then, they were washed twice in PBS and incubated with 120  $\mu$ L of a solution of HIgG in PBS for 30 min at 25° C at 650 rpm. After washing 3 times in PBS, the magneto-immuno sandwich was formed incubating the MBs with 120  $\mu$ L AuNPs modified with the  $\alpha$ HIgG for 30 min at 25° C at 650 rpm and washed 4 times before being re-suspended in 120  $\mu$ L of mQ water. In the real human serum measurements, we diluted the sample with a factor of 10<sup>6</sup> in PBS.

In order to perform the electrochemical detection, a drop of 25  $\mu$ L of the magnetosandwich complex was deposited onto a SPCE and the complexes were accumulated onto the working electrode by a magnet. Finally, 25  $\mu$ L of HCl 2M were added. The AuNPs of the immune-complexes catalyzed the hydrogen formation in 1M HCl solution.<sup>23</sup> This reaction produced a current, measured by chronoamperometry (holding the working electrode at a potential of +1.35 V for 1 min followed by a negative potential of -1.00 V for 100 s), whose intensity is directly related to the amount of AuNPs and so to the amount of analyte captured by the immunocomplexes.

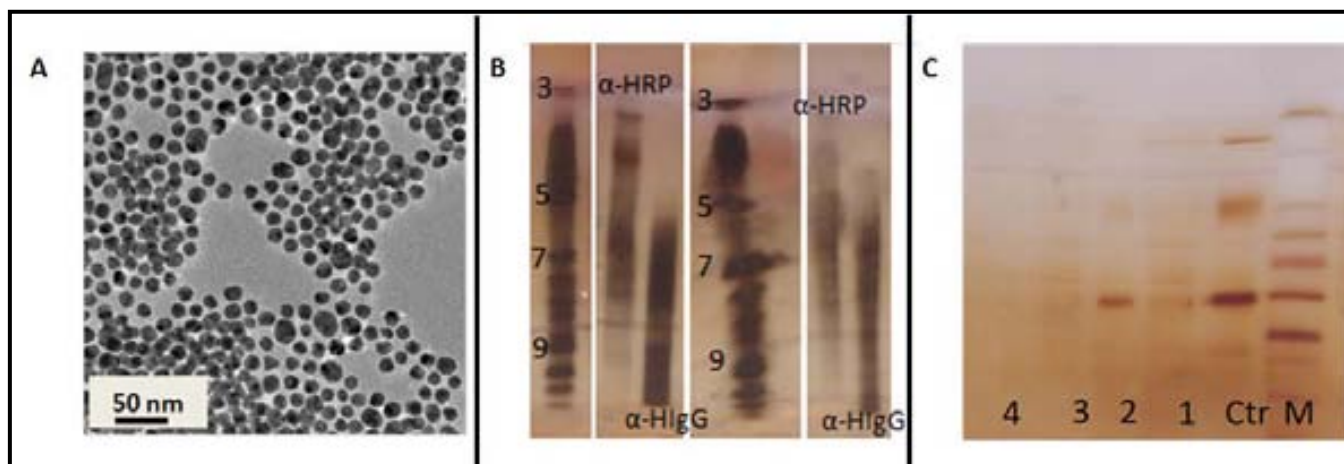


Fig. 2: (A) Transmission Electron Microscopy image of the synthesized AuNPs. (B) Isoelectric point measurement; both  $\alpha$ HRP and  $\alpha$ HIgG antibodies have an isoelectric point of 7. (C) SDS gel of supernatants after conjugates centrifugation, from the right to the left: M) marker, Ctr)  $\alpha$ HRP, 1) Ionic absorption without EDC, 2) Ionic desorption without EDC in Carbonate buffer pH 8, 3) Conjugates  $\alpha$ HRP/AuNP, 4) Conjugates  $\alpha$ HRP/AuNPs in Carbonate buffer pH 8.

### 3. Results and Discussion

#### 3.1. Gold Aggregation Test

As previously mentioned, the GAT gave the best conditions to carry out the random functionalization. In fact, the function of the NaCl is to displace the charges on the AuNP surface; this leads to the aggregation of the NPs, which can be followed measuring the absorbance of AuNP. In fact, in presence of aggregates, the wavelength of the plasmon peak of AuNPs shifts to higher values. This phenomenon cannot happen if the surface of the AuNPs is covered by antibodies, since the NaCl cannot break the Au-S bond. Thus, we found that the best conditions for the random functionalization of the AuNPs with  $\alpha$ HIgG and  $\alpha$ HRP were respectively 20  $\mu$ g/mL at pH 9, and 15  $\mu$ g/mL at pH 7. These conditions correspond to the pH values and antibody concentrations that avoid the AuNP aggregation.

#### 3.2 Isoelectric point measurements

The measurements of the isoelectric points of  $\alpha$ HRP and  $\alpha$ HIgG produced several bands; this was due to the fact that we were using antisera and so other serum proteins were present in the solution (Fig. 2B). However, comparing the two

different gels, we can estimate that the isoelectric points of both antibodies are around 7, since the most intense bands, corresponding to the  $\alpha$ HRP and  $\alpha$ HIgG can be found at pH 7. From this result, the MES buffer at pH 5 was chosen to carry out all the oriented functionalization.

#### 3.3 Characterization of the oriented conjugates

The evidence that, working at pH 5, there was ionic attraction between negatively charged AuNPs and antibodies was given by the Bradford assay measurements. The experiment was carried out without the activation of the COOH-groups with the EDC-chemistry; in this way, the formation of the peptide bond between the COOH-group of the PEG and the NH<sub>2</sub>-group of the antibody was not catalyzed, and so we assumed that the interaction between NPs and antibodies was

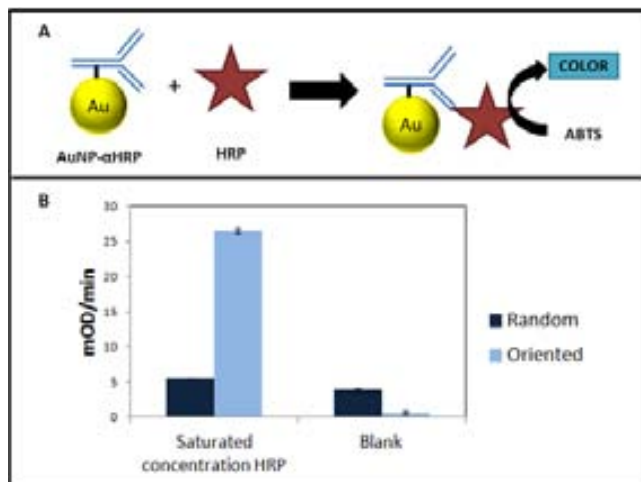


Fig. 3: (A) Scheme of the optical method used to qualitatively evaluate the orientation of the  $\alpha$ HRP antibody onto the AuNP surface. (B) Comparison of the results obtained using the random and oriented conjugation for a blank sample (without HRP) and for a saturated concentration of HRP.

due mainly to ionic interactions. We found that in the supernatant of the first sample the concentration of antibodies, which were not ionically adsorbed onto the AuNP, was  $13.87 \pm 5.52 \mu\text{g/mL}$ ; whereas in the second supernatant the concentration of the antibodies, which were ionically adsorbed onto the AuNP and then released by the carbonate buffer pH8, was  $12.74 \pm 2.21 \mu\text{g/mL}$ . The sum of the values is  $\sim 26 \mu\text{g/mL}$ , which was the concentration of antibody that we used for the incubation with the AuNPs. In addition, the concentration of the ionically adsorbed antibody is close to those of the GAT ( $15 \mu\text{g/mL}$ ), indicating that the entire surface of the AuNPs was fully covered with antibodies.

The next step was to prove that the conjugation was covalent. For this reason, the new labels were incubated in carbonate buffer pH 8, since it could desorb all the ionically adsorbed antibodies

(as shown by the previous Bradford results), but not those that are covalently attached. In this case, the supernatants were analyzed by SDS-PAGE. The results showed that all the antibodies of the new label were covalently attached to the surface of the AuNPs, since no bands can be seen in the row of the gel corresponding to this sample. On the other hand, the previous supernatants, which were obtained without the activation of the COOH-groups, revealed the two typical bands of the antibodies, corresponding to the light and heavy chains (Fig. 2C).

These two controls confirmed the ionic adsorption and the peptide bond formation.

### 3.4 Antigen capturing by oriented label versus random one

The advantage of using the  $\alpha$ HRP antibody was that the antigen, the horseradish peroxidase, is an enzyme that can catalyze a reaction that generates color in the presence of the proper substrate (Fig. 3A). This is a powerful tool to check how much antigen the antibodies have captured. In fact, it is possible to link the kinetic of the enzyme reaction with the amount of enzyme present in solution. This experiment gives qualitative information about the orientation of the antibodies onto the AuNP surface, since the amount of captured antigen is strictly related to the orientation of the antigen binding sites. The experiment was carried out using a saturated concentration of HRP with the aim to see which label could capture more antigens, considering the same amount of antibodies and AuNPs. The results (Fig. 3B) showed that the oriented functionalization allowed the recognition of an amount of HRP molecules of around 5 times more than the random technique.

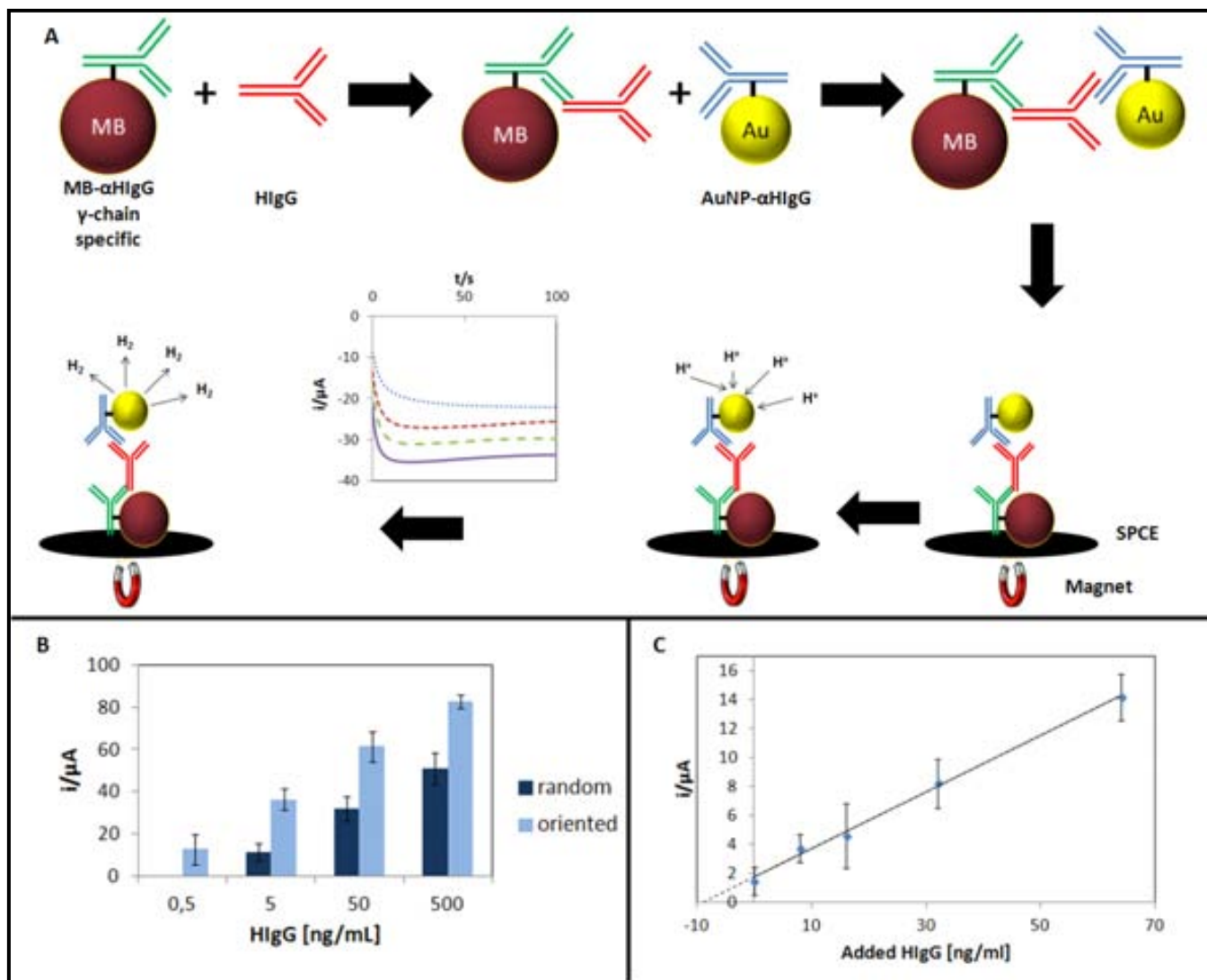


Fig. 4: (A) Scheme of the magnetosandwich immunoassay used to detect HlgG. In the inset a representative chronoamperometric results obtained using the new label (from up to down):  $\cdots$  0,  $---$  8,  $---$  32,  $---$  64 ng/ml of HlgG. (B) Results obtained subtracting the blank in HCl IM for random and oriented  $\alpha$ HlgG/AuNP labels. (C) Correlation curve obtained with the method of the standard additions of HlgG in human serum.

### 3.3. Signal amplification efficiency of AuNP labels in a magneto-sandwich immunoassay

The efficiency of both oriented and random conjugated AuNP labels were also compared in a magnetosandwich immunoassay for the electrochemical detection of HlgG in PBS buffer. The detection method is based on the AuNP ability of catalyzing the formation of hydrogen gas from hydrogen ions; this reaction generates a current that can be chronoamperometrically measured (Fig. 4A). In this way, it is possible to correlate the current intensity recorded at a fixed time (180 seconds) with the concentration of AuNPs in solution and so to the concentration of the antigen captured by the magnetosandwich. The obtained results are plotted in the Fig. 4B. A logarithmic relationship (correlation coefficient of 0.999 in both cases) between the HlgG concentration and the current intensity is found in the range of 0.5 to 500 ng/ml and of 5 to 500 ng/ml for the oriented and random label respectively. The reproducibility of the method shows a relative standard deviation (RSD) of 7% for the oriented label and 5% for the ran-

dom one ([HIgG]: 5 ng/mL; n = 6). The estimated limit of detection (LoD), calculated as the concentration of HIgG corresponding to three times the standard deviation of the estimate, was 0.19 and 1.9 ng/mL respectively using the oriented label and the random. This means that using the oriented label was possible to improve the LoD of almost one order of magnitude. This reflects the fact that there are more antigen binding sites available in the new label and so the probability of a recognition event between antibody and antigen is higher than using the random label.

Once proved that the new label could achieve the detection of less amount of analyte, we applied it for the detection of HIgG in a human serum to prove that it could be used also for real samples. Standard additions method was used to estimate the concentration of the sample minimizing the matrix effects.. A linear relationship between the standard addition of HIgG and the voltammetric peak current is found in the range 10–70 ng/mL, with a correlation coefficient of 0.998, adjusted to the following equation:

peak current ( $\mu\text{A}$ ) =  $-0.1958 [\text{added HIgG (ng/mL)}] + 1.7359$ . (Fig. 4C). The estimated concentration of HIgG in serum was  $8.86 \pm 0.4 \text{ mg/mL}$  (Standard addition: 0 ng/mL; n = 3). This value is within the expected range of IgG in serum, between 6 and 11 mg/mL.<sup>24,25</sup>

#### 4. Conclusion

A new label based on the oriented functionalization of AuNPs with Abs for immunosensing applications has been developed. It took advantage of the high density of positive charges onto the major plane of the antibodies, when they are in a solution with pH lower than their isoelectric point. In order to ionically orientate the antibodies, the AuNPs were modified with COOH-PEG, which allowed the formation of a stable negative intermediate that interacted with the major plane of the antibody to form a peptide bond. The formation, nature and orientation of the label have been characterized using an  $\alpha\text{HRP}$  antibody, confirming the entire hypothesis. Then its application as electrochemical label in a magnetosandwich immunoassay was performed. The limit of detection obtain was of 160 pg/ml which improved of one order of magnitude the one obtained using a label based on the random functionalization. Finally, it has been successfully used to detect the HIgG in a real human serum to prove its applicability in complex matrixes

We expect that this oriented antibody immobilization approach, developed for AuNP, the most used nanoparticle in biosensing technology, will have a great impact in several other electrochemical and optical biosensing applications with interest not only for proteins but also for cells (ex. cancer cells reported earlier) or even plasmonic based detection of biomarkers.<sup>26</sup>

#### Acknowledgements

We acknowledge MINECO (Spain) for the project MAT2011-25870, the E.U.'s support under FP7 contract number 246513 "NADINE", ERC-Starting Grant-NANOPUZZLE, European Regional Social Development Funds. We thank S. Puertas for fruitful discussion, I. Echaniz and S. Rivera for technical support and Yulan Hernández for the help with the AuNPs.

#### ASSOCIATED CONTENT

SPCE electrode production, Bradford assay and SDS procedure. This material is available free of charge via the Internet at <http://pubs.acs.org>.

#### AUTHOR INFORMATION

##### Corresponding Author

\* [arben.merkoci@icn.cat](mailto:arben.merkoci@icn.cat)

##### Author Contributions

The manuscript was written through contributions of all authors. / All authors have given approval to the final version of the manuscript.

## REFERENCES

- (1) Parolo, C.; Merkoçi, A. *Chemical Society Reviews* **2013**, *42*, 450–457.
- (2) Lei, J.; Ju, H. *Chemical Society reviews* **2012**, *41*, 2122–34.
- (3) Khlebtsov, N.; Dykman, L. *Chemical Society reviews* **2011**, *40*, 1647–71.
- (4) Daniel, M.-C.; Astruc, D. *Chemical reviews* **2004**, *104*, 293–346.
- (5) Jans, H.; Huo, Q. *Chemical Society reviews* **2012**, *41*, 2849–66.
- (6) Pumera, M.; Castañeda, M. T.; Pividori, M. I.; Eritja, R.; Merkoçi, A.; Alegret, S. *Langmuir* □: the ACS journal of surfaces and colloids **2005**, *21*, 9625–9.
- (7) Ambrosi, A.; Castañeda, M. T.; Killard, A. J.; Smyth, M. R.; Alegret, S.; Merkoçi, A. *Analytical chemistry* **2007**, *79*, 5232–40.
- (8) De la Escosura-Muñiz, A.; Sánchez-Espinel, C.; Díaz-Freitas, B.; González-Fernández, A.; Maltez-da Costa, M.; Merkoçi, A. *Analytical chemistry* **2009**, *81*, 10268–74.
- (9) Maltez-da Costa, M.; De la Escosura-Muñiz, A.; Nogués, C.; Barrios, L.; Ibáñez, E.; Merkoçi, A. *Nano letters* **2012**, *12*, 4164–71.
- (10) Maltez-da Costa, M.; De la Escosura-Muñiz, A.; Nogués, C.; Barrios, L.; Ibáñez, E.; Merkoçi, A. *Small (Weinheim an der Bergstrasse, Germany)* **2012**, *8*, 1–8.
- (11) Ambrosi, A.; Airò, F.; Merkoçi, A. *Analytical chemistry* **2010**, *82*, 1151–6.
- (12) Li, D. X.; Zhang, J. F.; Jang, Y. H.; Jang, Y. J.; Kim, D. H.; Kim, J. S. *Small (Weinheim an der Bergstrasse, Germany)* **2012**, *8*, 1442–8.
- (13) Boisselier, E.; Astruc, D. *Chemical Society reviews* **2009**, *38*, 1759–82.
- (14) Giljohann, D. a; Seferos, D. S.; Daniel, W. L.; Massich, M. D.; Patel, P. C.; Mirkin, C. a *Angewandte Chemie (International ed. in English)* **2010**, *49*, 3280–94.
- (15) Eustis, S.; el-Sayed, M. a *Chemical Society reviews* **2006**, *35*, 209–17.
- (16) Mout, R.; Moyano, D. F.; Rana, S.; Rotello, V. M. *Chemical Society reviews* **2012**, *41*, 2539–44.
- (17) De la Escosura-Muñiz, A.; Parolo, C.; Merkoçi, A. *Materials Today* **2010**, *13*, 24–34.
- (18) Puertas, S.; Batalla, P.; Moros, M.; Polo, E.; Del Pino, P.; Guisan, J. M.; Grazú, V.; De la Fuente, J. M. *ACS nano* **2011**, *5*, 4521–8.
- (19) Puertas, S.; Moros, M.; Fernández-Pacheco, R.; Ibarra, M. R.; Grazú, V.; De la Fuente, J. M. *Journal of Physics D: Applied Physics* **2010**, *43*, 474012.
- (20) Sanz, V.; Conde, J.; Hernández, Y.; Baptista, P. V.; Ibarra, M. R.; Fuente, J. M. *Journal of Nanoparticle Research* **2012**, *14*, 917.
- (21) Turkevich, J.; Stevenson, P.; Hillier, J. *Discuss. Faraday Soc.* **1951**, *55*–75.
- (22) De la Escosura-Muñiz, A.; Parolo, C.; Maran, F.; Mekoçi, A. *Nanoscale* **2011**, *3*, 3350–3356.
- (23) M. Maltez-da Costa, A. de la Escosura-Muñiz, A. Merkoçi, ^ *Electrochemistry Communications* **2010**, *12*, 1501–1504.
- (24) Stiehm, E. R.; Fudenberg, H. H. *Pediatrics* **1966**, *37*, 715.
- (25) Gonzalez-Quintela, a; Alende, R.; Gude, F.; Campos, J.; Rey, J.; Meijide, L. M.; Fernandez-Merino, C.; Vidal, C. *Clinical and experimental immunology* **2008**, *151*, 42–50.

- (26) De la Rica, R.; Stevens, M. M. *Nature Nanotechnology* **2012**, 7, 821–824.

## Supporting Information

### Antibody-oriented functionalization of gold nanoparticle labels for very sensitive electrochemical biosensing

Claudio Parolo<sup>1</sup>, Alfredo de la Escosura-Muñiz<sup>1</sup>, Ester Polo<sup>2</sup>, Valeria Grazú<sup>2</sup>, Jesús M. de la Fuente<sup>2,3</sup> and Arben Merkoçi<sup>1,4\*</sup>

<sup>1</sup> ICN2 - Institut Català de Nanociència i Nanotecnologia, Campus UAB, 08193 Bellaterra (Barcelona), Spain;

<sup>2</sup> Instituto de Nanociencia de Aragón (INA), University of Zaragoza, Campus Río Ebro, Edificio I+D, Mariano Esquillor, s/n, 50018 Zaragoza, Spain

<sup>3</sup> Fundación ARAID, Zaragoza, Spain

<sup>4</sup> ICREA - Institutio Catalana de Recerca i Estudis Avançats, 08010 Barcelona, Spain

#### Fabrication of screen-printed carbon electrodes (SPCEs)

The electrochemical transducers were homemade screen-printed carbon electrodes (SPCEs), consisting of three electrodes: working electrode WE, reference electrode RE and counter electrode CE in a single strip. The full size of the sensor strip was 29mm x 6.7mm, and the WE diameter was 3mm. The fabrication of the SPCEs was carried out in three steps. First, a graphite layer was printed onto the polyester sheet, using the screen-printing machine with the stencil (where it is the electron pattern). After curing for 15 minutes at 95°C, an Ag/AgCl layer was printed and cured for 15 minutes at 95°C. Finally, the insulating ink was printed and cured at 95°C for 20 minutes.

Figure S1 shows images of the 45-sensor sheet obtained following the detailed experimental procedure.

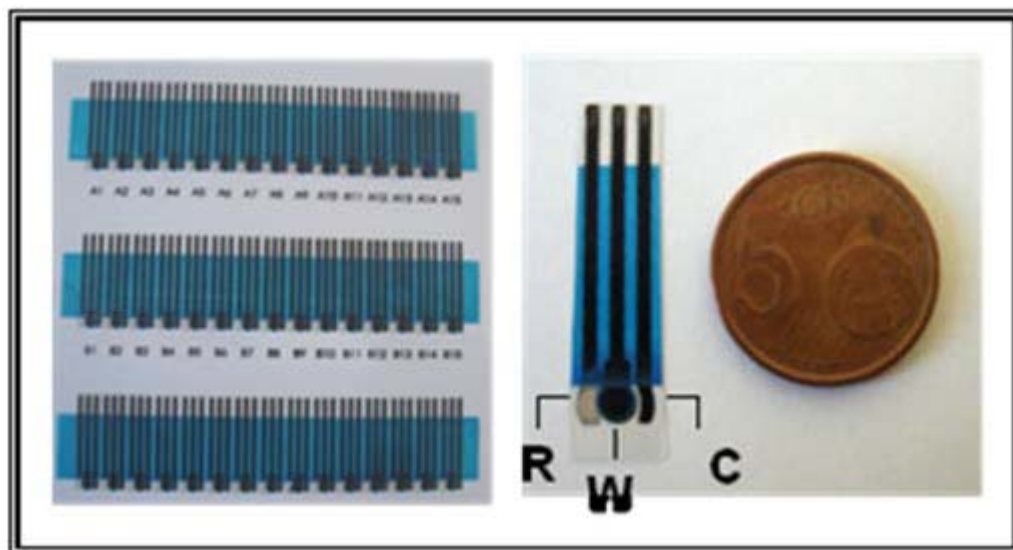


**Figure S1.** (Left) Images of the 45 SPCE sensors sheet obtained following the detailed experimental procedure. (Right) Detail of one SPCE, containing the three electrodes in the working area: R- Ag/AgCl reference electrode, W- carbon working electrode and C- carbon counter electrode.

## **Bradford Assay and SDS procedure**

The Bradford Assay is a colorimetric method for total protein quantitation. When coomassie dye binds protein in an acidic medium, an immediate shift in absorption maximum occurs from 465 nm to 595 nm with a concomitant color change from brown to blue.

In 96-well microplate 150  $\mu$ L of each supernatant were mixed with 150  $\mu$ L of Bradford reagent. After developing of the color, the wells were read measuring the absorbance at 595 nm.

The SDS gel electrophoresis with silver staining is a more reliable method than Bradford, but it also required more time. It consists in separating the protein depending on their molecular weight and then estimating their concentration with the silver staining.

The gel electrophoresis is done in a commercial available gradient gel, this means that the gel has a gradient of porous size, in this case from 4% to 20%, which allows separating proteins between 5 and 200 kDa. The run was performed for 2h and 30 min at 150 V and 100 mA.

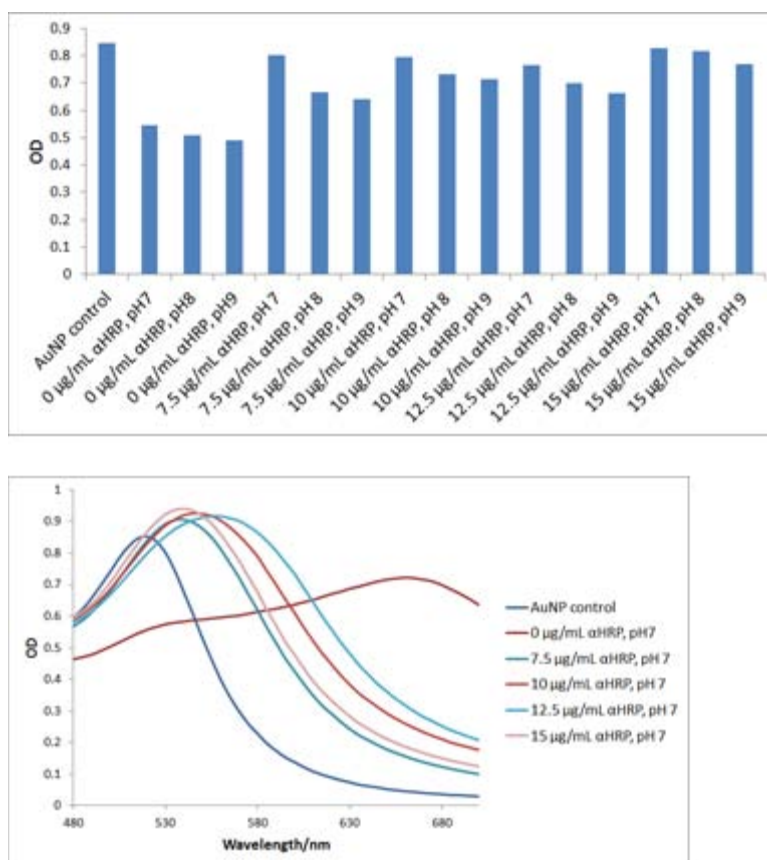


**Figure S2.** Gold aggregation test results for the optimization of the random conjugation.

### Articles accepted by the PhD comission

#### Related Publications

---

- 1) De la Escosura-Muñiz, A.; Parolo, C.; Merkoçi, A. Immunosensing using nanoparticles. *Materials Today*, 2010, 13, 24–34.
  - 2) Parolo, C.; Merkoçi, A. Paper-based nanobiosensors for diagnostics. *Chemical Society Reviews*, 2013, 42, 450–457.
  - 3) De la Escosura-Muñiz, A.; Parolo, C.; Maran, F.; Merkoçi, A. Size-dependent direct electrochemical detection of gold nanoparticles: application in magnetoimmunoassays. *Nanoscale*, 2011, 3, 3350–3356.
  - 4) Parolo, C.; Medina-Sánchez, M.; De la Escosura-Muñiz, A.; Merkoçi, A. Simple paper architecture modifications lead to enhanced sensitivity in nanoparticle based lateral flow immunoassays. *Lab on a chip*, 2013, 13, 386–90.
  - 5) Parolo, C.; De la Escosura-Muñiz, A.; Merkoçi, A. Enhanced lateral flow immunoassay using gold nanoparticles loaded with enzymes. *Biosensors and Bioelectronics*, 2012, 40, 412–416.
  - 6) Parolo, C.; Medina-Sánchez, M.; Montón, H.; De la Escosura-Muñiz, A.; Merkoçi, A. Paper-based electrodes for nanoparticles detection. *Particle & Particle System Characterization*, 2013, DOI: 10.1002/ppsc.201200124.
-



# Immunosensing using nanoparticles

Immunosensing technology is taking advantage of the latest developments in materials science and in particular from the nanomaterials field. Because of their unprecedented optical tunability as well as electrical and electrochemical qualities, we are seeing significant developments in the design of novel immunoassays; various conventional optical and electrical platforms which allow for future applications in several fields are being used. Properties of nanoparticles such as light absorption and dispersion are bringing interesting immunosensing alternatives. Nanoparticles are improving the sensitivity of existing techniques used for protein detection in immunoassays based on Surface Plasmon Resonance, Quartz Crystal Microbalance, Fluorescence spectroscopy etc. Electrochemical techniques are also taking advantage of electrical properties of nanoparticles. Redox properties of metal based nanoparticles, surface impedance change and conductance changes once nanoparticles are present as labelling tags or modifiers of transducer surfaces are also improving the technology. In most of the examples nanoparticle based biosensing systems are being offered as excellent screening and superior alternatives to existing conventional strategies/assays with interest for fields in clinical analysis, food quality, safety and security.

Alfredo de la Escosura-Muñiz<sup>a,b</sup>, Claudio Parolo<sup>a</sup>, Arben Merkoçi<sup>a,c,\*</sup>

<sup>a</sup> Nanobioelectronics & Biosensors Group, Institut Català de Nanotecnologia, CIN2 (ICN-CSIC), Esfera UAB, Barcelona, Spain.

<sup>b</sup> Instituto de Nanociencia de Aragón, Universidad de Zaragoza, Zaragoza, Spain.

<sup>c</sup> ICREA, Barcelona, Spain

\* E-mail: [arben.merkoci.icn@uab.es](mailto:arben.merkoci.icn@uab.es)

Recent developments in nanotechnology are having marked effects on different industries ranging from electronics to biomedical engineering, by producing a new group of nanomaterials such as nanoparticles (NPs), including quantum dots (QDs), with unique semiconducting and light-emitting properties amongst other characteristics. Nanomaterials are defined as having a size regime of less than 100 nanometers and, more specifically, QDs range from 2-10 nanometers. From the material point of view, NPs are so small that they exhibit characteristics that are often not observed in the bulk materials. For example, gold nanoparticles (AuNPs) have unique properties such as a strong absorption in the UV-Vis up to the NIR region. QDs have unique properties because at this size they behave differently to their bulk equivalents and exhibit unprecedented tunability, enabling completely new applications in science and technology. This has required the continuous search for novel routes of synthesis of fabricated NPs from different materials such as Au, Pt, Fe, Co, CdS, Pd, Cu etc.

Between the different applications the use of NPs for biosensing is showing an increased interest for several areas such as clinical analysis<sup>1,2</sup>, environmental monitoring<sup>3</sup> as well as safety and security.

NPs involvement in DNA, protein and even cell sensing systems have recently been the hottest topics in nanobiotechnology. Given the special importance of protein analysis we intend in this review to overview some of the major advances and milestones in the field of immunodetection systems based on NPs underlying the different approaches reported so far. Particular emphasis will be on the different optical<sup>4</sup> and electrochemical<sup>5,6</sup> detection methodologies where NPs are showing significant impact. In certain cases assays based upon nanomaterials have offered significant advantages over conventional diagnostic systems with regard to assay sensitivity, selectivity, and practicality<sup>7</sup>.

## Antibodies, modifications with nanoparticles and immunosensing

The structure of IgG, the most used antibody in immunosensing assays, has been determined by X-ray crystallography (Fig. 1a, upper part) which shows a Y-shape form consisting of three equal-sized portions, loosely connected by a flexible tether<sup>8</sup>. The antibodies are constituted by two heavy and two light polypeptide chains linked between them as shown in Fig. 1a (lower part). The C regions determine the isotype

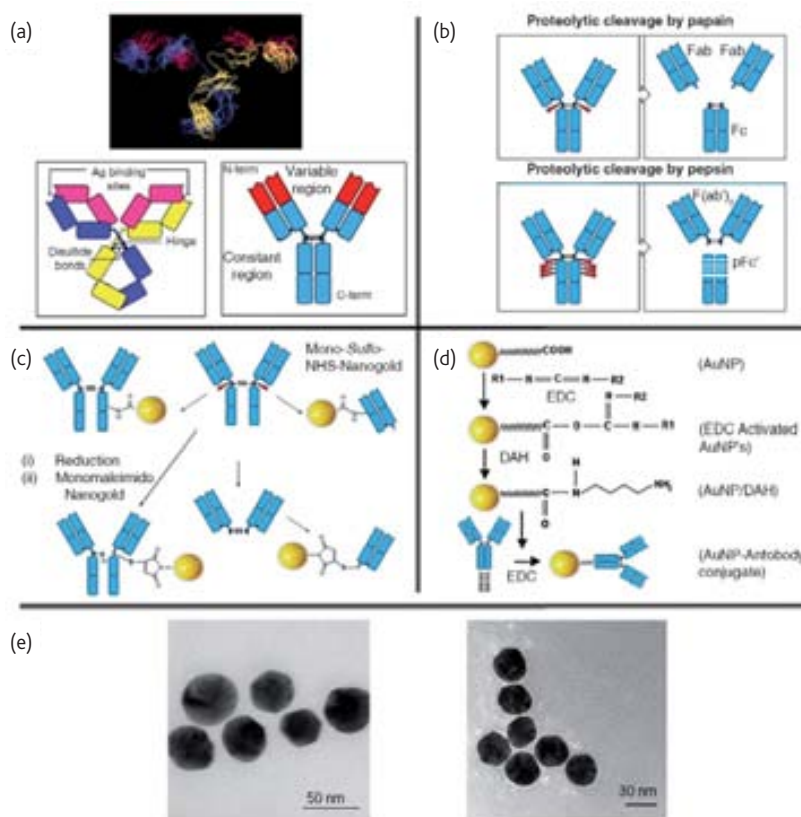


Fig. 1 (a) X-ray crystallographic structure of an IgG antibody (upper part); A schematic representation of IgG and a simplified scheme of the antibody's structure (lower part). (b) The papain (upper part) and the pepsin (lower part) cleavages. (c) Functionalization of a whole IgG or a Fab by a Mono-Sulfo-NHS-AuNP via free amino groups (upper part); monomaleimido AuNP binds the S atom after the reduction of the disulfide bond starting from the whole IgG (lower part, left) or from  $F(ab')_2$  (lower part, right). (d) An activated by EDC AuNP coated with glutathione, as spacer arm, reacts with an IgG, also activated by EDC. (e) TEM images of AuNPs (left part) and AuNPs conjugated with IgG (right part). Image shows a thin white layer, called "halo" effect, surrounding the surface of the AuNPs indicating coating with protein. Adapted from<sup>8-10</sup> and [www.nanoprobes.com](http://www.nanoprobes.com) with permission.

of the antibody whereas the variable regions of one heavy and one light chain constitute an antigen binding site (ABS). The digestion of antibody with papain (Fig. 1b upper part) and pepsin (Fig. 1b lower part) proteases produces several smaller fragments that may be used instead of the original antibody for immunosensing applications.

Immunoassays are based on the interaction between the antibody and the antigen, in particular between the ABS and the epitope. In fact this interaction gives high specificity and sensitivity to the immunoassay. In order to functionalize the Ig, the connection of labels through three main groups:  $-NH_2$ ,  $-COOH$  and  $-SH$  have been performed. Fig. 1c (upper part) shows two examples of conjugation of mono-sulfo-NHS-AuNPs with an antibody through the amino group. A conjugation of monomaleimido AuNPs (Fig. 1c, lower part) with an antibody, through the  $-SH$  group, is also shown. The use of the thiol group for the functionalization is a good way to control the direction of the bond between the label and the antibody, and prevent the involvement of the ABS. Fig. 1d is an example of conjugation through

the carboxyl group reported by Ahirwal *et al.*<sup>9</sup>. They connected the carboxi-term of the antibody with a AuNP by glutathione used as a spacer. The C-term region is a good point to attach the label, since it is far from the ABS and should allow the molecule interaction with the antigen. The AuNP modification with protein can even be observed by TEM (Fig. 1e)<sup>10</sup>.

In the following part the different immunosensing technologies ranging from optical (i.e. colorimetric) to electrical (i.e. voltammetry) techniques that involve the use of NPs will be discussed.

## Colorimetric detection

AuNPs have an extraordinarily high extinction coefficient, emanating from the inherent plasmonic properties<sup>11</sup>. Their optical properties are strongly dependent on the interparticle separation distance, and aggregation that cause a massive shift in the extinction spectrum manifested as a color change of suspensions from red to purple<sup>12</sup>. The clearly distinguishable color shifts facilitate a very simple sensor

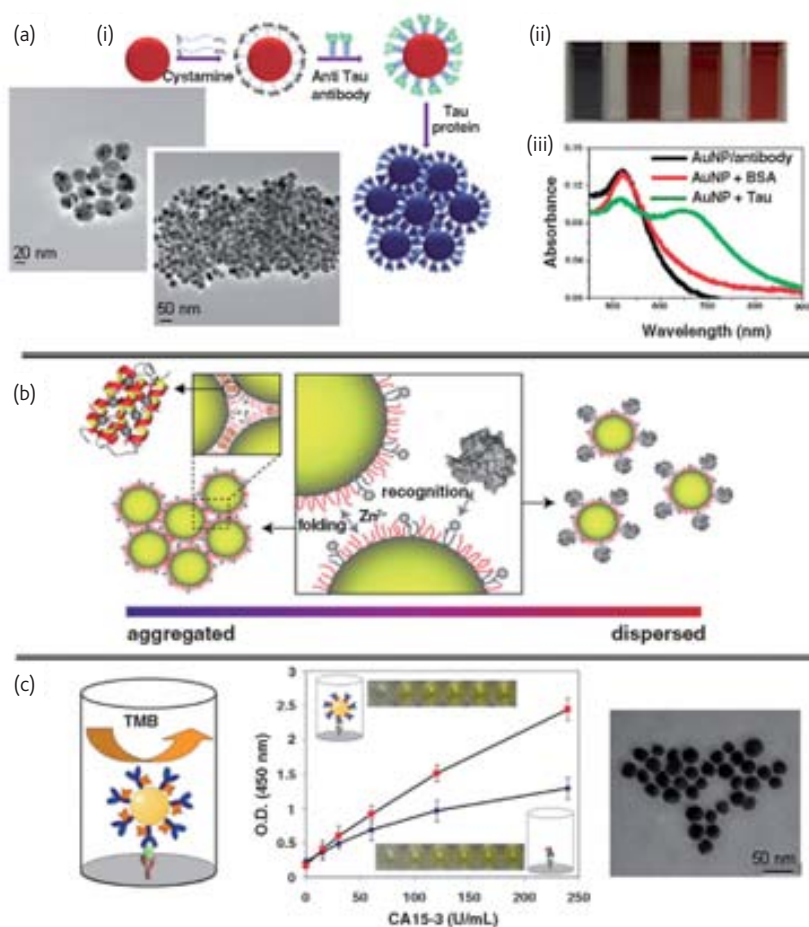


Fig. 2 (a) Colorimetric assay based on aggregation of AuNPs. (i) Schematic representation of the assay and TEM images of the antibody conjugated AuNPs before and after the aggregation; (ii) Photograph showing colorimetric change upon addition of increasing concentrations of specific antigen; (iii) Absorption profile variation of AuNP/antibody due to the addition of specific protein. (b) Colorimetric assay based on disaggregation of AuNPs. AuNPs modified with a polypeptide designed to allow folding induced particle aggregation triggered by  $Zn^{2+}$  and a polypeptide-based synthetic receptor for binding of protein analytes (c) Enhancement of enzymatic colorimetric assay by NPs carriers. AuNPs modified with antibodies labelled with an enzymatic label -HRP- exert an amplification effect on the enzymatic colorimetric signal. Adapted from<sup>16,20,22</sup> with permission.

readout that often can be performed by the naked eye. The use of controllable aggregation of AuNPs for biosensor applications was pioneered by Mirkin *et al.*<sup>13,14</sup> using DNA hybridization to induce an assembly of particles modified with single-stranded DNA. Most nanoparticle-based colorimetric sensors are designed in such a way that binding of an analyte causes particle aggregation, and consequently a colorimetric response<sup>15</sup>.

This sensing principle is recently used by Neely *et al.*<sup>16</sup> for the detection of Alzheimer's tau protein in the 1 pg/mL level using anti-tau antibody-coated AuNP. When anti-tau antibody-coated AuNPs are mixed with tau protein, a displacement in the wavelength of maximum absorbance of AuNPs is observed, allowing its sensitive detection (Fig. 2a). Interesting similar approaches have been reported for the detection of thrombin<sup>17</sup> and rabbit IgG<sup>18</sup> at 0.04 pM and 1.7 nM levels respectively. Glyconanoparticles have also been used as platforms of colorimetric assays for the detection of for example Cholera toxin<sup>19</sup> at 54 nM levels based on its interaction with the lactose contained in the glyconanoparticles.

Some recent works also approach the disaggregation of AuNPs due to the immunological reaction. This is the basis of the work reported by Aili *et al.*<sup>20</sup> based on polypeptide-functionalized AuNPs. The polypeptide is designed to specifically bind to human carbonic anhydrase II (model protein) and the AuNPs aggregation is induced by the Zn<sup>2+</sup> triggered dimerization. Folding of a second polypeptide also present on the surface of the AuNP, gives a readily detectable colorimetric shift that is dependent on the concentration of the target protein, allowing its detection at 10 nM levels (Fig. 2b).

In addition to AuNPs, other NPs such as AgNPs<sup>21</sup> have been used in a minor extent, as sensing elements of colorimetric detection methods.

Finally, it must be mentioned the use of AuNPs as carriers of enzymatic labels in colorimetric assays<sup>22</sup>, i.e. ELISAs, exerting an amplification effect of the enzymatic signal and improving the detection limits of the proteins (Fig. 2c).

## Fluorescence detection

QDs, semiconductor nanoparticles with spectral characteristics, have been intensively studied as unique fluorescent markers<sup>23,24</sup>. QDs with different emission bands that depend on their diameters can be used as labels and all can be excited by a single wavelength. This detection mode is reported by Soman *et al.*<sup>25</sup>. They used QDs with different emission bands labelled with different antibodies. The simultaneous detection of angiotensin-2 and mouse IgG model proteins is achieved in a simple way, with high sensitivity and selectivity (Fig. 3a). CdTe<sup>26</sup>, ZnO<sup>27</sup> and CdSe@ZnS<sup>28,29</sup> QDs are other examples where NPs have been used as direct fluorescent labels for the detection of proteins at very sensitive levels.

Another strategy for immunodetection approached over the last few years consists of the use of core-shell NPs formed by inert core nanoparticles (made of silica or polystyrene) and a shell of a fluorescent dye, mainly lanthanide chelates containing Europium (III). These modified NPs take advantage of the flexible surface modification of inert NPs and the narrow absorption and long tailing of the mentioned dyes, resulting in very sensitive immunoassays for prostate specific antigen<sup>30</sup>, human hepatitis B surface antigen<sup>31</sup> and interleukin-6<sup>32</sup> amongst others at clinical relevant concentrations.

Finally, it can be highlighted the use of NPs associated with charge complementary fluorescent polymers to produce quenched complexes, as performed by You *et al.*<sup>33</sup> (Fig. 3b).

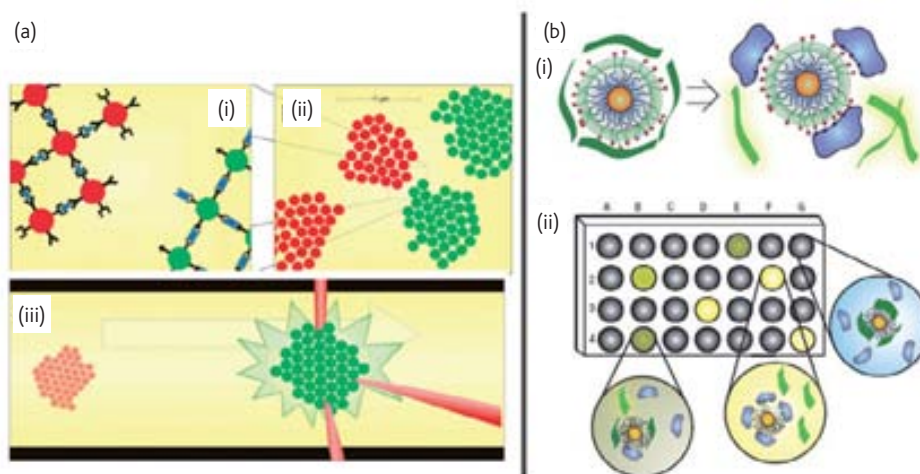


Fig. 3 (a) Fluorimetric detection of QDs. (i) Different QDs are functionalized with polyclonal antibodies for different antigens. Antigens bridge polyclonal antibodies forming two body QDs agglomerates; (ii) Continued agglomeration yields microparticles capable of characterization by i.e. flow cytometry. (iii) The fluorescence of the agglomerates flowing through a microfluidic channel is measured at multiple wavelengths. (b) Fluorophore displacement protein sensor array. (i) Displacement of quenched fluorescent polymer (dark green strips, fluorescence off; light green strips, fluorescence on) by protein analyte (in blue) with concomitant restoration of fluorescence; (ii) Fluorescence pattern generation through differential release of fluorescent polymers from AuNPs. The wells on the microplate contain different nanoparticle-polymer conjugates, and the addition of protein analytes produces a fingerprint for a given protein. Adapted from<sup>25,33</sup> with permission

## Surface plasmon resonance based detection

Surface plasmon resonance (SPR) offers a flow-through biosensing technology that measures very small changes in refractive index on a noble metal surface when mass binds to that surface. To conduct a typical protein-protein binding study, one of the protein partners is immobilized on a thin gold film. When the target protein from solution binds to the immobilized protein partner, the binding will cause a refractive index change at the surface layer, which is detected by SPR through resonance angle change of the reflected light<sup>34,35</sup>. One of the most popular commercial SPR systems available is the BIAcore™. The sensitivity of these label-free SPR-based immunosensors can be greatly enhanced by using for example AuNPs tags through the electronic coupling interaction between the localized surface Plasmon (LSP) of the NPs and the surface plasmon wave associated with the SPR gold film for example. In addition, the active area of the LSP-based sensor is smaller, decreasing the minimum detectable number of molecules involved in the binding event. In this way, human IgE at 1ng/mL levels in an aptamer based immunosensor<sup>36</sup> (Fig. 4a) and testosterone<sup>37</sup> at physiologically relevant range have been detected between others. The sensitivity of these assays can be improved even more by secondary enzymatic precipitation produced by enzymes that can be loaded on the surface of the AuNPs<sup>38</sup> and by the fluorescence coming from fluorescence-labeled antibodies loaded on the AuNPs, giving rise to the technique called localised surface Plasmon Resonance Coupled Fluorescence (LSPCF), with fiber optic detection<sup>39,40</sup>.

In addition to their surface plasmon resonance absorption, light scattering (LS) is another optical property of AuNPs that is of great interest for biomolecular detection<sup>41,42</sup>. The light-scattering cross-section of an AuNP with a diameter of 60 nm is 200-300 times stronger than that of a polystyrene bead of the same size, and 4-5 orders of magnitude stronger than that of a strong fluorescence dye, e.g., fluorescein<sup>41</sup>. For these reasons, several works have been recently reported developing immunoassays based on either the static,

linear, or nonlinear scattering properties of AuNPs<sup>43,44</sup>.

Finally, it can also be highlighted the use of the surface-enhanced Raman scattering (SERS) microscopy as very sensitive technique for the detection of NPs tags in immunoassays. SERS is observed for molecules on or nearby the surface of metallic nanostructures that can support localized surface Plasmon resonances. The signal levels observed in SERS are several orders of magnitude higher than in conventional Raman scattering, providing the sensitivity required for bioanalytical and biomedical applications<sup>45-47</sup>.

In addition to their extensive use as labels, AuNPs have been directly assembled on the sensing surface, in order to enhance the SPR<sup>48</sup> and SERS<sup>49</sup> signal as a label-free detection system. Furthermore, the AuNPs allow a better oriented immobilization of antibodies, improving the sensitivity and selectivity of the immunoassay (Fig. 4b).

## Direct electrical detection

The excellent electroactivity of AuNPs and heavy metal based QDs (i.e. CdS, ZnS, PbS QDs) for example allows the use of both electrical or electrochemical techniques for their detection, reaching low limits of detection (LOD) and consequently detects low concentrations of proteins<sup>50</sup>. NPs can be directly detected due to their own redox properties (of the gold or heavy metals atoms constituents for example) or indirectly due to their electrocatalytic properties toward other species like silver reduction etc.

Several NPs present excellent electroactivity, making direct electrical detection possible, being not necessary any preliminary dissolution step to liberate the metal ions in solution. This direct electrical detection of NPs comprises solid state analysis, where the metals forming the NPs are electrically detected. However, this type of detection needs direct contact between the electrode surface and the metal, and excludes from detection a large portion of non-touching particles. This phenomenon could result in a loss of sensitivity, in contrast with techniques exploiting the total NP dissolution where all metal ions are

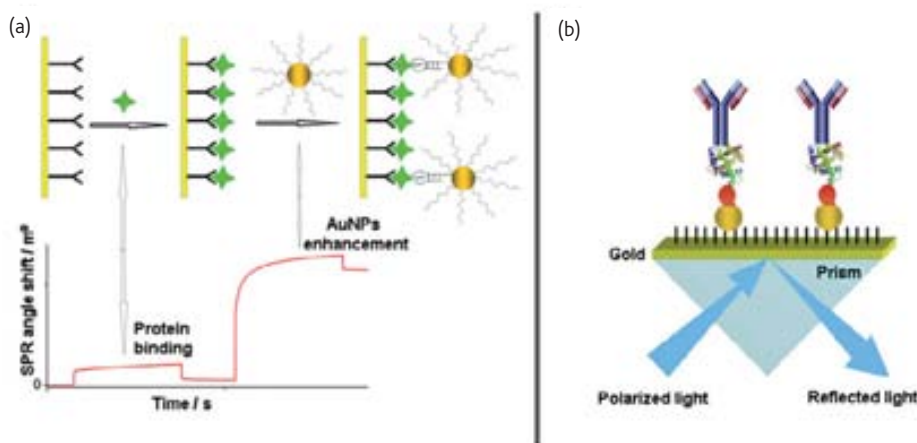


Fig. 4 (a) SPR enhancement by NPs labels. The use of AuNPs conjugated with aptamers in a sandwich assay allows the amplification of the SPR signal of the label-free assay. (b) SPR enhancement by NPs modifiers of the sensing surface. The use of AuNPs platforms allows the oriented immobilization of antibody onto the AuNPs assembled SPR immunosensor chips for the further immunoreaction. Adapted from<sup>36,49</sup> with permission.

detected. However, more rapid responses with acceptable LODs with a shorter analysis time and a more compact / integrated immunosensing assays are achieved with this direct detection.

The first work describing direct electrochemical detection of NPs was reported by Costa-García *et al.*<sup>51</sup>. Important contributions have since been made to direct electrochemical characterization or detection of metal and semiconductor NPs by our group and others, and some of the work has been reported regarding the voltammetric analysis of AuNPs and CdS QDs. In the case of the AuNPs<sup>52</sup>, the procedure involves absorption of AuNPs onto the electrode, followed by their electrochemical oxidation in a hydrochloric medium. The resulting tetrachloroaurate ions generated near the electrode surface are detected by differential pulse voltammetry. For CdS QDs<sup>53,54</sup>, the procedure is quite similar, but in this case the Cd (II) ions contained as defects in the CdS QDs crystalline structure are electrochemically reduced to Cd (0) and then immediately electro-oxidised to Cd (II), registering the oxidation peak. Based on these principles, solid-state detection of AuNPs<sup>55</sup> (Fig. 5a) and CdS QDs<sup>56</sup> have been applied in immunoassays for the detection of human IgG and carcinoembryonic antigen *respectively* at pM levels.

### Indirect electrical detections

The most reported way to electrochemically detect NPs involved in bioassays consists in their preliminary oxidative dissolution in acidic mediums, followed by the detection of the metal ions by a sensitive powerful electroanalytical technique such as anodic stripping voltammetry. Very low LODs, in the order of pM, are achieved due

to the release of a large number of metal ions from each NP and its effective "built-in" preconcentration step ensured by electrochemical stripping analysis. Dequaire *et al.*<sup>57</sup> pioneered the application of this NP detection method for the quantification of IgG as model analyte at pg/mL levels. Since then, AuNPs as well as other NPs, such as CdS@ZnS QDs<sup>58,59</sup> and CdSe@ZnS QDs<sup>60</sup> have been used for the sensitive detection (always in the pM level) of proteins as prostate specific antigen or interleukin 1- $\alpha$  respectively. Furthermore, one of the most important advantages that offers the use of QDs as electroactive labels is their ability to perform multidetection by using QDs made of different inorganic crystals, with different electrochemical responses. This electrochemical coding technology has been approached by Liu *et al.*<sup>61</sup> for the simultaneous measurements of proteins ( $\beta_2$ -microglobulin, IgG, bovine serum albumin and C-reactive protein) using ZnS, CdS, PbS and CuS QDs as tracers. (Fig. 5b).

It must also be mentioned that the high surface coupled with the easy bioconjugation, make NPs excellent carriers of other electroactive labels in immunoassays. The loading of NPs with other NPs (i.e. AuNPs loaded by CdS QDs<sup>62</sup>) (Fig. 5c) and with enzymes (i.e. AuNPs loaded by HRP<sup>63</sup> and SiNPs loaded by HRP<sup>64</sup> or AP<sup>65</sup>) (Fig. 5d) so as to obtain labels with an enhanced signal have been reported as an interesting alternative for electrochemical immunosensing systems.

Another alternative to detect NPs used as labels in protein detection assays consists in using their catalytic properties toward reactions of other species. The well-known catalytic properties of the AuNPs on the silver chemical reduction have been extensively approached in the last years.

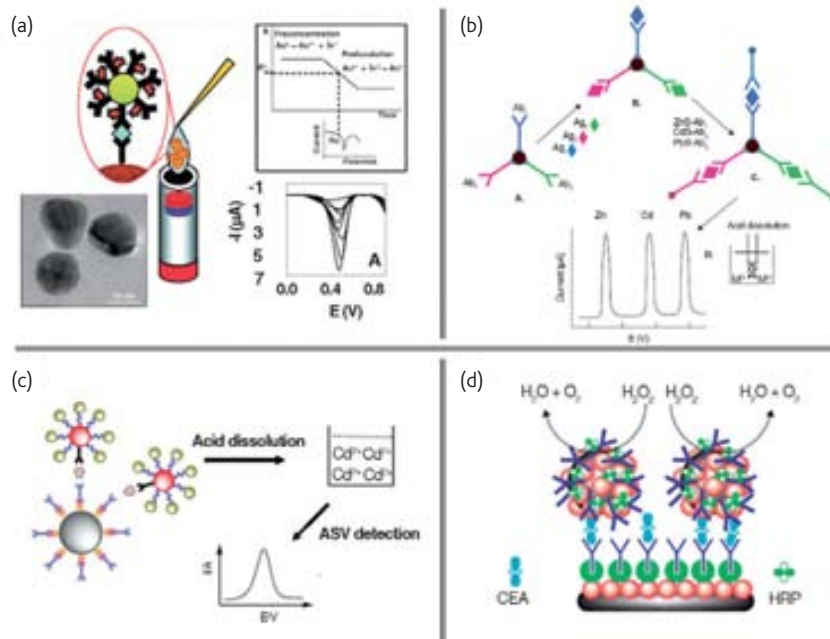


Fig. 5 (a) Electrical detection of NPs. Direct electrical detection of AuNPs tags without acidic dissolving, based on a pre-oxidation and later reduction of Au(III) ions generated. (b) Electrochemical detection of NPs. The electrochemical stripping detection of different QDs labels after their acidic dissolution, allows the multiple detection of proteins. (c) NPs as carriers of other NPs. AuNPs can be used as carriers of a high number of CdS QDs, giving rise to an amplified signal in the further stripping detection after acidic dissolution. (d) NPs as carriers of enzymes. AuNPs can also be used as carriers of a high number of HRP enzymes, exerting an amplification effect in the electrochemical enzymatic signal. Adapted from<sup>56,62-64</sup> with permission.

Recently, our group has developed a very sensitive methodology based on the selective electroreduction of silver ions on the surface of AuNPs in magnetosandwich assays, achieving LODs of human IgG in the fM level<sup>66</sup>, and has also exploited the catalytic properties of AuNPs on the hydrogen ions electroreduction in an acidic medium for the antigen-antibody interaction monitoring, applied for cancer cells detection<sup>67</sup> (Fig. 6).

Silver nanoparticles (AgNPs) also exhibit catalytic activity on the chemical reduction of silver ions added as 'substrate'. After that, the silver can be dissolved in for example an acidic medium and measured by anodic stripping voltammetry. This property has been exploited in sandwich immunoassays, for the sensitive detection of human IgG<sup>68</sup> at pM levels.

Finally, in addition to the catalytic activity on metal ions reduction the catalysis of other electrochemical reactions is also reported. For example, the catalytic activity of PtNPs on the reduction of  $\text{H}_2\text{O}_2$  to  $\text{H}_2\text{O}$ <sup>69</sup>, and of the core-shell Au@Pd NPs on the  $\text{O}_2$  reduction to  $\text{H}_2\text{O}$ <sup>70</sup> have been exploited by Polsky *et al.*, for the detection of thrombin (nM levels) and cytokine TNF- $\alpha$  (fM levels) respectively.

## Electromechanical detection: quartz crystal microbalances and microcantilevers

Microcantilevers and quartz crystal microbalances have emerged in the last few years as versatile biosensors demonstrating remarkable

achievements such as high sensitivity and label free detection<sup>71-73</sup> (Fig. 7a, left part). In the case of the quartz crystal microbalance, the bioreaction generates a change in the mass, reordering the charges in the surface of the piezoelectric material and giving rise to a change in the resonant frequency of the microbalance. The use of NP labels in sandwich assays can increase both the surface stress and the mass of the immunocomplex, allowing the increase in sensitivity of these electromechanical assays.

This was the case in work reported by Lee *et al.*<sup>74</sup> for the detection of prostate specific antigen at pg/mL levels using SiNPs as labels in a dynamic mode microcantilever based biosensor (Fig. 7a, right part and Fig. 7b). In a similar way, quartz crystal microbalance biosensors have been developed using AuNPs, as amplification agents for the detection of human IgG<sup>75</sup> and aflatoxin B1<sup>76</sup> at clinical relevant levels.

## NPs as modifiers of electrotransducing surfaces

The presence of NPs on the electrotransducer surface promotes the electron transfer, improving the electrochemical response coming from potentiometric and conductimetric responses. Furthermore, some NPs provide congenial microenvironments similar to that of redox proteins in a native system for retaining their bioactivity giving the protein molecules more freedom in orientation and

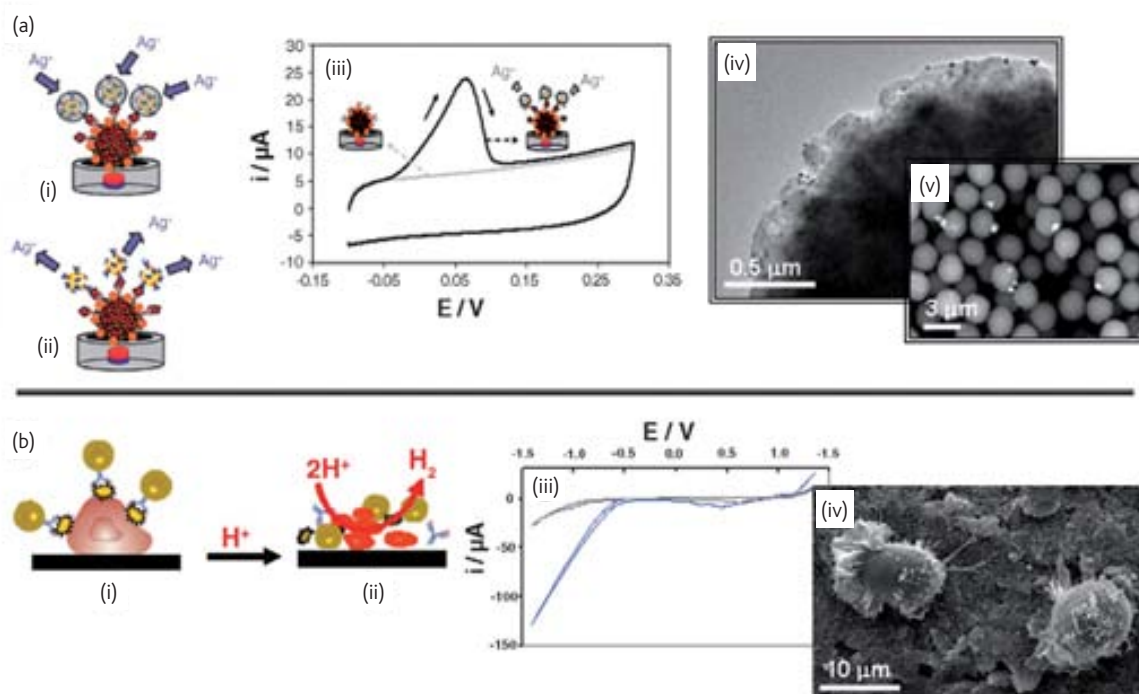


Fig. 6 Electrocatalytic detection of AuNPs. (a) Detection based on the catalytic properties of AuNPs on the silver electroreduction in a magnetosandwich immunoassay (i); the further silver reoxidation (ii) gives rise to a peak current that can be related with the protein concentration (iii); the AuNPs (small black points) can be observed by TEM analysis around the magnetic beads used as immobilization platforms (big black sphere) (iv); the silver crystals formed after the silver electrodeposition (white points) can be observed by SEM analysis around the magnetic beads (v). (b) Detection of cells (i) based on the catalytic properties of AuNPs on the hydrogen evolution in an acidic medium (ii); the presence of AuNPs gives rise to a shift in the reduction potential of the hydrogen ions to hydrogen (lower voltammetric curve) (iii); the cells on the electrotransducer surface can be observed by SEM (iv). From<sup>67,68</sup> with permission.

avoiding their denaturation. The introduction of NPs into the transducing platform is commonly achieved by their adsorption onto conventional electrode surfaces in various forms including that of a composite.

PtNPs directly electrogenerated<sup>77</sup>, AuNPs adsorbed<sup>78</sup>, AuNPs integrated in composites<sup>79,80</sup> or AuNPs immobilised on the electrotransducer surface through electrostatic forces on cationic polymeric layers<sup>81</sup> are representative examples of these nanostructured surfaces built for the detection of proteins such as human IgG,  $\alpha$ -fetoprotein, prostate specific antigen and hepatitis B surface antigen at clinical relevant levels.

In addition to the final conductometric, potentiometric and voltammetric detection it is remarkable to see the use of nanostructured surfaces containing AuNPs<sup>82,83</sup>, ZrO<sub>2</sub> NPs<sup>84</sup> and CoFe<sub>2</sub>O<sub>4</sub>@SiO<sub>2</sub> NPs<sup>85</sup> for improving the performance of quartz crystal microbalance based immunosensors.

### New trends: lateral flow and lab-on-a-chip

A lateral flow assay (LFA) is a prefabricated strip of a carrier material containing dry reagents that are activated by applying the fluid sample<sup>86</sup>. The fluid movement is driven by capillary forces and controlled by the wettability and feature size of the porous or microstructured substrate<sup>87</sup>. When the recognition elements are

antibodies, the test is called lateral flow immunoassay (LFIA). The first LFIA was the pregnancy test, which was based in the detection of human chorionic gonadotropin (HCG), and was introduced into the market in the middle of the '80s<sup>88</sup>. Nowadays several LFIAs to detect drug abuse, cardiac markers, and allergens are commercially available. The LFIA strip is generally divided in 4 zones: sample pad, conjugation pad, detection pad and absorbent pad used to wick the fluid through the membrane. In this way the amount of sample can be increased resulting in an increased sensitivity<sup>86</sup> (see details at Fig. 8a, upper part).

Two formats can be used in a LFIA: competitive and sandwich format. In the competitive format the sample analyte competes with a labelled analyte for the antibodies on the test line<sup>89</sup>. In another type of competitive format an analyte-protein conjugate is sprayed at the test line and the labelled antibody is applied onto the conjugation pad. In this way if the sample contains the analyte then the labelled antibody cannot bind to the test line<sup>90</sup> (Fig. 8b). The sandwich format can be used for analytes with more than one epitope. In this format the sample line is made of an antibody specific for one epitope of the analyte whereas the antibody conjugate with the labelled particles is specific for another epitope. In this way the analyte first binds the antibody of the conjugation pad and then the antibody of the test line. This format gives a signal proportional to the analyte concentration<sup>91</sup> (Fig. 8a, lower part).

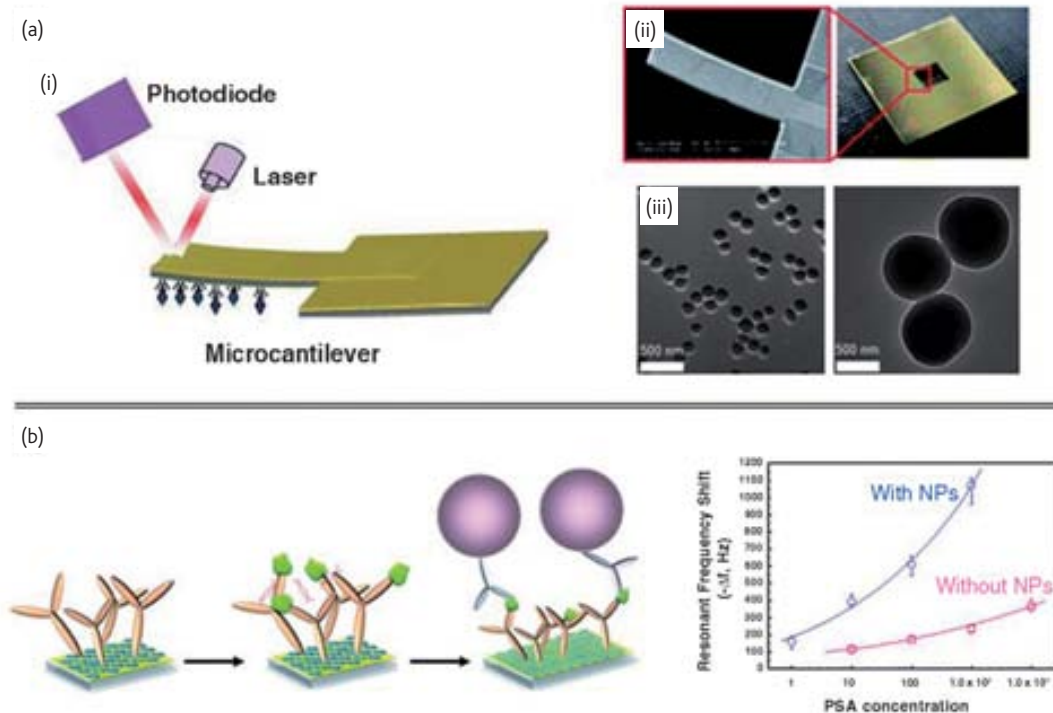


Fig. 7 (a) Electromechanical immunosensing using microcantilevers. (i) The immunoreaction produces a change in the laser reflectance angle on the microcantilever; (ii) SEM image of single microcantilever with dimension of 50 mm/150 mm/1.75 mm (width/length/thickness) (left) and photo image (right) of a unit device with twelve microcantilevers (right); (iii) TEM images of SiNPs used to amplify the label-free immunoassay. (b) Electromechanical detection enhancement by NPs. The sandwich assay using polyclonal antibody conjugated SiNPs allows the enhancement of the resonant frequency shift of the microcantilever described in (a-ii). Adapted from<sup>74,75</sup> with permission.

The detection methods are mainly colorimetric and give results mostly qualitative or semi quantitative, even if, in the last year, fluorescent and electrochemical detection produce some quantitative results using a readout device<sup>92,93</sup>. The responses usually come within 2 and 15 minutes. The highest optical detection limit obtained with a sandwich format LFIA is about 1 pg/mL<sup>94</sup>, whereas the electrochemical detection limit is about 10 pg/mL. The LFIA strips already have an important market presence due to their ease of use, low cost, at the point of care and fast. These qualities make them suitable for the home care and *in vitro* diagnostics. However, their applications in more complex samples are facing problems related to reproducibility and long-term operation.

Currently, the trend in the development of biosensing systems is towards the miniaturization of the whole analytical chain, from sampling to the detection of the analytes. The advantages of miniaturized systems in general and particularly of microfluidic based biosensors are for reducing the amount of sample and reagents, detection facility, minimal handling of hazardous materials and multiple and parallel sample detection capability. Techniques such as fluorescence, absorbance and electrochemistry have been used for the final detection of the immunoassay. The combination of these microfluidics chips with the use of NPs, gives rise to systems with improved performance for immunosensing.

With regard to the electrochemical detection, PDMS–glass hybrid electro-immunosensing chips have recently been reported by Lee's group<sup>95,96</sup> for the multiplex detection of cancer biomarkers ( $\alpha$ -fetoprotein, carcinoembryonic antigen and prostate specific antigen) at pM levels, using microbeads as antibody immobilization platforms and measuring the electrical resistance between microelectrodes and taking advantage of AuNPs labels and silver enhancement (Fig. 9a). In addition to the lower volumes of sample needed, the overall assay time were demonstrated to be reduced from 3–8 hours to about 55 minutes when compared to conventional immunoassays.

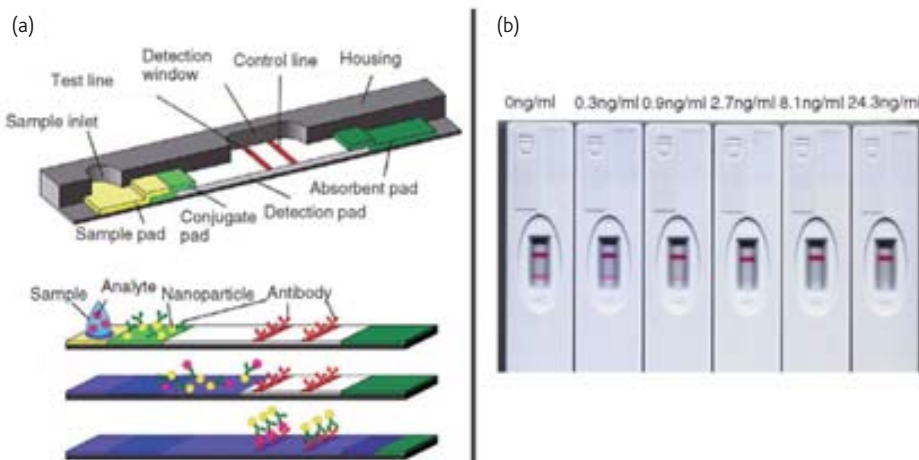


Fig. 8 Lateral flow immunoassay using NPs. (a) Schematic of a lateral flow strip (upper part) and lateral flow immunoassay (LFIA) based on a sandwich format (lower part). (b) Example of results obtained for a competitive LFIA. When increasing the concentration of the analyte, the intensity of test line decreases as expected. Adapted from<sup>88,91</sup> with permission.

## Instrument Citation

### Colorimetric detection

- Cary 500 scan UV-vis-NIR spectrophotometer (Varian, USA)
- Lamda 800 UV-vis spectrometer (Pekin-Elmer, USA).
- Shimadzu UV-1601PC spectrophotometer plate reader (Tecan Trading AG, Switzerland).
- Cary 500 scan UV-vis-NIR spectrophotometer (Varian, USA).

### Fluorescence detection

- BioTek Synergy HT microplate reader (BioTek, USA).
- Nanodrop ND-3300 fluorospectrometer (Thermo Scientific, USA).
- RF-5301 PC fluorospectrometer (Shimadzu Scientific Instruments, USA)
- SPECTRAmax M2e multi-mode microplate reader (Molecular Devices Inc, USA)
- Olympus IX 71 fluorescence inverted microscope (Olympus GmbH, Germany)

### Surface plasmon resonance based detection

- Autolab SPR systems (Eco Chemie, The Netherlands).
- BIAcore 2000TM (BIAcoreTM, USA).

### Electrical detection

- Potentiostat / Galvanostat Autolab 12 (Eco-chemie, The Netherlands)
- Potentiostat / Galvanostat Model 600D series (CH Instruments Inc, USA).

### Electromechanical detection

- EQCM cell system (CH Instruments, USA).
- Quartz crystal analyzer QCA922 (Seiko EG&G Co. Ltd. Japan).

### Other characterizations of nanoparticles

- Dynamic light scattering (Zetasizer Nano ZS (Malvern Instruments , U.K.))
- Flow cytometry (BD FACSAria flow cytometer (Beckton Dickinson, USA)
- Scanning Electron Microscope (SEM) (Jeol JSM-6300, Jeol Ltd, Tokio, Japan)
- Transmission Electron Microscope (TEM)  
Jeol JEM-2011, Jeol Ltd, Japan  
H800, Hitachi, Japan  
Philips CM20, Philips, The Netherlands

Alternatively, the multiplex detection of cancer biomarkers at clinical relevant levels has also been performed approaching the fluorescence properties of CdSe@ZnS in an anisotropically etched silicon chip<sup>97</sup> (Fig. 9b).

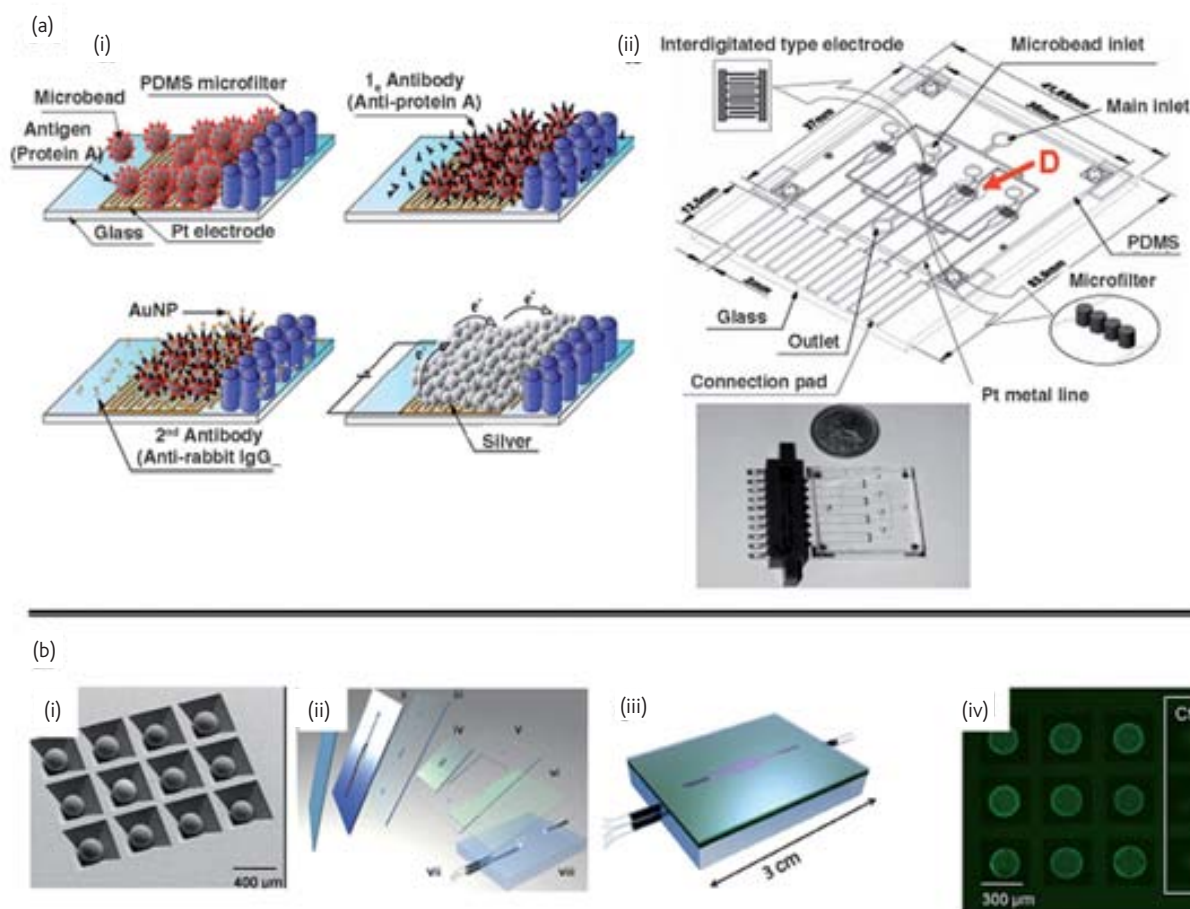


Fig. 9 (a) Electrochemical detection in a microfluidic chips using AuNPs labels. Illustration of the electrical immunoassay. (i) A sandwich immunoassay is carried out in a PDMS-glass chip, using magnetic beads as platforms and AuNPs labels and the final detection is performed by measuring the electrical resistance between microelectrodes, taking advantage of the silver enhancement catalyzed by AuNPs. (ii) 3-D drawing of the design of the PDMS-glass electro-immunosensing chip (the detection zone in the chip is indicated as "D") and photograph of the fabricated chip. (b) Fluorescent detection in a microfluidic chip using QDs labels. (i) SEM photomicrograph of beads in anisotropically etched silicon chip. (ii) PMMA chip layers fabrication; (iii) Sealed LOC assembly; (iv) Fluorescent image of beads after immunoassay including negative controls as imaged with one second of CCD camera integration (exposure) time. Adapted from<sup>96-98</sup> with permission.

## Conclusions and outlook


This is a brief overview of a rapidly increasing research field in immunosensing using nanoparticles. The research and applications in this field are at the crossroads of materials research, nanosciences, and molecular biotechnology. Since the nanoparticles and biomolecules typically meet at the same nanometer length scale, this interdisciplinary approach will contribute to the establishment of a novel field, descriptively termed immunosensing nanotechnology or nanoimmunosensing.

Future development of immunosensing technology will continually profit from the rapid current advances in material science and particularly that of nanomaterials science thus producing novel nanoparticles with improved physical and chemical properties. In addition, the current proteome research will also benefit since it provides data that allows the production of even more relevant bioreceptors crucial for this technology. These developments will

open the door to more effective nanoimmunosenors with a focus on biomedical applications.

In addition to the long term perspectives, today's advanced nanomaterials as well as the modern optical and electrochemical techniques originally developed for materials research, physics and biology are already being used in immunosensing applications or as model systems with an interest in basic research as well as to solve biological and clinical analysis problems. NP based immunosensing systems are proving to assist in the development of new and versatile protein detection methods. In most of the reported applications NPs are seen as immunoassay labels achieving higher sensitivities as well and multiplexing analysis. They are also used as modifiers of the electrochemical or optical transducing platforms.

Clearly, we are still far from the real nanosensors that can operate in an automatic mode in living organisms. However the progress in nano and microsystem technology including nanomotors may open the way to real nanosize sensors and even to a new class of immunosensors that in

an intelligent way could combine diagnostic and therapy in the so called theranostic<sup>98</sup> devices. This can probably significantly shorten the time from protein sensing (diagnostic) to therapy (i.e. cancer cell fighting) that would improve an individuals life and ensure a better safety and security. 

## Acknowledgments

We acknowledge funding from MEC for the projects MAT2008-03079/NAN, CSD2006-00012-“NANOBIOMED”- (Consolider-Ingenio-2010) and the JdC scholarship (A.de la Escosura-Muñiz).

## REFERENCES

- Agasti, S. S., et al., *Adv Drug Delivery Rev* (2010) **62** (3), 316.
- Durner, J., *Angew Chem Int Ed* (2009) **49**(6), 1026.
- Palchetti, I., and Mascini, M., *Analyst* (2008) **133**, 846.
- Seydack, M., *Biosens Bioelectron* (2005) **20**, 2454.
- Roy, S., and Gao, Z., *Nano Today* (2009) **4**, 318.
- Pumera, M., et al., *Sensors and Actuators B* (2007) **123**, 1195.
- Rosi, N. L., and Mirkin, C. A., *Chem Rev* (2005) **105**, 1547.
- Janeway, Jr, C. A., et al., *Immunobiology: The Immune System in Health and Disease*, 6th edition. Taylor & Francis Group, New York, 2005.
- Ahirwal, G. K., and Mitra, C. K., *Biosens Bioelectron* (2010) **25**, 2016.
- Thobhani, S., et al., *J Immunol Meth* (2010) **356**, 60.
- Storhoff, J. J., et al., *J Am Chem Soc* (2000) **122**, 4640
- Faraday, M., *Philos Trans R Soc* (1857) **147**, 145.
- Mirkin, C. A., et al., *Nature* (1996) **382**, 607.
- Storhoff, J. J., et al., *J Am Chem Soc* (1998) **120**, 1959.
- Stewart, M. E., et al., *Chem Rev* (2008) **108**, 494.
- Neely, A., et al., *ACS Nano* (2009) **3** (9), 2834.
- Chen, C. K., et al., *Biosens Bioelectron* (2010) **25**, 1922.
- Liu, Y., et al., *Biosens Bioelectron* (2009) **24**, 2853.
- Schofield, C. L., et al., *Anal Chem* (2007) **79**, 1356.
- Aili, D., et al., *Small* (2009) **5** (21), 2445.
- Wei, H., et al., *Anal Chem* (2008) **80**, 7051.
- Ambrosi, A., et al., *Anal Chem* (2010) **82**, 1151.
- Alivisatos, A. P., *J Phys Chem* (1996) **100**, 13226.
- Murray, C. B., et al., *J Am Chem Soc* (1993) **115**, 8706.
- Soman, C. P., and Giorgio, T. D., *Langmuir* (2008) **24**, 4399.
- Cui, R., et al., *Anal Chem* (2007) **79**, 8494.
- Dorfman, A., et al., *Adv Mater* (2006) **18**, 2685.
- Liu, Y., et al., *Anal Chem* (2007) **79**, 8796.
- Xie, H., et al., *Small* (2009) **5** (9), 1036.
- Näreoja, T., et al., *J Immunol Meth* (2009) **345**, 80.
- Zhang, H., et al., *Chem Mater* (2007) **19**, 5875.
- Hun, X., and Zhang, Z., *Biosens Bioelectron* (2007) **22**, 2743.
- You, C. C., et al., *Nature Nanotech* (2007) **2** (5), 318.
- Englebienne, P., et al., *Spectroscopy* (2003) **17**(2-3), 255.
- Homola, J., *Chem Rev* (2008) **108**, 462.
- Wang, J., et al., *Biosens Bioelectron* (2009) **25**, 124.
- Mitchell, J. S., and Lowe, T. E., *Biosens Bioelectron* (2009) **24**, 2177.
- Cao, C., and Sim, S. J., *Biosens Bioelectron* (2007) **22**, 1874.
- Hsieh, B. Y., et al., *Anal Chem* (2007) **79**, 3487.
- Chang, Y. F., et al., *Biosens Bioelectron* (2009) **24**, 1610.
- Jain, P. K., et al., *J Phys Chem B* (2006) **110**, 7238.
- Du, B. A., et al., *Angew Chem Int Ed* (2006) **45**, 8022.
- Xie, C., et al., *J Am Chem Soc* (2009) **131**, 12763.
- Jans, H., et al., *Anal Chem* (2009) **81**, 9425.
- Stiles, P. L., et al., *Annu Rev Anal Chem* (2008) **1**, 601.
- Schlüker, S., *Chem Phys Chem* (2009) **10**, 1344.
- Porter, M. D., et al., *Chem Soc Rev* (2008) **37**, 1001.
- Ko, S., et al., *Biosens Bioelectron* (2009) **24**, 2592.
- Han, X. X., et al., *Anal Chem* (2009) **81**, 3350.
- De la Escosura-Muñiz, A., et al., *Trends Anal Chem* (2008) **27** (7), 568.
- González-García, M. B., and Costa-García, A., *Bioelectrochem Bioenerg* (1995) **38**, 389.
- Pumera, M., et al., *Electrochim Acta* (2005) **50**, 3702.
- Merkoçi, A., et al., *Nanotechnology* (2006) **17**, 2553.
- Merkoçi, A., et al., *Nanotechnology* (2007) **18**, 35502.
- Ambrosi, A., et al., *Anal Chem* (2007) **79**, 5232.
- Ho, J. A., et al., *Anal Chem* (2009) **81**, 1340.
- Dequaire, M., et al., *Anal Chem* (2000) **72**, 5521.
- Liu, G., et al., *Anal Chem* (2007) **79**, 7644.
- Lin, Y. Y., et al., *Biosens Bioelectron* (2008) **23**, 1659.
- Wu, H., et al., *Electrochem Commun* (2007) **9**, 1573.
- Liu, G., et al., *Anal Chem* (2004) **76**, 7126.
- Ding, C., et al., *Biosens Bioelectron* (2009) **24**, 2434.
- Tang, D., et al., *Anal Chem* (2008) **80**, 1582.
- Wu, Y., et al., *Anal Chem* (2009) **81**, 1600.
- Qu, B., et al., *Talanta* (2008) **76**, 785.
- De la Escosura-Muñiz, A., et al., *Biosens Bioelectron* (2009) **24**, 2475.
- De la Escosura-Muñiz, A., et al., *Anal Chem* (2009) **81**, 10268.
- Chen, Z. P., et al., *Biosens Bioelectron* (2007) **23**, 485.
- Polsky, R., et al., *Anal Chem* (2006) **78**, 2268.
- Polsky, R., et al., *Chem Commun* (2007) **26**, 2741.
- Fritz, J., *Analyst* (2008) **133**, 855.
- Wu, G., et al., *Nature Biotech* (2001) **19**, 856.
- Milburn, C., et al., *J. Biomed Nanotech* (2005) **1** (1) 30.
- Lee, S. M., et al., *Lab Chip* (2009) **9**, 2683.
- Chu, X., et al., *Sens Actuat B* (2006) **114**, 696.
- Jin, X., et al., *Biosens Bioelectron* (2009) **24**, 2580.
- Huang, Y., et al., *Biosens Bioelectron* (2008) **24**, 600.
- Ding, C., et al., *Talanta* (2009) **78**, 1148.
- Liu, Y., *Thin Solid Films* (2008) **516**, 1803.
- Tang, D., et al., *Clin Biochem* (2006) **39**, 309.
- Mani, V., et al., *ACS Nano* (2009) **3**, 585.
- Ding, Y., et al., *Biomaterials* (2007) **28**, 2147.
- Zhang, Q., et al., *J Colloid Interface Science* (2008) **319**, 94.
- Wang, H., et al., *Biosens Bioelectron* (2009) **24**, 2377.
- Tang, D., et al., *Adv Funct Mater* (2007) **17**, 976.
- Posthuma-Trumpie, G. A., et al., *Anal Bioanal Chem* (2009) **393**, 569.
- Mark, D., et al., *Chem Soc Rev* (2010) **39**, 1153.
- Leuversing, J. H. W., et al., *J Immunol Meth* (1981) **45** (2), 183.
- Laitinen, M. P., and Vuento, M., *Biosens Bioelectron* (1996) **11** (12), 1207.
- Zhao, Y., et al., *J. Agric Food Chem* (2008) **56**, 12138.
- Van Amerongen, A., et al., *Clin Chim Acta* (1994) **229** (1-2), 67.
- Cosmi, B., et al., *Thromb Res* (2000) **100** (4), 279.
- Liu, G., et al., *Anal Chem* (2007) **79**, 7644.
- Tanaka, R., et al., *Anal Bioanal Chem* (2006) **385**, 1414.
- Ko, Y. J., et al., *Electrophoresis* (2008) **29**, 3466.
- Ko, Y. J., et al., *Sens Actuat B* (2008) **132**, 327.
- Jokerst, J. V., et al., *Biosens Bioelectron* (2009) **24**, 3622.
- Ho, Y. P., and Leong, K. W., *Nanoscale* (2010) **2**, 60.

## Paper-based nanobiosensors for diagnostics

Claudio Parolo<sup>a</sup> and Arben Merkoçi<sup>\*ab</sup>Cite this: *Chem. Soc. Rev.*, 2013, **42**, 450

Received 11th July 2012

DOI: 10.1039/c2cs35255a

www.rsc.org/csr

In this review we discuss how nanomaterials can be integrated in diagnostic paper-based biosensors for the detection of proteins, nucleic acids and cells. In particular first the different types and properties of paper-based nanobiosensors and nanomaterials are briefly explained. Then several examples of their application in diagnostics of several biomarkers are reported. Finally our opinions regarding future trends in this field are discussed.

## Introduction

In the last few years the development of new biosensors has increased significantly, especially in diagnostics, since it has been shown that an early diagnosis can change dramatically the development of a disease.<sup>1</sup> In particular, in the third world the availability of biosensors for the most common diseases could save many lives.<sup>2</sup> Unfortunately, the cost of biosensors and the lack of equipped centers and trained people are probably the hardest obstacles to the diffusion of adequate biosensors in

these regions.<sup>3,4</sup> The World Health Organization defined that diagnostics for developing countries should be defined as ASSURED: affordable, sensitive, specific, user-friendly, rapid and robust, equipment free and deliverable to end-users.<sup>5</sup>

Nanomaterials are bringing important advantages in the design of novel biosensing systems or improvements of the existing devices. Nanomaterial application in environmental monitoring (*i.e.* heavy metals<sup>6</sup>), nanoparticles uses for DNA,<sup>7</sup> proteins<sup>8</sup> and even cells (*i.e.* cancer diagnostics<sup>9</sup>) are showing great potential in enhancing biosensor sensitivity, stability and in general improvement of the cost-efficiency of the developed devices.

Although nanotechnology contains a high level of integrated technologies and knowledge, it is also bringing simple sensing

<sup>a</sup> Nanobioelectronics & Biosensors Group, Institut Català de Nanotecnologia, CIN2 (ICN-CSIC), Campus UAB, Barcelona, Spain

<sup>b</sup> ICREA, Barcelona, Spain. E-mail: arben.merkoci@icn.cat



Claudio Parolo

Claudio Parolo obtained his BSc in Biotechnology, at the University of Padova in July 2007. In October 2009 he obtained his Industrial Biotechnology MSc degree at the same university, with a Thesis on "Gold nanoparticles in nucleic acid biosensors", carried out at the Catalan Institute of Nanotechnology (ICN) (Barcelona, Spain) and co-supervised by Professors Arben Merkoçi and Flavio

Maran. He is currently a PhD student in the Nanobioelectronics and Biosensors Group at the ICN. His work focuses on the development of electrochemical and paper-based biosensors based on nanoparticles for the detection of protein and nucleic acid for diagnostic applications.



Arben Merkoçi

Arben Merkoçi is ICREA Professor and head of the Nanobioelectronics and Biosensors Group at Catalan Institute of Nanotechnology, in Barcelona. He obtained a PhD in Chemistry at the University of Tirana (Albania) and followed various postdoctoral researches in various international centers. His research is focused on the integration of biological molecules and other receptors with micro- and nanostructures

of interest for the design of novel sensors and biosensors. He is the author of over 150 manuscripts, special journal issues, and books and lastly serves as Editor of the Nanoscience and Nanotechnology Encyclopedic Series launched by John Wiley & Sons.

and biosensing concepts and technologies, which are making possible the development of even more easy-to-use and efficient biosensors. Paper-based nanobiosensors are the excellent example of ASSURED devices developed as a result of the synergy between nanotechnology and biosensing technology.

### Why paper-based biosensors?

Paper-based biosensors can be one of the answers to this demand. In fact they are affordable, paper is inexpensive and abundant; sensitive and specific, they can be based on immuno-reactions or nucleic acid hybridizations; user-friendly, the pregnancy test is one of the most used point-of-care (PoC) biosensors; rapid and robust, within a few minutes or less the response is developed; equipment free, they are mainly read with the naked eye, or, if a quantitative detection is required, the equipment is small and cheap; and finally deliverable to end-users, they are quite stable to a wide range of temperature and time.<sup>10</sup> Furthermore they can be developed using inkjet,<sup>11</sup> wax printing<sup>12</sup> or screen printing<sup>13</sup> technology, making them amenable to *in-situ* fabrication<sup>14</sup> with interest to be delivered or even produced in areas with limited resources.

### A little bit of history

The first paper-based sensor can be considered the invention of paper chromatography by Martin and Synge, who were awarded with the Nobel Prize in chemistry in 1952. Another milestone in the field was the commercialization of the pregnancy test, which can be considered one of the most used PoC biosensors and one of the first lateral flow assays (LFAs).<sup>6</sup> After the pregnancy test, other diagnostic PoC paper-based devices for diabetes and for the detection of biomarkers of pathogens and infectious diseases appeared in the market.<sup>15</sup> More recently the development in this field has been extended toward the microfluidic paper analytical devices ( $\mu$ PADs).<sup>16</sup>

### Different types of paper-based biosensors

The paper-based biosensor can be divided into three main categories: the dipstick assays, the LFAs and the  $\mu$ PADs (Table 1).

The dipstick assays are the simplest ones, since they are based on the blotting of the sample onto a paper pre-stored with reagents; the best known example is the pH strip. Their main disadvantage is the impossibility to design more sophisticated assays, which for diagnostic purposes are often necessary.

The LFAs have all the reagents pre-stored in the strip, as the dipstick, but they integrate also the flow of the sample. The flow gives a very important advantage to the sample: it passes through the different zones of the strip, which have different reagents for different functions. In this way many different assay designs like sandwich and competitive formats or multi-detection can be used. In particular a LFA is generally made of 4 different parts: the sample pad, the conjugation pad, the detection pad and the absorbent pad. The sample pad, made of cellulose, filters the sample from impurities and stores the dried assay buffer, which assures the optimal conditions for the analyte during all the flux. The conjugation pad, made of glass fibers, is used as dry-reagent storage for the labels. In this pad the binding reaction between the labels and the analyte starts. In the detection pad, made of nitrocellulose, the capture reagents are fixed and the signal is developed. Finally, cellulose filters are used as absorbent pad. The function of the absorbent pad is to wick the fluid through the membrane, in this way the amount of sample can be increased resulting in an increased sensitivity. The main drawbacks of the LFAs are the difficulty in obtaining multiplex and quantitative analysis.<sup>17</sup>

These drawbacks can be overcome using the  $\mu$ PADs. The  $\mu$ PADs are devices which integrate the paper advantages with those of microfluidics. In fact they are very cheap and do not need any pump or external source of energy to make the liquid flow through the channel, but at the same time they require a very low amount of sample and can be used for multiplexed and quantitative analysis.<sup>18</sup> They are made creating hydrophilic channels in hydrophobic paper. Many techniques such as photolithography, polydimethylsiloxane (PDMS) plotting, inkjet etching, plasma etching, cutting, and wax printing have been used to produce  $\mu$ PADs.<sup>19</sup>

### Different types of detection

The three different types of paper-based platforms exemplify differences in the type of detection. In fact the dipstick assays

**Table 1** Detection methods, advantages and disadvantages of the different paper-based biosensors

Type of paper-based biosensor	Possible detection methods	Advantages	Disadvantages
Dipstick	<ul style="list-style-type: none"> <li>Optical</li> </ul>	<ul style="list-style-type: none"> <li>Easy design</li> <li>Fast optimization</li> </ul>	<ul style="list-style-type: none"> <li>Just one step</li> <li>Only optical detection</li> <li>Mostly no quantification</li> </ul>
LFA	<ul style="list-style-type: none"> <li>Optical</li> <li>Electrochemical</li> </ul>	<ul style="list-style-type: none"> <li>Versatile</li> <li>Flow</li> <li>Electrochemical detection</li> <li>Possible quantification</li> </ul>	<ul style="list-style-type: none"> <li>Long optimization times</li> <li>Long fabrication</li> <li>Sample volume (around 100 <math>\mu</math>L)</li> </ul>
$\mu$ PAD	<ul style="list-style-type: none"> <li>Optical</li> <li>Electrochemical</li> <li>Chemiluminescence</li> <li>MEMS</li> </ul>	<ul style="list-style-type: none"> <li>Versatile</li> <li>Flow</li> <li>Different detection methods</li> <li>Quantification</li> <li>Small sample volume (less than 10 <math>\mu</math>L)</li> <li>Massive production</li> </ul>	<ul style="list-style-type: none"> <li>Long optimization times</li> </ul>

tend to be an easy optical detection, which is done with the naked eye, like pH strips, in the most cases. Regarding the LFAs, optical detection is the most frequent and is based on the use of strip readers, when quantitative results are required,<sup>20</sup> although integration of electrochemical detection within the LFA is also reported.<sup>21</sup> Finally the  $\mu$ PADs, besides being simple and using optical detection, can employ more sophisticated devices and techniques, like microplate readers,<sup>22</sup> chemiluminescence,<sup>23,24</sup> electrochemistry,<sup>25</sup> transmission of light through paper,<sup>4</sup> or piezoresistive MEMS sensors.<sup>26</sup> All these techniques would be useless in third world countries due to the price of the devices and the lack of trained people. To solve this problem Martinez *et al.* integrate the use of a normal digital camera. The camera can digitalize the optical signal of the paper-based sensor and send it to trained personnel, who can send back a quantitative response.<sup>27</sup>

### What nanotechnology can bring

In this context nanotechnology can improve the quality of the paper-based devices with the unique properties of the nanomaterials.<sup>28</sup> In the paper biosensors the nanomaterials are mainly used as labels or carriers<sup>29</sup> (Fig. 1A), but other special functions such as photocatalytic, antibacterial, anti-counterfeiting, Surface Enhanced Raman Scattering (SERS) and Surface Plasmon

Resonance (SPR) on the paper have also been reported.<sup>30</sup> The most used nanomaterials in paper-based devices are gold nanoparticles (AuNPs).<sup>31</sup> AuNPs have many properties, which make them excellent labels: easy functionalization, easy manipulation, biocompatibility, a strong red color, a characteristic surface Plasmon resonance and electrochemical activity that can be used in optical<sup>32</sup> (Fig. 1B) or electrical detection of antibodies, nucleic acids and even cancer cells. The AuNPs are not the only nanoparticles used in paper-based devices. Magnetic nanoparticles,<sup>33</sup> quantum dots (QDs),<sup>34</sup> liposomes,<sup>35</sup> carbon nanoparticles<sup>36,37</sup> and ceria nanoparticles<sup>38</sup> have also been reported.

### Protein detection

The development of sensitive, easy-to-use and cheap biosensors for the detection of proteins is of tremendous interest for diagnostics applications. In fact many diseases can be related to the higher/lower presence of a protein or to its different isoforms.<sup>39</sup> Many paper-based sensors have been developed using different strategies. Here we try to summarize the different techniques and nanoparticles that can be used.

The main format used in paper nanobiosensors to detect proteins is the sandwich assay, based on a pair of antibodies (immunosandwich formation) as reported below. Li *et al.* detected nitrated ceruloplasmin, a significant biomarker for cardiovascular disease, lung cancer, and stress response to smoking, using a sandwich assay LFA based on the measurement of the QD fluorescence using a portable device (Fig. 2A). The authors reached a limit of detection (LoD) of  $8 \text{ ng mL}^{-1}$  in a spiked human plasma sample.<sup>40</sup> Other works enhanced the sensitivity of the sandwich format. One was proposed by Parolo *et al.* using the AuNPs both as labels, reaching a LoD of  $6 \text{ ng mL}^{-1}$  of HlgG, and as carriers of HRP, achieving a LoD of  $200 \text{ pg mL}^{-1}$ .<sup>41</sup> A different mechanism of enhancement was proposed by Choi *et al.*, combining two different size AuNPs in the same sandwich to detect the Troponin I with a LoD of  $10 \text{ pg mL}^{-1}$  (Fig. 2B) in serum samples of patients with myocardial infarction.<sup>42</sup> The sandwich format also has been used by Lin *et al.* to develop an electrochemical LFA reaching a LoD of  $20 \text{ pg mL}^{-1}$  of prostate specific antigen in human serum. In this case the authors used core-shell CdSe-ZnS nanoparticles as labels.<sup>43</sup>

The following two works are based also on the sandwich format but instead of using antibodies, the authors used aptamers or DNA sequences. Xu *et al.* detected thrombin in human plasma, achieving a LoD of  $2.5 \text{ nM}$ , using a LFA based on the use of aptamers combined with AuNPs. They demonstrated that aptamers are equivalent or superior to antibodies in terms of specificity and sensitivity for thrombin detection, respectively (Fig. 2C).<sup>44</sup> Fang *et al.* developed a LFA for the rapid detection of the DNA-binding protein c-jun. They used the sandwich format using AuNPs functionalized with a DNA probe specific for the c-jun and a capture antibody specific for the same protein in the test line. The biosensor was tested with crude HeLa cells lysate and it visually detected c-jun activity in  $100 \text{ g}$  of protein lysate.<sup>45</sup>

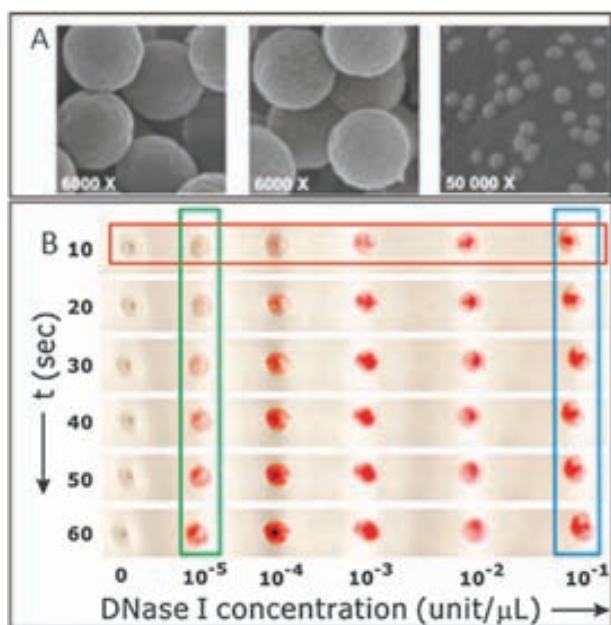


**Fig. 1** Nanomaterials in paper biosensors. (A) From the left to the right: scanning electron microscopy (SEM) images of the microspheres deposited on the diagnostic membrane alone, with nanoparticles, and with nanoparticles at a larger magnification. Reprinted from ref. 29 with permission from IOP. (B) DNase I-sensing assays on hydrophobic paper as functions of assay time and DNase I concentration. More red color is observed when more target analyte is added (red box) or longer assay time was utilized (green box). Note that the color intensity eventually reaches a plateau. For example, when a target analyte at a high concentration ( $10^{-1} \text{ unit } \mu\text{L}^{-1}$ ) was applied (blue box), a maximum signal was reached very quickly ( $\sim 10\text{--}20 \text{ s}$ ), after which no further color change was observed. Reprinted with permission from ref. 32. Copyright 2008, American Chemical Society.

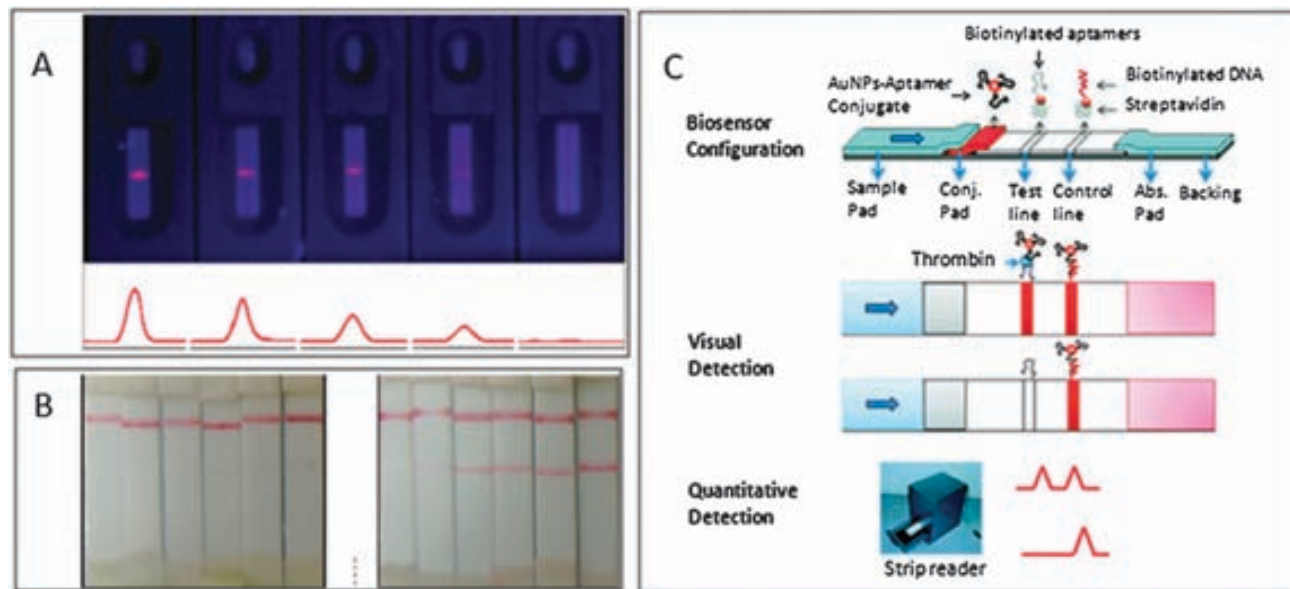


**Fig. 2** Paper-based biosensor for protein detection. (A) Fluorescence imaging of QD-based LF for (from the left to the right)  $10 \text{ g mL}^{-1}$ ,  $1 \mu\text{g mL}^{-1}$ ,  $100 \text{ ng mL}^{-1}$ ,  $10 \text{ ng mL}^{-1}$  nitrated ceruloplasmin and  $10 \mu\text{g mL}^{-1}$  ceruloplasmin without nitration. The bottom curves are the corresponding readout using a strip reader. Reprinted with permission from ref. 40. Copyright 2010, American Chemical Society. (B) Detection of troponin I with varying concentrations by the conventional LFA (left) and the dual AuNP conjugate-based LFA (right). Reprinted from ref. 42. Copyright 2010, with permission from Elsevier. (C) Schematic illustration of the configuration and measurement principle of the aptamer-based strip biosensor. Reprinted with permission from ref. 44. Copyright 2009, American Chemical Society.

Some very interesting works about the detection of proteins in paper-based biosensors, based on enzymatic reactions, have been published; in a near future such devices will probably integrate nanoparticles in order to enhance their performances. Martinez *et al.* were the first in creating a  $\mu\text{PAD}$  for the detection of protein. They could detect the total amount of protein in a urine sample, as low as  $0.38 \mu\text{M}$ , integrating the tetrabromophenol blue in a  $\mu\text{PAD}$ .<sup>16</sup> Particularly interesting is the work of Cheng *et al.*, who developed a paper-based ELISA (P-ELISA). They obtained a 96 well paper device, which can be read with a normal spectrophotometer to perform the classical ELISA test. P-ELISA showed to be faster and cheaper than a conventional ELISA and with a similar level of sensitivity and specificity. In particular the authors obtained a limit of detection of  $54 \text{ fmol per zone}$ , which is approximately ten times lower than that obtained by ELISA experiments in 96-well plates for the same antigen–antibody pair.<sup>46</sup> The paper-based ELISA format was recently used by Wang *et al.* to perform a multi detection of tumoral markers. In their work the authors introduced, besides the chemiluminescence detection, the modification with chitosan of the surface to enhance the efficiency of immobilization of the antibodies. They reached to detect with a linear range:  $0.1\text{--}35.0 \text{ ng mL}^{-1}$  for  $\alpha$ -fetoprotein,  $0.5\text{--}80.0 \text{ U mL}^{-1}$  for cancer antigen 125 and  $0.1\text{--}70.0 \text{ ng mL}^{-1}$  for carcinoembryonic antigen.<sup>23</sup>

## Nucleic acid detection

The detection of nucleic acids is used for genetic tests but also for the detection of pathogens, making these molecules extremely important in diagnostics.<sup>47</sup> The samples used are

generally pre-amplified using PCR or isothermal techniques in order to have a sufficient amount of DNA to be detected or they are synthetic DNA sequences. Furthermore, the connection of DNA sequences with the paper generally occurs through the use of a pair of proteins, like biotin–avidin or antigen–antibody, which makes a bridge between the DNA and the paper.

He *et al.* could detect as low as  $10 \text{ aM}$  of a synthetic target DNA with a LFA test without the use of any instrument. To achieve this result they used an enzyme–AuNP dual label to add the red color produced by the deposition of an insoluble enzymatic catalytic product to the red color produced by the AuNPs (Fig. 3A).<sup>48</sup>

Elenis *et al.* developed a multiplex LFA which was able to detect 10 different DNA sequences. In particular, they spotted onto the membrane polystyrene microspheres functionalized with different DNA sequences specific for the different PCR products. In this way the probes were more exposed to the sample than if they were attached directly to the membrane. The detection was done using AuNPs modified with an antibody specific for the biotin. In fact, the PCR was performed with biotinylated primers in order to have the biotin only if the primers matched perfectly with the target sequences. In this way they could detect the target sequences in a range of  $2\text{--}80 \text{ fmol}$  of extended primer with the naked eye.<sup>29</sup> Konstantou *et al.* detected with a LFA the somatic mutation JAK2V617F, related to *polycythemia vera* and *thrombocythemia*, incorporated as clonal biomarker in WHO diagnostics criteria. The authors used primers modified with biotin or digoxin into a triprimer PCR in order to detect a single-nucleotide polymorphism (SNP) in clinical samples. In fact the digoxin primer matches just with the mutant allele, producing a small product, whereas the biotinylated primer

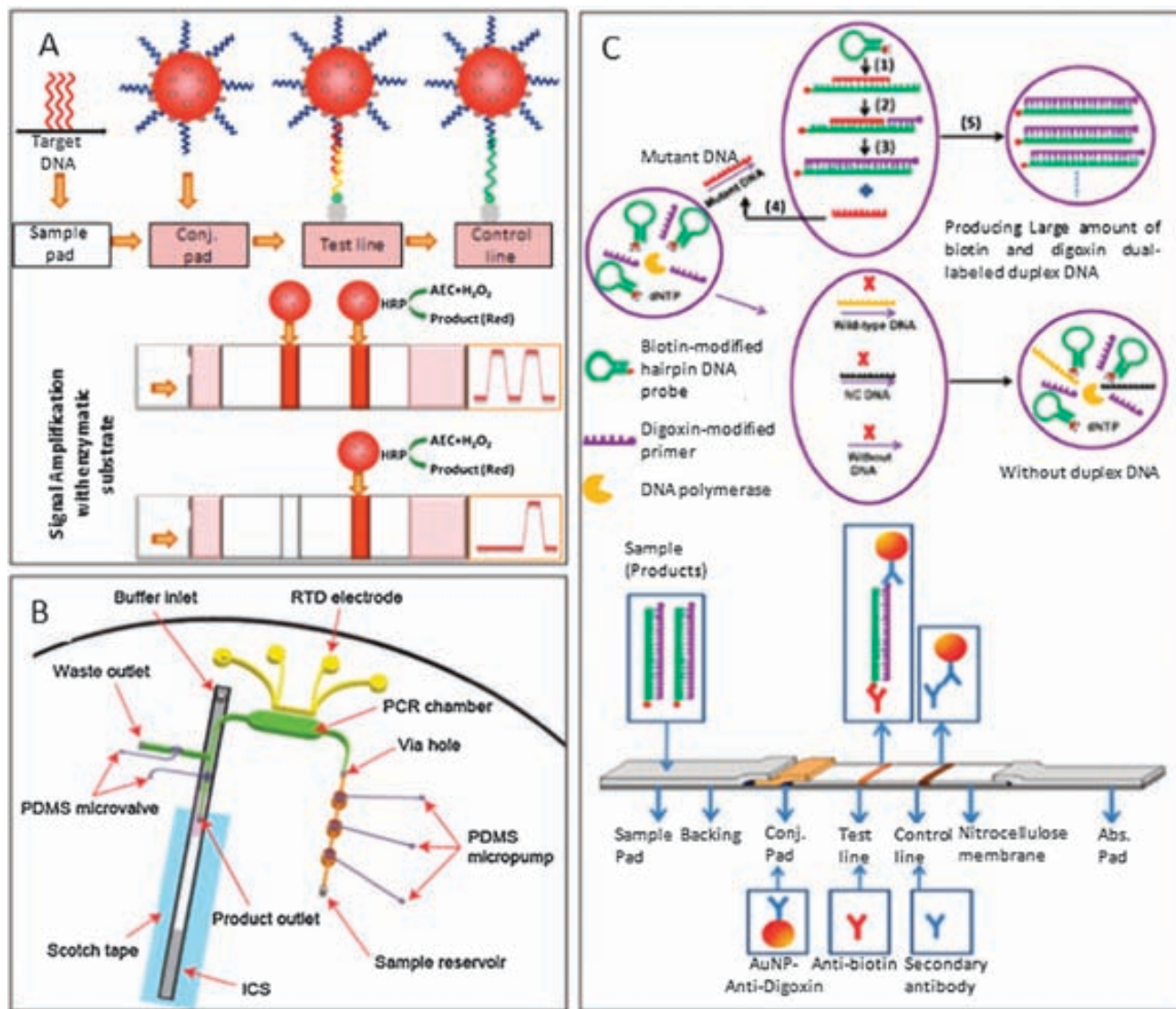


**Fig. 3** (A) From the top to the bottom: schematic illustration of capturing HRP-AuNP-DNA conjugates on the test and control zones of lateral flow nucleic acid biosensor and signal enhancement of biosensor in the presence of enzymatic substrate. AEC: 3-amino-9-ethylcarbazole. Reprinted from ref. 48. Copyright 2010, with permission from Elsevier. (B) Schematic of the integration of a RT-PCR microchamber with a lateral flow strip. Reprinted from ref. 50. Copyright 2011, with permission from Elsevier. (C) At the top: scheme of the isothermal strand-displacement polymerase reactions with the formation of digoxin and biotinylated duplex DNA complexes. At the bottom: scheme of the LF used to check the ISDPR products. Reprinted from ref. 51. Copyright 2011, with permission from Elsevier.

always matches producing a long product. Both products are further hybridized with dA probes and then pipetted onto the sample pad to be recognized by AuNPs modified with oligo dT. The detection is done using streptavidin at a control line and an antibody specific for digoxin at a detection line.<sup>49</sup>

A very interesting device was proposed by Kim *et al.*, combining a microfluidic reverse transcription PCR (RT-PCR) reactor with a LFA to detect H1N1 virus (Fig. 3B). First the RT-PCR was performed obtaining amplicons labelled with Texas Red and biotin, due to primers modified with Texas Red and the biotin labelled dUTPs, respectively. Then the amplicons were first recognized by AuNPs modified with an antibody specific for the Texas Red and then the complexes were captured by the streptavidin molecules of the detection pad. The limit of detection of around 14 pg RNA template was achieved.<sup>50</sup>

The next work reported in this review used an isothermal amplification technique instead of the classical PCR. He *et al.* developed a LFA to detect visually the mutation in the R156H gene of keratin. The authors first amplified the gene with an isothermal strand-displacement polymerase reaction (ISDPR) using primers modified with digoxin and biotin (Fig. 3C). Then they could detect the products using a sandwich assay based on AuNPs functionalized with an antibody specific for the digoxin and an antibody specific for the biotin in the test line. The LoD reached was as low as 1 fM.<sup>51</sup> Lie *et al.* integrated the AuNPs in the ISDPR avoiding any conjugation pad in the LFA. Using human clinical blood samples, the authors detected up to 25 ng mL<sup>-1</sup>, whereas using synthetic sequences the sensor reached detecting 0.01 fM.<sup>52</sup>

Even if the work of Ali *et al.* does not include any nanoparticle, it deserves to be mentioned, since the authors designed

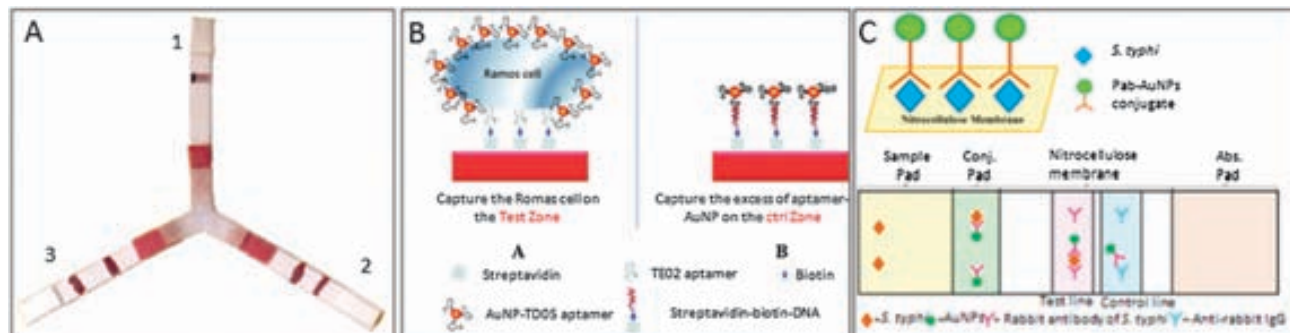


**Fig. 4** Paper-based biosensor for cell detection. (A) Behavior of the LFA for the detection of *S. aureus* using: (1) *S. aureus*, (2) *P. aeruginosa*, (3) *S. aureus* + *P. aeruginosa*. Reprinted from ref. 53. Copyright 2011, with permission from Elsevier. (B) Schematic diagram of the detection of Ramos cells on aptamer-nanoparticle strip biosensor. Reprinted with permission from ref. 54. Copyright 2009, American Chemical Society. (C) Comparison between the scheme of the dot blot immunoassay for *S. typhi* detection and one of the sandwich immunochromatographic strip tests for the detection of *S. typhi* proposed by Preechakasedkit *et al.* Reprinted from ref. 55. Copyright 2011, with permission from Elsevier.

a paper strip which is capable of DNA amplification using the rolling circle amplification (RCA) technique, another isothermal alternative to the PCR. The authors took advantage of a previous work, where they showed that poly(*N*-isopropylacrylamide) microgels coupled with DNA oligonucleotides were compatible with enzymatic reactions.<sup>11</sup> Briefly they could detect up to 100 pM of a DNA target, which was used as a template for the DNA ligase in order to connect a capture sequence with a primer sequence. The new DNA molecule is further amplified by RCA, which generates an extremely long ssDNA that can be detected using a complementary DNA functionalized with a fluorescent dye.<sup>1</sup>

## Cell based devices

Paper-based devices that integrate cells either as receptors for indirect detection of proteins or other species or for their direct detection also have been developed. It must be pointed out that most of the cells cannot run intact through the porous of the membranes used, but they can be attached to the surface of the paper.

Li *et al.* developed a LFA for the detection of whole-cell antigens of *Pseudomonas aeruginosa* and *Staphylococcus aureus* based on the use of AuNPs functionalized with specific

antibodies as labels (Fig. 4A). The authors obtained a detection range of the bacteria lines within 500–5000 CFU mL<sup>−1</sup>; furthermore in this work they described the fabrication of a compact portable device which converts the color intensity of the gold nanoparticles into a quantitative voltage reading proportional to the bacterial concentration in the sample.<sup>53</sup> Liu *et al.* developed an aptamer-AuNP strip biosensor for the detection of circulating cancer cells, reaching a detection limit of 4000 Ramos cells with the naked eye and 800 Ramos cells with a portable strip reader within 15 min. Furthermore the cells were detected also in human blood samples (Fig. 4B).<sup>54</sup> Finally Preechakasedkit *et al.* developed a LFA based on immunosandwich with AuNPs for the detection of *Salmonella typhi* in human serum (Fig. 4C). The LoD reached by the authors was 1.14 × 10<sup>5</sup> cfu mL<sup>−1</sup> within 15 min, which is better than a dot blot immunoassay.<sup>55</sup>

Some other interesting works although do not use any nanomaterial but due to their interesting innovation are also revised. The first work done by Struss *et al.* described the development of a portable filter-paper-based strip biosensor for the detection of bacterial quorum sensing signaling molecules, *N*-acylhomoserine lactones (AHLs). They reached a LoD of 10 nM of AHL and they could also successfully use the device for physiological samples. Briefly they dried onto a filter

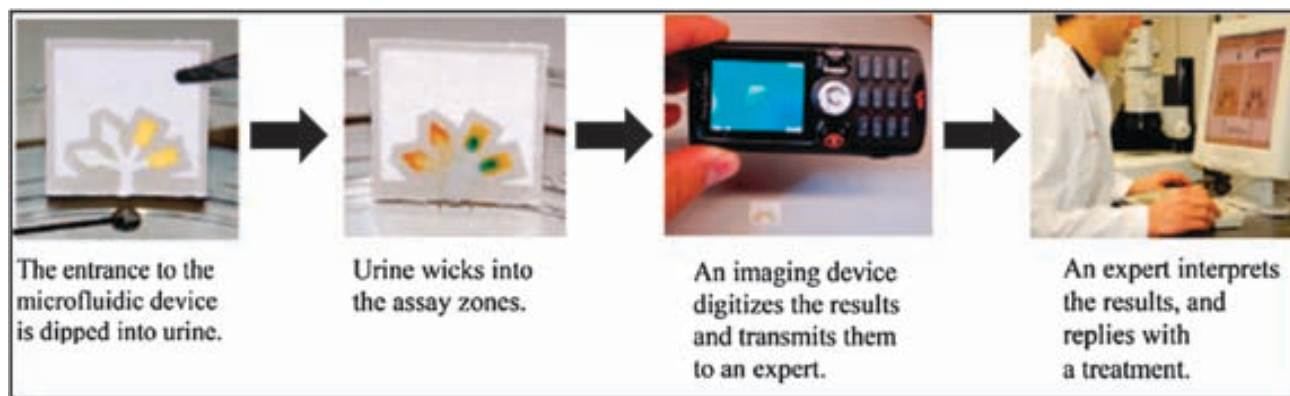


**Fig. 5** General strategy for performing inexpensive bioassays in remote locations and for exchanging the results of the tests with offsite technicians. Reprinted with permission from ref. 27. Copyright 2008, American Chemical Society.

paper strip the genetically engineered bacterial cells, which use  $\beta$ -galactosidase as reporter protein. The saliva samples were applied to the strip.<sup>56</sup>

Finally Derda *et al.* presented a strategy to have a 3D control of cell cultures using layers of chromatography paper. Briefly they impregnated each layer with an extracellular matrix hydrogel precursor containing living cells and then they gelled it in place. In this way it is possible to manipulate each layer stacking and destacking it very easily and study the effect of the gradient of O<sub>2</sub> concentration. Finally the authors improved the technique using a 96 well paper plate, which enables parallel cultures and rapid analysis of various cell types and cellular responses.<sup>57</sup>

## Future trends

In the near future the paper-based diagnostic nanobiosensors are expected to bring improvements in terms of sensitivity enhancement as well as the multiple molecules detection capability. In addition the most useful for their applicability as PoC devices will be the possibility to communicate the results to specialized personnel. In this way some works related to paper-based diagnostic technology and communication systems have been already reported, especially by Martinez *et al.*<sup>14,27</sup> The authors used a normal phone camera to send the result of the assay to a laboratory, where a specialized person can analyze it and send back to the biosensor user the response of the test (Fig. 5). This technology will tremendously enhance the healthcare in extreme places like the developing world and battle fields, where not always is possible the intervention of specialized people or the use of expensive measuring instruments.

One of the focuses of the research in the design of the paper biosensors is to make these devices more robust, sensitive and multiplex. Examples are the works done by Fu and co-workers, where they increased the properties of a LFA making it a 2D-LFA,<sup>58</sup> and Martinez *et al.*, who decided to create fully enclosed microPADs, printing toner on the top and bottom of the devices using a laser printer.<sup>59</sup>

Considering in particular the nucleic acid detection, the major efforts will be probably focalized in the use of isothermal amplification techniques instead of the classical PCR. In fact the isothermal technique can be cheaper and easier to be used also in countries with fewer resources, without losing sensitivity and sensibility.

## Conclusions

The paper-based nanobiosensors are shown to be excellent tools for diagnostics. In particular, their nature makes them available for PoC applications, since they are portable and easy to use. Furthermore, the fast response is essential in many situations such as illness diagnostics which later require a fast treatment. The integration of small strip reader or electrochemical sensor in a paper-based device improves the quantification of the analytes, reaching higher sensitivity and lower detection limits. Paper-based diagnostics are suitable for large

scale production, since they can be fabricated using even already existing or similar office machines making them a very cheap and efficient technology. Finally the integration of nanomaterials within these devices is expected to bring advances to their stability/robustness, shelf lifetime and bringing novel detection opportunities including multidetection capability besides other improvements of their analytical performance.

## Acknowledgements

We acknowledge MEC (Madrid) for the project MAT2011-25870 and E.U. for the FP7 "NADINE" project (contract number 246513). C.P. also thanks the *Generalitat de Catalunya* for the PhD scholarship.

## Notes and references

- 1 M. M. Ali, S. D. Aguirre, Y. Xu, C. D. M. Filipe, R. Pelton and Y. Li, *Chem. Commun.*, 2009, 6640–6642.
- 2 D. Mabey, R. W. Peeling, A. Ustianowski and M. D. Perkins, *Nat. Rev. Microbiol.*, 2004, **2**, 231–240.
- 3 P. Yager, T. Edwards, E. Fu, K. Helton, K. Nelson, M. R. Tam and B. H. Weigl, *Nature*, 2006, **442**, 412–418.
- 4 A. K. Ellerbee, S. T. Phillips, A. C. Siegel, K. a. Mirica, A. W. Martinez, P. Striehl, N. Jain, M. Prentiss and G. M. Whitesides, *Anal. Chem.*, 2009, **81**, 8447–8452.
- 5 R. W. Peeling, K. K. Holmes, D. Mabey and A. Ronald, *Sex. Transm. Infect.*, 2006, **82**(Suppl. 5), v1–v6.
- 6 G. Aragay, J. Pons and A. Merkoçi, *Chem. Rev.*, 2011, **111**, 3433–3458.
- 7 A. Merkoçi, M. Aldavert, S. Marin and S. Alegret, *TrAC, Trends Anal. Chem.*, 2005, **24**, 341–349.
- 8 A. de la Escosura-Muñiz, C. Parolo and A. Merkoçi, *Mater. Today*, 2010, **13**, 24–34.
- 9 M. Perfézou, A. Turner and A. Merkoçi, *Chem. Soc. Rev.*, 2011, **41**, 2606–2622.
- 10 W. Zhao and A. van der Berg, *Lab Chip*, 2008, **8**, 1988–1991.
- 11 S. Su, M. M. Ali, C. D. M. Filipe, Y. Li and R. Pelton, *Biomacromolecules*, 2008, **9**, 935–941.
- 12 E. Carrilho, A. W. Martinez and G. M. Whitesides, *Anal. Chem.*, 2009, **81**, 7091–7095.
- 13 A. Savolainen, Y. Zhang, D. Rochefort, U. Holopainen, T. Erho, J. Virtanen and M. Smolander, *Biomacromolecules*, 2011, **12**, 2008–2015.
- 14 A. W. Martinez, S. T. Phillips, G. M. Whitesides and E. Carrilho, *Anal. Chem.*, 2010, **82**, 3–10.
- 15 J. H. Leuvering, P. J. Thal, M. van der Waart and A. H. Schuurs, *J. Immunoassay*, 1980, **1**, 77–91.
- 16 A. W. Martinez, S. T. Phillips, M. J. Butte and G. M. Whitesides, *Angew. Chem., Int. Ed.*, 2007, **46**, 1318–1320.
- 17 G. a. Posthuma-Trumpie, J. Korf and A. van Amerongen, *Anal. Bioanal. Chem.*, 2009, **393**, 569–582.
- 18 A. R. Rezk, A. Qi, J. R. Friend, W. H. Li and L. Y. Yeo, *Lab Chip*, 2012, **12**, 773–779.

- 19 W. Dungchai, O. Chailapakul and C. S. Henry, *Analyst*, 2011, **136**, 77–82.
- 20 M. M. Dudek, N. J. Kent, P. Gu, Z. H. Fan and A. J. Killard, *Analyst*, 2011, **136**, 1816–1825.
- 21 R. F. Carvalhal, M. S. Kfoury, M. H. D. O. Piazzetta, A. L. Gobbi and L. T. Kubota, *Anal. Chem.*, 2010, **82**, 1162–1165.
- 22 E. Carrilho, S. T. Phillips, S. J. Vella, A. W. Martinez and G. M. Whitesides, *Anal. Chem.*, 2009, **81**, 5990–5998.
- 23 S. Wang, L. Ge, X. Song, J. Yu, S. Ge, J. Huang and F. Zeng, *Biosens. Bioelectron.*, 2012, **31**, 212–218.
- 24 C.-G. Shi, X. Shan, Z.-Q. Pan, J.-J. Xu, C. Lu, N. Bao and H.-Y. Gu, *Anal. Chem.*, 2012, **84**, 3033–3038.
- 25 Z. Nie, C. a. Nijhuis, J. Gong, X. Chen, A. Kumachev, A. W. Martinez, M. Narovlyansky and G. M. Whitesides, *Lab Chip*, 2010, **10**, 477–483.
- 26 X. Liu, M. Mwangi, X. Li, M. O'Brien and G. M. Whitesides, *Lab Chip*, 2011, **11**, 2189–2196.
- 27 A. W. Martinez, S. T. Phillips, E. Carrilho, S. W. Thomas, H. Sindi and G. M. Whitesides, *Anal. Chem.*, 2008, **80**, 3699–3707.
- 28 S. Song, Y. Qin, Y. He, Q. Huang, C. Fan and H.-Y. Chen, *Chem. Soc. Rev.*, 2010, **39**, 4234–4243.
- 29 D. S. Elenis, P. C. Ioannou and T. K. Christopoulos, *Nanotechnology*, 2011, **22**, 155501.
- 30 Y. H. Ngo, D. Li, G. P. Simon and G. Garnier, *Adv. Colloid Interface Sci.*, 2011, **163**, 23–38.
- 31 S. Lou, J.-Y. Ye, K.-Q. Li and A. Wu, *Analyst*, 2011, **137**, 1174–1181.
- 32 W. Zhao, M. M. Ali, S. D. Aguirre, M. A. Brook and Y. Li, *Anal. Chem.*, 2008, **80**, 8431–8437.
- 33 S. Puertas, M. Moros, R. Fernández-Pacheco, M. R. Ibarra, V. Grazú and J. M. de la Fuente, *J. Phys. D: Appl. Phys.*, 2010, **43**, 474012.
- 34 X. Zhu, L. Chen, P. Shen, J. Jia, D. Zhang and L. Yang, *J. Agric. Food Chem.*, 2011, **59**, 2184–2189.
- 35 S. Shukla, H. Leem and M. Kim, *Anal. Bioanal. Chem.*, 2011, **401**, 2581–2590.
- 36 M. Blažková, B. Javůrková, L. Fukal and P. Rauch, *Biosens. Bioelectron.*, 2011, **26**, 2828–2834.
- 37 D. P. Kalogianni, L. M. Boutsika, P. G. Kouremenou, T. K. Christopoulos and P. C. Ioannou, *Anal. Bioanal. Chem.*, 2011, **400**, 1145–1152.
- 38 M. Ornatska, E. Sharpe, D. Andreescu and S. Andreescu, *Anal. Chem.*, 2011, **83**, 4273–4280.
- 39 M.-I. Mohammed and M. P. Y. Desmulliez, *Lab Chip*, 2011, **11**, 569–595.
- 40 Z. Li, Y. Wang, J. Wang, Z. Tang, J. G. Pounds and Y. Lin, *Anal. Chem.*, 2010, **82**, 7008–7014.
- 41 C. Parolo, A. de la Escosura-Muñiz and A. Merkoçi, *Biosens. Bioelectron.*, 2012, DOI: 10.1016/j.bios.2012.06.049.
- 42 D. H. Choi, S. K. Lee, Y. K. Oh, B. W. Bae, S. D. Lee, S. Kim, Y.-B. Shin and M.-G. Kim, *Biosens. Bioelectron.*, 2010, **25**, 1999–2002.
- 43 Y.-Y. Lin, J. Wang, G. Liu, H. Wu, C. M. Wai and Y. Lin, *Biosens. Bioelectron.*, 2008, **23**, 1659–1665.
- 44 H. Xu, X. Mao, Q. Zeng, S. Wang, A.-N. Kawde and G. Liu, *Anal. Chem.*, 2009, **81**, 669–675.
- 45 Z. Fang, C. Ge, W. Zhang, P. Lie and L. Zeng, *Biosens. Bioelectron.*, 2011, **27**, 192–196.
- 46 C.-M. Cheng, A. W. Martinez, J. Gong, C. R. Mace, S. T. Phillips, E. Carrilho, K. a. Mirica and G. M. Whitesides, *Angew. Chem. Int. Ed.*, 2010, **49**, 4771–4774.
- 47 A. M. Caliendo, *Clinical infectious diseases: an official publication of the Infectious Diseases Society of America*, 2011, 52(Suppl. 4), S326–S330.
- 48 Y. He, S. Zhang, X. Zhang, M. Baloda, A. S. Gurung, H. Xu, X. Zhang and G. Liu, *Biosens. Bioelectron.*, 2011, **26**, 2018–2024.
- 49 J. K. Konstantou, A. C. Iliadi, P. C. Ioannou, T. K. Christopoulos, N. I. Anagnostopoulos, E. Kanavakis and J. Traeger-Synodinos, *Anal. Bioanal. Chem.*, 2010, **397**, 1911–1916.
- 50 Y. T. Kim, Y. Chen, J. Y. Choi, W.-J. Kim, H.-M. Dae, J. Jung and T. S. Seo, *Biosens. Bioelectron.*, 2012, **33**, 88–94.
- 51 Y. He, K. Zeng, S. Zhang, A. S. Gurung, M. Baloda, X. Zhang and G. Liu, *Biosens. Bioelectron.*, 2012, **31**, 310–315.
- 52 P. Lie, J. Liu, Z. Fang, B. Dun and L. Zeng, *Chem. Commun.*, 2012, **48**, 236–238.
- 53 C.-Z. Li, K. Vandenberg, S. Prabhulkar, X. Zhu, L. Schneper, K. Methee, C. J. Rosser and E. Almeida, *Biosens. Bioelectron.*, 2011, **26**, 4342–4348.
- 54 G. Liu, X. Mao, J. a. Phillips, H. Xu, W. Tan and L. Zeng, *Anal. Chem.*, 2009, **81**, 10013–10018.
- 55 P. Preechakasedkit, K. Pinwattana, W. Dungchai, W. Siangproh, W. Chaicumpa, P. Tongtawe and O. Chailapakul, *Biosens. Bioelectron.*, 2011, **31**, 562–566.
- 56 A. Struss, P. Pasini, C. M. Ensor, N. Raut and S. Daunert, *Anal. Chem.*, 2010, **82**, 4457–4463.
- 57 R. Derda, S. K. Y. Tang, A. Laromaine, B. Mosadegh, E. Hong, M. Mwangi, A. Mammoto, D. E. Ingber and G. M. Whitesides, *PLoS One*, 2011, **6**, e18940.
- 58 E. Fu, T. Liang, J. Houghtaling, S. Ramachandran, S. A. Ramsey and B. Lutz, *Cellulose*, 2011, 7941–7946.
- 59 K. M. Schilling, A. L. Lepore, J. a. Kurian and A. W. Martinez, *Anal. Chem.*, 2012, **84**, 1579–1585.

Cite this: *Nanoscale*, 2011, **3**, 3350[www.rsc.org/nanoscale](http://www.rsc.org/nanoscale)

PAPER

## Size-dependent direct electrochemical detection of gold nanoparticles: application in magnetimmunoassays†

Alfredo de la Escosura-Muñiz,<sup>a</sup> Claudio Parolo,<sup>a</sup> Flavio Maran<sup>b</sup> and Arben Mekoçi<sup>\*ac</sup>

Received 15th April 2011, Accepted 30th May 2011

DOI: 10.1039/c1nr10377f

The effect of the AuNPs size, ranging from 5 nm to 80 nm, on the electrochemical response of screen-printed carbon electrodes (SPCEs) used as electrochemical transducers is investigated for the first time. A simple hydrodynamic modelling and calculation at the nanoscale level is applied so as to find the effect of the size of AuNP upon the electrochemical response. The results show that the best electrochemical response for AuNP suspension for the same concentration of total gold is obtained for the 20 nm sized nanoparticles. It is concluded that the Brownian motions avoid a better response for smaller AuNPs that should in fact be related with the best electrochemical signal due to their higher surface area. Finally, the size effect is studied for AuNPs acting as electroactive labels in an immunosensor that employs magnetic beads as platforms of the bioreactions. The best response for the 5 nm AuNPs in this case is due to the fact that in the immunosensing conditions the Brownian motions are minimized because the AuNPs contact with the electrotransducer surface is induced by the immunoreaction and the fast magnetic collection of the nanoparticles used as antibody labels upon application of a magnetic field.

### Introduction

Investigations on nanoparticles (NPs) have rapidly increased in recent years due to their size and shape-dependent physical, chemical and electrochemical properties, which make them extremely useful in sensing and biosensing applications.<sup>1</sup> The size and the composition of NPs are advantageous over the corresponding bulk structure because a target binding event, *e.g.* DNA hybridization or immunoreaction, involving NPs may cause significant effects on their optical (change of light absorption or emission) or electrochemical properties (oxidation or reduction current generated at transducing platform), thereby offering novel options and tools for efficient bioanalysis. In fact, these properties offer signal-transduction modes, including simultaneous approaches (optical and electrochemical),<sup>2–5</sup> that are not available with other materials and systems.

Applications of NPs in biosensing strongly relate to their properties that, in turn, can be tuned through specifically devised synthetic procedures (quality of NPs) and later modifications (chemical and biological). NP-preparation procedures, in colloidal solutions or grown on solid substrates, have been extensively reviewed.<sup>6</sup> Along with advances in synthesis allowing one to control size, shape, and composition of nanostructured materials, our knowledge on how to tailor the NP-binding affinities for various biomolecules through surface modification and engineering has improved significantly. These advancements are now being used to device electrochemical-related applications of NPs in enzyme-based sensors, immunosensors and DNA sensors.<sup>7–10</sup>

In this context, gold nanoparticles (AuNPs) stand out from the variety of other nanoparticles and quantum dots because of their biocompatibility<sup>11</sup> and unique electronic, optical, and catalytic properties.<sup>12–16</sup> In particular, AuNPs applications are extensively investigated and tested in immunocytochemistry and cell biology.<sup>17</sup> AuNPs have also been used in a variety of analytical,<sup>18,19</sup> and sensing applications, including DNA,<sup>20,21</sup> and immuno-sensing.<sup>22</sup> Although the majority of sensing systems so far described rely on the optical properties of AuNPs, we are currently observing a noticeable growth of AuNP-based immuno<sup>23</sup> and DNA electrochemical assays.<sup>7,8</sup> The vast majority of these electrochemical approaches is based on chemical dissolution of AuNPs in toxic solutions (*i.e.* HBr/Br<sub>2</sub>) followed by accumulation and stripping analysis of the resulting Au(III) solution. These solutions are highly toxic and therefore

<sup>a</sup>CIN2 (ICN-CSIC), Catalan Institute of Nanotechnology, Campus de la UAB, 08193 Bellaterra (Barcelona), Spain. E-mail: arben.merkoci.icn@uab.es; Fax: +34935868020; Tel: +34935868014

<sup>b</sup>Dipartimento di Scienze Chimiche, Università degli Studi di Padova, Padova, Italy. E-mail: flavio.maran@unipd.it; Fax: +390498275135; Tel: +390498275147

<sup>c</sup>ICREA, Barcelona, Spain; Fax: +34932687700; Tel: +34932687700

† Electronic supplementary information (ESI) available: Detailed experimental procedures and related figures, calculations for the estimation of the settling velocity and deposition time for AuNPs of different sizes and tables summarizing these and other calculations. See DOI: 10.1039/c1nr10377f

alternative approaches based on direct electrochemical detection of AuNPs to replace the chemical oxidation agent are sought. In addition to indirect electrocatalytic methods,<sup>24,25</sup> we<sup>2,26,27</sup> and others<sup>4,5</sup> developed a direct detection method based on adsorption of the AuNPs on the surface of the electrotransducer, electrooxidation of the AuNPs to Au(III), and reverse electroreduction to Au(0), which generates a well defined cathodic peak constituting the actual analytical signal. This methodology has been optimized for 20 nm AuNPs on carbon paste and graphite–epoxy electrodes, but the effect of the AuNPs size on the electrochemical signal and the use of other kinds of electrotransducers, such as screen-printed electrodes, have not yet been studied and possibly exploited in biosensors. The size-dependence of the optical properties of AuNPs has been extensively studied, but this effect on the electrochemical properties has not yet been clarified.

Here, we report the size-dependent direct electrochemical detection of AuNPs using screen-printed carbon electrodes (SPCEs) as electrochemical transducers.

## Experimental section

### Chemicals and instruments

Gold nanoparticle solutions (supplied diameters: 5, 20, 40, 60, and 80 nm) were purchased from BBI International (UK). Streptavidin-coated Magnetic Beads (M-280), with 2.8  $\mu\text{m}$  size, were purchased from Dynal Biotech (Invitrogen, Spain). Biotin conjugate-goat anti-human IgG (Sigma B1140, developed in goat and gamma chain specific), human IgG from serum, goat IgG from serum and anti-human IgG (Sigma A8667, developed in goat is whole molecule) were purchased from Sigma-Aldrich. All buffer reagents and other inorganic chemicals were supplied by Sigma, Aldrich or Fluka, unless otherwise stated. All chemicals were used as received and all aqueous solutions were prepared using doubly distilled water.

The phosphate buffer solution (PBS) consisted of 0.01 M phosphate buffered saline, 0.137 M NaCl, 0.003 M KCl (pH 7.4). Blocking buffer solution consisted of a PBS solution with added 5% (w/v) bovine serum albumin (pH 7.4). The binding and washing (B&W) buffer consisted of a PBS solution containing 0.05% (v/v) Tween 20 (pH 7.4).

A thermostatic centrifugator Sigma 2-16 PK (Fisher Bioblock Scientific, France) was used to purify the conjugates of gold nanoparticles with antibodies.

A semi-automatic screen-printing machine DEK248 (DEK International, Switzerland) was used for the fabrication of the screen-printed carbon electrodes (SPCEs). The reagents used for this process were Autostat HT5 polyester sheet (McDermid Autotype, UK), Electrodag 423SS carbon ink, Electrodag 6037SS silver/silver chloride ink, and Minico 7000 Blue insulating ink (Acheson Industries, The Netherlands).

Electrochemical measurements were performed at room temperature with an Autolab 20 (Eco-chemie, The Netherlands) connected to a PC.

Spectrophotometric measurements were performed using a Spectramax® M2E multi-mode microplate reader (Molecular Devices Inc, UK).

An Inductively Coupled Plasma Mass Spectrometer (ICP-MS) model 7500ce (Agilent Technologies, USA) was used to calculate the total gold in the samples.

A Transmission Electron Microscope (TEM) Jeol JEM-2011 (Jeol Ltd, Japan) was used to characterize the gold nanoparticles. An ultrasonic bath (JP selecta, Spain) was used to prevent agglomeration in the gold nanoparticles solutions before the TEM measurements.

The electrochemical transducers used for the *in situ* growth of the cells were homemade screen-printed carbon electrodes (SPCEs) consisting of a working electrode, a reference electrode, and a counter electrode inserted on a single strip (for details of the fabrication procedure and images of a SPCE and the 45-sensor sheet, see the ESI†).

### AuNPs characterizations

ICP-MS and spectrophotometric analyses were performed to estimate the concentration of AuNPs and total gold contained in each AuNPs solution used for the electrochemical studies. The size and shape of the AuNPs was assessed by transmission electron microscopy. The experimental procedures for these analyses are detailed in the ESI†.

### AuNPs conjugation with antibodies

The conjugation of different sized AuNPs (5, 20, and 80 nm of diameter) to anti-human IgG antibodies was performed according to the following procedure, which we previously optimized:<sup>2,24</sup> 2 mL of a AuNPs suspension, containing 84  $\mu\text{M}$  of total gold, was mixed with 100  $\mu\text{L}$  of 100  $\mu\text{g mL}^{-1}$  of the antibody solution and incubated at 25 °C for 20 min. After that a blocking step with 150  $\mu\text{L}$  of 1 mg  $\text{mL}^{-1}$  BSA, incubating at 25 °C for 20 min was performed. Finally, a centrifugation was carried out in order to purify the conjugate AuNP/anti-human IgG. Centrifugation was performed under different conditions, depending on the size of the AuNPs:

- 5 nm AuNPs: 21 000  $\times$  g, 4 °C, 45 minutes, 2 times.
- 20 nm AuNPs: 14 000  $\times$  g, 4 °C, 10 minutes, 2 times.
- 80 nm AuNPs: 11 000  $\times$  g, 4 °C, 2 minutes, 2 times.

Finally, the conjugate AuNPs/anti-human IgG was reconstituted in  $\text{H}_2\text{O}$  (Milli-Q).

### Magnetosandwich immunoassay using as labels AuNPs of different sizes

The preparation of the magnetic beads (MBs) based sandwich type immunocomplex was performed following a method that we previously optimized.<sup>2,24</sup> MBs modified with streptavidin were used to immobilize specific antibodies against human IgG. After the capture of the human IgG in the sample. The sandwich was formed with secondary specific antibodies conjugated with AuNPs. A blank (control) assay was performed using goat IgG instead of human IgG at the same concentration. The experimental procedure is detailed in the ESI†.

### Electrochemical analysis

The electrochemical analysis of AuNPs was performed by placing 25  $\mu\text{L}$  of the AuNPs solution on the working electrode

area of the SPCEs and leaving the AuNPs to adsorb for 2 minutes. After that, 25  $\mu\text{L}$  of a HCl 0.2 M solution were added, covering the three electrodes area. The pre-concentration step, meant to oxidize AuNPs to  $\text{AuCl}_4^-$ , was performed at +1.25 V (vs. Ag/AgCl) for 120 s in a quiescent solution. Immediately after the electrochemical oxidation, differential pulse voltammetry was performed by scanning from +1.25 V to 0.0 V (step potential 10 mV, modulation amplitude 50 mV, scan rate 33.5 mV s $^{-1}$ ), resulting in the analytical signal caused by reduction of  $\text{AuCl}_4^-$  at +0.45 V.

For the magnetosandwich immunoassay measurements, we applied the same protocol, but for placing the magnetic beads solution instead of the AuNPs solution on the SPCE. A magnet was placed on the opposite side of the strip relative to the working electrode.

## Results and discussion

### Direct electrochemical detection of gold nanoparticles

The size and shape of the AuNPs were first determined by transmission electron microscopy (TEM) analysis. Fig. 1A shows the TEM images obtained for most of the AuNPs studied, together with the corresponding size distribution. As can be observed, Gaussian distributions were obtained, being the main values (and their deviations) of 6.5 ( $\pm 1.1$ ), 8.5 ( $\pm 1.7$ ), 17.5 ( $\pm 2.0$ ), 38.3 ( $\pm 4.5$ ), 54.9 ( $\pm 6.1$ ) and 73.9 ( $\pm 8.9$ ) nm for the “5”, “10”, “20”, “40”, “60” and “80” nm supplied values respectively. However, in order to facilitate the understanding of the results, the values given by the NPs supplier only are mentioned along the text.

UV-vis absorption spectroscopy of the AuNPs solutions, in the 528–540 nm range where the gold plasmon resonance band appears,<sup>28</sup> evidenced absence of aggregation. As expected, the wavelength of the maximum of absorbance undergoes a red shift as the AuNPs size increases. An estimation of the concentration of AuNPs was obtained by measuring the optical density at

450 nm and knowing the molar decadic extinction coefficient ( $\epsilon$ ) at this wavelength, which has been previously calculated for each AuNP size by Haiss *et al.*<sup>29</sup> (see the calculations in the ESI†).

A key step of our procedure for the electrochemical detection of AuNPs consists in an efficient adsorption of AuNPs onto the surface of the electrotransducer, which will allow their further oxidation and then reduction of the ensuing oxidized gold species. The efficient adsorption of 20 nm AuNPs onto the surface of the SPCEs, according to the experimental procedure detailed in Experimental section, seems to be evidenced in the SEM images shown in Fig. 1B, where in spite of the rugosity of the carbon surface it seems that the AuNPs are adsorbed and spread onto the carbon surface without agglomerates formation; this is important for allowing a reproducible electrochemical detection in the further steps.

We previously reported results about the direct electrochemical detection of AuNPs on graphite–epoxy composite electrodes.<sup>2,26,27</sup> We are now reporting data concerning further important issues. One aspect we addressed was to study the electrochemical features of this AuNP-based approach by using SPCEs, which provide an advantageous platform in terms of miniaturization, low volume of samples, single use possibilities, and convenient mass-production related technology. In addition to the use of a novel transducing surface, main objective of this work was to study the effect of the AuNP size on the electrochemical signal. In particular, we anticipated that this issue would have had important effects on both the sensitivity and the reproducibility of the affinity bioassays (*i.e.* DNA sensors or immunosensor) requiring the use of labels.

Fig. 2A shows cartoons of the detection steps pertaining to AuNPs with three different sizes (small, medium, large); AuNP suspensions consist of the same number of AuNPs. After the AuNPs are deposited onto the SPCE surface from the appropriate suspension (step 1), their partial electrochemical oxidation (step 2), generating a high surface concentration of Au(III) ions by the electrotransducer, occurs. Anodic stripping of the adsorbed AuNPs is then followed by a potential scan to reductive potentials (step 3): the peak current for reduction of Au(III) ions to Au(0) is related to the original surface concentration of the AuNPs.

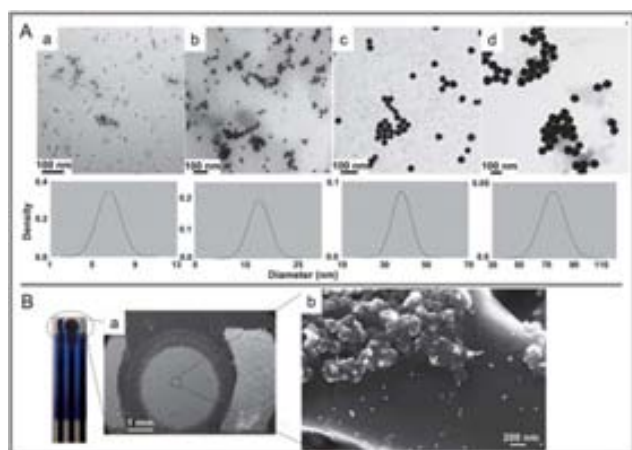


**Fig. 1** (A) TEM images obtained for 5 nm (a), 20 nm (b), 40 nm (c) and 80 nm (d) AuNPs solutions and the corresponding size distributions. (B) SEM images of the SPCE electrotransducer (a) and the 20 nm AuNPs deposited on the carbon working area from a solution of  $1 \times 10^{10}$  AuNPs per mL, following the experimental procedure detailed in the Experimental section at 100 000 $\times$  amplifications (b).

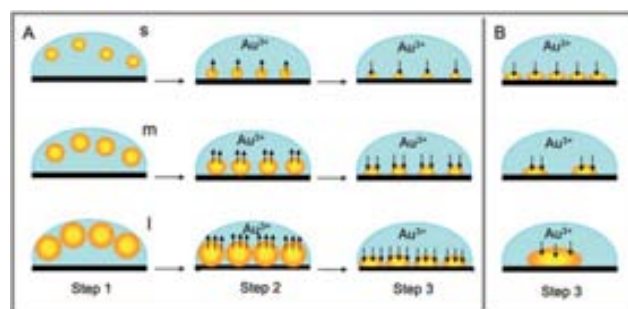


**Fig. 2** (A). Schematic, not in scale, of the three steps used for introduction and detection of small (s), medium (m) and large (l) size AuNP suspension of the same number of AuNPs using a SPCE. Step 1 corresponds to AuNP deposition onto SPE surface. Step 2 corresponds to gold ion release/oxidation upon the application of a +1.25 V potential during 120 s. Step 3 corresponds to gold ion deposition/reduction onto the SPE by scanning from +1.25 V to 0.0 V. (B). Schematic of the third step only in the case when the total gold concentration is the same.

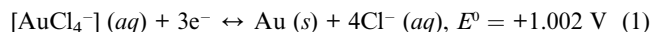
For the same number of nanoparticles, AuNPs of different sizes were also expected to provoke different behaviors in terms of reduction peak potentials for Au(0) deposition. The value of the peak current was expected to be higher for larger AuNPs (for the same number of nanoparticles) due to their higher surface area generating a higher surface concentration of released gold ions during the oxidation step. As depicted in the cartoon of step 3, deposition of gold occurs onto smaller, residual AuNPs, as during the stripping step AuNPs are partially oxidized (being their size slightly reduced). Due to an ‘incomplete stripping’,<sup>30</sup> the remaining AuNPs, of different area, act as an array of nanoelectrodes that catalyze the further electrodeposition, that consequently should occur at different potentials in comparison to the bare carbon electrode.

On the other hand, it is conceivable that if one starts from the same total gold ion concentration (see Fig. 2B), smaller AuNPs would result in the detection of larger peak currents, as small NPs are present in a larger number, provide a higher quantity of surface atoms (the ratio between the surface and the core gold atoms increases as the NP is made smaller), and increase the area of contacting surface between them and the electrotransducing surface. Furthermore, the reduction potential of the gold ions should be shifted to less negative potentials, due to a better array-like effect for smaller compared to larger sizes NPs.

To verify our expectations, we carried out experiments focusing on two sets of conditions for the AuNP suspensions. In the first set we used AuNP suspensions with varying core sizes but with the same number of nanoparticles. In the second set we kept the total amount of gold constant: because of the different core sizes, this procedure resulted in AuNP suspensions containing a different number of nanoparticles.

### Size-effect on the voltammetric response for the same number of gold nanoparticles

As a first step, the effect of the AuNPs size on the electrochemical signal for the same concentration of AuNPs, previously determined by UV-vis spectrophotometry, was evaluated. As it is detailed in the Experimental section, an oxidation potential of +1.25 V was applied to the adsorbed AuNPs in order to release the Au(III) ions (step 2, Fig. 2A). In the case of gold, the standard state in the pure crystalline bulk metal, and the generation of Au(III) ions from the AuNPs in a hydrochloric medium is given by:<sup>31</sup>



For convenience, the shape of AuNPs is taken as that of a perfect sphere and, accordingly, the volumes of single 5, 20 and 80 nm diameter particles are calculated to be  $5.23 \times 10^{-19}$ ,  $2.09 \times 10^{-18}$  and  $8.36 \times 10^{-18} \text{ cm}^3$ , respectively. By taking the density of the AuNP to be that of bulk gold ( $\rho$ ),  $19.3 \text{ g cm}^{-3}$ , the atomic mass ( $M$ ) to be  $196.967 \text{ g mol}^{-1}$ , and Avogadro's number ( $N_A$ ) to be  $6.022 \times 10^{23}$ , the approximate numbers of atoms per particle ( $N$ ) are 3859, 246 960 and 15 806 976, respectively, according to the following equation:<sup>32,33</sup>

$$N = \Pi \rho D^3 N_A / 6M \quad (2)$$

where  $D$  is the diameter of the NP.

These values are much greater than the number of atoms needed to start producing ‘bulk character’<sup>34ab</sup> and, as such, to have the same standard potential,  $E^0$ , of gold, as this value is quoted for all species in their standard states. The range of particle sizes considered in this work, in a similar mode as for Compton's silver nanoparticles<sup>35</sup> is narrow, and therefore, it is assumed that the value of this standard potential is the same for the different-sized AuNPs studied. It means that the potential of +1.25 V applied is oxidative enough to oxidize the surface of the AuNPs and to generate Au(III) ions.

After the oxidation step, we applied a negative-going differential pulse voltammetry (DPV) scan to the SPCE and obtained voltammograms such as those shown in Fig. 3A. The results show that gold ion reduction onto larger AuNPs occurs at less negative potentials ( $\sim 60 \text{ mV}$  shift) than observed for smaller size particles, due to an increased nanoarray like effect (Fig. 2A, step 3). Regarding the peak current, directly related to the quantity of gold ions and indirectly to the AuNP quantity, Fig. 3A shows that the maximum analytical signals, obtained by following the experimental procedure described in Experimental section, were obtained for the largest NP employed, *i.e.*, the 80 nm AuNPs. The same behavior was observed for different AuNP concentrations, as shown in the plots of Fig. 3B (full data are provided in the ESI†). As for the peak potential, the increase of the DPV peaks as the AuNP size also increases is in agreement with the expected behavior, because for the same number of NPs the number of released gold ions (and, consequently, of those available for the following reduction step) can be related with the number of surface atoms in the AuNPs, which in turn is related to the size of the AuNPs (Fig. 2A, step 2).

### Size-effect on the voltammetric response for the same concentration of total gold

The effect of the AuNPs size onto the electrochemical response for the same concentration of total gold, previously determined by inductively coupled plasma mass spectrometry (ICP-MS), was also studied. We expected (Fig. 2B) that for the same quantity of total gold, smaller AuNPs would have yielded a higher electrochemical signal, as for smaller AuNPs a higher surface area, implying a higher number of surface atoms (see a summary table in the ESI†), is in contact with the working electrode surface.

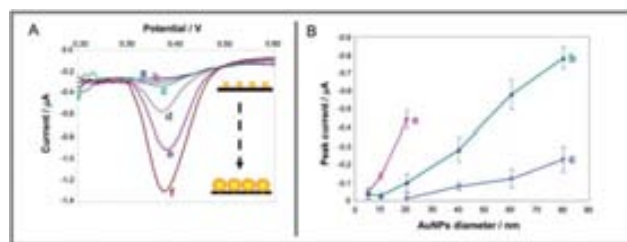


**Fig. 3** (A) Differential pulse voltammograms obtained for AuNPs of different diameters in solutions containing  $1 \times 10^{10}$  AuNPs per mL. (a) 5 nm, (b) 10 nm, (c) 20 nm, (d) 40 nm, (e) 60 nm, (f) 80 nm. Step potential: 10 mV, modulation amplitude: 50 mV, scan rate  $33.5 \text{ mV s}^{-1}$  (non-stirred 0.1 M HCl solution, room temperature). (B) AuNPs size dependence on the analytical signal for different AuNP concentrations: (a)  $1 \times 10^{11}$ , (b)  $1 \times 10^{10}$ , (c)  $1 \times 10^9$  AuNPs per mL.

Consequently, a higher number of Au(III) ions would be released from the bulk metal due to the electrochemical oxidation step, giving rise to a higher voltammetric peak recorded during the ions reduction step. The DPVs obtained for different AuNPs at a total gold concentration of 200  $\mu\text{M}$  are shown in Fig. 4A. The predicted behavior is indeed observed in the range 20–80 nm (c, d, e voltammograms). In these experiments, a positive shift of the reduction potential ( $\sim 30$  mV) was observed for the smaller AuNPs. This can be attributed again to the array effect of the remaining AuNPs and its promoting role on the reduction of Au(III) ions to Au(0). As also predicted, the peak current is smaller for larger AuNPs. However, for AuNPs in the range from 5 to 20 nm (voltammograms a, b, and c: voltammogram c, corresponding to the 20 nm AuNP, is included for comparison purposes) we found the opposite effects in terms of both reduction potential and peak current intensity. The shift of the reduction potential ( $\sim 80$  mV) is even more pronounced. This general trend was consistently observed for different total gold concentrations tested, as shown in the plots of Fig. 4B.

An explanation to these contradictory results may be related to the Brownian effects<sup>36</sup> governing the motion of these smaller particles. Any minute particle suspended in a liquid (or gas) moves chaotically under the action of collisions with surrounding molecules. The frictional force—also called drag force—exerted on spherical objects with very small Reynolds numbers (e.g., nanoparticles) in a continuous viscous fluid can be calculated by the Stokes law:<sup>37</sup> if the particles are falling in a viscous fluid by their own weight due to gravity, then a terminal velocity, also known as the settling velocity, is reached when this frictional force combined with the buoyant force exactly balance the gravitational force. From equations derived from this law, the settling velocity of the AuNPs of different sizes from the suspension to the electrode surface and the necessary falling time

to the electrode surface from an arbitrary distance can be estimated. These approximated calculations are detailed in the ESI†, showing that for the 5 nm AuNPs, the expected time of AuNPs deposition of those situated at a distance of, say, 50 nm (an arbitrary distance chosen as long enough to put in evidence the different behaviors between the smaller and the larger AuNPs in relatively short, *i.e.* 2 minutes, adsorption time) over the electrotransducer surface would be 32 minutes. This means that, after drop casting the AuNPs suspension onto the electrode surface, a deposition time of 2 minutes (used in the detection procedure) is not long enough to guarantee quantitative adsorption of AuNPs smaller than 20 nm onto the electrode surface. If part (or even most) of the AuNPs are still not adsorbed onto the electrotransducer surface, the electrochemical signal coming from the AuNPs will dramatically decrease. On the other hand, the AuNPs of 20–80 nm situated at the same 50 nm distance from the electrode surface will be totally adsorbed within the 2 minutes deposition time. A cartoon of the process hypothesized to occur on the electrode surface is shown in Fig. 4C.

Overall, the results obtained under the same experimental protocol indicate that, for the same quantity of total gold, efficiency is optimized with the 20 nm AuNPs. In other words, for the same quantity of gold the best way to exploit the electrochemical properties of AuNPs is to use the 20 nm sized ones. Smaller AuNPs suffer the problem of the longer times required to be adsorbed onto the electrode surface due to Brownian effects.

#### Application in a magnetoinmunoassay

We also studied the effect of the AuNPs size on the electrochemical signal when the NPs are used as labels in an immunoassay system based on the use of magnetic particles as immobilization platform. Under these conditions, we expected that the Brownian effects would have been minimized because independent of their size all AuNPs would be attracted onto the electrotransducer surface upon application of the magnetic field.

To study the effect of size, AuNPs of different sizes were conjugated with antibodies (see Experimental section) and used as labels in a magnetosandwich immunoassay that we previously optimized for 20 nm AuNPs,<sup>2,24</sup> using magnetic beads (MB) as platforms of the immunoreactions (see Experimental section). Briefly, it consists in the immobilization of biotin-modified anti-human IgG antibodies onto the surface of streptavidin-coated magnetic beads followed by the human IgG capturing from the sample. Finally the sandwich is completed through the immunoreaction with anti-human IgG–AuNP antibodies (MB/anti-human IgG/Human IgG/anti-human IgG–AuNP). It is well known that magneto-based immunoassays present improved properties in terms of sensitivity and selectivity, due to the pre-concentration of the analyte, the separation from the matrix of the sample and the immobilization/collection on the transducer surface, achieved using a magnetic field. Fig. 5A shows the electrochemical signals obtained for the same total concentration of gold with different AuNP sizes (5, 20, and 80 nm) used as labels in the described magnetoinmunoassay. The voltammetric peak current values show that a higher peak current was obtained for the 5 nm AuNPs. In addition, the peak potential was found to shift to less negative potentials as the AuNP size

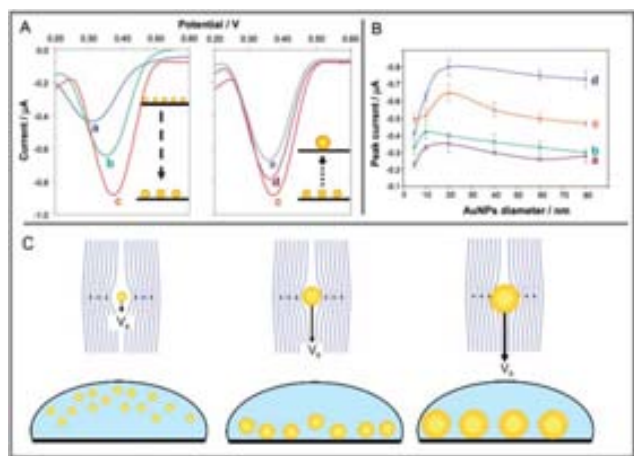


**Fig. 4** (A) Differential pulse voltammograms obtained for AuNPs of different sizes—(a) 5 nm, (b) 10 nm, (c) 20 nm, (d) 60 nm, (e) 80 nm—containing a concentration of total gold of 200  $\mu\text{M}$ . DPV parameters as in Fig. 3A (non-stirred 0.1 M HCl solution, room temperature). (B) AuNPs size dependence on the analytical signal for different total gold concentrations: (a) 10  $\mu\text{M}$ , (b) 20  $\mu\text{M}$ , (c) 50  $\mu\text{M}$ , (d) 200  $\mu\text{M}$ . (C) Scheme of the process occurring on the electrode surface for the different AuNP sizes.  $V_s$  stands for “setting velocity” as detailed in the Experimental section.

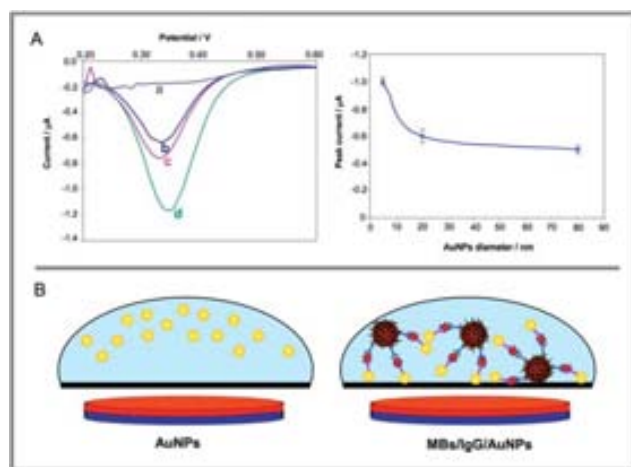


**Fig. 5** (A) (Left) Differential pulse voltammograms obtained for magnetosandwich immunoassays performed using AuNP labels of different sizes: (b) 80 nm, (c) 20 nm and (d) 5 nm. (a) Curve corresponds to a blank immunoassay carried out with goat IgG instead of human IgG and AuNPs labels of 5 nm. (Right) Corresponding AuNP labels size dependence on the analytical signals obtained for the magnetosandwich immunoassay using as electrochemical labels AuNPs of different sizes prepared from solutions of 84  $\mu$ M of total gold as detailed in the Experimental section. DPV parameters as in Fig. 3A (non-stirred 0.1 M HCl solution, room temperature). (B) Scheme of the process on the electrode surface—where a magnet has been placed under the working electrode area—for only AuNPs (left) and for the AuNPs attached to magnetic beads through the immunoassay (right).

decreased. These results confirm that the Brownian effects are not relevant when the AuNPs are attached to the MBs through the immunoreaction (as schematized in Fig. 5B) being these attracted afterward by a magnet placed under the working electrode surface. Therefore, under magnetosandwich conditions, the higher surface area of the smaller AuNPs gives rise to the best electrochemical response.

## Conclusions

The electrochemical properties of gold nanoparticles suspensions are strongly depended on the size and the hydrodynamic properties of the solvent. By considering only the NPs' size and for a fixed quantity of gold, smaller size NPs generate higher voltammetric signals. On the other hand, owing to the solvent effect and while working at a constant electrochemical measuring time, larger NPs generate higher signals. Our analysis points to Brownian effects as the main factor governing the efficiency of smaller size NPs. Conversely, while working in a bioassay system such as magnetimmunoassay employing magnetic particles, the mentioned effect is suppressed due to the fact that the NPs labels are attracted to the electrotransducer surface upon application of a magnetic field as witnessed by the increase of the voltammetric signal for the smallest NPs.

However we consider that the Brownian effect should be carefully considered according to the experimental conditions. For example, in an integrated biosensing system where the antibodies (or DNA capture probes) are directly immobilized onto the transducing surface the approaching of NPs upon the

recognition event would highly depend on the size. This consideration should be crucial for microfluidics based biosensing system (*i.e.* lab-on-a-chip) designs employing NPs based labeling technology. The design of optical based biosystems also might take advantages of such an approximation that would enlarge the importance of such phenomena.

These results are considered to provide an important piece of information to obtain a better understanding of the properties of AuNPs and, more generally, for the optimization of AuNPs-based electrochemical bioassays relevant not only to proteins but also to DNA and cells sensing.

We acknowledge MICINN (Madrid) for the projects PIB2010JP-00278 and IT2009-0092, the E.U.'s support under FP7 contract number 246513 "NADINE" and the NATO Science for Peace and Security Programme's support under the project SfP 983807.

## Notes and references

- 1 N. L. Rosi and C. A. Mirkin, *Chem. Rev.*, 2005, **105**, 1547–1562.
- 2 A. Ambrosi, M. T. Castañeda, A. J. Killard, M. R. Smyth, S. Alegret and A. Merkoçi, *Anal. Chem.*, 2007, **79**, 5232–5240.
- 3 H. P. Huang, Y. L. Tan, J. J. Shi, G. X. Liang and J. J. Zhu, *Nanoscale*, 2010, **2**, 606–612.
- 4 A. Merkoçi, *FEBS J.*, 2007, **274**, 310–316.
- 5 A. De la Escosura-Muñiz, A. Ambrosi and A. Merkoçi, *TrAC, Trends Anal. Chem.*, 2008, **27**, 568–584.
- 6 W. Parak, D. Gerion, T. Pellegrino, D. Zanchet, C. Micheel, S. C. Williams, R. Boudreau, M. A. Le Gros, C. A. Larabell and A. P. Alivisatos, *Nanotechnology*, 2003, **14**, R15–R27.
- 7 E. Katz, I. Willner and J. Wang, *Electroanalysis*, 2004, **16**, 19–44.
- 8 J. Wang, *Anal. Chim. Acta*, 2003, **500**, 247–257.
- 9 A. Merkoçi, M. Aldavert, S. Marín and S. Alegret, *TrAC, Trends Anal. Chem.*, 2005, **24**, 341–349.
- 10 E. Katz and I. Willner, *Angew. Chem., Int. Ed.*, 2004, **43**, 6042–6108.
- 11 M. C. Daniel and D. Astruc, *Chem. Rev.*, 2004, **104**, 293–346.
- 12 J. Wang, G. Liu, R. Polsky and A. Merkoçi, *Electrochem. Commun.*, 2002, **4**, 722–726.
- 13 G. Liu, H. Wu, J. Wang and Y. Lin, *Small*, 2006, **2**, 1139–1143.
- 14 J. H. Kim, K. S. Seo and J. Wang, *IEEE Sens. J.*, 2006, **6**, 248–253.
- 15 N. Jha and S. Ramaprabhu, *Nanoscale*, 2010, **2**, 806–810.
- 16 M. Seydack, *Biosens. Bioelectron.*, 2005, **20**, 2454–2469.
- 17 K. Aslan and V. H. Pérez-Luna, *Langmuir*, 2002, **18**, 6059–6065.
- 18 W. P. Faulk and G. M. Taylor, *Immunochemistry*, 1971, **8**, 1081–1083.
- 19 M. Pumera, J. Wang, E. Grushka and R. Polsky, *Anal. Chem.*, 2001, **73**, 5625–5628.
- 20 L. M. Demers, C. A. Mirkin, R. C. Mucic, R. A. Reynolds, R. L. Letsinger, R. Elghanian and G. A. Viswanadham, *Anal. Chem.*, 2000, **72**, 5535–5541.
- 21 A. P. Alivisatos, K. P. Johnson, X. Peng, T. E. Wislon, C. J. Loweth, M. P. Bruchez and P. G. Schultz, *Nature*, 1996, **382**, 609–611.
- 22 M. A. Hayat, *Colloidal Gold, Principles, Methods and Applications*, Academic Press, New York, 1989.
- 23 A. De la Escosura-Muñiz, C. Parolo and A. Merkoçi, *Mater. Today*, 2010, **13**, 24–34.
- 24 A. De la Escosura-Muñiz, M. Maltez-da Costa and A. Merkoçi, *Biosens. Bioelectron.*, 2009, **24**, 2475–2482.
- 25 A. De la Escosura-Muñiz, C. Sánchez-Espinell, B. Díaz-Freitas, A. González-Fernández, M. Maltez-da Costa and A. Merkoçi, *Anal. Chem.*, 2009, **81**, 10268–10274.
- 26 M. Pumera, M. Aldavert, C. Mills, A. Merkoçi and S. Alegret, *Electrochim. Acta*, 2005, **50**, 3702–3707.
- 27 M. Pumera, M. T. Castañeda, M. I. Pividori, R. Eritja, A. Merkoçi and S. Alegret, *Langmuir*, 2005, **21**, 9625–9629.
- 28 D. McFarland, C. L. Haynes, C. A. Mirkin, R. P. Van Duyne and H. A. Godwin, *J. Chem. Educ.*, 2004, **81**, 544A–544B.
- 29 W. Haiss, N. T. K. Thanh, J. Aveyard and D. G. Fernig, *Anal. Chem.*, 2007, **79**, 4215–4221.

- 
- 30 M. E. Hyde, C. E. Banks and R. G. Compton, *Electroanalysis*, 2004, **16**, 345–354.
- 31 J. L. Lingane, *J. Electroanal. Chem.*, 1962, **4**, 332–342.
- 32 X. Liu, M. Atwater, J. Wang and Q. Huo, *Colloids Surf., B*, 2007, **58**, 3–7.
- 33 R. H. Terrill, T. A. Postlethwaite, C. H. Chen, C. D. Poon, A. Terzis, A. Chen, J. E. Hutchison, M. R. Clark and G. Wignall, *J. Am. Chem. Soc.*, 1995, **117**, 12537–12548.
- 34 R. Sardar, A. M. Funston, P. Mulvaney and R. W. Murray, *Langmuir*, 2009, **25**, 13840–13851; R. W. Murray, *Chem. Rev.*, 2008, **108**, 2688–2720.
- 35 S. E. Ward-Jones, F. W. Campbell, R. Baron, L. Xiao and R. G. Compton, *J. Phys. Chem. C*, 2008, **112**, 17820–17827.
- 36 R. Brown, *Philos. Mag.*, 1828, **4**, 161–173.
- 37 *Encyclopædia Britannica*, 11th edn, 1911.

# Supplementary Information

## Size-dependent direct electrochemical detection of gold nanoparticles: application in magnetoimmunoassays

Alfredo de la Escosura Muñiz <sup>a</sup>, Claudio Parolo <sup>a</sup>, Flavio Maran <sup>b</sup> and Arben Mekoçi <sup>a,c\*</sup>

<sup>a</sup>CIN2 (ICN-CSIC), Catalan Institute of Nanotechnology, Campus de la UAB, 08193 Bellaterra (Barcelona) Spain

<sup>b</sup> Dipartimento di Scienze Chimiche, Università degli Studi di Padova, 35122 Padova, Italy

<sup>c</sup> ICREA, Barcelona, Spain

### **Screen-printed carbon electrodes (SPCEs) fabrication.**

The full size of the sensor strip was 29 mm x 6.7 mm, and the working-electrode diameter was 3 mm. The fabrication of the SPCEs was carried out in three steps. First, a graphite layer was printed onto the polyester sheet, using the screen-printing machine with the stencil (where it is the electron pattern). After curing for 15 minutes at 95°C, an Ag/AgCl layer was printed and cured for 15 minutes at 95°C. Finally, the insulating ink was printed and cured at 95°C for 20 minutes.

Images of the 45-sensor sheet obtained following the above experimental procedure and details of one of the SPCE are shown in figure S1.

### **AuNPs characterizations.**

- *ICP-MS analysis*: The amount of total of gold in the AuNPs solutions was obtained by ICP-MS analysis. The samples were diluted in 1% HNO<sub>3</sub> and inserted in the ICP-MS spectrometer to obtain their total content of gold, expressed in mg L<sup>-1</sup>.

- *Spectrophotometric analysis*: The spectrophotometric analysis of the different AuNPs solutions was performed by placing 275 µL of each solution on a plate of a 96-well plate, and measuring the OD in the range of 300 -750 nm. The concentration of AuNPs in each sample was calculated as detailed in the following section.

- *TEM images*: The size and shape of the different AuNPs studied was observed in the transmission electron microscope. The AuNPs solutions were first sonicated in an ultrasonic bath and then a drop of 4 µL was placed in a disk of copper and let to dry during 2 hours before the measurements.

### **Estimation of the concentration of AuNPs from UV-Vis spectra**

Knowing the value of  $\epsilon_{450}$ , the particle concentration (c) in mol L<sup>-1</sup> can be calculated from the absorption (A) at 450 nm for a standard path length (l) of 1 cm according to:

$$c = A_{450}/\epsilon_{450}$$

The values of  $\epsilon_{450}$  for each AuNP size has been calculated and experimentally verified in the range between 5-100 nm by Haiss's group (ref. 28 in the main text), being  $7.20 \times 10^6$ ,  $6.15 \times 10^7$ ,  $5.41 \times$

$10^8$ ,  $4.92 \times 10^9$ ,  $1.73 \times 10^{10}$ ,  $3.89 \times 10^{10}$  and  $6.44 \times 10^{10} \text{ M}^{-1} \text{ cm}^{-1}$  for 5, 10, 20, 40, 60, 80 and 100-nm AuNPs respectively. Absorbance spectra for different AuNPs solutions and the estimation of the concentration of each solution are summarized in figure S2.

### **Estimation of settling velocity and deposition time for AuNPs of different sizes**

The frictional force exerted on spherical objects with very small Reynolds numbers (e.g., nanoparticles) in a continuous viscous fluid can be calculated by the Stokes Law:

$$F_d = 6 \pi \mu R V$$

where  $F_d$  is the frictional force (in N),  $\mu$  is the fluid's dynamic viscosity (Pa s),  $R$  is the radius of the spherical object (m), and  $V$  is the particle's velocity ( $\text{m s}^{-1}$ ).

If the particles are falling in a viscous fluid by their own weight due to gravity, then a terminal velocity, also known as the settling velocity, is reached when this frictional force combined with the buoyant force exactly balance the gravitational force. The resulting settling velocity (or terminal velocity) is given by the following equation, derived from the Stokes Law:

$$V_s = 2 (\rho_p - \rho_f) g R^2 / 9 \mu$$

where  $V_s$  is the particles' settling velocity ( $\text{m s}^{-1}$ ) (vertically downwards if  $\rho_p > \rho_f$ , upwards if  $\rho_p < \rho_f$ ),  $g$  is the gravitational acceleration ( $\text{m s}^{-2}$ ),  $\rho_p$  is the mass density of the particles ( $\text{kg m}^{-3}$ )  $\rho_f$  is the mass density of the fluid ( $\text{kg m}^{-3}$ ) and  $\mu$  is the fluid's dynamic viscosity (Pa s).

Considering a gold density of  $19.3 \text{ g cm}^{-3}$  and a fluid viscosity of  $1 \text{ mPa s}$ , the settling velocity of the AuNPs of different sizes from the suspension to the electrode surface and the necessary falling time to the electrode surface from an arbitrary distance of 50 nm can be estimated (Table S1).

### **Magnetosandwich immunoassay using as labels AuNPs of different sizes**

Briefly, 150  $\mu\text{g}$  (15  $\mu\text{L}$  from the stock solution) of the magnetic beads solution (MBs) were transferred into 0.5 mL Eppendorf tube. The MBs were washed twice with 150  $\mu\text{L}$  of B&W buffer.

The MBs were then re-suspended in 108  $\mu\text{L}$  of B&W buffer and 42  $\mu\text{L}$  (from stock solution 0.36 mg  $\text{mL}^{-1}$ ) of biotinylated anti-human IgG were added. The resulting MB and anti-human IgG (goat IgG for the blank assay) solution was incubated for 30 min at temperature 25  $^{\circ}\text{C}$  with gentle mixing in a TS-100 ThermoShaker. The formed MB/anti-human IgG were then separated from the incubation solution and washed 3 times with 150  $\mu\text{L}$  of B&W buffer. The preparation process was followed by resuspending the MB/anti-human IgG in 150  $\mu\text{L}$  of blocking buffer (PBS-BSA 5%) to block any remaining active surface of MBs and incubated at 25 $^{\circ}\text{C}$  for 60 min. After the washing steps with B&W buffer, the MB/anti-human IgG were incubated at 25  $^{\circ}\text{C}$  for 30 min with 150  $\mu\text{L}$  of 1  $\mu\text{g mL}^{-1}$  of human IgG antigen, forming by this way the immunocomplex MB/anti-human IgG/Human IgG. Finally, after the washing steps, the MB/anti-human IgG/Human IgG immunocomplex was incubated at 25  $^{\circ}\text{C}$  for 30 min with 150  $\mu\text{L}$  of the previously synthesized AuNPs/anti-human IgG complex.

A blank (control) assay is performed using goat IgG instead of human IgG at the same concentration.

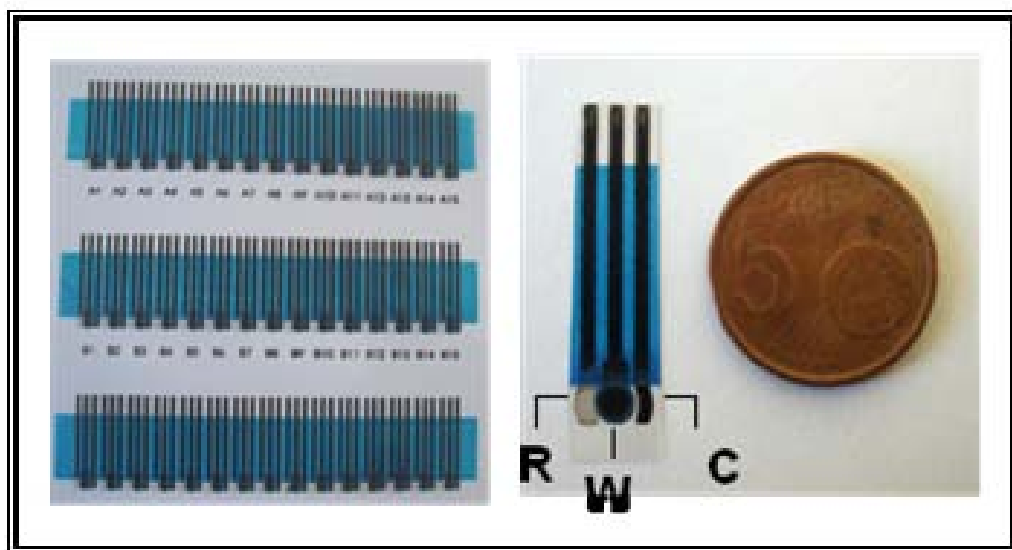


**Figure S1.** (Left) Images of the 45 SPCE sensors sheet obtained following the detailed experimental procedure. ( Right) Detail of one SPCE, containing the three electrodes in the working area: R - Ag/AgCl reference electrode, W- carbon working electrode and C- carbon counter electrode.

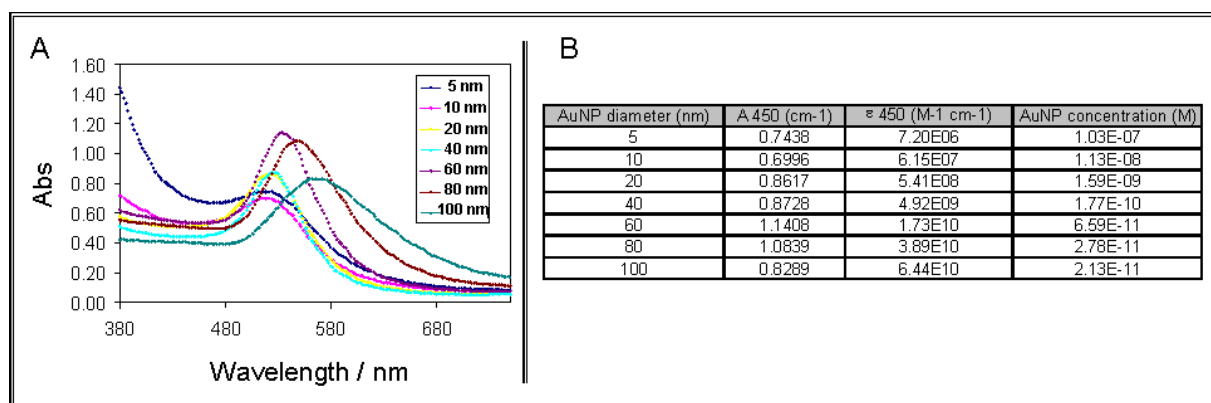


**Figure S2.** (A) Absorbance spectra of different AuNPs solutions and (B) estimation of the concentration of each solution.

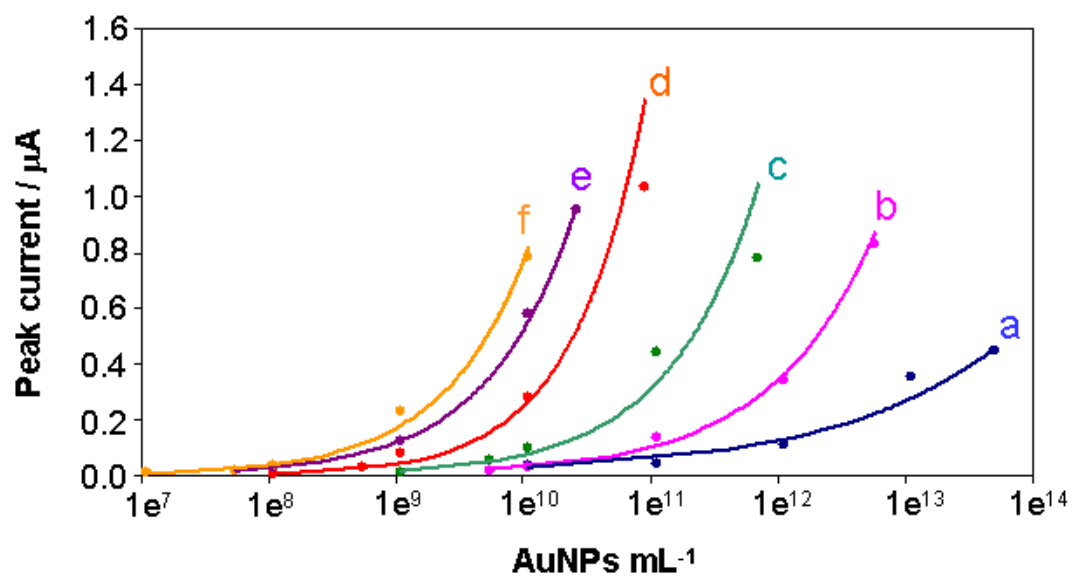


**Figure S3.** Full data of the electrochemical results obtained for different concentrations of AuNPs of different sizes: (a) 5 nm, (b) 10 nm, (c) 20 nm, (d) 40 nm, (e) 60 nm, (f) 80 nm.

<b>AuNP diameter</b> (nm)	<b>Velocity</b> (cm/min)	<b>Time*</b> (min)
5	1.57 e-6	31.97
10	6.30 e-6	7.99
20	2.52 e-5	2.00
40	1.01 e-4	0.50
60	2.27 e-4	0.22
80	4.04 e-4	0.12

\* Considering an arbitrary distance of 50 nm that the AuNP has to travel from the solution to the electrode.

**Table S1.** Estimation of the falling velocity and time required for AuNPs of different sizes traveling from the solution to the electrode surface.

<b>AuNPs diameter (nm)</b>	<b>N° atoms per nanoparticle</b>	<b>N° NPs in 1 mol atoms</b>	<b>N° NPs in 25µL of 50 µM gold solution</b>	<b>N° surface atoms in 25 µL of 50 µM gold solution</b>
5	3859	$1.50 \times 10^{20}$	$1.95 \times 10^{11}$	$1.99 \times 10^{14}$
20	246960	$2.44 \times 10^{18}$	$3.05 \times 10^9$	$5.00 \times 10^{13}$
80	15806976	$3.81 \times 10^{16}$	$4.76 \times 10^7$	$1.25 \times 10^{13}$

**Table S2.** Estimation of the number of surface atoms contained in 25 µL of a 50 µM gold solution of AuNPs of different sizes.

## PAPER

[View Article Online](#)  
[View Journal](#) | [View Issue](#)

# Simple paper architecture modifications lead to enhanced sensitivity in nanoparticle based lateral flow immunoassays†

Cite this: *Lab Chip*, 2013, 13, 386Claudio Parolo,<sup>a</sup> Mariana Medina-Sánchez,<sup>a</sup> Alfredo de la Escosura-Muñiz<sup>a</sup> and Arben Merkoçi<sup>\*ab</sup>Received 11th October 2012,  
Accepted 25th October 2012

DOI: 10.1039/c2lc41144j

[www.rsc.org/loc](http://www.rsc.org/loc)

Lateral flow immunoassays (LFIA) are ideal biosensors to detect proteins, but their lack of sensitivity hinders their extensive use. We report a strategy that yields up to an 8-fold improvement in the sensitivity of a gold nanoparticles-based LFIA by changing the sizes of the pads. Theoretical flow simulations of the developed LFIA architectures are in accordance with the experimental results.

## Introduction

Sensitive methods for the detection of proteins are of tremendous interest in everyday diagnostics, since many proteins are biomarkers of diseases.<sup>1</sup> Early detection of such biomarkers could allow treatment to start in the early stages of a disease, making it possible to save many lives. This is particularly important in third world countries, where advanced and expensive technologies are unavailable to most people.<sup>2,3</sup> The same situation can be found in remote or dangerous regions or on battlefields, where the conditions do not allow the use of complicated devices and trained personnel cannot be present. For these reasons, it is of extreme importance to develop biosensors which fulfil the requirements of an ASSURED biosensor:<sup>4</sup> affordable, sensitive, specific, user-friendly, rapid and robust, equipment free and deliverable to end-users.

Lateral flow immunoassays (LFIA) can be considered as biosensors which fit the definition of ASSURED technology. Since the first pregnancy test was sold in the mid-1970s, LFIAs have gained much more importance in the field of biosensing.<sup>5</sup> However, some limitations have prevented their wide adoption by other fields, where quantitative analysis together with better sensitivity are required. In order to answer these demands, the integration of several nanomaterials into paper based biosensors has already been investigated.<sup>6,7</sup> Taking advantage of the outstanding properties of nanometer-scale materials, it is possible to improve the performance of the biosensors.<sup>8–11</sup> Examples of nanomaterials used in lateral flow assays are gold nanoparticles (AuNPs),<sup>12–15</sup> quantum dots,<sup>16,17</sup>

carbon nanotubes,<sup>18</sup> magnetic nanoparticles,<sup>19,20</sup> and liposomes,<sup>21,2</sup> amongst others.

In this article, we show both theoretically and experimentally how simple changes in the architecture of an AuNP based LFIA, such as the width of the sample and conjugation pads, can be translated into an increase in sensitivity and an improved detection limit for this analytical device.

## Materials and methods

### Chemicals and equipment

All the materials used for the production of the strips were purchased from Millipore (Billerica MA 08128, USA): sample and absorbent pads (CFSP001700), conjugation pad (GFCP00080000), detection pad (SHF2400425) and backing card (HF000MC100). The membranes were characterized using Scanning Electron Microscopy (SEM) (ZEISS MERLIN FE-SEM). Human IgG whole molecule (HIGG) (I2511), antibody anti-human IgG ( $\alpha$ HIGG) whole molecule (produced in goat; I1886), antibody anti-human IgG  $\gamma$  chain specific biotinylated (produced in goat; B1140) and all the chemical reagents (analytical grade) used for the preparation of AuNPs and buffer solutions were purchased from Sigma Aldrich (Spain). Anti-goat IgG ( $\alpha$ GIgG) (produced in chicken; ab86245) was purchased from Abcam (UK). The stirrer used was a TS-100 Thermo shaker (BioSan, Latvia). A thermostatic centrifuge (Sigma 2-16 PK, Fisher Bioblock Scientific, France) was used to purify the AuNP-antibody conjugates. An IsoFlow reagent dispensing system (Imagen Technology, USA) was used to dispense the detection and control lines. A strip reader (COZART, SpinReact, UK) was used for quantitative measurements. A guillotine (Dahle 533, Germany) was used to cut the strips. mQ water, produced using a Milli-Q system ( $>18.2$  M $\Omega$  cm<sup>-1</sup>) purchased from Millipore (Sweden), was used for the preparation of all solutions.

<sup>a</sup>Nanobioelectronics & Biosensors Group, Institut Català de Nanotecnologia, CIN2 (ICN-CSIC), Campus UAB, Barcelona, Spain

<sup>b</sup>ICREA, Barcelona, Spain. E-mail: [arben.merkoci@icn.cat](mailto:arben.merkoci@icn.cat)

† Electronic supplementary information (ESI) available. See DOI: 10.1039/c2lc41144j

The mathematical simulations were done using the chemical reaction engineering module of Comsol Multiphysics 3.4 software, taking advantage of the equations of transport in porous media.

### Preparation and modification of gold nanoparticles

AuNPs of  $20.99 \pm 2.72$  nm in diameter were synthesized according to the citrate reduction of  $\text{HAuCl}_4$  (as pioneered by Turkevich *et al.*<sup>22</sup>); details of the synthesis can be found in the ESI† together with the experimental procedure for the functionalization of AuNPs with  $\alpha\text{HIgG}$   $\gamma$  chain specific. The AuNPs modified with antibodies were concentrated 5 times in 2 mM borate buffer pH 7.4 containing 10% of sucrose after a centrifugation step.

### Preparation of LFIA strips

The sample pad was pre-treated by dipping it into 10 mM PBS buffer pH 7.4, containing 5% BSA and 0.05% Tween20 and then drying it for 30 min at 60 °C. The conjugation pad was dipped into the AuNP solution and then dried for 1 h under vacuum. The control and the detection lines were obtained by dispensing  $\alpha\text{HIgG}$  whole molecule and  $\alpha\text{GIgG}$  respectively onto the detection pad. The antibody solutions ( $1 \text{ mg mL}^{-1}$  in 10 mM phosphate buffer pH 7.4) were dispensed at a rate of  $1 \mu\text{L cm}^{-1}$  using an IsoFlow reagent dispensing system. The pad was then dried at 37 °C for 30 min. After that, the different pads were laminated on the backing card in the following order: first, the detection pad, then the absorbent pad at the end of the backing card and overlapping the detection pad, next, the conjugation pad overlapping the detection pad and finally the sample pad on the beginning of the backing card and overlapping the conjugation pad (see Fig. 1A). All of the overlaps were around 1 mm.

After lamination, the strips were cut using a guillotine to define the external edges and then with a manual cutter to define the internal ones. In order to study the effects of the sample and conjugation pad sizes, two different setups were used: one where only the sample pad size was changed and another where both the sample and the conjugation pad sizes were changed. In both cases the surface area studied was  $1 \times$ ,  $2 \times$  and  $3 \times$  the original one.

### Assay procedure

For the 1X, 2X and 3X strip sizes, the assays were performed by pipetting 200, 400 and 600  $\mu\text{L}$  of the HIgG solution respectively onto the bottom of the sample pad. A blank and three different concentrations of HIgG were studied: 6, 60 and 600  $\text{ng mL}^{-1}$  in 10 mM PBS pH 7.4. The assay took around 10 min to develop the color of the lines and 10 min for the washing step, performed by pipetting the same amount of buffer onto the sample pad. The strip was finally cut to a uniform width of 8 mm in order to be read by the strip reader.

The assay follows an immunosandwich format: the  $\alpha\text{HIgG}$  ( $\gamma$ -chain specific) antibodies, attached to the AuNPs, recognize the  $\gamma$ -chain of the HIgG of the sample. The AuNP- $\alpha\text{HIgG}$  ( $\gamma$ -chain specific)-HIgG conjugates are stopped by the  $\alpha\text{HIgG}$  (whole molecule) antibodies which are fixed at the detection line. The stronger the red color of the AuNPs at the detection line, the higher the concentration of the analyte (HIgG)

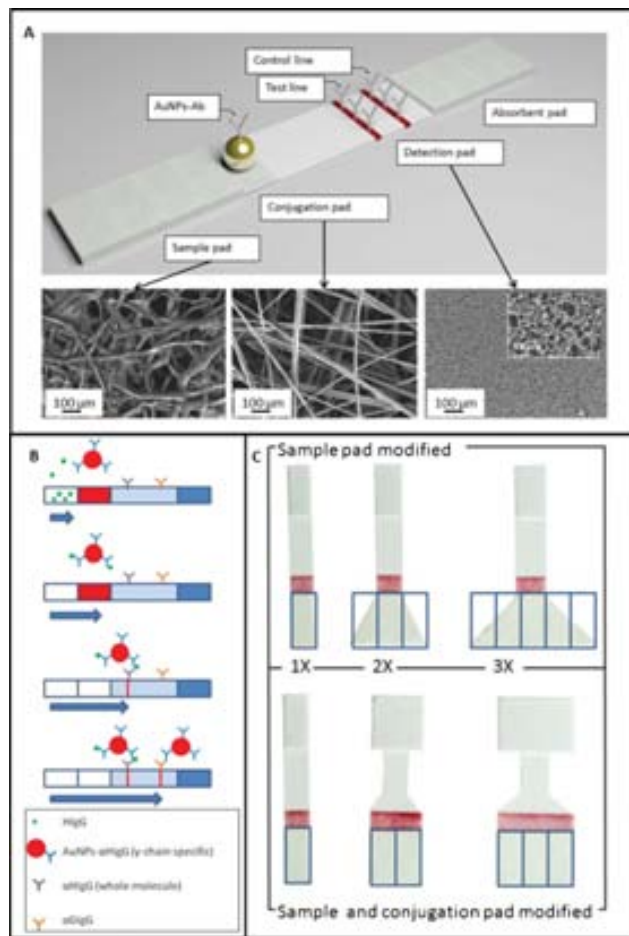


**Fig. 1** (A) Scheme, not to scale, of a LFIA strip based on a sandwich format (above) and SEM images of the different pads (below). (B) Scheme of the formation of the immune-complex during the flow. (C) Different setups for LFIAs: with only the sample pad 1X, 2X and 3X (above) and with both the conjugation and sample pads 1X, 2X and 3X (below).

present in the sample (Fig. 1B). Furthermore the  $\alpha\text{GIgG}$  at the control line recognizes  $\alpha\text{HIgG}$  ( $\gamma$ -chain specific) in the complexes which are not stopped at the detection line, confirming that the assay worked properly.

### Mathematical simulations

The flow in strip membranes is usually described by the Navier–Stokes equation (pore-free region) and the Brinkman equations (porous region). The most common way to deal with pore-free and porous media flow in a system is to couple Darcy's law, which does not account for viscous effects, with the Navier–Stokes equations. However, depending on the pore size distribution of the porous media and the fluid's properties, it is not always appropriate to neglect viscous effects. The Brinkman equations account for momentum transport through viscous effects and through pressure gradients in porous media, and can be considered an extension of Darcy's law, which is a derived constitutive equation that describes the flow of a fluid through a porous medium (see eqn (1)).<sup>23</sup>

$$Q = \frac{kA}{\mu} \left( \frac{dP}{dL} \right) \quad (1)$$

where  $Q$  is the flow rate (in units of volume per time unit),  $k$  is the relative permeability (typically in millidarcys),  $A$  is the cross sectional area (in square meters),  $\mu$  is the viscosity of the fluid (in centipoises),  $L$  is the length of the porous media (in meters) and  $dP/dL$  is the pressure change per unit length. The constants for the different pads were calculated empirically measuring the volume of water absorbed by each pad. In this way it was possible to estimate the porosity and the permeability of the different pads (see ESI†).

The initial conditions defined for the simulation were: porosity and permeability of the membranes (empirically calculated, as detailed at the ESI†) and the viscosity and density of the fluid (water). On the other hand, for the boundary conditions the initial velocity was calculated from the volume of the liquid introduced into the membrane (200, 400, and 600  $\mu\text{L}$  for the 1X, 2X and 3X strips respectively), the cross sectional area and the time necessary to absorb the respective volume. So for the 1X, 2X and 3X strips, the velocities were  $1.47 \times 10^{-3}$ ,  $2.94 \times 10^{-3}$  and  $4.41 \times 10^{-3} \text{ m s}^{-1}$  respectively.

## Results and discussion

### Effect of the architecture of the sample pad

A scheme of the LFIA used for the detection of HlgG as a model analyte is shown in Fig. 1B. Firstly, the effect of changing the sample pad size on the sensitivity of the LFIA was evaluated. The sample pads were designed to have a trapezoid shape to facilitate the flow. In order to obtain the sample pads with areas 2 and 3 times larger, the shorter base of the trapezoid (the one in contact with the conjugation pad) was fixed at 8 mm wide, whereas the longer base was increased to 24 mm and 40 mm respectively, as detailed in Fig. 1C. The strip reader outputs % values corresponding to the intensity of the lines: the weaker the intensity of the line, the higher the % value. The blank of each strip was subtracted from the results obtained in order to compensate for possible non-specific interactions.

In Fig. 2A it is possible to see how the strips looked following an assay with  $60 \text{ ng mL}^{-1}$  of HlgG. There are no clear differences in sensitivity for the different geometries used. In fact as shown in Fig. 2B there are two opposing effects that influenced the assay: the amount of analyte and the speed of the flow. Using bigger sample pads it is possible to use a greater volume of sample, and consequently more analyte is available, but this induces an increase in the speed of the flow, which reduces the time that the AuNP labels have to bind the analyte. The flow is also faster in the detection pad, decreasing the time to recognize the immuno-complexes formed by the antibodies of the test and control lines. As represented by the arrows in the figure, in the 1X format the AuNP speed is low giving enough time to have good recognition of the analyte, but the analyte amount is not high. The 2X format has a higher

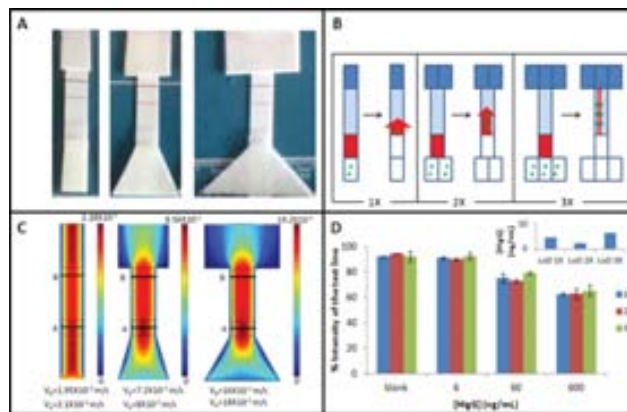


**Fig. 2** (A) Photos of LFIA with different sample pad architectures for  $60 \text{ ng mL}^{-1}$  HlgG. (B) Scheme of the two opposite effects: the amount of analyte vs. the speed of the flow for the LFIA using a bigger sample pad. The red arrows represent the speed of the AuNPs in the flow and the green point stated for the analyte. (C) Results of the flow speed simulations for sample pads with different sizes. (D) Effect of the relative size of the sample pad on the quantitative measurement of different HlgG concentrations and the corresponding LODs obtained (inset).

flow speed than the 1X but is still not fast enough to compromise the interaction between the antibodies and the analyte; furthermore the amount of analyte is larger, increasing the possibility of recognition by the AuNPs. Finally, in the 3X format the flow is very fast, not giving enough time for the AuNP complexes to interact with the antigen, consequently decreasing the sensitivity of the assay even though the quantity of analyte is larger.

These phenomena were also evaluated using mathematical simulations (see Fig. 2C). For each geometry the flow speed was calculated at the level of the conjugation pad and the test line. For the 1X geometry, the speeds were calculated to be  $2.1 \times 10^{-3}$  and  $1.95 \times 10^{-3} \text{ m s}^{-1}$  respectively. For the 2X, they were  $8 \times 10^{-3}$  and  $7.2 \times 10^{-3} \text{ m s}^{-1}$  and for the 3X they were  $18 \times 10^{-3}$  and  $16 \times 10^{-3} \text{ m s}^{-1}$ .

The graph in Fig. 2D shows the results obtained with the strip reader. They are in accordance with the theoretical calculations. In fact, there is no clear positive effect on the sensitivity of the LFIA when changing only the sample pad size. For the strips with a 2 times bigger sample pad, it was possible to observe a slight increase in the sensitivity of the assay, probably due to the higher volume of sample, which implies a higher amount of analyte. However, the results obtained using the strips with the 3 times larger sample pad show that the sensitivity of the assay is lower than with the sample pad of the original size. This can be explained considering that in the 3X configuration, the flow has a speed of approximately one order of magnitude higher than the 1X. Furthermore, the AuNPs are re-suspended by a fixed amount of liquid and they are dragged by it. This means that only the analyte present in this volume of liquid can be recognized by the AuNP labels, showing that use of an excess sample volume is not useful.

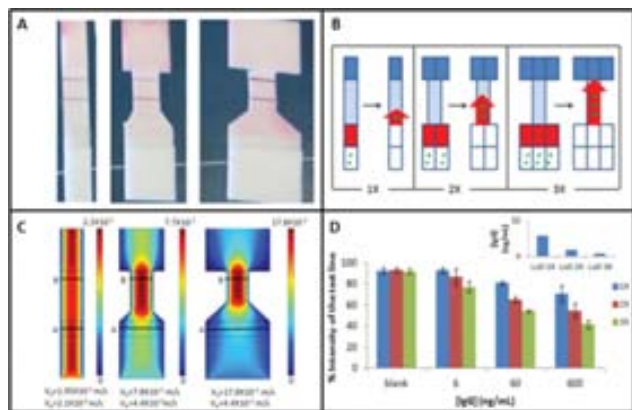


**Fig. 3** (A) Photos of LFIA with different sample and conjugation pad architectures after  $60 \text{ ng mL}^{-1}$  HlgG assays. (B) Scheme of the two opposite effects: the amount of analyte vs. the speed of the flow for the LFIA using bigger sample and conjugation pads. The red arrows represent the speed of the AuNPs in the flow and the green point stated for the analyte. (C) Results of the flow speed simulations for sample and conjugation pads with different sizes. (D) Effect of the relative sizes of the sample and conjugation pads on quantitative measurements for different HlgG concentrations and the corresponding LODs obtained (inset).

### Effect of different architectures for both sample and conjugation pad

In the second study, both the conjugation and the sample pads were changed. Here, the shapes of the sample and conjugation pads remain rectangular, so they were simply made 2 and 3 times bigger (Fig. 1C). Fig. 3A shows how the strips look after an assay using  $60 \text{ ng mL}^{-1}$  of HlgG. An increase in the intensity of the band is evident with increasing the sizes of sample and conjugation pads. In fact, as shown in Fig. 3B, using these configurations, the flow speed in the conjugation pad does not change significantly, giving enough time for the AuNPs labels to recognize the analyte. In addition, using a larger volume meant that there were more analyte molecules to be detected and since the conjugation pad was bigger, more AuNPs could be used as labels. This enabled the formation of a higher number of immuno-complexes. When the flow passed to the detection pad, there was an increase in the flow speed, but this phenomenon was compensated by the larger number of labels, which recognized the analyte. This theory was confirmed by the mathematical simulations (Fig. 3C): for the conjugation pad, the speed values were of the same order:  $2.1 \times 10^{-3}$ ,  $4.4 \times 10^{-3}$  and  $4.4 \times 10^{-3} \text{ m s}^{-1}$  for 1X, 2X and 3X respectively. However for the detection pad, a large increase is observed when increasing the size, with values of  $1.95 \times 10^{-3}$ ,  $7.8 \times 10^{-3}$  and  $17.8 \times 10^{-3} \text{ m s}^{-1}$  respectively. The results obtained with the strip reader (Fig. 3D) confirmed all of the previous data, showing the limits of detection for the 1X, 2X and 3X strips to be 5.89, 1.83 and  $0.7 \text{ ng mL}^{-1}$  respectively. This means that a 3-fold increase in the width of the conjugation and sample pads gives an 8-fold improvement in the limit of quantification.

These results could be further improved by increasing the difference in width between the detection pad and the conjugation and sample pads. This can be achieved by making

the conjugation and sample pads wider and/or making the detection pad smaller. However, some drawbacks are envisaged: with bigger conjugation and sample pads, a greater volume of sample as well as a larger amount of label is required. Furthermore, smaller detection pads would not be compatible with the strip reader. Another point to be considered is the shape of the strips: longer strips would allow a softer pre-concentration, which would probably produce more reproducible results. This can also be achieved placing the detection line closer to the end of the detection pad.

## Conclusions

We have demonstrated that very simple changes to the LFIA architecture, such as increasing the size of both the conjugation and the sample pads, can improve its performance in terms of the sensitivity of the assay. Flow speed simulations also corroborate the experimental results and represent useful tools in designing novel lateral flow architectures. The proposed designs can be easily applied to any type of LF strip without changing the fabrication method; moreover it is simple and cheap, enabling its use in point-of-care applications, even at the doctor's surgery or in undeveloped countries. Studies using a different method of detection, based on the use of a camera, and the use of a wax printer, in order to define better the shape of the LFIA, have already started in our lab and they will enable further decreases in the size of the detection pad, allowing greater improvements in the sensitivity of the device.

## Acknowledgements

We acknowledge MEC (Madrid) for the project MAT2011-25870, the EU's support under FP7 contract number 246513 "NADINE" and the NATO Science for Peace and Security Programme's support under the project SfP 983807.

## References

- 1 D. Mabey, R. W. Peeling, A. Ustianowski and M. D. Perkins, *Nat. Rev. Microbiol.*, 2004, **2**, 231–240.
- 2 P. Yager, T. Edwards, E. Fu, K. Helton, K. Nelson, M. R. Tam and B. H. Weigl, *Nature*, 2006, **442**, 412–418.
- 3 A. K. Ellerbee, S. T. Phillips, A. C. Siegel, K. a Mirica, A. W. Martinez, P. Striehl, N. Jain, M. Prentiss and G. M. Whitesides, *Anal. Chem.*, 2009, **81**, 8447–8452.
- 4 R. W. Peeling, K. K. Holmes, D. Mabey and A. Ronald, *Sex. Transm. Infect.*, 2006, **82**, v1–6.
- 5 G. a Posthuma-Trumple, J. Korf and A. van Amerongen, *Anal. Bioanal. Chem.*, 2009, **393**, 569–582.
- 6 S. Song, Y. Qin, Y. He, Q. Huang, C. Fan and H.-Y. Chen, *Chem. Soc. Rev.*, 2010, **39**, 4234–4243.
- 7 C. Parolo and A. Merkoçi, *Chem. Soc. Rev.*, 2013, DOI: 10.1039/c2cs35255a.

- 8 G. Aragay, J. Pons and A. Merkoçi, *Chem. Rev.*, 2011, **111**, 3433–3458.
- 9 M. Perfézou, A. Turner and A. Merkoçi, *Chem. Soc. Rev.*, 2012, **41**, 2606–2622.
- 10 A. de la Escosura-Muñiz, C. Parolo and A. Merkoçi, *Mater. Today*, 2010, **13**, 24–34.
- 11 M. Medina-Sánchez, S. Miserere and A. Merkoçi, *Lab Chip*, 2012, **12**, 2000–2005.
- 12 Y. He, S. Zhang, X. Zhang, M. Baloda, A. S. Gurung, H. Xu, X. Zhang and G. Liu, *Biosens. Bioelectron.*, 2011, **26**, 2018–2024.
- 13 S. Lou, J.-Y. Ye, K.-Q. Li and A. Wu, *Analyst*, 2012, **137**, 1174–1181.
- 14 W. Zhao, M. M. Ali, S. D. Aguirre, M. A. Brook and Y. Li, *Anal. Chem.*, 2008, **80**, 8431–8437.
- 15 C. Parolo, A. de la Escosura-Muñiz and A. Merkoçi, *Biosens. Bioelectron.*, 2013, **40**, 412–416.
- 16 X. Zhu, L. Chen, P. Shen, J. Jia, D. Zhang and L. Yang, *J. Agric. Food Chem.*, 2011, **59**, 2184–2189.
- 17 Z. Zou, D. Du, J. Wang, J. N. Smith, C. Timchalk, Y. Li and Y. Lin, *Anal. Chem.*, 2010, **82**, 5125–5133.
- 18 A. Abera and J.-W. Choi, *Anal. Methods*, 2010, **2**, 1819–1822.
- 19 S. Puertas, M. Moros, R. Fernández-Pacheco, M. R. Ibarra, V. Grazú and J. M. de la Fuente, *J. Phys. D: Appl. Phys.*, 2010, **43**, 474012.
- 20 D. Tang, J. C. Saucedo, Z. Lin, S. Ott, E. Basova, I. Goryacheva, S. Biselli, J. Lin, R. Niessner and D. Knopp, *Biosens. Bioelectron.*, 2009, **25**, 514–518.
- 21 S. Shukla, H. KimLeem and M. Kim, *Anal. Bioanal. Chem.*, 2011, **401**, 2581–2590.
- 22 J. Turkevich, J. Stevenson and P. Hillier, *Discuss. Faraday Soc.*, 1951, **11**, 55–75.
- 23 S. Chen and G. D. Doolen, *Annu. Rev. Fluid Mech.*, 1998, **30**, 329–364.

## Supplementary information

Simple paper architecture modifications lead to enhanced  
sensitivity in nanoparticle based lateral flow immunoassay

*Claudio Parolo<sup>1</sup>, Mariana Medina-Sánchez<sup>1</sup>, Alfredo de la Escosura-Muñoz<sup>1</sup>, Arben  
Merkoçi<sup>1,2\*</sup>*

<sup>1</sup> Nanobioelectronics & Biosensors Group, Institut Català de Nanotecnologia, CIN2  
(ICN-CSIC), Campus UAB, Barcelona, Spain

<sup>2</sup> ICREA, Barcelona, Spain

\*Corresponding author: arben.merkoci@icn.cat Tel: +34935868014; fax:  
+34935813797

### **Preparation of gold nanoparticles (AuNPs)**

All glassware used in this preparation was thoroughly cleaned in aqua regia overnight and rinsed with double distilled H<sub>2</sub>O and reflux was used for all the procedure which was done as follows: a 50 mL aqueous solution of 0.01% HAuCl<sub>4</sub> was heated to boiling and vigorously stirred in a 250 mL round-bottom flask; 5 mL of 40 mM sodium citrate were added quickly to this solution. Boiling was continued for an additional 10 min. The solution was cooled to room temperature with a continuous stirring for another 15 min. The colloids were stored in dark bottles at 4° C.

### **AuNPs modification with antibodies**

The AuNPs were then conjugated with the antibody  $\alpha$ HIgG  $\gamma$  chain specific. Briefly, 1.5 ml of AuNPs solution was adjusted to pH 9 with 10mM borate buffer pH 9.2. Then, without stopping the stirring, 100  $\mu$ L of the antibody solution (100  $\mu$ g/mL) were added drop by drop and the resulting solution was incubated for 20 min at 650 rpm. Then 100  $\mu$ L of 1 mg/mL BSA aqueous solution were added drop by drop and the stirring was continued for other 20 min at 650 rpm. Finally the solution was centrifuged at 14000 rpm for 20 min. The supernatant was removed and the pellet of AuNPs was re-suspended in 300  $\mu$ L of 2 mM borate buffer pH 7.4 containing 10% of sucrose.

### **Empirical calculation of pad constants**

The porosity and permeability constants of sample, conjugation and detection pads were calculated measuring the change in a fixed volume of PBS (PBS density = 1,97g/mL) after dipping the different pads as shown in figure S1. The sizes of the pads are also shown in figure S1. The porosities of the absorbent, conjugation and detection pad were respectively: 0.47, 0.23, 0.31; whereas the permeability were:  $7.5 \times 10^{-6}$ , 1.85

$\times 10^{-6}$ ,  $4.91 \times 10^{-7} \text{ m}^2$ , calculated considering the transversal area of the membrane and its porosity.

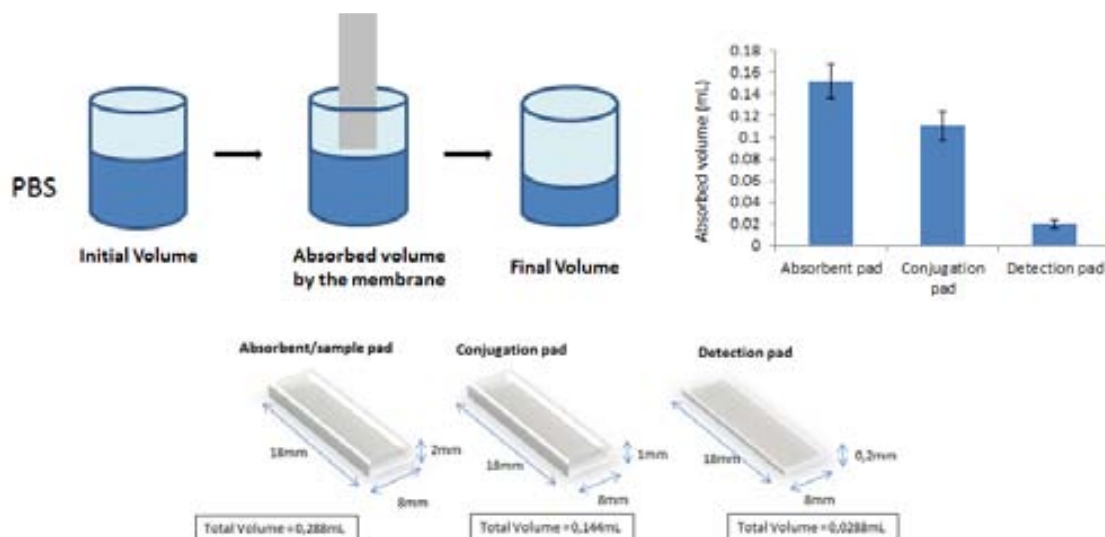


**Figure S1:** On the left: scheme of the experiment used to calculate the porosity and permeability of the membranes. On the right: results obtained for the different membranes. On the bottom: sizes and total volumes of the membranes used.



## Short communication

## Enhanced lateral flow immunoassay using gold nanoparticles loaded with enzymes

Claudio Parolo<sup>a</sup>, Alfredo de la Escosura-Muñiz<sup>a</sup>, Arben Merkoçi<sup>a,b,\*</sup><sup>a</sup> Nanobioelectronics & Biosensors Group, CIN2 (ICN-CSIC), Catalan Institute of Nanotechnology, Campus UAB, Bellaterra (Barcelona), Spain<sup>b</sup> ICREA, Barcelona, Spain

## ARTICLE INFO

Available online 30 June 2012

## Keywords:

Lateral flow immunoassay  
 Human immunoglobulin  
 Gold nanoparticle  
 Horseradish peroxidase  
 3,3',5,5'-Tetramethylbenzidine (TMB)  
 3-Amino-9-ethylcarbazole (AEC)  
 3,3'-Diaminobenzidine tetrahydrochloride (DAB) with metal enhancer

## ABSTRACT

The use of gold nanoparticles (AuNPs) as labeling carriers in combination with the enzymatic activity of the horseradish peroxidase (HRP) in order to achieve an improved optical lateral flow immunoassay (LFIA) performance is presented here.

Briefly in a LFIA with an immune-sandwich format AuNPs are functionalized with a detection antibody already modified with HRP, obtaining an 'enhanced' label. Two different detection strategies have been tested: the first one following just the red color of the AuNPs and the second one using a substrate for the HRP (3 different substrates are evaluated), which produces a darker color that enhances the intensity of the previous red color of the unmodified AuNPs. In such very simple way it is gaining sensitivity (up to 1 order of magnitude) without losing the simplicity of the LFIA format, opening the way to other LFIA applications including their on-demand performance tuning according to the analytical scenario.

© 2012 Elsevier B.V. All rights reserved.

## 1. Introduction

The detection of protein is of tremendous interest in diagnostics, since many biomarkers for many diseases are actually proteins and their early detection could save many lives, especially in the third world countries (Mabey et al., 2004). In fact, whereas in the industrialized world many complex and expensive techniques are available, in third world countries these techniques cannot be used because of their high cost and the lack of trained personnel (Yager et al., 2006; Ellerbee et al., 2009). The same situation can be found in small ambulatory, remote regions and battlefields. In this context the development of easy to use, point of care (PoC) and cheap biosensors is essential. A possible answer to this demand is the lateral flow immunoassay (LFIA), which is a platform that can be defined as ASSURED: affordable, sensitive, specific, user-friendly, rapid and robust, equipment free and deliverable to end-users (Peeling et al., 2006; <http://www.who.int/>) LFIA is based on the recognition of one or more analytes of interest, mainly proteins, by using antibodies. The antibodies are fixed onto a nitrocellulose membrane and they interact with the analyte either in sandwich or competitive formats using a proper label. The main advantage compared with

other immunosensors is that the entire assay can be done in one step and in a few minutes (Posthuma-Trumpie et al., 2009). Anyway the limit of detection (LoD) is generally not as good as other assays like ELISA; this limitation is the main reason to the lack of extensive use in clinical laboratories, even being one of the most used PoC biosensors, since the first pregnancy test sold in 1970s.

On the other hand, nanomaterials (NMs) and especially nanoparticles have been widely used in many biosensors ranging from protein (de la Escosura-Muñiz et al., 2010) to nucleic acid (Merkoçi et al., 2005) detection and with different techniques (both optical and electrochemical) due to their unique properties which make them excellent labels and carriers. Gold nanoparticles (AuNPs) are the most used NM in LFIA (Lou et al., 2011; Yang et al., 2011) but not the only one; actually also magnetic nanoparticles, quantum dots (QDs) (Zou et al., 2010; Zhu et al., 2011), liposomes (Edwards and Baemner, 2006; Shukla et al., 2011), carbon nanotubes (Wang et al., 2009, 2012; Abera and Choi, 2010), carbon nanoparticles (Ornatska et al., 2011) have also been used for such purposes. Although the peculiar properties of materials help to increase the sensitivity of the LFIA, this must be further increased to expand the application range in diagnostics. One of these advantageous properties consists in their ability to act as carriers of a high number of enzymes so as to increase their availability to catalyze the detection reaction. This approach was already performed in different biosensors like ELISA (Ambrosi et al., 2010) and lateral flow for nucleic acid (He et al., 2011; Mao et al., 2009).

\* Corresponding author at: Institut Català de Nanotecnologia, ETSE-Edifici Q, 2<sup>a</sup> planta, Campus UAB, 08193 Bellaterra (Barcelona) Spain.  
 Tel.: +34935868014; fax: +34935868020.

E-mail address: [arben.merkoci@icn.cat](mailto:arben.merkoci@icn.cat) (A. Merkoçi).

In this article we discuss the development of a LFIA based on the use of AuNPs not only as labels but also as carriers of enzymatic labels. AuNPs produce red bands at the detection and control lines of the LFIA when acting as direct labels, but if they are coupled with an antibody modified with HRP they can also act as carriers. 3,3',5,5'-Tetramethylbenzidine (TMB); 3-Amino-9-ethylcarbazole (AEC); 3,3'-Diaminobenzidine tetrahydrochloride (DAB) with metal enhancer as substrates of the HRP are evaluated since they produce insoluble chromogens which cannot be moved by the flow, concentrating the color at the lines. The developed LFIAs offer two different detection alternatives: one produced just by the red color of the AuNPs and other more sensitive produced by the substrate of the HRP achieving an 'on-demand' tuning of the biosensing performance. Its application for protein detection, after related optimizations, could open the way to several uses with interest in diagnostics, safety and security between other fields.

## 2. Experimental section

### 2.1. Materials

All the materials used for the production of the LFIA strips were purchased from Millipore (Billerica, MA 08128, USA): sample and absorbent pads (CFSP001700), conjugation pad (GFCP00080000), detection pad (SHF2400425) and the backing card (HF000MC100). A guillotine Dahle 533 (Germany) was used to cut the strips. The sample pad buffer consisted of 10 mM PBS pH 7.4 with 5% BSA and 0.05% Tween20; the conjugation pad buffer was 2 mM borate buffer pH 7.4 with 10% of sucrose; the antibody buffer was 10 mM phosphate pH 7.4. An IsoFlow reagent dispensing system (Image Technology, USA) was used to dispense the detection and control lines. A strip reader (COZART — SpinReact, UK) was used for quantitative measurements.

Hydrogen tetrachloroaurate (III) trihydrate ( $\text{HAuCl}_4 \cdot 3\text{H}_2\text{O}$ , 99.9%) and trisodium citrate ( $\text{Na}_3\text{C}_6\text{H}_5\text{O}_7 \cdot 2\text{H}_2\text{O}$ ) were purchased from Sigma-Aldrich (Spain) to synthesize AuNPs. A Transmission Electron Microscope (TEM) Jeol JEM-2011 (Jeol Ltd., Japan) and a scanning electron microscope Merlin<sup>®</sup> FE-SEM (Carl Zeiss, Germany) were used to characterize the AuNPs.

For the AuNP conjugation: the borate buffer solution (BB) was prepared with 0.1 M boric acid and adjusted to pH 9.2 with 5 M NaOH. Blocking buffer solution consisted of mQ water with 1 mg/mL bovine serum albumin (BSA). The stirrer used was a TS-100 Thermo shaker (Spain). A thermostatic centrifuge Sigma 2-16 PK (Fisher Bioblock Scientific, France) was used to purify the conjugates of AuNPs/antibodies.

Human IgG whole molecule (I2511), anti-human IgG whole molecule (produced in goat; I1886), anti-human IgG  $\gamma$  chain specific HRP modified (produced in goat; A6029) and all the chemical reagents (analytical grade) used for the preparation of buffer solutions were purchased from Sigma-Aldrich (Spain). Anti-goat IgG (produced in chicken; ab86245) was purchased from Abcam (UK).

The HRP substrates: TMB (T0565), AEC (AEC101), and DAB with metal enhancer (D0426) were purchased from Sigma-Aldrich (Spain).

mQ water, produced using Milli-Q system ( $> 18.2 \text{ M}\Omega \text{ cm}^{-1}$ ) purchased from Millipore (Sweden), was used for the preparation of all the solutions.

### 2.2. Methods

#### 2.2.1. Preparation and modification of gold nanoparticles

AuNPs of 20 nm diameter were prepared according to the citrate reduction of the  $\text{HAuCl}_4$  method pioneered by Turkevich et al. (1951), as stated in the [Supplementary material](#).

The prepared AuNPs were further modified with the antibody anti-human IgG  $\gamma$  chain specific HRP modified. The functionalization process is described in the [Supplementary material](#). The AuNPs/antibody conjugates were further centrifuged at 14,000 rpm for 20 min at 4° C in order to concentrate them 5 times in 2 mM borate buffer pH 7.4 with 10% of sucrose.

#### 2.2.2. Preparation of the LFIA strips

First the sample pad was prepared by dipping it into a sample pad buffer solution and then drying it at 60° C for 2 h. The conjugation pad was prepared by soaking it with the AuNPs/antibody conjugate, prepared as described above, and then drying it at room temperature under vacuum for 2 h. Finally the antibodies anti-human IgG whole molecule and anti-goat IgG, diluted in the antibody buffer at a concentration of 1 mg/mL, were spotted onto the detection pad to form the detection and control lines respectively, using the IsoFlow reagent dispensing system. The detection pad was dried at 37° C for 1 h.

The different pads were subsequently laminated onto the baking card with an overlap between them of around 2 mm, in order to allow the sample to flow (see [Fig. 1](#)). Finally they were cut 8 mm wide and stored in dry conditions at 4° C up to a week. The long term stability was not the object of this study but considering the pregnancy test which can be stable up to several weeks one could expect (in a case of mass production for commercial purposes) similar performance.

#### 2.2.3. LFIA procedure

Sample solutions were prepared by diluting different amounts of Human IgG (HIgG) in PBS, obtaining different analyte concentrations: 0.5 ng/mL, 5 ng/mL, 50 ng/mL, and 500 ng/mL. PBS without analyte was considered as blank. The assay procedure consisted of first dispensing 200  $\mu\text{L}$  of sample solution onto the sample pad and keeping for 15 min until the flow is stopped. Then 200  $\mu\text{L}$  of PBS was dispensed in order to wash away the excess of AuNPs/antibody. The strips were read with the strip reader to obtain the calibration curve corresponding to the AuNPs used as 'direct' labels. After the first reading step, the LFIA strips were dipped for 5 min into the different HRP substrates, and washed with mQ water to stop the reaction and prevent saturation of the signals. The strips were finally read again with the reader.

## 3. Results and discussion

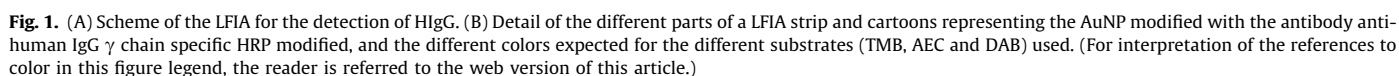
### 3.1. AuNP/antibody conjugates characterization

The AuNPs were characterized first by UV–vis analysis to calculate their concentration (it resulted  $2.1 \times 10^{-4} \text{ M}$ ) and to have an estimation of their size, which resulted to be around 20 nm in diameter since the wavelength of the peak was 520 nm ([de la Escosura-Muñiz et al., 2011](#)) ([Fig. 1SA](#)). Then they were also visualized by transmission electron microscopy (TEM) to have a more accurate size distribution, resulting in a diameter of  $21 \pm 3 \text{ nm}$  ([Fig. 1SB](#)).

The detection lines obtained for different concentrations of HIgG were also visualized by scanning electron microscopy (SEM). In [Fig. 1SC](#) it is possible to see the AuNPs (the white spots) in the test line of a LFIA after detecting 500 ng/mL of HIgG, whereas [Fig. 1SD](#) shows another zone of the detection pad without AuNPs.

### 3.2. Evaluation of the LFIA performance using AuNPs as both direct labels and carriers of enzymatic labels

The prepared LFIA strips gave rise to two different signals. The first one corresponds to the red color of the AuNPs, whereas the second one corresponds to the color of the chromogen produced



The first HRP substrate tested was the TMB. As stated in [Section 2](#) the TMB used in these experiments produced an insoluble blue-violet chromogen, which is deposited at the level of the control and test lines (as shown in [Fig. 2](#)); in this way the color is not dispersed along the strip. After stopping the HRP activity the strips were read with the strip reader. The results obtained are shown in the graph of [Fig. 2](#), where the improvement in the sensitivity seems to be clear. By using non-modified AuNPs

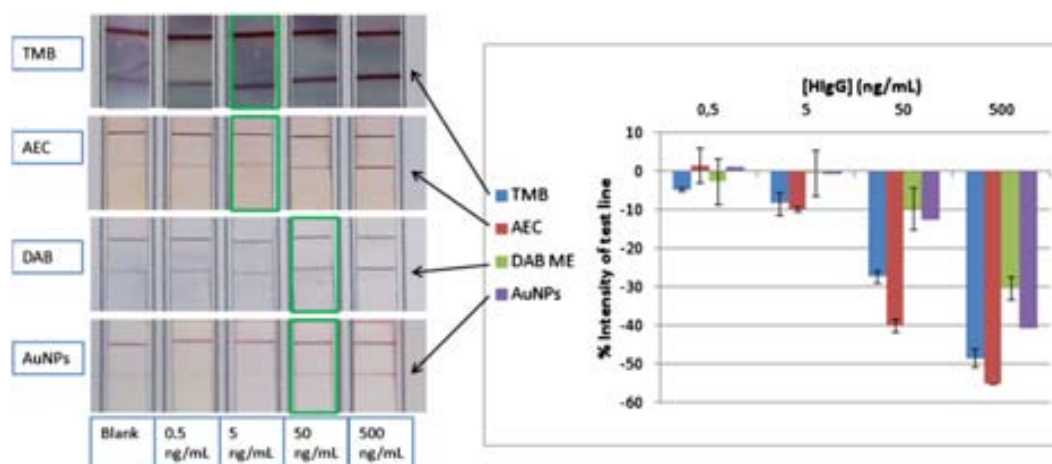


**Fig. 2.** (Left) Photos of the LFIA strips for different concentrations of HlgG and the different substrates. The limits of detection obtained for the naked eyes are highlighted. (Right) Graph of the results obtained with the strip reader. Experimental conditions as explained in the text.

as labels it was difficult to distinguish between a blank and 5 ng/mL of HlgG with the naked eye; on the other hand using the TMB the difference between the blank and the samples is evident, even at 5 ng/mL. The limit of detection obtained using the reader was of 200 pg/mL.

The second substrate used was the AEC, which produces an insoluble red chromogen. This substrate was already used by Liu's group in a LF for the detection of nucleic acids (He et al., 2011; Mao et al., 2009). As in the case of TMB substrate also the AEC enables an increase of the sensitivity of the assay, allowing detection up to 5 ng/mL with the naked eye as shown in Fig. 2. The limit of detection using the strip reader in this case was 310 pg/mL.

Finally the DAB with metal enhancer was tested. This HRP-substrate developed a gray/black insoluble compound. Surprisingly, it did not produce any appreciable increment in the sensitivity of the LFIA, being the minimum concentration detected with the naked eye of around 50 ng/mL, also shown in Fig. 2. The limit of detection using the reader (1.6 ng/mL) was only a little bit lower than the one obtained for the unmodified AuNPs (2 ng/mL, as explained before).

It is also noticed in a higher colored background in the case of the enzymatic reactions, probably due to a not completely washing of the strips.

The reproducibility of responses ( $n=3$ ) for a 50 ng/mL HlgG concentration was also studied, and relative standard deviations (RSD) of 1.3% for AuNPs, 5.6% for TMB, 1.5% for AEC and 16% for DAB were obtained.

The obtained results show that the use of the enzymatic reactions catalyzed by the HRP loaded on AuNPs using TMB and AEC as substrates of the enzyme allows an enhancing of the sensitivity of the LFIA of around one order of magnitude compared to the results obtained just from the direct measurement of the AuNPs as non-modified optical labels. In particular the TMB was the substrate which gave the best limit of quantification compared with the others (Fig. 2). TMB is also cheaper compared with DAB. Furthermore it has an important advantage compared to the other substrates studied in this work: it is ready to use. In fact both AEC and DAB need to be prepared freshly, using deionized water and mixing of at least two reagents. These characteristics make these two substrates not so suitable for LFIA applications, since they are more time consuming and could increase the possibility of human errors leading to an increase of the irreproducibility of the results. It has also been noted that the AEC produces a red chromogen whose color can be added to

the red color of the AuNPs and the background resulted less intense than the one of the TMB.

#### 4. Conclusions

A LFIA strip, with AuNPs loaded with HRP enzymatic labels was obtained. The use of such a label allows increasing order of magnitude the limit of quantification in a LFIA for the detection of Human IgG used as model protein. The strips prepared gave two different detection ranges: one less sensitive considering just the red color of the AuNPs and other more sensitive considering the color produced by the HRP substrates. Three different HRP substrates were tested and the TMB resulted the most suitable for LFIA applications compared with AEC and DAB with metal enhancer. This result could open the way to the use of LFIA in more diagnostics applications, especially in an ambulatory/laboratory context, due to the lower limit of quantification obtained. Furthermore, the use of various substrates offers the possibility to the 'on-demand' tuning of the sensitivity of the device adapting it to the analytical scenario.

#### Acknowledgments

We acknowledge the MEC (Madrid) for the Project no. MAT2011-25870, the E.U.'s support under FP7 Contract no. 246513 "NADINE" and the NATO Science for Peace and Security Program's support under the Project no. SFP 983807.

#### Appendix A. Supporting information

Supplementary data associated with this article can be found in the online version at <http://dx.doi.org/10.1016/j.bios.2012.06.049>.

#### References

- Abera, A., Choi, J.-W., 2010. *Analytical Methods* 2, 1819.
- Ambrosi, A., Airò, F., Merkoçi, A., 2010. *Analytical Chemistry* 82, 1151–1156.
- de la Escosura-Muñiz, A., Parolo, C., Maran, F., Merkoçi, A., 2011. *Nanoscale* 3, 3350.
- de la Escosura-Muñiz, A., Parolo, C., Merkoçi, A., 2010. *Materials Today* 13, 24–34.
- Edwards, K.A., Baumann, A.J., 2006. *Analytical and Bioanalytical Chemistry* 386, 1335–1343.

- Ellerbee, A.K., Phillips, S.T., Siegel, A.C., Mirica, K.A., Martinez, A.W., Striehl, P., Jain, N., Prentiss, M., Whitesides, G.M., 2009. *Analytical Chemistry* 81, 8447–8452.
- He, Y., Zhang, S., Zhang, X., Baloda, M., Gurung, A.S., Xu, H., Zhang, X., Liu, G., 2011. *Biosensors and Bioelectronics* 26, 2018–2024.
- < [http://www.who.int/std\\_diagnostics/about\\_SDI/priorities.htm](http://www.who.int/std_diagnostics/about_SDI/priorities.htm) >.
- Lou, S., Ye, J.-Y., Li, K.-Q., Wu, A., 2011. *Analyst* 137, 1174–1181.
- Mabey, D., Peeling, R.W., Ustianowski, A., Perkins, M.D., 2004. *Microbiology* 2, 231–240.
- Mao, X., Ma, Y., Zhang, A., Zhang, L., Zeng, L., Liu, G., 2009. *Analytical Chemistry* 81, 1660–1668.
- Merkoci, A., Aldavert, M., Marin, S., Alegret, S., 2005. *TrAC Trends in Analytical Chemistry* 24, 341–349.
- Ornatska, M., Sharpe, E., Andreescu, D., Andreescu, S., 2011. *Analytical Chemistry* 83, 4273–4280.
- Peeling, R.W., Holmes, K.K., Mabey, D., Ronald, A., 2006. *Sexually Transmitted Infections* 82 (Suppl. 5), v1–v6.
- Posthuma-Trumpie, G.A., Korf, J., van Amerongen, A., 2009. *Analytical and Bioanalytical Chemistry* 393, 569–582.
- Shukla, S., Leem, H., Kim, M., 2011. *Analytical and Bioanalytical Chemistry* 401, 2581–2590.
- Turkevich, J., Stevenson, P., Hillier, J., 1951. *Discussions of the Faraday Society* 11, 55–75.
- Wang, L., Chen, W., Xu, D., Shim, B.S., Zhu, Y., Sun, F., Liu, L., Peng, C., Jin, Z., Xu, C., Kotov, N.A., 2009. *Nano Letters* 9, 4147–4152.
- Wang, P., Ge, L., Yan, M., Song, X., Ge, S., Yu, J., 2012. *Biosensors and Bioelectronics* 32, 238–243.
- Yager, P., Edwards, T., Fu, E., Helton, K., Nelson, K., Tam, M.R., Weigl, B.H., 2006. *Nature* 442, 412–418.
- Yang, W., Li, X.-Bing, Liu, G.-Wen, Zhang, B.-Bing, Zhang, Y., Kong, T., Tang, J.-Jia, Li, D.-Na, Wang, Z., 2011. *Biosensors and Bioelectronics* 26, 3710–3713.
- Zhu, X., Chen, L., Shen, P., Jia, J., Zhang, D., Yang, L., 2011. *Journal of Agricultural and Food Chemistry* 59, 2184–2189.
- Zou, Z., Du, D., Wang, J., Smith, J.N., Timchalk, C., Li, Y., Lin, Y., 2010. *Analytical Chemistry* 82, 5125–5133.

# Supplementary material

**Enhanced lateral flow immunoassay using gold nanoparticles loaded with enzymes**

*Claudio Parolo<sup>1</sup>, Alfredo de la Escosura-Muñiz<sup>1</sup>, Arben Merkoçi<sup>1,2\*</sup>*

<sup>1</sup> Nanobioelectronics & Biosensors Group, Institut Català de Nanotecnologia, CIN2  
(ICN-CSIC), Campus UAB, Barcelona, Spain.

<sup>2</sup> *ICREA, Barcelona, Spain*

Phone number: +34935811976; Fax number: +34935812379

\*E-mail: [arben.merkoci@icn.cat](mailto:arben.merkoci@icn.cat)

### **Preparation of gold nanoparticles**

Gold nanoparticles of 20 nm of diameter were prepared according with the citrate reduction of  $\text{HAuCl}_4$ , method pioneered by Turkevich. (Turkevich, 1951) Briefly: 50 mL aqueous solution of 0.01%  $\text{HAuCl}_4$  was heated to boiling and vigorously stirred in a 250 mL round-bottom flask; 5 mL of 40 mM sodium citrate were added quickly to this solution. Boiling was continued for additional 10 min. The solution was cooled to room temperature with a continuous stirring for another 15 min. The colloids were stored in dark bottles at 4°C. All glassware used in this preparation was thoroughly cleaned in aqua regia overnight and rinsed with double distilled  $\text{H}_2\text{O}$  and reflux was used for all the procedure.

### **AuNPs modification with antibodies**

The antibody anti-human IgG  $\gamma$  chain specific HRP modified was conjugated to the AuNPs: the pH of 1.5 mL of AuNPs was corrected to 7.4 with borate buffer. Then 100  $\mu\text{L}$  of the antibody solution (100  $\mu\text{g}/\text{mL}$ ) were added drop by drop and the resulting solution was incubated for 20 min at 650 rpm. Then 100  $\mu\text{L}$  of 1 mg/mL BSA in  $\text{H}_2\text{O}$  mQ were added drop by drop and the stirring was continued for other 20 min at 650 rpm. Finally the solution was centrifuged at 14000 rpm for 20 min. The supernatant was removed and the pellet of AuNPs was re-suspended in 300  $\mu\text{L}$  of 2 mM borate buffer pH 7.4 with 10% of sucrose.

### Regression line data

Substrate	Equation	R
AuNPs	$y = -8.708\ln(x)+16.12$	0.973
TMB	$y = -6.521\ln(x)-4.1016$	0.964
AEC	$y = -8.709\ln(x)-1.7567$	0.985
DAB with metal enhancer	$y = -6.475\ln(x)+11.918$	0.977

y= % of the intensity of the test line

x= concentration of HIgG [ng/mL]

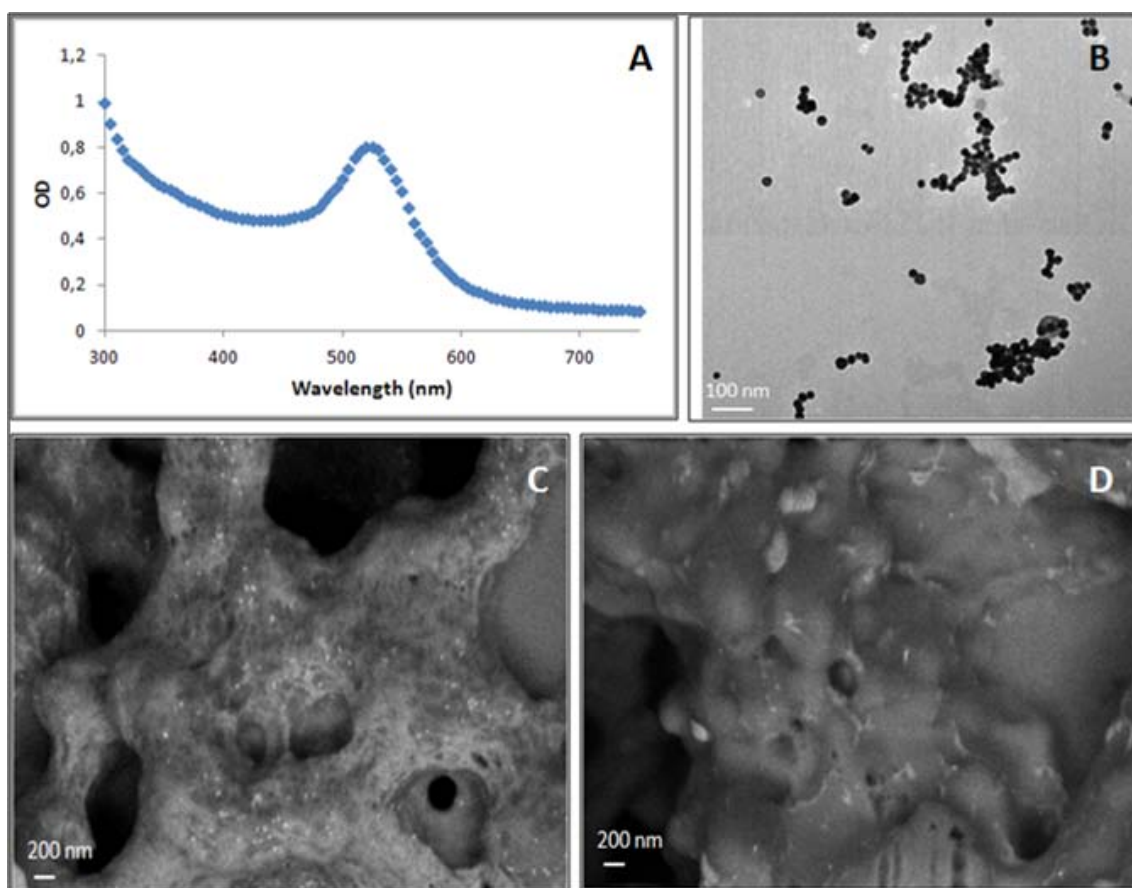


**Figure 1S.** (A) UV-Vis spectra of AuNPs. (B) TEM image of AuNPs. (C) SEM image of the test line of the LFIA detecting 500 ng/mL HIgG; the white spots represent the AuNPs. (D) SEM image of the detection pad without AuNPs.

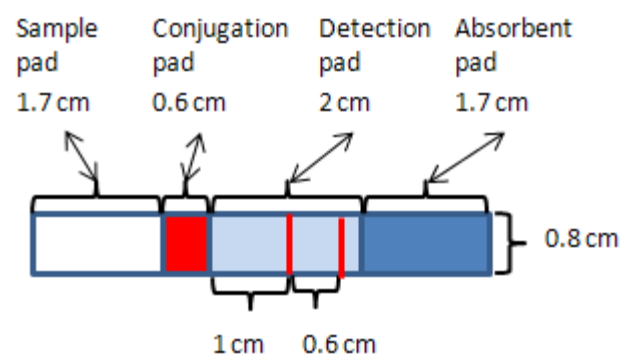


**Figure 2S.** Scheme of the strip sizes.

# Paper-Based Electrodes for Nanoparticle Detection

Claudio Parolo, Mariana Medina-Sánchez, Helena Montón, Alfredo de la Escosura-Muñiz, and Arben Merkoçi\*

In general, the success of a sensor depends not only on the efficient recognition of the analyte, but it is also affected by the detection method and the platform used.<sup>[1]</sup> In this context, the development of sensitive, robust, and cheap electrodes is essential for the progress of electrochemical based (bio)sensors. Many different kinds of electrodes, used as a sensing platform, are reported: glassy carbon electrodes, gold electrodes, micro-electrodes, screen-printed carbon electrodes (SPCEs), etc.<sup>[2]</sup> In our opinion, the integration of SPCEs in a point of care platform, such as lateral flow sensor, is easier, and the resulting device easy to be used.<sup>[3–5]</sup> In addition, due to their small sizes, low cost, fast, and versatile fabrication, using screen printing technology, the resulting device is cheaper in comparison with other types of electrodes, such as those based on sputtering or other micro and nanofabrication technologies. SPCEs are usually printed on polymeric materials, such as polyester, due to overall the mechanical properties of this platform, beside their low cost. These materials have two main drawbacks: they are not safely disposable and the sample to be analyzed needs pretreatments (i.e., incubations, washings, labeling etc.) outside the electrode. These problems can be overcome by the use of paper as a platform for the production of SPCEs, instead of plastic materials.<sup>[6–8]</sup> In fact, paper electrodes can be safely disposed by burning them. Their inherent microfluidic capability combined with an easy insertion of sample pretreatment pads including electrochemical detectors makes these devices the best candidate in terms of full integration of all the steps required for the detection of a sample.<sup>[9,10]</sup>

Paper-based nanobiosensors are showing to be the best sensing platforms for point of care applications.<sup>[11]</sup> They combine the advantages of the paper with those of nanomaterials, in general and especially of nanoparticles. The paper-based nano-biosensors, developed so far, are based mainly on optical detection of gold nanoparticles (AuNPs) plasmon signal.<sup>[12]</sup> Although such detection technologies are successfully applied for DNA,<sup>[13]</sup> proteins,<sup>[14]</sup> or cells,<sup>[15]</sup> there is still a big demand to improve the sensitivity and decrease the detection limits. Given the simplicity and robustness of electrochemical detection, its integration with lateral flow seems to be the best choice. The

efforts to achieve such integration are usually limited to a simple mechanical approximation of electrochemical detector with lateral flow paper platform. In fact, it is possible to develop paper-based sensors (such as lateral flow assays, microfluidic paper-based devices, etc.), where the paper SPCEs can be easily integrated and the entire device can be easily burned after use.<sup>[16]</sup> Furthermore, the sensitivity of such electrodes is generally expected to be higher than the others, because the surfactants of the inks can be absorbed by the paper, making the conductive material more exposed. In addition, they have a bigger electroactive surface available, since the matrix of the paper has a porous 3D structure.<sup>[17]</sup> To clarify such phenomena, characterizations of paper SPCEs and polyester SPCEs by scanning electron microscopy (SEM), confocal laser scanning microscopy (CLSM), and the studies of their hydrophobicity and porosity are firstly discussed. Then, the results obtained using paper SPCEs are compared with those obtained with polyester SPCEs for the detection of AuNPs and CdSe@ZnS quantum dots (QDs) with different electrochemical techniques. These very sensitive paper SPCEs are produced by combining screen printing, wax printing, and plasma cleaner.

First, we characterized the surface of the electrodes by SEM. Figure 1A,B shows the images of the paper and polyester platforms before printing any ink. A higher porosity of the paper can be clearly observed. In Figure 1C,D, it is possible to see the carbon-based working electrodes (WE) of polyester SPCE and paper SPCE respectively. In the paper SPCE, it is observed that in addition to the higher porosity of the substrate, the carbon ink is also printed on a microporous like pattern of around 185  $\mu\text{m}$ , which apparently increases the roughness of the WE and, in addition, may allow free space for an easy penetration of the sample. Such structures, in addition to the porous nature of the paper, make the WE having an enhanced electroactive surface easily accessible by the analyte. These ink-printed structures are observed only after printing (they are not present in Figure 1B) and are due to the nitrocellulose properties. We suggest that during the screen-printing process, when the ink is squeezed out of the mesh, the surfactants are quickly absorbed by the paper, making the carbon material accumulated into certain areas ordered according to the micropore distribution in the used mask. Such ordered carbon areas cannot be observed when the same ink is printed onto polyester, due to the fact that the ink, once is getting out from the mesh, keeps containing the same amount of solvent and consequently the same fluidity, causing an almost uniform coverage with carbon. As expected, the printed WE onto the polyester surface (SPCE) is very flat compared with the one of paper SPCE. This difference in the WE structure is probably one of the most important factors in the better electrochemical behavior of paper SPCEs

C. Parolo, M. Medina-Sánchez, H. Montón,  
Dr. A. de la Escosura-Muñiz, Prof. A. Merkoçi  
Nanobioelectronics & Biosensors Group  
Institut Català de Nanotecnologia, CIN2 (ICN-CSIC)  
Campus UAB, Barcelona, Spain  
E-mail: arben.merkoci@icn.cat  
Prof. A. Merkoçi  
ICREA, Barcelona, Spain



DOI: 10.1002/ppsc.201200124

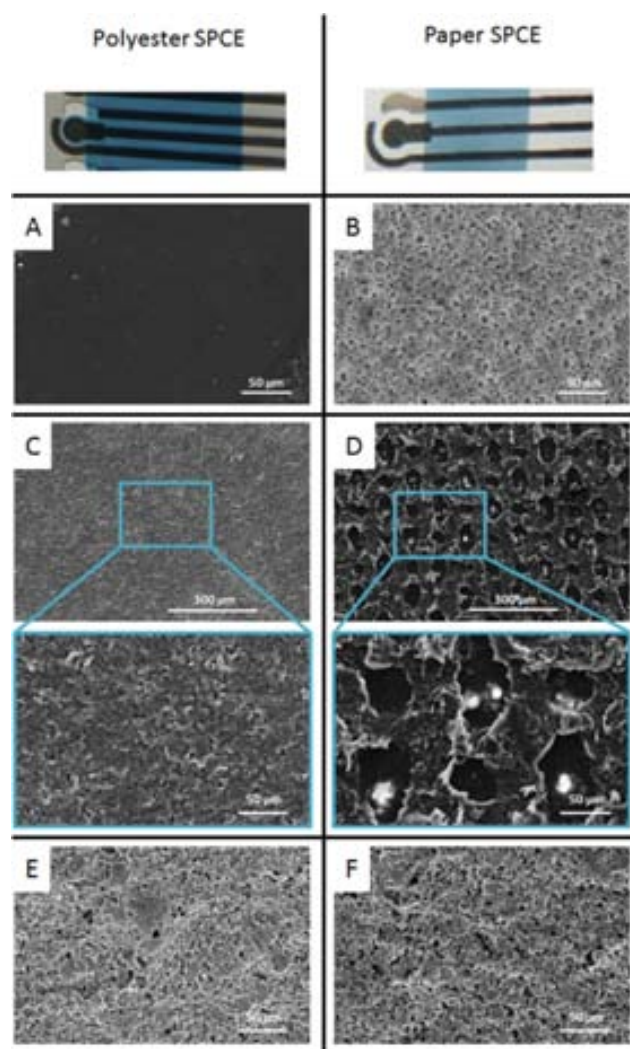


**Figure 1.** Microscopy images of polyester and paper-based SPCEs and SEM characterizations of: A) polyester sheet, B) nitrocellulose membrane (paper), C) carbon ink printed onto polyester, D) on paper at two different magnifications, E) silver ink printed onto polyester, and F) on paper.

compared with the polyester ones, as will be shown below. In the case of the silver layers, no observable differences are noticed between polyester and paper, as shown in Figure 1E,F, due to the different behavior (more fluidity) in comparison with the carbon ink.

CLSM  $\times 10$ – $12$  Mas used to confirm such observations by scanning the depth of the electrode along the z-axis using the reflection mode and z-stacks (Figure 2A,B). The periodic pattern in the WE of the paper SPCE and the much more homogeneous surface of the WE in polyester are evidenced in the plan view. Moreover, in order to see in depth the X and Y profiles of the WEs, a cross-section of the z-stack was performed (the dashed cross represents the exact site where the virtual cuts are performed). It is possible to see the periodic changes in the surface both in the X and Y profiles of the paper SPCE, while in the polyester one no remarkable changes of the surface can be observed.

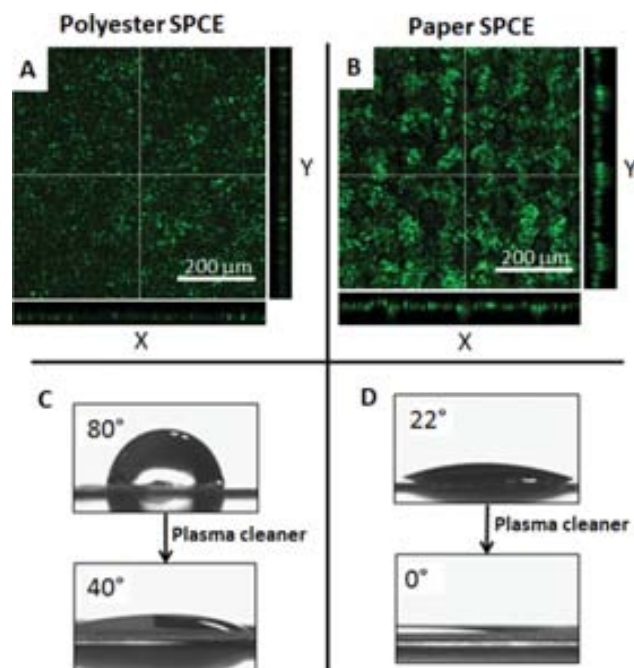


**Figure 2.** CLSM and hydrophilicity characterizations of the carbon WE printed onto polyester (left column) and on paper (right column). A,B) CLSM plan views and cross-section of the z-stack and C,D) contact angle study before (up) and after (down) plasma treatment.

The study of the hydrophilicity, of both carbon-printed surfaces, was also performed after plasma exposition (see Figure S2, Supporting Information). This plasma treatment is applied in order to introduce hydroxyl groups. The presence of such groups increases the hydrophilicity of the surface, causing a better and faster entrance of the sample into the porous surface of the WE, and increasing the contact area between the WE and the analyte. The increment in the humectability was confirmed by contact angle studies, as shown in Figure 2C,D. As expected, the untreated polyester is more hydrophobic than the untreated paper, as shown by the resulting contact angles of  $80^\circ \pm 0.5^\circ$  and  $22^\circ \pm 0.5^\circ$ , respectively. After the plasma treatment (1 min of exposure), the contact angle for the polyester decreased to  $40^\circ \pm 0.5^\circ$ , whereas the paper value could not be measured, because the liquid was immediately absorbed. The obtained results indicate that the plasma treatment is effective in making the paper SPCE more hydrophilic, enabling its application in water medium sensing (see Figure S2, Supporting Information).

The improved characteristics of the paper SPCEs was evaluated for the electrochemical detection of gold nanoparticles (AuNPs) and CdSe@ZnS quantum dots (QDs), which are of great interest for further applications in bioassays, where these NPs will be used as electroactive labels. To obtain a better sensing performance, all the electrochemical measurements were performed using the electrodes treated with plasma. The detailed experimental conditions for the detection of each NPs are detailed in the Supporting Information.

In the case of the AuNPs, two different methods, previously optimized on polyester SPCEs for the detection of these

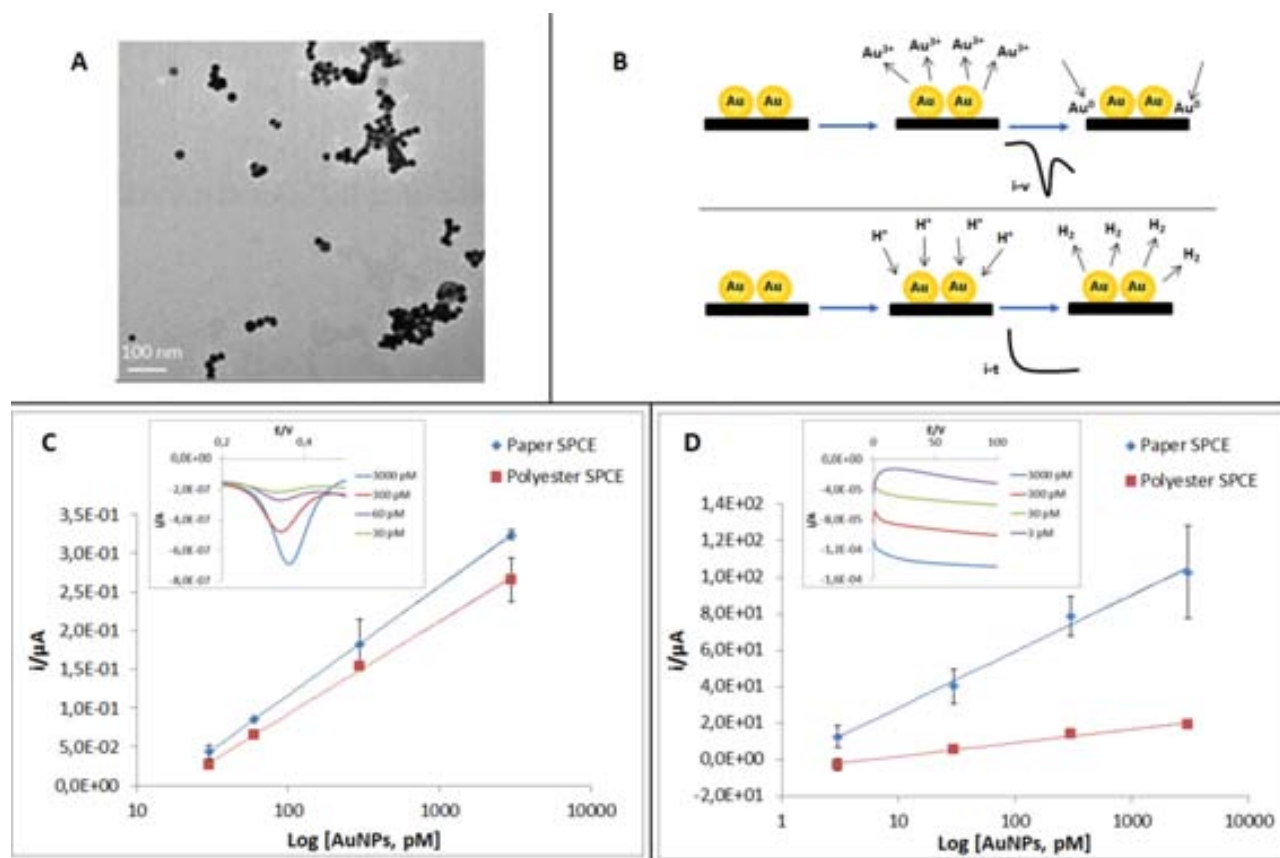


**Figure 3.** A) Transmission electron microscopy (TEM) images of AuNPs. B) Electrochemical principles for the detection of AuNPs: Direct voltammetric detection (top) and catalytic detection of AuNPs through the hydrogen evolution reaction (HER; bottom). C) Calibration curves of direct voltammetric detection of AuNPs, obtained measuring the peak values; in the inset representative signals obtained with paper SPCE at different concentration of AuNPs. D) Calibration curves of catalytic detection of AuNPs, obtained considering the current values at 100 s; in the inset representative signals obtained with paper SPCE at different concentration of AuNPs are shown.

NP labels in immunoassays, were tested with the two kinds of electrodes. Firstly, suspensions of 20 nm AuNPs of different concentrations were voltammetrically detected following a previously optimized method.<sup>[18]</sup> It consists in the electrochemical oxidation of the Au(0) to AuCl<sub>4</sub><sup>-</sup>, followed by the differential pulse voltammetric (DPV) reduction back to Au(0) (Figure 3B), which generates a peak of current directly related with the quantity of AuNPs. The results obtained, shown in Figure 3C, demonstrate that also with paper SPCEs was possible to directly detect AuNPs, obtaining sensitivity and reproducibility values of the same order of magnitude of polyester SPCEs, noticing even a slightly better sensitivity in the case of the paper. In particular, the limits of detection for paper SPCEs and polyester SPCEs were respectively  $15 \times 10^{-12}$  M and  $25 \times 10^{-12}$  M of AuNPs.

The second method tested was based on the hydrogen evolution reaction (HER) catalyzed by AuNPs and was followed chronoamperometrically. The value of the current registered at a 100 s is related with the quantity of AuNPs. This method leads to an efficient indirect detection of AuNPs by measuring the current produced during H<sub>2</sub> formation catalyzed by AuNPs (Figure 3D). This AuNP quantification technique is known to be more sensitive than the direct voltammetric detection and has been used in many biosensors ranging from protein<sup>[19]</sup>

to cancer cell<sup>[20,21]</sup> detections. The results show a clear increment in the signal using paper SPCEs. The limits of detection obtained were respectively  $3 \times 10^{-12}$  M and  $24 \times 10^{-12}$  M for paper SPCEs and polyester SPCEs. The bigger improvement obtained using paper instead of polyester, respect the direct detection of gold, can be related to the 3D structure of the WE, which allows an easier flow of protons toward the electrode area, pushing forward the H<sub>2</sub> evolution (hydrogen gas also escape faster through the generated micropores) reaction. This makes the paper SPCE an excellent platform to perform the whole catalytic cycles, with interest for an efficient AuNP quantification.

Finally, the last application of paper SPCEs was the direct voltammetric detection of CdSe@ZnS QDs in PBS buffer, without the need of a previous acidic dissolution of the NPs. This methodology has also been previously reported for QD detection on polyester SPCEs.<sup>[22]</sup> It consists in the electrochemical reduction of the Zn(II), contained in the NP, to Zn(0) followed to a square wave voltammetric (SWV) oxidation back of the Zn(0) to Zn(II), which generates a peak of currents at -0.9 V, which is related with the quantity of these NPs (Figure 4B). The results showed a very good trend, reaching a limit of detection of  $11 \times 10^{-6}$  M of QDs in a PBS solution (Figure 4C) using paper SPCEs. In this experiment, the data obtained with polyester SPCE are

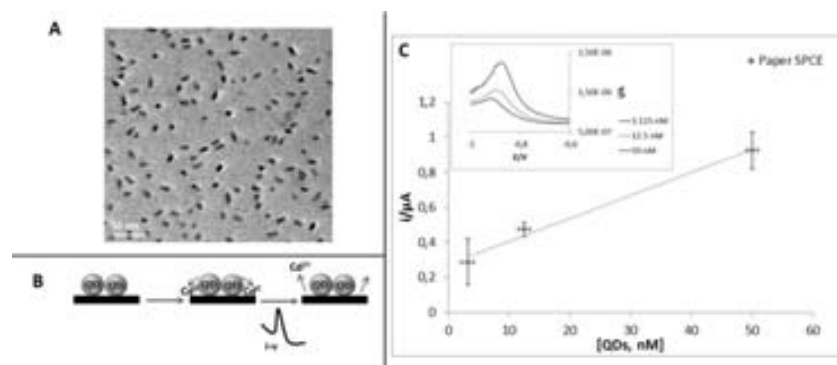


**Figure 4.** A) TEM images of CdSe@ZnS QDs. B) Electrochemical principle for the direct voltammetric detection of QDs. C) Calibration curve of direct voltammetric detection of QDs; in the inset representative signals obtained with paper SPCE at different concentration of QDs are shown. The response of polyester SPCE were not representative.

not shown, because such electrodes could not detect even the highest concentration of QDs evaluated.

In conclusion, we have developed very sensitive paper SPCEs by combining screen printing, wax printing, and plasma cleaner. This complete integrated paper-based SPCE shows a better response in comparison with state-of-the-art screen-printed platforms, such as polyester. We have also clarified such better response, due to the 3D structure of the electrode and the formation of microporous structures, which allowed a higher surface interaction between the nanoparticles and the WE. Furthermore, the use of plasma exposition makes the surface more hydrophilic. The detections of AuNPs and CdSe@ZnS QDs demonstrate that paper SPCEs can be used with a wide range of electrochemical techniques. Finally, the better electrochemical responses, compared with those obtained with polyester SPCE, make evident that the paper SPCE can be integrated in many biosensing platforms for several applications, where nanoparticles are used as labels either for DNA, protein, or even cell detection. In addition, fast and sensitive detection of electroactive nanoparticles with interest for environmental control can be done.

The developed paper-based sensor may improve, in a significant mode, the lateral flow-based devices, and opens the way to new real world applications of electrochemical sensing technology, which is still lacking from the separation between sample introduction, pretreatment, and incubations (immuno-reactions, DNA reactions) with detection. Having the electrochemical detector well integrated within paper microfluidics will further strengthen the efficiency of the resulting biosensing technologies. We envisage that, given the easy deposition of electrodes onto paper, combined with the flexibility and variability of paper platforms and wax printing, paper-based electrodes and sensors will be strong devices, with interest, not only in (bio)sensing, but also energy related applications,<sup>[23–25]</sup> where efficient “green solutions” are always welcome.

## Experimental Section

**Paper SPCEs Fabrication:** The nitrocellulose membrane HF240 was purchased from Millipore. A first insulating/hydrophobic layer of wax

was printed on it using a Xerox ColorQube 8570 wax printer (Xerox Corp., USA). Then, the membrane was heated at 150 °C for 30 s on a hot plate (VWR, USA). Finally, when the membrane was cooled to room temperature, the carbon ink and the Ag/AgCl ink were screen printed onto the paper. After each printing, the membrane was heated at 90 °C for 15 min.

**Polyester SPCE Fabrication:** On a polyester sheet, purchased by Mac Dermid Autotype, UK, three different layers were printed, in order: first the carbon ink, then the silver ink, and finally an insulating ink. For carbon and silver, the procedure was the same of the paper SPCEs, whereas the insulating ink was cured at 120 °C for 15 min.

**Plasma Cleaner.** All the electrodes were treated with plasma (from Harrick Plasma, E. U). First 3 min of vacuum were applied and then 1 min of plasma (30 W).

**NPs Preparations:** AuNPs of 20 nm of diameter were prepared according with the citrate reduction of HAuCl<sub>4</sub>, method pioneered by Turkevich,<sup>[26]</sup> as stated in the Supporting Information.

CdSe@ZnS QDs were purchased from (Invitrogen, USA).

**Assay Procedure:** The direct electrochemical detection of AuNPs was performed by placing 25 µL of the AuNPs solution on the working electrode area and leaving the AuNPs to adsorb during 2 min. After that, 25 µL of a HCl 0.2 M solution were added, covering the three electrodes area. A pre-concentration step to oxidize AuNPs to AuCl<sub>4</sub><sup>−</sup> was performed at +1.25 V (vs Ag/AgCl) for 120 s in a non-stirred solution. Immediately after the electrochemical oxidation, DPV was performed by scanning from +1.25 V to 0.0 V (step potential 10 mV, modulation amplitude 50 mV, scan rate 33.5 mV s<sup>−1</sup>, non-stirred solution), resulting in an analytical signal due to the reduction of AuCl<sub>4</sub><sup>−</sup> at +0.45 V.

The chronoamperograms, of the electrocatalytic detection of AuNPs, were obtained placing a mixture of 25 µL of 2 M HCl and 25 µL of the AuNP solution (different concentrations) onto the surface of the electrodes and, subsequently, holding the working electrode at a potential of +1.35 V for 1 min and then a negative potential of −1.00 V for 100 s.

The direct voltammetric detection of CdSe/ZnS QDs were obtained placing a drop of 50 µL of the desired QD in PBS concentration was suspended on the surface of the electrode and a potential of −0.15 V was applied for 60 s (conditioning step). Later, in the accumulation step, a deposition potential of −1.5 V for 120 s was applied to promote the electrochemical reduction of Zn<sup>2+</sup> ions contained in the shell structure of QD to Zn<sup>0</sup>. Then, the reduced zinc is oxidized back to zinc ions by SWV scanning from −1.5 V to −0.15 V (step potential 3 mV, modulation amplitude 30 mV and frequency 15 Hz), resulting in an analytical signal.

## Supporting Information

Supporting Information is available from the Wiley Online Library or from the author.

## Acknowledgements

M.M.-S. and H.M. contributed equally to this work. The authors acknowledge MEC (Madrid) for the project MAT2011–25870.

Received: November 12, 2012

Revised: April 7, 2013

Published online:

- [1] A. de la Escosura-Muñiz, C. Parolo, A. Merkoçi, *Mater. Today* **2010**, 13, 24.
- [2] D. W. Kimmel, G. LeBlanc, M. E. Meschievitz, D. E. Cliffel, *Anal. Chem.* **2012**, 84, 685.
- [3] L. Ge, J. Yan, X. Song, M. Yan, S. Ge, J. Yu, *Biomaterials* **2012**, 33, 1024.
- [4] P. Wang, L. Ge, M. Yan, X. Song, S. Ge, J. Yu, *Sens. Bioelectron.* **2012**, 32, 238.
- [5] Z. Nie, C. A. Nijhuis, J. Gong, X. Chen, A. Kumachev, A. W. Martinez, M. Narovlyansky, G. M. Whitesides, *Lab Chip* **2010**, 10, 477.
- [6] W. Dungchai, O. Chailapakul, C. S. Henry, *Anal. Chem.* **2009**, 81, 5821.
- [7] R. F. Carvalhal, M. S. Kfoury, M. H. D. O. Piazzetta, A. L. Gobbi, L. T. Kubota, *Anal. Chem.* **2010**, 82, 1162.
- [8] D. Zang, L. Ge, M. Yan, X. Song, J. Yu, *Chem. Commun.* **2012**, 48, 4683.
- [9] S. Ge, L. Ge, M. Yan, X. Song, J. Yu, J. Huang, *Chem. Commun.* **2012**, 48, 9397.
- [10] X. Liu, M. Mwangi, X. Li, M. O'Brien, G. M. Whitesides, *Lab Chip* **2011**, 11, 2189.
- [11] C. Parolo, A. Merkoçi, *Chem. Soc. Rev.* **2013**, 42, 450.
- [12] K. Saha, S. S. Agasti, C. Kim, X. Li, V. M. Rotello, *Chem. Rev.* **2012**, 112, 2739.
- [13] P. Lie, J. Liu, Z. Fang, B. Dun, L. Zeng, *Chem. Commun.* **2012**, 48, 236.
- [14] C. Parolo, A. de la Escosura-Muñiz, A. Merkoçi, *Biosens. Bioelectron.* **2012**, 40, 412.
- [15] C.-Z. Li, K. Vandenberg, S. Prabhulkar, X. Zhu, L. Schneper, K. Methee, C. J. Rosser, E. Almeida, *Biosens. Bioelectron.* **2011**, 26, 4342.
- [16] Z. Nie, F. Deiss, X. Liu, O. Akbulut, G. M. Whitesides, *Lab Chip* **2010**, 10, 3163.
- [17] D. Zang, L. Ge, M. Yan, X. Song, J. Yu, *Chem. Commun.* **2012**, 4683.
- [18] A. de la Escosura-Muñiz, C. Parolo, F. Maran, A. Merkoçi, *Nanoscale* **2011**, 3, 3350.
- [19] M. Maltez-da Costa, A. de la Escosura-Muñiz, A. Merkoçi, *Electrochem. Commun.* **2010**, 12, 1501.
- [20] M. Maltez-da Costa, A. de la Escosura-Muñiz, C. Nogués, L. Barrios, E. Ibáñez, A. Merkoçi, *Nano Lett.* **2012**, 12, 4164.
- [21] M. Maltez-da Costa, A. de la Escosura-Muñiz, C. Nogués, L. Barrios, E. Ibáñez, A. Merkoçi, *Small* **2012**, 8, 3605.
- [22] M. Medina-Sánchez, S. Miserere, S. Marín, G. Aragay, A. Merkoçi, *Lab Chip* **2012**, 12, 2000.
- [23] N. K. Thom, K. Yeung, M. B. Pillion, S. T. Phillips, *Lab Chip* **2012**, 12, 1768.
- [24] L. Yuan, X. Xiao, T. Ding, J. Zhong, X. Zhang, Y. Shen, B. Hu, Y. Huang, J. Zhou, Z. L. Wang, *Angew. Chem. Int. Ed.* **2012**, 51, 4934.
- [25] L. Ge, P. Wang, S. Ge, N. Li, J. Yu, M. Yan, J. Huang, *Anal. Chem.* **2013**, 85, 3968.
- [26] J. Turkevich, P. C. Stevenson, P. Hillier, *Discuss. Faraday Soc.* **1951**, 11, 55.

# Supporting Information

## **Paper-based electrodes for nanoparticles detection**

By *Claudio Parolo, Mariana Medina-Sánchez, Helena Montón, Alfredo de la Escosura-Muñiz, and Arben Merkoçi\**

[\*] Prof. A. Merkoçi, C. Parolo, M. Medina-Sánchez, H. Montón, Dr. A. de la Escosura-Muñiz  
Nanobioelectronics & Biosensors Group,  
Institut Català de Nanotecnologia, CIN2 (ICN-CSIC),  
Campus UAB, Barcelona, Spain.  
Prof. A. Merkoçi  
ICREA, Barcelona, Spain

Phone number: +34935868014; Fax number: +34935868020

\*E-mail: [arben.merkoci@icn.cat](mailto:arben.merkoci@icn.cat)

### Effect of the plasma treatment

In the fig 1-S it is possible to see how the plasma affect positively the electrochemical detection of AuNPs in paper SPCE, both for direct and indirect detection.

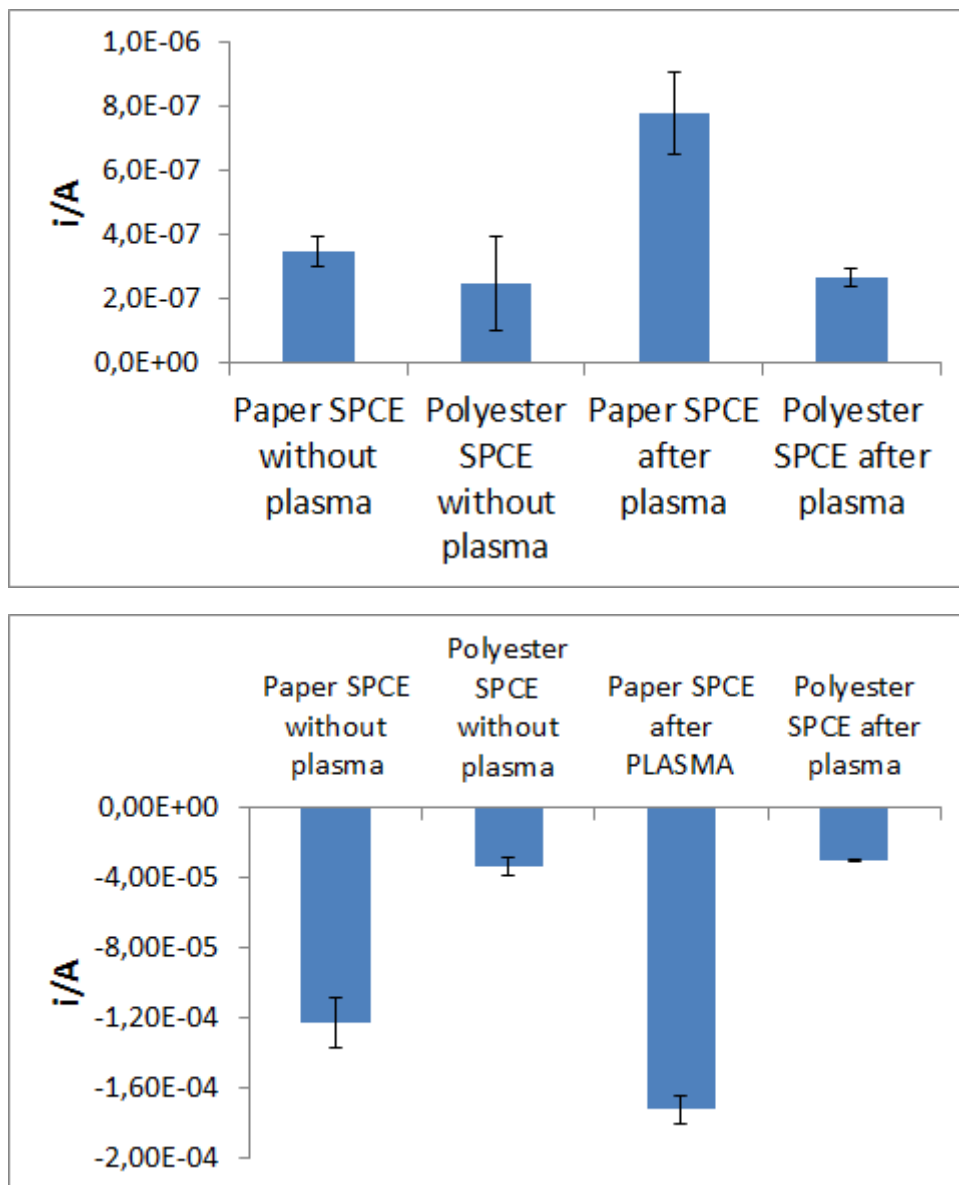


**Fig. 1-S:** Electrochemical direct detection of AuNPs (top) and indirect detection of AuNPs (bottom) with paper and polyester SPCE treated or not with plasma for 3nM AuNPs concentration.

### Preparation of gold nanoparticles

Gold nanoparticles of 20 nm of diameter were prepared according with the citrate reduction of  $\text{HAuCl}_4$ , method pioneered by Turkevich.(Turkevich, 1951) Briefly: 50

mL aqueous solution of 0.01%  $\text{HAuCl}_4$  was heated to boiling and vigorously stirred in a 250 mL round-bottom flask; 5 mL of 40 mM sodium citrate were added quickly to this solution. Boiling was continued for additional 10 min. The solution was cooled to room temperature with a continuous stirring for another 15 min. The colloids were stored in dark bottles at 4° C. All glassware used in this preparation was thoroughly cleaned in aqua regia overnight and rinsed with double distilled  $\text{H}_2\text{O}$  and reflux was used for all the procedure.

### **Rugosity study using CLSM**

Analyzing a single section of the z-stack we can also determine the random/flat or patterned/rugous by studying the intensity. The intensity value of each pixel in the selected ROI (red line) is displayed in the graph below the image. In polyester WE we can see continuous but non-periodic changes in a small range of intensity, whereas in paper WE we can observe that the decrease/increase of the intensity is stronger, periodic and matching with the pattern observed in the image.

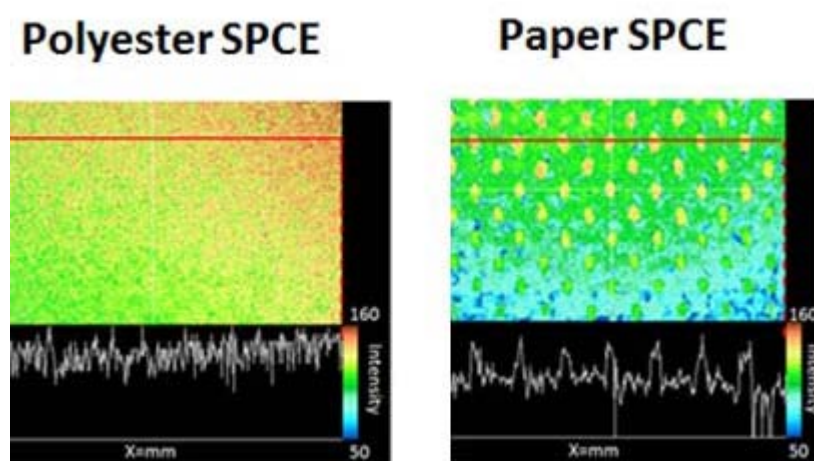


**Fig. 2-S:** Analysis of the intensity of a single z-stack for polyester SPCE (on the left) and paper SPCE (right)

### **Direct voltammetric detection of AuNPs**

The direct electrochemical detection of AuNPs was performed by placing 25  $\mu\text{L}$  of the AuNPs solution on the working electrode area and leaving the AuNPs to adsorb during 2 minutes. After that, 25  $\mu\text{L}$  of a HCl 0.2 M solution were added, covering the three electrodes area. A pre-concentration step to oxidize AuNPs to  $\text{AuCl}_4^-$  was performed at +1.25 V (vs Ag/AgCl) for 120 s in a non-stirred solution. Immediately after the electrochemical oxidation, differential pulse voltammetry (DPV) was performed by scanning from +1.25 V to 0.0 V (step potential 10 mV, modulation amplitude 50 mV, scan rate 33.5 mV s<sup>-1</sup>, non-stirred solution), resulting in an analytical signal due to the reduction of  $\text{AuCl}_4^-$  at +0.45 V.

### **Electrocatalytic detection of AuNPs**

Chronoamperograms were obtained by placing a mixture of 25  $\mu\text{L}$  of 2 M HCl and 25  $\mu\text{L}$  of the AuNP solution (different concentrations) onto the surface of the electrodes and, subsequently, holding the working electrode at a potential of +1.35 V for 1 min and then a negative potential of -1.00 V for 100 s.

### **Direct voltammetric detection of CdSe/ZnS QDs**

A drop of 50  $\mu\text{L}$  of the desired QD in PBS concentration was suspended on the surface of the electrode and a potential of -0.15 V was applied for 60 s (conditioning step). Later, in the accumulation step, a deposition potential of -1.5 V for 120 s was applied to promote the electrochemical reduction of  $\text{Zn}^{2+}$  ions contained in the shell structure of QD to  $\text{Zn}^0$ . Then, the reduced zinc is oxidized back to zinc ions by SWV scanning from -1.5 V to -0.15 V (step potential 3 mV, modulation amplitude 30 mV and frequency 15 Hz), resulting in an analytical signal.

## Annex B

### Articles accepted by the PhD comission

#### Related Publications

---

- 1) De la Escosura-Muñiz, A.; Parolo, C.; Merkoçi, A. Immunosensing using nanoparticles. *Materials Today*, 2010, 13, 24–34.
  - 2) Parolo, C.; Merkoçi, A. Paper-based nanobiosensors for diagnostics. *Chemical Society Reviews*, 2013, 42, 450–457.
  - 3) De la Escosura-Muñiz, A.; Parolo, C.; Maran, F.; Merkoçi, A. Size-dependent direct electrochemical detection of gold nanoparticles: application in magnetoimmunoassays. *Nanoscale*, 2011, 3, 3350–3356.
  - 4) Parolo, C.; De La Escosura-muñiz, A.; Polo, E.; Grazú, V.; de la Fuente, J. M.; Merkoçi, A. Antibody-oriented functionalization of gold nanoparticle labels for very sensitive electrochemical biosensing. Submitted *Anal. Chem.* 2013.
  - 5) Parolo, C.; Medina-Sánchez, M.; De la Escosura-Muñiz, A.; Merkoçi, A. Simple paper architecture modifications lead to enhanced sensitivity in nanoparticle based lateral flow immunoassays. *Lab on a chip*, 2013, 13, 386–90.
  - 6) Parolo, C.; De la Escosura-Muñiz, A.; Merkoçi, A. Enhanced lateral flow immunoassay using gold nanoparticles loaded with enzymes. *Biosensors and Bioelectronics*, 2012, 40, 412–416.
  - 7) Parolo, C.; Medina-Sánchez, M.; Montón, H.; De la Escosura-Muñiz, A.; Merkoçi, A. Paper-based electrodes for nanoparticles detection. *Particle & Particle System Characterization*, 2013, DOI: 10.1002/ppsc.201200124.
-





**Acknowledgments**

**Agraïments**

**Agradecimientos**

**Ringraziamenti**



## Acknowledgments/Agraïments/Agradecimientos/Ringraziamenti

In this part, I want to thank all the people who helped me during these 3 years, using the languages I am used to talk with them. The list is very long but each of them has really given me a support to finish this thesis.

### **Barcelona** – Nanobioelectronics and Biosensors group

No se puede que empezar agradeciendo a **Arben** que desde el primer día, cuando era aún un estudiante de máster en Erasmus a Barcelona, ha demostrado de creer en mí y me ha hecho siempre pensar en grande. No creo que se pueda pedir más de un jefe! (Inolvidable la cena ligera a base de pizza en Slovenia!)

Y obviamente en seguida toca a **Alfredo** (el Xavi Hernández del grupo), que me direccionó en el día a día haciéndome poner los pies en el suelo (y a veces en el campo de futbol) y aprender a ser más metódico, a parte obviamente de todas las correcciones de artículos, presentaciones etc. De verdad una gran guía!

Y bueno, como no dar una mención especial a **Anna** Puma... ops... quería decir Puig... definirla secretaria sería poco, definirla lab manager también... decimos simplemente que sin ella este laboratorio no podría funcionar! Pero sobre todo gracias por tu amistad y conexión cerebral! Jeje!

Ahora viene lo difícil... quería decir algo personal a cada uno del grupo... pero me doy cuenta que ha pasado así tanta gente que tardaría muchísimo a escribir un párrafo por cada uno... así que no tomaros a mal si os dedico solo una palabra o una frase! Para no olvidarme de nadie sigo el orden de la web nanobiosensors.org! Jejeje!

Muchas gracias a:

Las postdocs: **Carmen** y **Sandrine**... que al final podían considerarse como una única entidad! Están conocidas también como Reina del Cuzco y Princesa de Paris (ahora está intentando expandirse a México para poder decir que “nunca baja el sol en su imperio!”). Aunque no hemos trabajado directamente juntos me ha gustado hablar con vosotras y tomar respectivamente la sangría más car(gad)a de Barcelona y el aperitivo-mojito!

**Miquelito**... el hombre que ha recorrido todas las montañas de Cataluña con su inseparable mochila! Ha sido divertido estar en el mismo grupo!

## **Acknowledgments/Agraïments/Agradecimientos/Ringraziamenti**

**Cholesito**, Mariluz, Marisol, P endy, ecc e cc... una mujer con mas nombres de las palabras en un diccionario. No se cuentan las cervezas/patatas que nos hemos tomado a la E TSE. Eres una de las personas más listas que conozco así como con la risa mas fuerte!

**Maria**... que hablando de risas ruidosas no tiene nada que envidiar a Marisol! Jajaja! Que decirte Maria... gracias de verdad! Si el primer año me lo he pasado así a gusto en Barcelona ha sido en buena parte gracias a ti! Eres una crack tanto a trabajo como fuera del lab!

**Adaris**... una explosión cubana en el medio de Cataluña! A parte de compartir el sufrimiento con las tiras de LF, me he divertido a intercambiar visiones distintas de la vida!

**Mariana**... podría copiar y pegar lo que he dicho de Maria (excepto la risa ruidosa)... has sido como una hermana el primer año! Además que habiendo llegado con 15 días de diferencia hemos hecho todo el doctorado en paralelo! Estoy seguro que tendrás mucho éxito!

**Helena**... creo que la afirmación más frecuente que la gente nos ha hecho ha sido “parecéis un matrimonio (de abuelos)”... y esto describe muy bien todo... dos formas de hacer las cosas que más distintas no podrían ser, pero que al mismo tiempo se compensan. A esto sumamos comidas compartidas, horas midiendo células hasta las tantas, miles de millas en coche across USA y un viaje a Hawaii comiendo cocooo... de verdad “Grazie mille di tutto”!

**Eden**... ha sido siempre interesante hablar de ciencia contigo... ya entender cuando me explicas de agopuntura me cuesta un poquito más :-p! Que el espíritu del Absinth te acompañe siempre!

**Flavio**... detto anche Pino-san... perchè bisogna ammetterlo: un tocco di italianità/juventinità in più nel laboratorio ci voleva! Adesso pure controllore dell'ordine dopo il ritiro spirituale giapponese! Sempre un appoggio sicuro quando si tratta di farsi una birretta in compagnia!

## Acknowledgments/Agraïments/Agradecimientos/Ringraziamenti

**LuLu...** con Adaris, otro componente del Lateral Flow team! Siempre, o casi, con una sonrisa en el laboratorio! Además tengo que agradecerle un montón por el más bonito diario de viaje que se haya visto nunca! Tienes un don por las manualidades!

**Luis...** bueno tío... que de cirte... eres una de las personas más eclécticas que he conocido! Ha sido un placer trabajar, ir de viaje y de fiesta juntos! Tienes un potencial enorme: fantasía, comunicación y sobretodo sabes juntarte con cualquier tipo de persona!

El **Chamo...** un personaje increíble! Profesional, amistoso, aventurero y con un lado de locura que nunca viene mal! Además tienes el poder “afro” en tus genes! Estoy seguro que irás muy lejos!

**Abdelmoneim**, alias “Moni”... it was a pleasure working with you and learning about ferrocene! You are also a Juve-supporter! We have to organize a trip in Tunisia, man!

And also the people who passed in the lab during my PhD: **Anna, Jihane, Amal, Lenka1, Lenka2, Giselle, Serdar1, Serdar2, Misa, Deniz, Ruslan, Erika, André, Laura, Wilanee, Welter, Nicholas, Maelle, Irene.**

Pero aquí no se ha terminado la sección del grupo, ya que hay unas personas que ya no están en el grupo pero merecen una citación especial:

**Gemma...** chavalina! Per tu vaig a tractar de escriure en Catalán... moltes gracies per tot... ets una maquina! En part t’he sempre mirat com un modelo d’imitar, i no podria haver escollit a un millor! Però sobre tot... PUFF! I con això ja ho he dit tot!

**Marisa...** con Maria ha cíaais el comité de bienvenida al grupo! Muchas gracias para enseñarme los secretos de la magento-sandwich y aun mas para los secretos de la pastelería portuguesa! Espero que la caldera siga funcionando bien! jejeje

**Briza...** lo primero que se me pasa por la cabeza es “sonrisa”! Daba siempre mucho gusto entrar a la oficina y verte allí! Además tus vestidos molan un mogollón!

**Sergi...** otro mítico personaje! Nos hemos divertido mucho durante el doctorado y esto también ha sido muy importante! Si no me equivoco tenemos, de andalucia, un asunto pendiente con unos mexicanos!

## Acknowledgments/Agraïments/Agradecimientos/Ringraziamenti

**Tiziana**... indubbiamente meriti una menzione speciale quella ragazza italiana “mas loca” che si abbia visto mai!

The next two are adopted group members:

**Carlos**... si tenias un problema, él te lo arreglaba en un segundo, además de hacer el mejor asado argentino que haya probado nunca! Cuidado con ese bate!

**Francesco**... non saprei in che sezione metterti, se barcelona-gruppo, barcelona-amici, italia-amici... però ormai vieni considerato all’unanimità come uno del gruppo... a parte del fatto che come Cip&Ciop non debba aggiungere nulla più di un “Grazie mille vecio!”

### – ICN

Gracias por el soporte administrativo/técnico a: **Rosa, Anabel, Stewe, Mireia, Montse, Belen, Marcos!** Y unas gracias especiales a **Damaso** por la impagable ayuda con la portada de la tesis!

### – UAB

Un gracias a **Maria Josep** y al **equipo de postgrado** para el soporte burocrático.

### – Tusamigossonmisamigos

Unas gracias muy grandes quiero darlas a mis compis de piso para haberme aguantado en estos 3 años y pico: **Laura, Berta, Maria, Rocio, Carlos, Cris, Jordi, Nuria, Katia, Albert.**

Y a todos los demás (espero acordarme de todos!) para la alegría que me habéis dado en estos años: **Alex, Alexis, Ane, Aritz, Arnau, Aurora, Crisa, Monica, Natalia, Ofelia, Rosa, Tamara, Vane, Veronica, Victor.**

Y para las noches de Trivial a **Carla, Ariadna, Grego, Fito, Tesla.**

### – BioNANOSurf Group

Y como no dar las gracias a los chic@s del grupo del Prof. **Jesús de la Fuente**? Fue una mini-estancia muy intensa sea a nivel de trabajo que humano! La verdad que desde el primer día mi hicisteis sentir como uno más del grupo y esto hizo que el trabajo salió

## Acknowledgments/Agraïments/Agradecimientos/Ringraziamenti

muy bien y que al mismo tiempo pude disfrutar de Zaragoza y de la bbq... así que muchas gracias a: **Jesús, Ester, Sara, Sara, Valeria, Yulán, Dani, María, Bea, Pablo!**

### **Boston** – Whitesides group

I want to thank **Prof. Whitesides** to let me spend 6 fruitful months in his laboratory. My experience in Harvard University could not be possible without the help I received from **T.J., Melissa and Tracy!**

My very special gratitude goes for **Wenjie** and **Jane**, who have been my scientific guides in Boston.

And if my stay in Whitesides lab, beside the very high quality scientific level, has been also a reach human experience, it is all due to people (actually “Friends” is the right word) like **Barb, Shuji** and his wonderful family, **Dennis** and **Nikoleta, Felice, Abraham, Alok, Hai Dong, Mathieu, Sen Wai, Ramses** and the **Spanish group**, and all the others.

### **Italia** – Università di Padova

Un grazie al Prof. **Flavio Maran** perchè se que l giorno 6 anni fa non mi avesse proposto di andare a Barcellona non avrei mai potuto trovarmi dove sono adesso.

### **Italia** – Amici

Un grazie a **Alessandra** per avermi incoraggiato all’inizio di questa avventura.

Grazie a **Matteo, Carlo, Vincenzo, Valeria, Giulia, Nadia, Martina** per rimanere sempre i soliti vecchi buoni amici.

### **Italia** – **Este**

Infine, i ringraziamenti più sentiti vanno ai miei genitori, **Annamaria e Carlo**, perchè hanno sempre avuto fiducia in me e mi hanno sempre supportato moralmente (ed economicamente!) durante tutti questi anni. Un grazie speciale anche al la nonna Mascarona Francesca e al nonno Bepi d’Arian Giuseppe, così come a tutti zii, cugini, parenti e amici vari.